Rockefeller University
Digital Commons @ RU

Student Theses and Dissertations

2013

Telomere-Driven Tetraploidy and its Relevance to Cancer

Teresa Davoli

Follow this and additional works at: http://digitalcommons.rockefeller.edu/student_theses_and_dissertations

 Part of the Life Sciences Commons

Recommended Citation
Davoli, Teresa, "Telomere-Driven Tetraploidy and its Relevance to Cancer" (2013). *Student Theses and Dissertations*. Paper 235.

This Thesis is brought to you for free and open access by Digital Commons @ RU. It has been accepted for inclusion in Student Theses and Dissertations by an authorized administrator of Digital Commons @ RU. For more information, please contact mcsweej@mail.rockefeller.edu.

TELOMERE-DRIVEN TETRAPLOIDY AND ITS RELEVANCE TO CANCER

A Thesis Presented to the Faculty of
The Rockefeller University
in Partial Fulfillment of the Requirements for
the degree of Doctor of Philosophy

by

Teresa Davoli

June 2013

©Copyright by Teresa Davoli 2013

TELOMERE-DRIVEN TETRAPLOIDY AND ITS RELEVANCE TO CANCER

Teresa Davoli, Ph.D.

The Rockefeller University 2013

Aneuploidy, i.e. the state of having an abnormal chromosome number, is a hallmark of human solid tumors. A fraction of aneuploid tumors is near-diploid and can be explained by individual chromosome gains and losses in mitosis. The remaining fraction is subtetraploid, containing an increased chromosome number, ranging from 60 to 90 chromosomes. Mounting evidence argues that tetraploidization, i.e. whole genome doubling, followed by chromosome loss is likely to represent an early event in the development of subtetraploid tumors. The origin of tetraploidization in cancer is still unclear. Here we describe a new potential mechanism of tetraploidization in cancer, originating from telomere dysfunction, a widespread phenomenon in early tumorigenesis. Prolonged telomere deprotection caused by inactivation of the telomeric proteins POT1a and POT1b leads to tetraploidy in p53/Rb deficient mouse cells. Irreversible telomere deprotection and other forms of persistent DNA damage induce a prolonged G2 phase followed by by-pass of mitosis, re-entry into S phase, and whole genome reduplication. Endoreduplication requires an ATM and/or ATR-dependent DNA damage signal, blocking the activation of Cdk1/CyclinB and mitosis. Furthermore, we demonstrate tetraploidization through endoreduplication or mitotic failure in human fibroblasts and mammary epithelial cells undergoing replicative telomere crisis in the absence of p53 and Rb. Using an inducible system to generate transient telomere dam-

age, we show that telomere-driven tetraploidization enhances the tumorigenic transformation of mouse cells. Finally we showed that breast cancer cell lines with high chromosome numbers display higher frequency of telomeric fusions compared to near-diploid lines, suggesting previous telomere crisis during their development. Collectively, these data suggest a potentially widespread mechanism for tetraploidization resulting from excessive telomere shortening in early precancerous lesions, promoting the evolution of a subtetraploid cancer karyotype.

Acknowledgements

First, and most of all, I would like to thank my advisor, Titia de Lange, for her steadfast support during these years of graduate school. Her scientific insight, intuition, and fearless willingness to tackle big questions will always represent a fount of inspiration for me. Despite her extremely active scientific life, Titia has dedicated to me, as well as the entire lab, an incredible amount of time and effort. This is very rare, if not unique, for a scientist of her level. I am very grateful for her dedication to extend my scientific knowledge, to discuss every step in my research project, and to teach me how to critically interpret experimental data. I am also extremely grateful to Titia for the time she has dedicated to improving my ability to effectively communicate scientific knowledge and research. Besides her scientific mentorship, Titia has been very supportive during difficult moments in the past few years.

I am very thankful to the members of my thesis committee, Fred Cross and Sohail Tavazoie, for their advice and support. I am grateful to Fred for his encouragement and guidance in the first years of graduate school. The level of scientific insight and acumen he has shared with me and others during classes has been inspirational. His dedication to teaching and mentoring of students is rare and invaluable. I would like to thank Sohail for his expert advice on cancer-related issues in my research project, not only during the thesis committee meetings, but also in informal meetings especially in the last years. His support and help allowed us to start a scientific collaboration with researchers and clinicians at Memorial Sloan Kettering Cancer Center. Besides his scientific encouragement, I am also extremely grateful to Sohail for

helping me and my boyfriend, Lorenzo, in the face of unforeseen difficulties. I would also like to express my appreciation to David Pellman for accepting the invitation to serve as the external examiner in my thesis committee.

Among many people who shared reagents, I am extremely thankful to Atsushi Miyawaki from RIKEN, Japan for having shared with us the FUCCI system for live cell imaging. I am very grateful to Martha Stampfer at Berkeley Laboratory for sharing several human mammary epithelial cell lines and her expertise on experimental procedures. In addition, I thank Scott Lowe, Pier Giuseppe Pelicci, Oscar Fernandez-Capetillo, and Jos Jonkers for sharing cell lines and retroviral constructs with us. I also thank Anna Jauch from Heidelberg University for collaborating with us on a small part of the project.

I am thankful to all present and past members of the de Lange lab I have had the opportunity to meet and work with during these years. They have rendered the lab a scientifically stimulating and collaborative environment. I extend a very special thanks to Devon White, not only for taking care of our mice colonies, but also for his invaluable skills and patience in teaching me some technical procedures with mice. I am grateful to Eros Lazzerini Denchi, who mentored me during my rotation and first months in the lab. His support and guidance were extremely important in the first steps of my research project. I am also very grateful to many postdocs and students for constant engagement in scientific (and non-scientific) discussion and for making the lab a fun place to work: Agnel Sfeir, Ylli Doksani, Hiro Takai, Michal Zimmermann, Isabelle Schmutz, Courtney Lovejoy, Katja Kratz, Shaheen Kabir, David Frescas, Francisca Lottersberger, Yi Gong, Nazario Bosco and Tatsuya Kibe. I

express my gratitude also to Wendi Li, Kaori Takai, and Rosie Mejia for organizing and taking care of the lab. Moreover, I am thankful for the Dean's office, where everybody has been very helpful and supportive especially in the last months. I also express my appreciation to Svetlana Mazel and Alison North form the Flow Cytometry and Bioimaging facilities, respectively, for their help and assistance.

Finally, I would like to thank my family for watching over me from the other side of the Atlantic ocean and always supporting my choices, even if sometimes difficult for the distance separating us. I thank my father, Oreste, for always encouraging me to eat enough, and making sure that every time I was back in Italy I would return to the US with lots of Parmesan cheese. I thank my mother, Maria Lucia, for her support and also for her genuine interest in biomedical questions related to important medical issues, an interest that I have always shared with her. I thank Lorenzo for having taught me how to use Latex software, which I used to write this thesis. Most of all I thank Lorenzo for having shared with me this exciting, and sometimes challenging, experience overseas in the past years and more to come. I also thank Paola, Andrea, Dee, Susa, Ashley, Brendan, Eva, Tina, Marlyn, Simona and many other friends here in NY for their constant support and friendship in these years.

Table of Contents

List of Figures

List of Abbreviations

ATM	Ataxia-telangiectasia mutated
ATR	ATM- and Rad3-related
BRCA2	Breast Cancer 2 susceptibility protein
BrdU	Bromo-deoxyuridine
Cdk	Cyclin-dependent kinase
Chk1	Checkpoint kinase 1
Chk2	Checkpoint kinase 2
DAPI	4,6-diamidino-2-phenylindole
eGFP	Enhanced green fluorescent protein
FISH	Fluorescence in situ hybridization
HDR	Homology-directed repair
HPV-E6/E7	Human papillomavirus protein E6/E7
IF	Immunofluorescence
IF-FISH	Immunofluorescence - Fluorescence in situ hybridization
KO	Knock-out
MEF	Mouse embryonic fibroblasts
NHEJ	Non-Homologous End-Joining
OHT	4-Hydroxytamoxifen
POT1a/b	Protection Of Telomeres 1a/b
PD	Population Doubling
Ras	Harvey Rat Sarcoma viral oncogene homolog
s.d.	Standard deviation
shRNA	Short hairpin RNA
SV40-LT	Simian virus 40; Large T antigen
Terc	Telomerase RNA Component
hTERT	HumanTelomerase Reverse Transcriptase
TopBP1	Topoisomerase (DNA) II Binding Protein 1
TRF1	Telomere repeat binding factor 1
TRF2	Telomere repeat binding factor 2
53BP1	p53 Binding Protein 1

Chapter 1

Introduction

1.1 Polyploidy in physiology and evolution

1.1.1 Organismal Polyploidy During Evolution

Organismal polyploidy is very common in plants (frequency estimated between 30 and 80%; Otto and Whitton, 2000), especially in the flowering plants (angiosperms; Masterson, 1994), probably due both to frequent formation of diploid gametes (0.5% of gametes are estimated to be diploid) and to frequent species hybridization (Fig. 1.1A). In contrast, organismal polyploidy is rare among animals, mainly due to problems in embryonic development and sex determination (Otto and Whitton, 2000). Polyploidy is sporadically found in insects (90 species) and some vertebrates (100 species among amphibians, reptiles and fishes; Otto and Whitton, 2000, Fig. 1.1A). In mammals, organismal polyploidy is poorly tolerated and it is responsible for 5-10% of spontaneous abortions in humans (Creasy et al., 1976). The only tetraploid mammals

are the red vizcacha rat (*Tympanoctomys barrerae*) and its close relatives, Fig. 1.1A).

Despite being rare in animals, polyploidy is thought to have played an important role during evolution. Many plants and animals are considered ancient polyploids (or paleopolyploids), i.e. to have arisen through one or more whole genome duplications during their evolution, followed by silencing, loss and divergence of many of the duplicated genes (Wolfe, 2001; Pennisi, 2001). For example, the genome of *Arabidopsis thaliana* contains many syntenic duplicated regions that have been proposed to derive from multiple genome-wide polyploidization events (Ku et al., 2000). A longstanding hypothesis, dating back to Ohno's ideas in 1970, proposes that two events of polyploidization occurred during the early evolution of the vertebrate lineage ('the 2R hypothesis', Ohno, 1970; Fig. 1.1B). One of the initial genetic observations supporting this hypothesis was the fact that many invertebrate single-copy genes have four vertebrate orthologues ('1:4 relationship'). For example, the single copy Hox gene cluster in the Drosophila genome is present in four copies in mammals, each located on a different chromosome (Graham et al., 1989; Schughart et al.; 1989, Garcia-Fernandez and Holland, 1994). Other examples of the 1:4 relationship include genes encoding for the fibroblast growth factor receptors and the major histocompatibility complex. Importantly, the quadruplicated paralogous chromosomal regions frequently show collinear gene order and the same centromere-to-telomere orientation, suggesting an *en-bloc duplication*, instead of individual independent duplications. Recent studies have refined the 2R model and specified the timing of whole-genome duplications at the

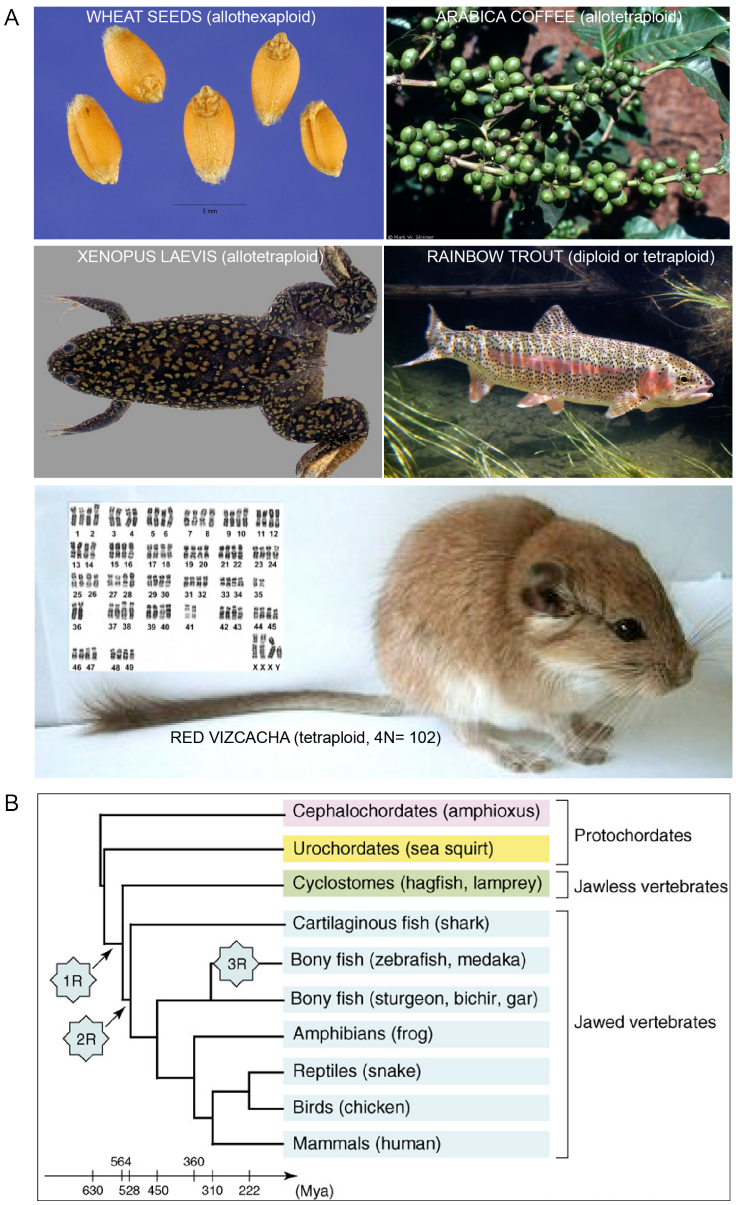

Figure 1.1: **Examples of organismal polyploidy and the 2R hypothesis.** (A) Examples of natural polyploid species among plants and animals (from *http* : *//polyploidy.org/index.php/Parade*$_o$*f*$_P$*olyploids*). The red vizcacha rat (*Tympanoctomys barrerae*) and its close relatives are the only tetraploid mammals. (B) Recent version of the 2R (3R) hypothesis, which assumes two rounds of genome duplication, the first after the emergence of urochordates and the second before the radiation of jawed vertebrates (from Kasahara, 2007). A third duplication is thought to have occurred during the evolution of fishes.

origin of vertebrates. The first duplication is supposed to have occurred after the emergence of urochordates and the second before the radiation of jawed vertebrates (Fig. 1.1B, Kasahara, 2007). A third genome duplication (3R) is thought to have occurred during the evolution of ray-finned fishes (Jallion et al., 2004).

The occurrence of paleopolyploidy argues that polyploidy does not necessarily result in an evolutionary dead end. It has been argued that polyploidy can confer an adaptive advantage because of mutational robustness. In the polyploid genome, the consequences of gene deletions or inactivating mutations can be buffered by the presence of the additional gene copies (Crow and Wagner, 2006). By limiting loss of fitness or viability, polyploidy can reduce the risk of extinction, especially of small and bottle-necked populations (as in preneoplastic cell populations, see below). However, a drawback of increased masking of gene mutations is a high mutational load (higher frequency of gene mutations in the population), that can impair the survival of a polyploid species compared to their diploid counterpart (Otto and Whitton, 2000). A second advantage of polyploidy is the increased gene subfunctionalization and neofunctionalization, leading to increased evolution rate and directional selection (Crow and Wagner, 2006). Moreover, doubling of the whole genome may allow doubling of all the genes in the same pathway preventing unbalanced effects that can result from duplication of single genes or single chromosomal regions (Freeling and Thomas, 2006). On the other hand, the effect of a new beneficial mutation can be lower in polyploids than in diploids since the number of remaining WT alleles is higher (Otto and Whitton, 2000). Finally, for

partially unknown reasons, newly formed polyploids show greater genome instability than the diploids counterpart, showing a higher rate of chromosome missegregation and in some cases higher level of endogenous DNA damage lesions and increased dependence on the DNA repair pathways (Hashimoto et al., 1996; Comai et al., 2000; Andalis et al., 2004; Mayer and Aguilera, 1990; Storchova et al., 2006). If high levels of genome instability can hamper survival and fitness, an increased mutation rate is also able to promote development of new gene functions and adaptive evolution especially in the presence of a sustained selective pressure (Colegrave and Collins, 2008). Theoretical models of adaptive evolution have been developed to determine the conditions of increased adaptive evolution of polyploids versus diploids. The prediction is that polyploids can adapt more rapidly than diploids if the population size is small and if the beneficial mutations that are selected for are at least partially dominant (Otto and Whitton, 2000). This hypothesis has been experimentally verified in yeast (diploids versus haploids; Paquin and Adams, 1983; Zeyl et al., 2003; Anderson et al., 2003; Anderson et al., 2004; Thompson et al., 2006).

1.1.2 Cellular Polyploidy in Normal Physiology

Cellular polyploidy is frequently observed in terminally differentiated and specialized tissues of multicellular organisms from plants (Galbraith et al., 1991), insects (such as gut, epidermis, salivary glands; Smith and Orr-Weaver, 1991) and mammals (Biesterfeld et al., 1994). A common theme is the occurrence of polyploidy in cells that provide nutrients, proteins or nucleotides to support the developing embryo, as it happens in plant endosperm, in nurse and follic-

ular cells in the Drosophila ovary and in trophoblast giant cells of mammalian placenta (Lee et al., 2009). Another common target of polyploidization are tissues specialized in nutrient uptake and storage such as leaves and root hairs in plants and intestinal cells in Drosophila and C. elegans.

In mammals, the conversion from diploidy to polyploidy is part of normal development and differentiation in at least three specialized cell types (Fig. 1.2). A striking case of developmental polyploidization is the placental trophoblast giant cell (TGC), which can reach a DNA content of up to 1000C (Ullah et al., 2009a; Ullah et al., 2009b). TGC polyploidization begins with a differentiation step induced when FGF4 signaling abates. The drop in FGF4 increases the expression of the Cdk inhibitor p57 (Ullah et al., 2008), which, together with a reduction in the translation of Cyclin B (Palazon et al., 1998), blocks Cdk1/CycB-mediated mitosis. The ensuing endocycles appear to involve oscillation of Cdk2/CycE activity and p57 (Hattori et al., 2000), inducing alternating S and G phases. TGCs have lowered amounts of geminin (Gonzalez et al., 2006), which may be a prerequisite for pre-RC formation in these amitotic cycles. Because no mitosis occurs between S-phases, the replicated chromatids are not separated, forming cohesin-linked polytene chromosomes similar to those of Drosophila salivary glands (Ilgren, 1981). The endocycles have been proposed to accelerate TGC growth by shortening the cell cycle and simultaneously increasing the number of chromosomes (Gardner and Davies, 1993; Goncalves et al., 2003).

Figure 1.2: **Examples of developmentally programmed polyploidization.** Three mammalian cell types show prominent polyploidization under physiological conditions: trophoblasts, megakaryocytes and hepatocytes. The schematics show the alterations in the cell cycle that allow polyploidization to occur. Trophoblast giant cells from (Rossant and Cross, 2001); Megakaryocytes from *http* : *//blass.com.au/definitions/* megakaryocyte; Hepatocytes from *http* : *//www.vivo.colostate.edu/hbooks/pathphys/digestion/liver/histocytes.html*. See text for detailed discussion.

Trophoblast giant cells (512N)

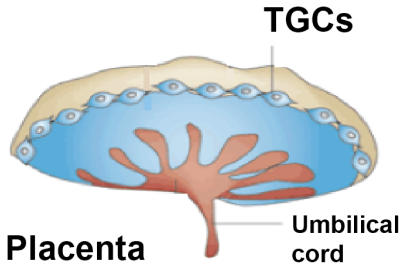

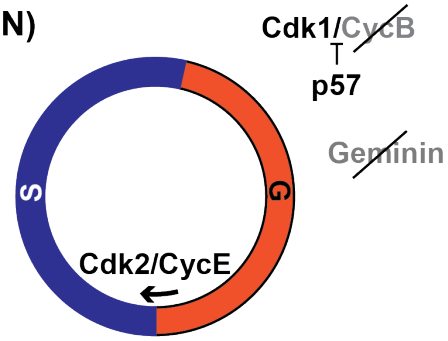

Megakaryocytes (16N-128N)

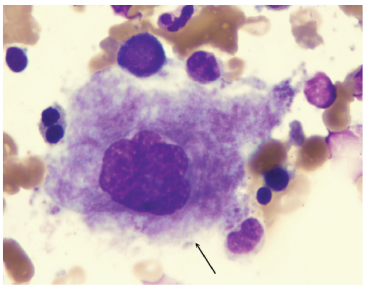

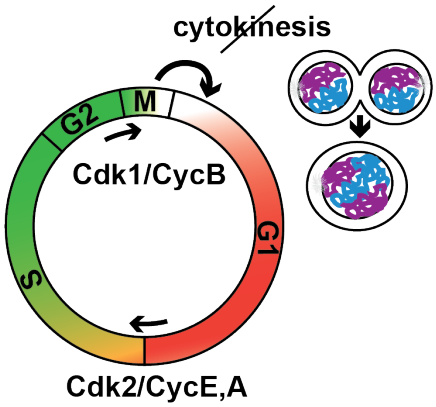

Hepatocytes (4N, 8N)

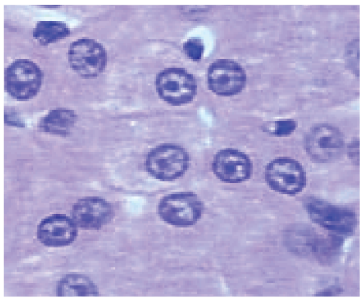

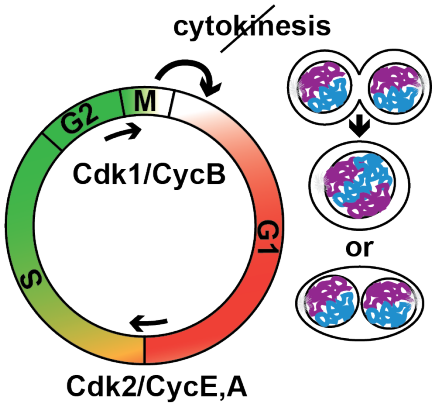

Whereas TGCs skip mitosis altogether, megakaryocytes become polyploid through an abortive mitosis (endomitosis) in which anaphase and telophase can occur but cytokinesis fails (Fig. 1.2). The abortive mitosis appears to be due to suboptimal levels of Cdk1/CycB activity and premature degradation of Cyclin B (Ravid et al., 2002). Although the clusters of duplicated chromosomes temporarily separate and a mid-zone forms, the cleavage furrow regresses and all chromosomes eventually end up in a single nucleus. The resulting cell is in a G1-like state, progresses through S phase, and enters another round of endomitosis, repeating the process several times to form polyploid cells up to 128N (modal ploidy of 16N; Winkelmann et al., 1987).

A third example of polyploidization involving an abortive mitosis is represented by hepatocytes (reviewed in (Celton-Morizur and Desdouets, 2010); Fig. 1.2). During liver growth, there is a progressive increase in the frequency of tetraploid (4N) and octoploid (8N) hepatocytes (Watanabe et al., 1978). These cells often have two 2N (or 4N) nuclei and arise from a failure in cytokinesis, perhaps due to an increase in insulin signaling (Celton-Morizur et al., 2010; Guidotti et al., 2003; Margall-Ducos et al., 2007). Multi-nucleated hepatocytes can also arise from cell-cell fusion (Duncan et al., 2009) and hepatocytes with a single 4N or 8N nucleus readily arise when anaphase is inhibited or telomeres are damaged (Wirth et al., 2006; Lazzerini Denchi et al., 2006). Hepatocytes are particularly prone to increasing their ploidy in response to DNA damage whereas most other cells undergo apoptosis. This attribute may be related to the altered manner in which the hepatocyte p53 pathway responds to DNA lesions (Fei et al., 2002).

A fourth type of polyploidization is seen in skeletal muscle and osteoclasts where cell fusion generates polynucleated terminally-differentiated cells (Yaffe and Feldman, 1965; Vignery, 2000). Polyploidy has also been observed sporadically under physiological conditions in lactating mammary gland, urothelium, mesothelium and Purkinje neurons (Biesterfeld et al., 1994), but how these whole genome duplications arise is less clear.

The benefits of programmed polyploidy are not fully understood. Polyploidy results in a decreased surface to volume ratio for both the whole cell and the nucleus, thereby minimizing membrane requirements but also lowering the efficiency of transport (Henery et al., 1992; Comai, 2005). Polyploid cells, including hepatocytes and placental giant trophoblasts, often serve to provide nutrients and metabolites. It has therefore been proposed that polyploidization increases the metabolic capacity of a tissue, possibly by funneling energy toward gene duplication and protein synthesis, instead of cell division and membrane synthesis (Joubes and Chevalier, 2000; Lee et al., 2009). Although megakaryocytes do not have a nourishing function, they can be similarly viewed as a stockpile of components needed to generate platelets. A 32N megakaryocyte can give rise to about 3,000 platelets (Ravid et al., 2002). Assuming that for every 2-fold ploidy increase, there is an approximately 2-fold increase in volume (Henery et al., 1992), at least 16 diploid megakaryocytes would be necessary to deliver the same number of platelets. Considering the diminished requirement for membrane synthesis in a single 32N cell versus 16 diploid cells, polyploidization of megakaryocytes might be an efficient way to direct membrane synthesis towards the production of platelets and would

avoid the energy expenditure of cell divisions. Recently, it has been proposed that tetraploidization of hepatocytes has the benefit of generating genetic variability. During liver regeneration, tetraploid hepatocytes can undergo a reductive mitosis creating aneuploid daughter cells with a near-diploid chromosome number (Duncan et al., 2010). These aberrant divisions are most likely the consequence of multipolar mitoses generated by supernumerary centrosomes. As the resulting aneuploid cells could carry re-assorted alleles, this genetic variation might increase the chance of resistance to exogenous stress.

1.1.3 Tetraploidization with aging and stress

In several tissues, tetraploid or octoploid cells appear with aging and under pathological conditions. For instance, the incidence of polyploidy increases with age in hepatocytes and vascular smooth muscle cells (Celton-Morizur and Desdouets, 2010; Hixon and Gualberto, 2003) and human fibroblasts and endothelial cells become tetraploid with *in vitro* replicative aging (Wagner et al., 2001; Walen, 2006). An increase in polyploidy is also observed in cardiomyocytes with cardiac overloading, congenital heart disease, and hypertension (Staiger et al., 1975; Adler and Costabel, 1975) and in hepatocytes with oxidative stress or telomere damage (Gorla et al., 2001; Lazzerini Denchi et al., 2006). Furthermore, polyploidization occurs in inflammatory bronchial lesions (Lothschutz et al., 2002) and in wound healing (Oberringer et al., 1999). The mechanisms and consequences of tetraploidization in these pathological settings are largely unknown.

1.2 Maintenance of the diploid mammalian genome

The diploid state of mammalian somatic cells is guarded by control mechanisms that act throughout the cell cycle to prevent the occurrence and/or proliferation of cells with deviant DNA contents (Fig. 1.3). The cyclin-dependent kinases (Cdks) and their cyclin subunits regulate key protein phosphorylation events such that DNA replication and mitosis alternate, driving the cell cycle forward; the initiation of DNA replication is controlled by a system that prevents re-replication; and the integrity of the diploid genome and the correct separation of newly-replicated sister chromatids is ensured by two types of checkpoints (the spindle assembly checkpoint or SAC and the DNA damage checkpoints). These controls are highlighted in Figure 1.3 and discussed briefly below.

Chromosome non-disjunction is prevented by regulatory pathways, generally known as "error correction" pathways, which promote correct kinetochore-microtubule attachments (for review see (Musacchio and Salmon, 2007)). An additional level of control is exerted by the SAC on the cell cycle. The SAC blocks anaphase until all chromosomes have achieved bi-oriented attachment to the mitotic spindle (Fig. 1.3). The dissolution of sister chromatids in anaphase requires activation of the APC/C (anaphase promoting complex/cyclosome, referred to as APC here), a ubiquitin ligase that together with either Cdc20 or Cdh1 targets mitotic proteins for degradation by the proteasome. APC/Cdc20 is inhibited by a signal emanating from unattached kinetochores. Once all

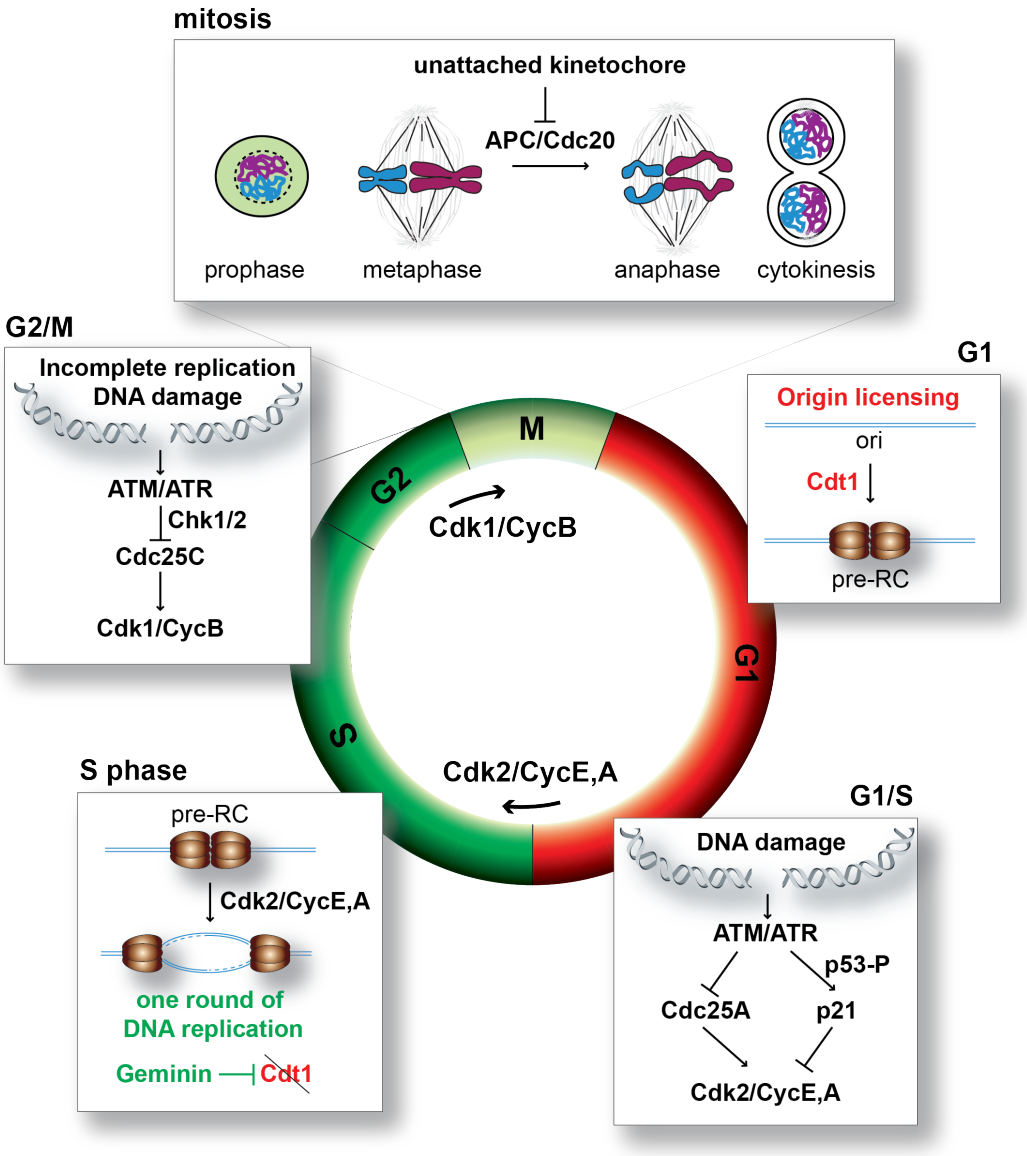

Figure 1.3: **How mammalian somatic cells maintain a diploid genome.** The schematic outlines the normal somatic cell cycle and highlights the three main mechanisms by which the diploid genome is kept intact: assurance of correct chromosome segregation in mitosis; regulation of DNA replication; and the DNA damage checkpoint. See text for detailed discussion.

chromosomes are correctly aligned on the spindle, the SAC is switched-off and APC/Cdc20 becomes active, leading to degradation of securin. With securin gone, separase can cleave the cohesin that holds the sister chromatids together and one copy of each duplicated chromosome is segregated to the daughter cells.

After mitosis, a regulatory pathway controls the initiation of DNA replication such that each sequence is only replicated once in the following S phase (Fig. 1.3; for review see (Remus and Diffley, 2009)). Replication origins are licensed at the end of mitosis and in the beginning of G1 by the formation of the pre-replication complex (pre-RC). The formation of the pre-RC requires Cdt1, which accumulates in G1 and is degraded upon entry into S phase after a ubiquitinylation step that depends on the initiation of DNA replication. In S and G2, origin re-licensing is prevented both by the degradation Cdt1 and the expression of geminin, an inhibitor of Cdt1. This system is reset by the APC/Cdh1-mediated degradation of geminin at the end of mitosis and the rise of Cdt1 in G1. As a result, replication origin licensing is coupled to progression through mitosis.

The integrity of the diploid chromosome complement is monitored by the DNA damage response pathways (for review see (Ciccia and Elledge, 2010)). Two related PI3-kinase-like protein kinases, the ATM and ATR kinases, can initiate a DNA damage checkpoint. The ATM kinase is activated by double-strand DNA breaks (DSBs) whereas ATR responds to pathological single-stranded DNA (ssDNA), including ssDNA generated by DNA replication problems or resection of a DSB. ATM and ATR phosphorylate and activate down-

stream effector kinases (Chk2 and Chk1, respectively), which in turn phosphorylate proteins that enforce cell cycle arrest. Replication of damaged DNA, a potentially deleterious event, is prevented by blocking cell cycle progression into S phase. This is achieved through inactivation of the Cdc25A phosphatase (required for activation of Cdk2) and activation of the p53 pathway (resulting in upregulation of the Cdk inhibitor p21). Because the effect of Cdc25A inactivation is transient, permanent arrest in G1 and induction of senescence and/or apoptosis is absent from p53 deficient mouse cells. In human cells, however, DNA damage also results in upregulation of p16, which can induce a G1 arrest through preventing the phosphorylation of Rb (reviewed in (Gil and Peters, 2006)). In G2, incompletely replicated DNA and broken chromosomes activate the G2/M checkpoint. In this setting, ATM and/or ATR signaling delays entry into mitosis primarily by inactivating Cdc25C, which is needed for the activation of Cdk1/CycB. In p53/Rb-deficient cells, this is the main checkpoint to prevent cell division in the presence of DNA damage. In addition to kinetochores and replication start sites, a third chromosomal element, the telomere (see below) plays a critical role in the stability of the diploid chromosome complement, as it is described below in detail.

1.3 Mammalian telomeres: end-protection and role in cancer

1.3.1 Telomere end-protection

Mammalian telomeres represent the ends of linear chromosomes and are composed of double-stranded (TTAGGG)n tandem repeats, varying in length between 10-15 kb in humans (de Lange et al., 1990; Hastie et al., 1990) to 30-50 kb in laboratory mice (Kipling and Cooke, 1990) and end in a G-rich single stranded 3'overhang (McElligott and Wellinger, 1997; Makarov et al., 1997). Telomeres are maintained by telomerase, comprised of a telomere-specific reverse transcriptase (TERT) and a TTAGGG RNA template (Terc), which together mediate the sequential addition of telomeric repeats (Cong et al., 2002). Telomeres are bound by a six-protein complex called shelterin (Fig. 1.4; Palm and de Lange, 2008). Shelterin is anchored to the telomeres through three DNA binding proteins which specifically recognize telomeric DNA: the single-stranded DNA binding protein POT1 (POT1a and POT1b in the mouse) and the two double-stranded DNA binding proteins TRF1 and TRF2. TRF1 and TRF2 bind duplex telomeric DNA as homodimers through their SANT/Myb domains (Chong et al., 1995; Bilaud et al., 1997; Broccoli et al., 1997; Bianchi et al., 1997). POT1 contains two OB-folds through which it can bind to single-stranded G-rich telomeric sequences (Baumann and Cech, 2001; Lei et al., 2004). The three DNA-binding components in shelterin are bridged by TIN2 and TPP1. TPP1 heterodimerizes with POT1 and mediates its localization at telomeres (Liu et al., 2004; Ye et al., 2004; Hockemeyer et

al., 2007, Kibe et al., 2010). Moreover TPP1 interacts with TERT, and is thought to mediate its recruitment to the telomeres (Xin et al., 2007). TIN2 can bind TRF1, TRF2 and TPP at the same time, bridging the TPP1/POT1 part of the complex to the ds DNA-bound TRF1/TRF2 (Houghtaling et al., 2004; Ye et al., 2004; O'Connor et al., 2006). TIN2 also contributes to TRF2 localization and stability at the telomeres (Ye et al., 2004, Takai et al., 2011). The sixth component of shelterin, Rap1, constitutively binds to TRF2 in a 1:1 stoichiometric ratio, and depends on TRF2 for its telomeric localization and stability (Li et al., 2000; Celli and de Lange, 2005).

In addition to recruitment and regulation of telomerase, the main function of shelterin is to prevent telomeres from being recognized as double-stranded DNA breaks. Inactivation of specific components of the shelterin complex leads to activation of one or multiple branches of the DNA damage signaling and repair pathways. Inactivation of TRF2 results in ATM activation, Chk2 phosphorylation and cell cycle checkpoint activation (Karlseder et al., 1999; Celli and de Lange, 2005; Denchi and de Lange, 2007). The activation of the DNA damage response is evident by the accumulation of phosphorylated histone H2AX and the DNA damage factor 53BP1 specifically at telomeres (Takai et al., 2003). Loss of TRF2 also leads to NHEJ of telomeric ends resulting in chromosome fusions that are incompatible with cell division and survival (van Steensel and de Lange, 1998; Smogorzewska et al., 2002). The mechanisms by which TRF2 inhibits ATM activation and NHEJ at telomeres is not fully understood. The most widely accepted hypothesis is based on the discovery that the 3'overhang can strand invade into the upstream double-

stranded region, forming the t-loop structure and that TRF2 can promote t-loop formation *in vitro* (Griffith et al., 1999; Stansel et al., 2001). The t-loop based model proposes that TRF2 inhibits ATM activation and NHEJ by promoting the formation of the t-loop configuration, which can hide and protect the very end of telomeres. However, this hypothesis requires further testing *in vivo*.

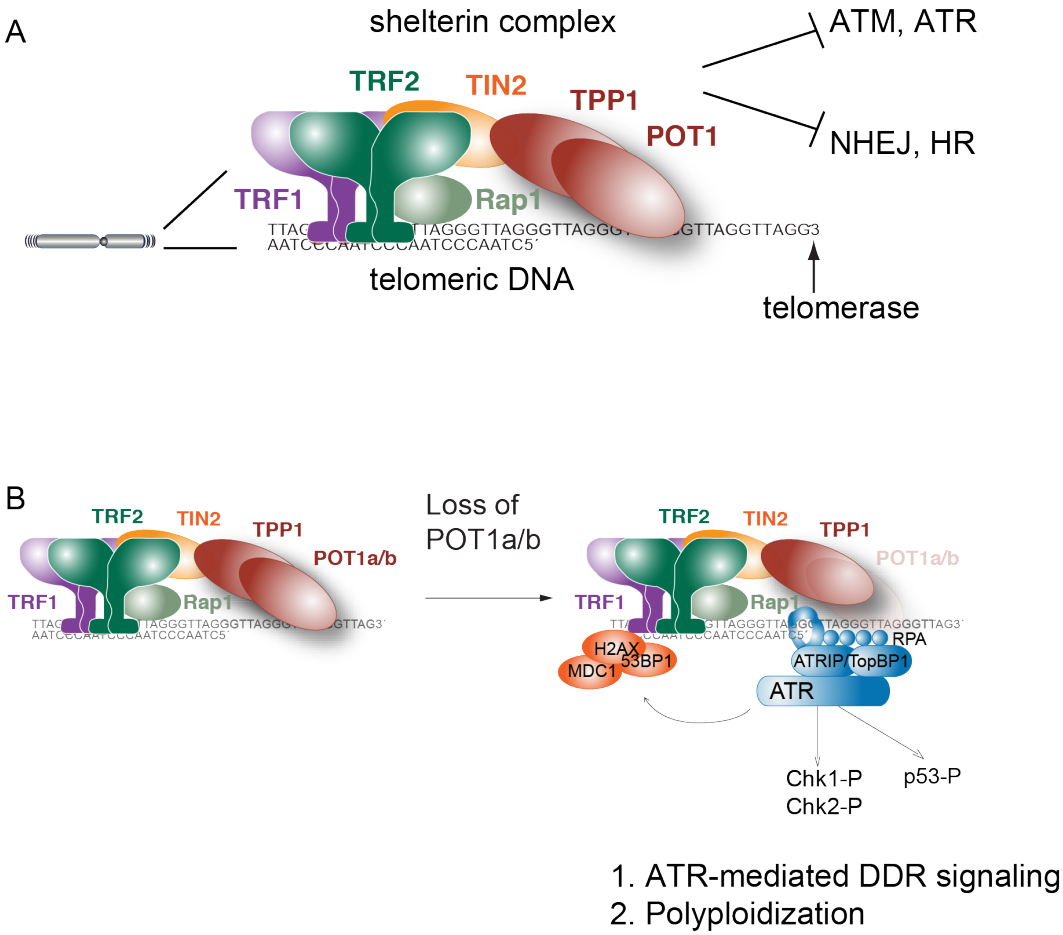

Figure 1.4: **Telomere end protection.** (A) Telomeres are bound to a multiprotein complex called shelterin which prevents the activation of the DNA damage signaling and repair pathways. (B) Deletion of POT1a/b at telomeres results in activation of ATR-dependent DNA damage response at telomeres and polyploidization.

The presence of POT1a (and to some extent POT1b) at the telomeres inhibits the activation of ATR at mouse telomeres (Fig. 1.4 B; Denchi and de Lange, 2007; Gong and de Lange, 2010). In the absence of POT1a/b, telomeres are rendered dysfunctional as judged by the accumulation of 53BP1 and a Chk1-dependent cell cycle checkpoint is induced (Wu et al., 2006 ; Denchi and de Lange, 2007).The prevention of ATR signaling relies mainly on POT1a, while POT1b has an additional independent role in preventing aberrant increase of the telomeric overhang (Hockemeyer et al., 2006). As for the DNA damage repair pathway, deletion of POT1a and POT1b results in a low level of post-replicative telomere fusions (Hockemeyer et al., 2006; Wu et al., 2006). TRF1 also contributes to the inhibition of the ATR pathway at telomeres, but only indirectly, by promoting efficient replication of the telomeric DNA (Sfeir et al., 2009). The homology-directed repair pathway at telomeres is prevented by the general DNA damage factor Ku in combination with POT1 and Rap1 (Wu et al., 2006; Sfeir et al., 2010).

The mechanism of ATR inhibition by POT1a/b is not yet completely clear. The ssDNA binding factor POT1 can bind to the telomeric overhang and to the displaced G-strand of the D-loop present in the t-loop configuration. The presence of POT1a (and POT1b) at the telomeric overhang is thought to prevent the binding of RPA, the first step required for ATR activation (Gong and de Lange, 2010). The low abundance of POT1 as compared to RPA and its comparable *in vitro* binding affinity for telomeric DNA (even in the presence of TPP1) cannot explain the ability of POT1 to prevent RPA binding at the telomeric DNA *in vivo* (Takai et al., 2010; Takai et al., 2011). One way

to explain the RPA exclusion model, is to assume that TIN2/TPP1 tether POT1 to the telomeres, through their binding to the rest of the shelterin. As a consequence, POT1 tethering would increase its local concentration at the telomeres, allowing it to outcompete RPA for telomere binding (Kibe et al., 2010; Takai et al., 2011). Theoretically this hypothesis could be tested *in vivo* by tethering to mammalian telomeres a different factor able to bind mammalian telomeric DNA, in the absence of POT1.

An additional consequence of POT1a/b deletion in mouse cells (when deficient concomitantly for p53 and Rb) is the induction of polyploidization, observed as multiple discrete peaks in the DNA profile (Hockemeyer et al., 2006). The occasional metaphase spreads that can be harvested from POT1a/b deficient cells, show diplo- and quadruplo-chromosomes, i.e. chromosomes composed of four (or eight) chromatids held together at the centromere (Hockemeyer et al., 2006; Kibe et al., 2010). Similar to the loss of POT1, inactivation of TPP1, which is required for localization of POT1 to the telomeres, results in ATR-dependent DNA damage response at telomeres and polyploidization (Kibe et al., 2010). Although TRF2 loss also leads to polyploidization, there is an important difference compared to POT1 inactivation. In the absence of TRF2, chromosome ends readily fuse by NHEJ, while in the absence of POT1a/b, the percentage of chromosome fusions is very low (Celli and de Lange, 2005; Hockemeyer et al., 2006). Therefore, while polyploidy after TRF2 loss can be explained by mitotic failure due to chromosome fusions, the prediction is that in the absence of POT1a/b, polyploidization is mediated by a different mechanism, which does not require the block of mitosis by

chromosome fusions.

1.3.2 Telomere shortening in human somatic cells

In humans and other primates (but not in rodents), telomerase activity is restricted to the germline and some adult stem cell compartments (Shay and Wright, 2005). As a consequence, telomeres of human somatic cells undergo progressive shortening during cellular proliferation, which eventually limits the cells' lifespan (Fig. 1.5; Bodnar et al., 1998; Shay and Wright, 2005). Short telomeres becomes unprotected, can be recognized as sites of DNA damage and normally lead to apoptosis and senescence through activation the p53 and Rb pathways (d'Adda di Fagagna et al., 2003). While in mouse cells, cell cycle arrest (or apoptosis) after telomere dysfunction is primarily mediated by p53 and its target p21, in humans, inhibition of Rb pathway through the induction of the Cdk inhibitor p16INK4a contributes to the induction of the G1/S arrest (Jacobs and de Lange, 2004; Smogorzewska and de Lange, 2002). In the absence of proficient p53 and Rb pathways, human cells do not undergo senescence and prolonged proliferation enhances telomere shortening until extremely short telomeres induce high genome instability and lead to cell death, a stage called telomere crisis (Fig. 1.5; Wright and Shay, 1992; Shay et al., 1993; Shay and Wright, 2005). The reason why short telomeres activate the DNA damage response is still unclear. One possibility is that they are not long enough to recruit a sufficient amount of shelterin factors necessary for the inhibition of ATM and ATR.

Similarly to the context of telomere deprotection after shelterin inactiva-

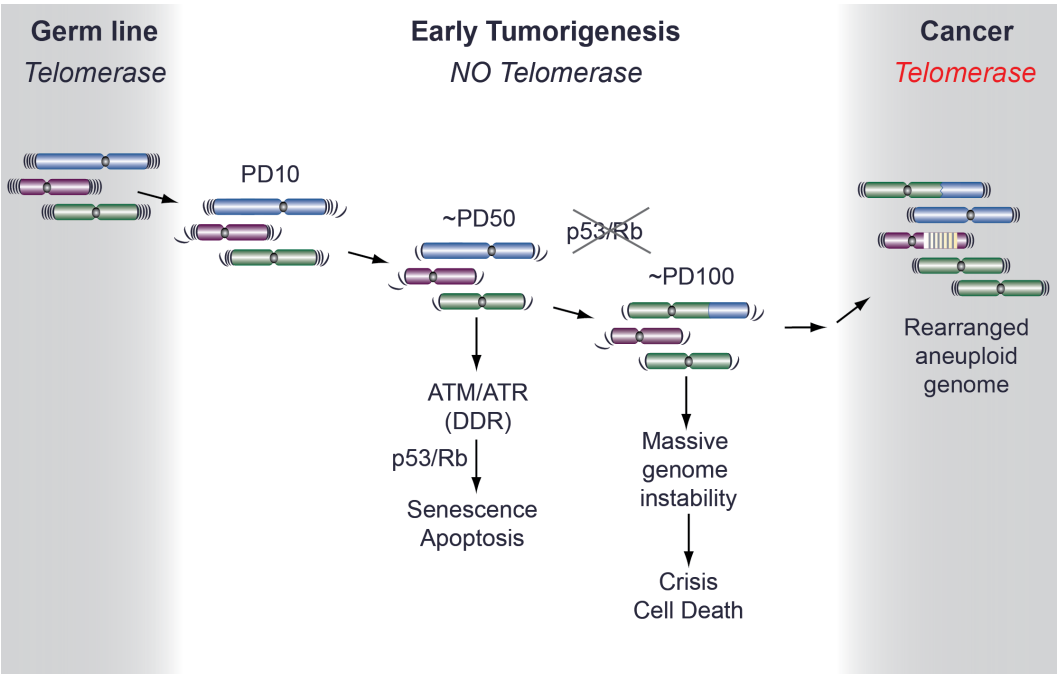

Figure 1.5: **Telomere shortening during tumorigenesis.** Telomere shortening during cellular proliferation of human somatic cells occurs in early tumorigenesis and normally leads to senescence or apoptosis. In the absence of functional p53 and Rb pathways, cells continue to proliferate until telomere crisis. Later in tumor progression telomerase is reactivated allowing immortalization and evolution of the tumor cells. See text for detailed discussion (PD: population doubling).

tion, short telomeres in senescent cells and crisis cells can be processed by the NHEJ pathway, leading to chromosome end-to-end fusion. As Barbara McClintock first recognized in the 1940s, dicentric chromosomes (formed by the terminal fusion of two broken chromosomes) can form anaphase bridges which can in turn break and be rejoined again in the following cell cycle (McClintock, 1941). These Breakage-Fusion-Bridge (BFB) cycles can result in genomic rearrangements and curb cell proliferation. While senescence normally involves a p53/p21 and Rb/p16 mediated permanent arrest in G1/S with minor genomic instability (Benn, 1976; Saksela and Moorhead, 1963), BFB cycles and the resulting chromosome rearrangements are frequently observed in cells in crisis (Shay et al., 1993).

1.3.3 Role of telomere dysfunction during tumorigenesis

Telomere shortening is frequently observed in human tumorigenesis (de Lange et al., 1990; Hastie et al., 1990). Although aberrant reactivation of telomerase in cancer allows healing of telomeric ends, most of the advanced-stage cancers show short telomeres (de Lange et al., 1990; Hastie et al., 1990), which bear witness of the cellular replicative history. Telomere shortening is thought to play a complex role during tumorigenesis. It can function either as a tumor suppressor or as a tumor promoter, depending on the tumor stage and on the integrity of cell cycle checkpoints, mainly the p53 and p16/Rb pathways.

By limiting the lifespan of human somatic cells, telomere shortening represents a tumor suppressor pathway. As a result of sustained proliferation,

telomere shortening is frequently observed in the early pre-invasive stages of human epithelial cancers, such as breast, colon and prostate cancers (Miura et al., 1997; Meeker et al., 2004; Meeker et al., 2002; Zhang et al., 2004a). In more advanced tumors, this barrier to cell survival and proliferation is usually counteracted by telomerase reactivation, which occurs in 80-90% of human cancers (Kim et al., 1994) or by an alternative mechanism of telomere elongation (Lundblad and Blackburn, 1993; Bryan et al., 1995; Bryan et al., 1997). Inhibition of telomerase can impair the viability of human cancer cells, demonstrating that their proliferation relies on telomere maintenance (Hahn et al., 1999). Furthermore, modeling of telomere shortening in the mouse showed that it is able to suppress tumorigenesis in some contexts through the activation of the p53 pathway (Gonzalez-Suarez et al., 2000; Greenberg et al., 1999). Therefore, the combination of telomere shortening and the cell cycle checkpoint pathways represents a barrier to tumorigensis. When the p53 (and Rb in human cells) pathway is impaired the outcome is different. In this context, telomere shortening can promote tumorigenesis and genome instability. Late generation Terc-/- p53-/- or p53+/- mice (deficient for the telomerase RNA component and for p53) show increased tumorigenesis as compared to the telomerase proficient controls (Artandi et al., 2000). Interestingly, telomere shortening can shift the tumor spectrum and the associated karyotype toward the common tumor types of aged humans (Artandi et al., 2000). In Terc-/- p53-/- mice the near-diploid lymphomas and sarcomas commonly observed in p53+/- mice are replaced by epithelial carcinomas with a complex aneuploid karyotype, resembling the karyotype of most human solid tumors (Artandi et

al., 2000). These data indicate that once the checkpoint controls are inactive, prolonged cell proliferation in the presence of very short telomeres can promote tumorigenesis and genome instability (Fig. 1.5). Breakage-fusion-breakage cycles result in gene mutation such as deletions, loss of heterozygosity and amplifications but also in chromosomal rearrangements, especially non-reciprocal translocations and inversions (de Lange, 2005). A large body of evidence suggests that telomere deprotection contributes to genome instability in human cancer. Anaphase bridges are observed in the early cancer stages when telomeres are short and telomerase activity is still undetectable (Rudolph et al., 2001; O'Sullivan et al., 2002; Chin et al., 2004; Finley et al., 2006). Analysis of the telomere length and the nature of the telomeric fusions in tumor samples showed evidence of telomere crisis during the progression of chronic lymphocytic leukemia (Lin et al., 2010). Finally, tumors arising from telomerase competent cells, such as leukemias and some lymphomas usually show very low levels of genome instability (Hilgenfeld et al., 1999; Broccoli et al., 1995).

In the context of telomere-mediated tumorigenesis, it is important to highlight that reactivation of telomerase, which occurs usually in the early invasive lesions, is necessary for the tumor to progress to a full malignant state and metastatic potential (Ding et al., 2012). In terms of genome instability, reactivation of telomerase can limit genomic instability ongoing in early cancerous lesions, stabilizing the cancer genome (Colegrave and Collins, 2008).

1.4 Aneuploidy and tetraploidy in human cancer

1.4.1 Chromosome instability in human cancer

Most human solid tumors are aneuploid. Karyotypic analysis of cancer cell lines has revealed a wide range of chromosome numbers ranging from hypodiploid to hypertetraploid. A substantial fraction of this aneuploidy, in particular the near-diploid chromosome numbers, can be explained from individual chromosome gains and losses due to defects in the segregation of sister chromatids (Fig. 1.6, reviewed in (Holland and Cleveland, 2009). This type of chromosome instability (CIN) leads to one chromosome gain or loss event in approximately five cell divisions (Lengauer et al., 1997). In rare cases, the cause of CIN has been assigned to defects in the SAC, cohesion, or the regulation of kinetochore-microtubule attachment (see for review (Thompson et al., 2010)). Mutations in Adenomatous Polyposis Coli in colon carcinoma can also result in a CIN phenotype (Kaplan et al., 2001; Fodde et al., 2001) and loss of Rb has been shown to cause aneuploidy and could therefore explain CIN in many human cancers (Manning et al., 2010; van Harn et al., 2010; Coschi et al., 2010). Aneupoloidy can also be caused by oncogene-induced replication stress, which has been proposed to occur in many early neoplastic lesions or defect in the DNA damage repair machinery (see for review (Negrini et al., 2010)). In addition, cells with supernumerary centrosomes, formed through a tetraploidization event or deregulation of the centrosome cycle, will often mis-segregate chromosomes due to transient formation of multipolar spindles

(Ganem et al., 2009). Finally, the formation of micronuclei that derive from chromosome missegregation, can result in chromosome pulverization and might explain a recently described process of genomic instability called chromothrypsis (Stephens et al., 2011; Crasta et al., 2012).

An important but under-explored cause of CIN in the early stages of human cancer is telomere dysfunction, as described earlier (reviewed in (de Lange, 2005)). A unique feature of this source of chromosome instability is that it is episodic, ultimately resulting in aneuploid cancer genomes that are stabilized once telomerase has restored telomere function. In this regard, it will be of interest to understand which cancers show ongoing CIN and which have a stable aneuploid chromosome complement.

1.4.2 Evidence for tetraploidization in human cancer

The CIN-type of chromosome mis-segregation does not, however, explain cancers with a triploid or near-tetraploid chromosome number (Fig. 1.6, Fig. 1.7). At the mis-segregation rate of approximately 1 per 5 cell divisions observed in colorectal cancer cell lines, it would require more than 200 PD to generate a clone with close to 90 chromosomes. This number of cell divisions is very high in the context of the etiology of human cancer. In addition, each intermediate in the multi-step CIN pathway would have to be viable.

Data on the distribution of chromosome numbers in human cancer is consistent with the proposal of a second, distinct pathway for tumors with high chromosome numbers. For many tumors, the chromosome numbers are distributed in two peaks, one representing tumors that are near-diploid and one represent-

ing tumors with a chromosome number between triploid and tetraploid genome , see examples in Fig. 1.6). This bimodal distribution argues against a single mechanism underlying aneuploidy. To account for aneuploidy with high chromosome numbers (arbitrarily set at >68 chromosomes in Fig. 1.7), it was proposed that these cancers originate from an unstable tetraploid intermediate (Shackney et al., 1989). As discussed above, tetraploid cells are known to frequently mis-segregate chromosomes due to their supernumerary centrosomes (Ganem et al., 2009). Tetraploid cells will therefore readily generate subclones with the hypo-tetraploid or hyper-triploid chromosome numbers observed in cancer.

Figure 1.6: **Evidence for tetraploidization in cancer.** (A) First reported evidence of polyploidy (Atkin and Richards, 1956) and diplochromosomes (Levan, 1956) in human cancer. (B, C) The bargraphs show the distribution of chromosome numbers in pancreatic carcinoma (B) and in osteosarcoma (C). The data was derived from the Mitelman database ($http://cgap.nci.nih.gov/Chromosomes/Mitelman$). The karyotype of all the pancreatic carcinoma and osteosarcoma tumors in the database were retrieved and used for the frequency distribution shown. For the monoclonal tumors, the average number of chromosomes is given. For multiclonal tumors, if the difference between the chromosome numbers of the clones was less than 10, the average is given. Otherwise, the 2 distinct clones were considered as 2 different karyotypes. Representative karyotype of pancreatic cancer from $http://www.path.cam.ac.uk/index.html$ (Capan-2 cell line); representative karyotype of osteosarcoma tumor from (Scheel et al., 2001).

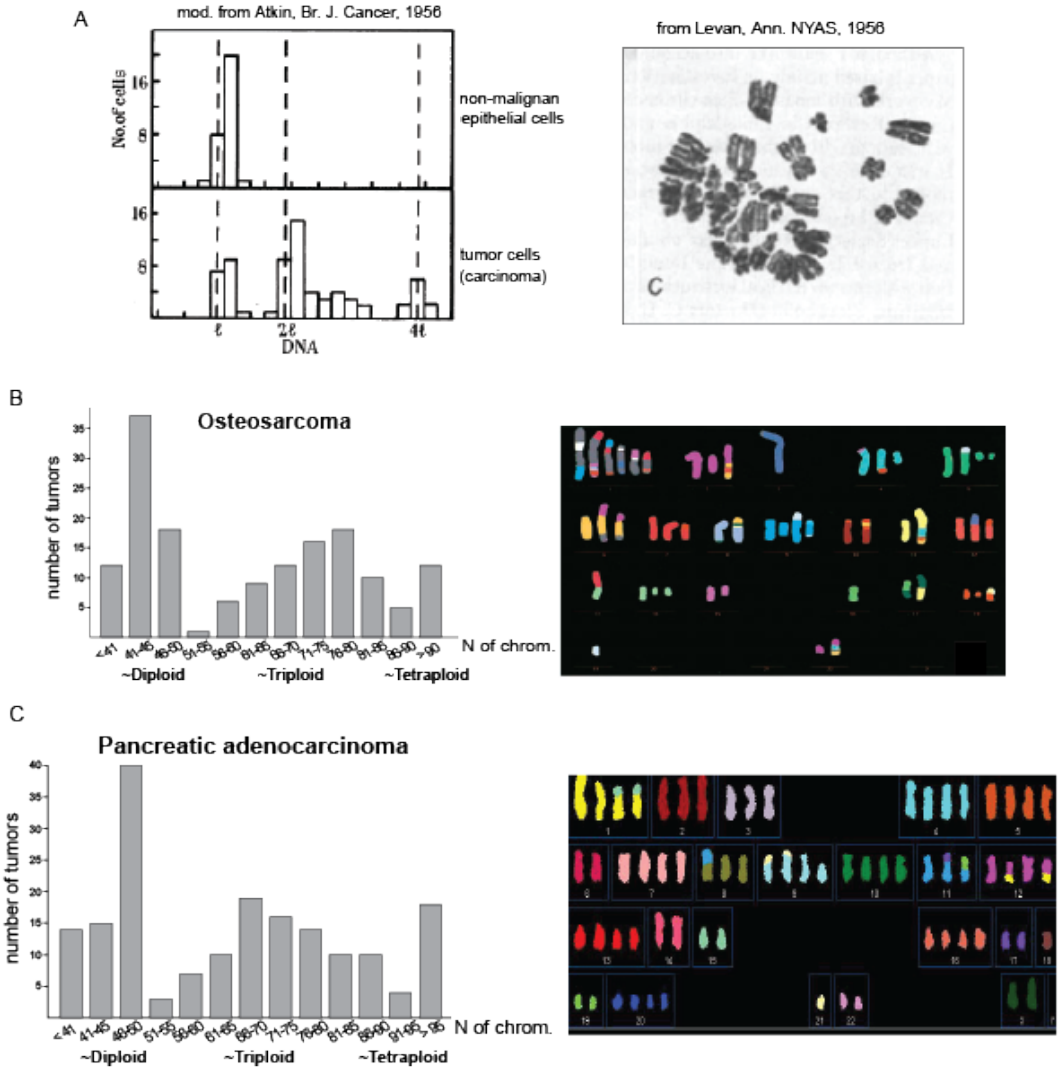
A
mod. from Atkin, Br. J. Cancer, 1956
No.of cells
16
8
16
8
non-malignan epithelial cells
tumor cells (carcinoma)
ℓ
2ℓ
4ℓ
DNA
from Levan, Ann. NYAS, 1956
C
B
Osteosarcoma
number of tumors
N of chrom.
~Diploid
~Triploid
~Tetraploid
C
Pancreatic adenocarcinoma
number of tumors
N of chrom.
~Diploid
~Triploid
~Tetraploid

Consistent with an initial tetraploidization event preceding the final aneuploid state, cells with supernumerary centrosomes have been observed in many tumor types, including breast cancer (Lingle et al., 1998; Ottesen, 2003), pancreatic cancer (Sato et al., 1999), prostate cancer (Pihan et al., 2001), as well as lung and colon carcinoma (Pihan et al., 1998). Multiple centrosomes appear in pre-invasive carcinomas (Lingle et al., 2002; Pihan et al., 2003) and correlate with abnormal multipolar mitosis and chromosomal instability (Lingle et al., 2005). In some tumor types, there is direct evidence for the development of aneuploidy from a transient 4N state. In Barretts esophagus, which predisposes to the development of esophageal adenocarcinoma, tetraploid cells precede the development of further aneuploidy (Galipeau et al., 1996; Reid et al., 1996). The tetraploid state is lost in 1-2 years, consistent with transient tetraploid cells that lose chromosomes at high frequency (Galipeau et al., 1996). Similarly during the evolution of cervical, breast cancer and bladder cancer, there is evidence for whole genome duplication followed by chromosome losses (Kirkland et al., 1967; Olaharski et al., 2006; Dutrillaux et al., 1991; Ottesen, 2003; Shackney et al., 1995b; Shackney et al., 1995a). Tetraploidization also occurs in hyperplastic lesions of the pancreas (Tanaka et al., 1984), in localized prostate cancer (Montgomery et al., 1990; Deitch et al., 1993; Pihan et al., 2001) and some colon adenomas (Hamada et al., 1988; Levine et al., 1991). Collectively, these observations argue that tetraploidization in the early stages of tumorigenesis is not a rare phenomenon.

Tumor type (n)	tumors with >68 chromosomes[a]	Inactivation of p53 pathway[b]	Inactivation of Rb pathway[c]	References
Liver adenocarcinoma (26)	54%	30-60%	40-60%	Martin and Dufour, 2008
Osteosarcoma (143)	42%	40-60%	60-70%	Sandberg and Bridge, 2003
Pancreatic adenocarcinoma (140)	41%	50-75%	80-95%	Maitra and Hruban 2008
Lung adenocarcinoma (160)	36%	40-60%	50-80%	Sekido et al., 2003
Cervical carcinoma (60)	34%	>90%[d]	>90%[d]	Moody and Laimins, 2010
Neuroblastoma (286)	31%	10-30%[e]	5-20%[e]	Brodeur, 2003; Van Maerken et al., 2009
Hodgkin lymphoma (247)	31%	20-50%	10-30%	Bal et al., 2005; Kupper et al., 2009
Prostate adenocarcinoma (220)	28%	20-30%	30-50%	Abate-Shen and Shen, 2000
Skin squamous cell carcinoma (32)	28%	60-80%	30-50%	Pons and Quintanilla, 2006
Soft tissue sarcoma (35)	25%	30-50%	30-60%	Leach et al.,1993; Polsky et al., 2006
Colon adenocarcinoma (345)	24%	60-70%	20-30%	Ruas and Peters, 1998; Fearon, 2010
Ovarian adenocarcinoma (445)	23%	50-70%	30-50%	Bast et al., 2009
Testis Seminoma or Teratoma (230)	23%	10-25%	30-60%	Bartkova et al., 2003
Astrocytoma grade III-IV (545)	22%	30-40%	30-50%	Gladson et al., 2010
Esophageal adenocarcinoma (26)	19%	40-50%	40-60%	Wong et al., 2001; Maley, 2007
Bladder transitional cell carcinoma (160)	17%	30-50%	50-70%	Mitra and Cote, 2009
Breast adenocarcinoma (772)	17%	20-30%	40-50%	Shackney and Silverman, 2003
Kidney carcinoma (1238)	13%	10-30%	10-30%	Aaltomaa 1999; Noon et al., 2010
Malignant melanoma (350)	13%	10-20%	30-50%	Ibrahim and Haluska, 2009
Stomach carcinoma (115)	11%	30-40%	20-30%	Wu et al., 2010

Figure 1.7: **Incidence of hypertriploid karyotypes, inactivation of p53 pathway and Rb pathway.** [a] Based on http://cgap.nci.nih.gov/Chromosomes/Mitelman. For each tumor type, a search of the tumors containing a chromosome number >68 was performed and the % of tumors >68 was calculated. The total number of tumors for each type is indicated (n). [b] Frequency of inactivativation of the p53 pathway, including p53 mutation (databases http://www-p53.iarc.fr/, http://p53.free.fr/index.html and specific references) or LOH and MDM2 amplification (Momand et al., 1998) [c] Frequency of inactivation of the Rb pathway, including mutation, LOH or methylation of Rb, p16, p18 and amplification or overexpression of CyclinD or CDK4/6 genes (Ruas and Peters, 1998; Sharpless and Chin, 2003) [d] In cervical cancer p53 and Rb inactivation are mediated by HPV-E6 and HPV-E7 proteins, respectively (Moody and Laimins, 2010). [e] The frequency of inactivation of p53 and Rb pathway in neuroblastoma is not completely clear since most studies have been performed on cell lines (Brodeur, 2003; Van Maerken et al., 2009).

1.4.3 Causes of tetraploidy in cancer

Two main mechanisms of tetraploidization in cancer have been proposed: cell fusion, failure in cytokinesis or failure in other steps in mitosis (Fig. 1.8). Cell fusion generates a bi-nucleate intermediate that can produce daughter cells with single 4N nuclei in G1. Experimentally induced fusion of primary human fibroblasts has been shown to enhance their *in vitro* transformation with potent oncogenes (Duelli et al., 2007). Cell fusion can be caused by viral infection (see for review (Duelli and Lazebnik, 2007)). For instance, infection with human papilloma virus (HPV), which contributes to the etiology of cervical cancer, has been shown to cause cell fusion (Hu et al., 2009; Gao and Zheng, 2010). The virus that causes cell fusion could also be unrelated to cancer development since the fusion partner could be a non-neoplastic infected cell that donates its chromosomes to a cancerous neighbor.

Several types of failure in progression through, or exit from, mitosis can give rise to a cell with double the chromosome number. Failure in cytokinesis usually generates a transient bi-nucleate state, which will yield mono-nucleated G1 daughter cells with 4N DNA content after the next cell division (Fig. 1.8). This type of tetraploidization is observed upon increased expression of either of two regulators of the anaphase promoting complex, Mad2 and Emi1 (Sotillo et al., 2007; Lehman et al., 2006). Mad2 and Emi1 are overexpressed in a variety of human cancers (Sotillo et al., 2007; Lehman et al., 2007), possibly due to loss of the Rb pathway, which controls their transcription through E2F. Furthermore, Mad2 overexpression might induce tetraploidization through inactivation of MLKP2, a kinesin required for cytokinesis (Lee et al., 2010).

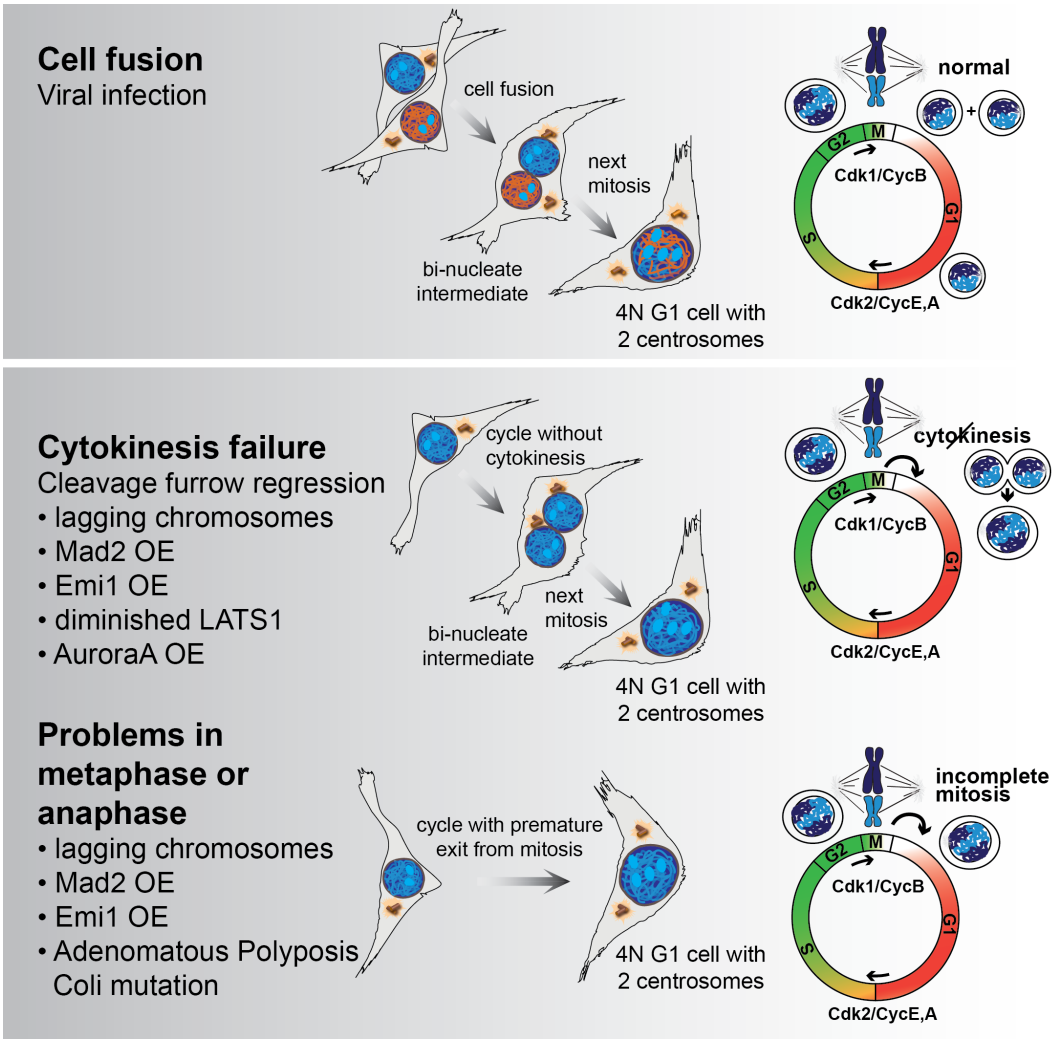

Figure 1.8: **Proposed mechanisms for tetraploidization in cancer.** The schematic shows the main mechanisms by which tetraploidization has been proposed to arise in the early stages of tumorigenesis: cellular fusion, failure in cytokinesis, in metaphase or anaphase. See text for discussion (OE: overexpression).

Cytokinesis failure also occurs upon inhibition of LATS1, a kinase needed for the regulation of actin polymerization in mitosis (Yang et al., 2004). LATS1 is a tumor suppressor in Drosophila and is frequently lost in soft tissues sarcoma (Hisaoka et al., 2002), astrocytoma (Jiang et al., 2006), and breast cancer (Takahashi et al., 2005). Finally, failure in cytokinesis is associated with over-expression of AuroraA, a kinase critical for mitosis (Bischoff et al., 1998; Zhou et al., 1998; Meraldi et al., 2002; Zhang et al., 2004b). High levels of AuroraA, in some cases due to gene amplification, are frequent in cancer (Lehman et al., 2007). In light of these potential causes of cytokinesis failure, it will be of interest to determine whether there is evidence for an initial tetraploidization step in tumors with elevated Mad2/Emi1/AuroraA or defective LATS1.

Cells with lagging chromosomes or acentric fragments can show failure in cytokinesis because the cleavage furrow can regress when there is chromatin in the mid-zone (Mullins and Biesele, 1977). Since a myriad of pathways can result in lagging chromosomes or acentric fragments, many genetic defects could potentially result in a low frequency of tetraploidization through this mechanism.

Problems earlier in mitosis are also likely to be responsible for some tetraploidization events. Interestingly, tetraploidization occurs in cells with defects in the Adenomatous Polyposis Coli, the colon carcinoma gene that is part of the Wnt-signaling pathway (Fodde et al., 2001; Kaplan et al., 2001). This APC protein (distinct from the anaphase promoting complex/cyclosome) binds to microtubules and its absence affects the kinetochore-microtubule interaction in a manner that induces disordered metaphases, lagging chromosomes, and chro-

mosome mis-segregation responsible for CIN in APC-driven colon carcinoma (Kaplan et al., 2001; Fodde et al., 2001; Dikovskaya et al., 2007; Dikovskaya et al., 2004; Caldwell et al., 2007; Draviam et al., 2006). The function of the SAC is not greatly affected by these APC mutations (Radulescu et al., 2010) nor is the SAC strongly activated by the disordered metaphases in APC-mutant cells (Draviam et al., 2006). Whether tetraploidization of APC-mutant cells is a direct consequence of the lagging chromosomes is not yet clear.

1.4.4 Role of p53 in culling tetraploid clones

Tetraploid cells generated by experimentally-induced mitotic failure undergo a p53-dependent arrest (Andreassen et al., 2001; Meraldi et al., 2002; Fujiwara et al., 2005). This activation of the p53 pathway is also thought to occur in other cases of tetraploidization, but the mechanism underlying this phenomenon is not understood. It is unlikely that the p53 pathway is activated by tetraploidy per se or by the presence of extra centrosomes (Uetake and Sluder, 2004; Wong and Stearns, 2005). Although the signal(s) that upregulate p53 remain to be determined, the challenges of navigating mitosis with supernumerary centrosomes make tetraploid cells more prone to sustaining DNA damage, explaining why they proliferate better in the absence of p53 (Ganem et al., 2009). In agreement, the frequency of inactivation of the p53 pathway inactivation and the occurrence of near-tetraploid karyotypes are positively correlated (Fig. 1.7 and Fig. 1.9A).

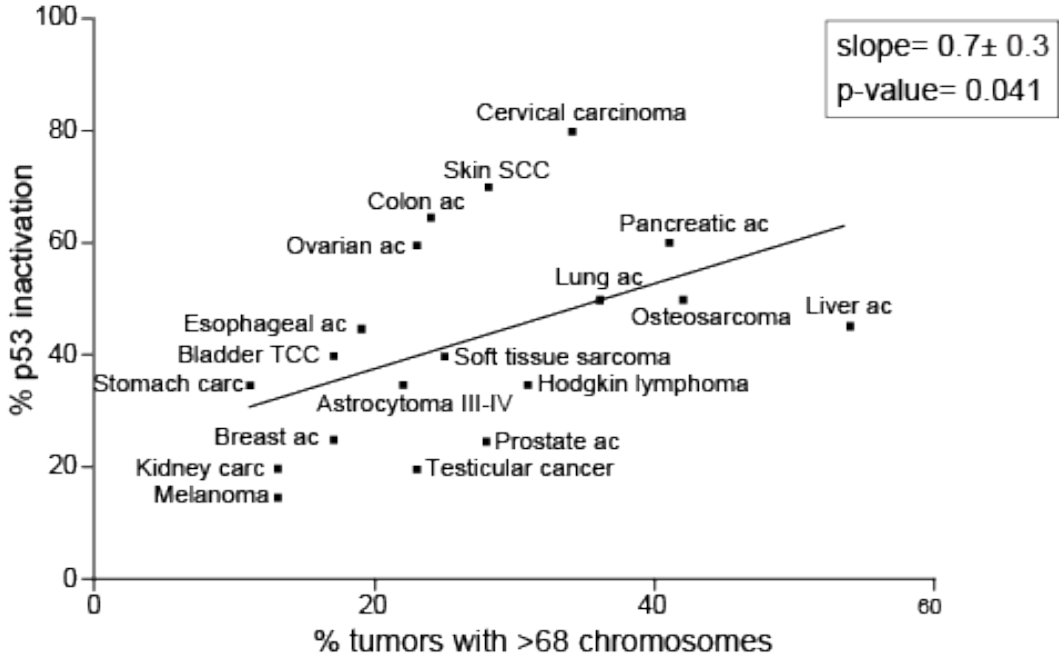

Figure 1.9: **Correlation between the frequency of p53 inactivation and near-tetraploid karyotypes.** The graphs shows the correlation between the frequency of inactivation of the p53 pathway and the percentage of karyotypes with high chromosome number (hypertriploid karyotypes, data from Fig. 1.7) for the indicated cancers. Analysis of linear regression shows significant correlation (slope and p-value are reported, from F-test using Prism-5 software). TCC: transitional cell carcinoma; SCC: squamous cell carcinoma; ac: adenocarcinoma; carc: carcinoma

1.4.5 Consequences of tetraploidy in cancer

The challenge for the incipient cancer cell is to evolve the right combination of genetic alterations that support unbridled proliferation at inappropriate sites. Aneuploidy per se does not confer an advantage in this regard but the re-assortment of mutated alleles in the process leading to aneuploidy does. Tetraploidization and its associated aneuploidy are particularly well-suited to accelerate tumor genome evolution for two reasons. First, tetraploidy is likely to enhance robustness in the face of a mutator phenotype as it will buffer the consequences of chromosome losses, gene deletions, and inactivating mutations. This idea was tested directly by comparing diploid and haploid yeast (Thompson et al., 2006) and is likely to hold for diploid versus tetraploid mammalian cells in which imprinting and haplo-insufficiency render part of the genome functionally haploid. Thus, tetraploidy is expected to allow tumor cells to sustain a higher incidence of mutations thereby increasing the chance of adaptive changes. Second, tetraploid cells have an increased rate of chromosome mis-segregation (Mayer and Aguilera, 1990; Storchova et al., 2006) as a consequence of supernumerary centrosomes and transient multipolar spindles (Ganem et al., 2009, Silkworth et al., 2009). Supernumerary centrosomes can limit the proliferation of newly formed tetraploid cells by inducing multipolar mitoses, which usually result in an unviable progeny. Cells can negotiate these problems through elimination/inactivation of centrosomes or by clustering them in two groups so that a bipolar spindle is formed (reviewed in (Godinho et al., 2009)). In the latter case, a transient multipolar spindle can occur before centrosome clustering, resulting in increased frequency of merotelic kine-

tochore attachments and chromosome missegregation. Centrosome clustering appears to be the dominant route by which (sub-) tetraploid cancer cells avoid multipolar spindles and factors required for this clustering are potential targets for cancer therapy (Kwon et al., 2008). Overall, tetraploidy has the potential to increase the chance that an evolving tumorigenic clone will accumulate and tolerate the mutations needed for its progression to a malignant state.

Finally, as described before, mathematical models predict that polyploids can adapt more rapidly than diploids if the population size is small and if the beneficial mutations that are selected for are at least partially dominant (Otto and Whitton, 2000). From these conclusions we can derive some predictions about the effect of polyploidy during tumorigenesis. Most likely, a polyploid state would be advantageous in bottle-neck phases when the cell population is small due to high selective pressure and low cellular adaptation, as precancerous cell populations, which are usually small at high risk of extinction. Other 'bottleneck' phases during tumorigenesis probably involve the initial steps of metastasis and of relapse after cancer treatment (such as surgery or chemotherapy). Secondly, the prediction is that for tetraploid precancerous cells dominant mutations activating oncogenes will be more advantageous than recessive mutations inactivating tumor suppressor genes.

In this thesis I will describe a new potential mechanism of tetraploidization during tumorigenesis. This mechanism is induced by prolonged telomere dysfunction, both after deletion of POT1a/b in mouse cells and after extensive telomere shortening in human somatic cells during crisis. Persistent telomere damage after deletion of POT1a/b activates the DNA damage re-

sponse signaling pathway and lead to endoreduplication cycles where multiple S-phases occur in the absence of intervening mitotic event. In human cells during telomere crisis tetraploidization occurs through mitotic failure or endocycles. Tetraploid mouse cells derived after transient telomere dysfunction show increased transformation potential *in vitro* and *in vivo*. Finally, we provide evidence of telomere crisis in breast cancer cell lines with an increased chromosome number as compared to near-diploid cell lines.

Chapter 2

Results

2.1 Persistent telomere damage induces bypass of mitosis and tetraploidy

2.1.1 Polyploidy in response to persistent DNA damage signaling

We used previously described SV40 large T antigen (SV40LT) immortalized MEFs carrying conditional alleles for POT1a and POT1b from which both POT1 genes can be deleted with Cre recombinase ($POT1a^{F/-}POT1b^{F/F}$; Hockemeyer et al., 2006). In these POT1a/b double knockout (DKO) cells, SV40LT interferes with the function of p53, which can block polyploidization (Carder et al., 1993; Andreassen et al., 2001; Margolis et al., 2003). As expected, POT1a/b DKO cells showed a DNA damage response as shown by the accumulation of 53BP1 foci and phosphorylation of Chk1 and Chk2 and displayed

polyploidization characterized by FACS profiles with discrete 8N and 16N peaks (Fig. 2.1A-D). The polyploid cell fraction (here defined as the fraction of cells with a DNA content >4N) increases from a basal level of 7-8% to 20-25% at day 4 after introduction of Cre, and to 35-40% at day 6 (Fig. 2.1A, C). Consistent with polyploidization, depletion of the POT1 proteins resulted in cells containing supernumerary centrosomes (Fig. 2.1E).

To determine whether the polyploidy of POT1a/b DKO cells was due to a DNA damage signal, we generated POT1a$^{F/-}$POT1b$^{F/F}$ATM$^{-/-}$ SV40LT-immortalized MEFs and treated the cells with an shRNA to ATR (Denchi and de Lange, 2007; Fig. 2.2A-C). As an ATM/ATR-proficient control, we used littermate-derived, POT1a$^{F/-}$POT1b$^{F/F}$ATM$^{+/-}$ SV40LT immortalized MEFs infected with the shRNA vector. As expected, inhibition of ATM and ATR affected the phosphorylation of Chk1 and Chk2 in response to deletion of POT1a/b (Fig. 2.2B). Importantly, inhibition of ATM and ATR signaling diminished the induction of polyploidy (Fig. 2.2A, C). Consistent with the ATR kinase being primarily responsible for the DNA damage signal in POT1a/b DKO cells, inhibition of ATR alone reduced the fraction of polyploid cells, whereas inhibition of ATM had a lesser effect (Fig. 2.2D, E). Measurement of BrdU incorporation rates indicated that ATR knockdown did not affect DNA replication per se (Fig. 2.2F). Polyploidization in the POT1a/b DKO cells was also diminished by knockdown of Chk1 and Chk2 (Fig. 2.3A-C) or treatment with UCN01 (Fig. 2.3D, E), which inhibits Chk1 and, to lesser extent, Chk2. These data establish that a DNA-damage signaling cascade involving ATM/ATR and Chk1/Chk2 is required for polyploidization in response to

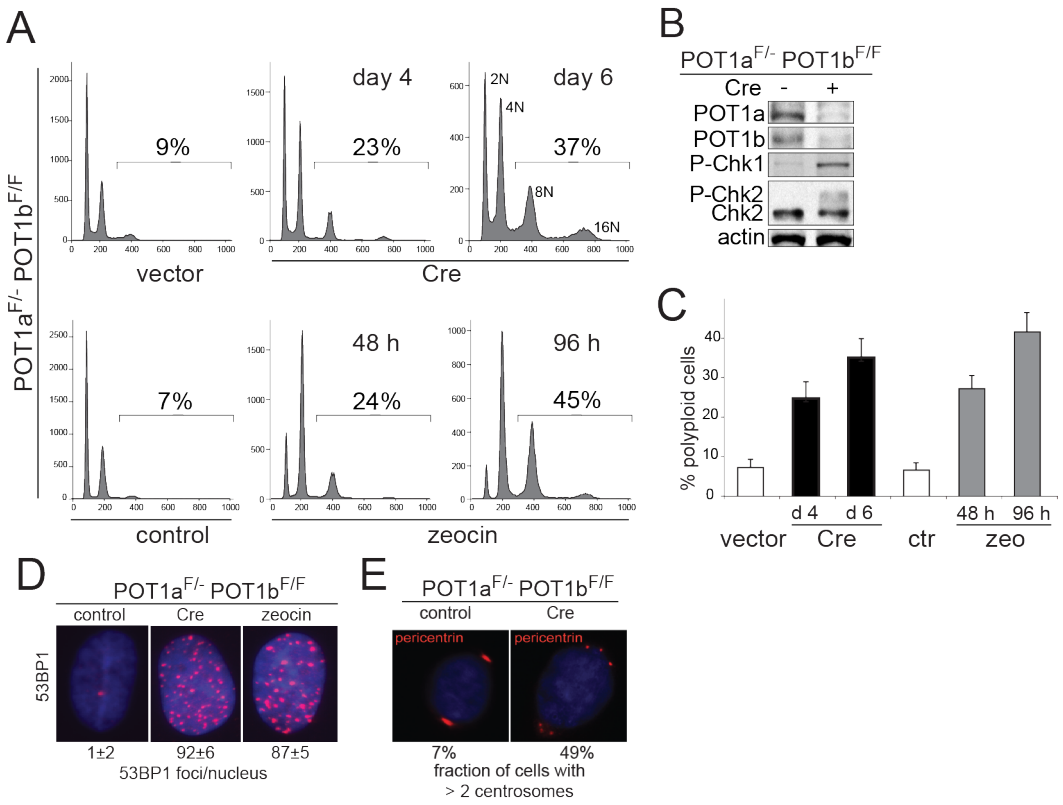

Figure 2.1: **Polyploidy is induced by telomere-specific or genome-wide persistent DNA damage.** (A) Polyploidization upon deletion of POT1a/b or continuous zeocin treatment. POT1a$^{F/-}$POT1b$^{F/F}$ MEFs were treated with Cre, the vector control, zeocin, or left untreated and analyzed by FACS at the indicated time points The % cells with DNA content >4N is given. Representative FACS analyses are shown. (B) Immunoblotting showing POT1a/b deletion and Chk1 and Chk2 phosphorylation in POT1a$^{F/-}$POT1b$^{F/F}$ MEFs after introduction of Cre. (C) Quantification of polyploidy induced by POT1a/b deletion or continuous zeocin. POT1a$^{F/-}$POT1b$^{F/F}$ MEFs were treated and analyzed as in (A). The bars show the average values and SDs of 3 independent experiments. (D) 53BP1 foci in POT1a/b DKO cells and zeocin-treated cells. POT1a$^{F/-}$POT1b$^{F/F}$ MEFs were treated with Cre, zeocin, or left untreated as in (A) and processed for IF for 53BP1 (red; DNA stained with DAPI (blue)). Average 53BP1 foci/nucleus and SEMs are given (n>50). (E) Supernumerary centrosomes in POT1a/b DKO cells. Centrosomes were detected by immunofluorescence for pericentrin in POT1a/b knockout cells and controls (no Cre). The percentage of cells containing more than 2 centrosomes was scored on >50 cells for each group.

telomere dysfunction.

The telomere damage in the POT1a/b DKO cells is unusual because it is not efficiently repaired and therefore elicits a DNA damage signal that persists. Irreparable telomere damage, and an accompanying persistent ATM kinase signal, also occurs when TRF2 is deleted from cells that are NHEJ-deficient due to lack of DNA ligase IV ($Lig4^{-/-}$; Celli and de Lange, 2005). Consistent with the findings in the POT1a/b DKO cells, Cre-mediated deletion of TRF2 from $TRF2^{F/-}Lig4^{-/-}p53^{-/-}$ MEFs induced endoreduplication and diplochromosomes, although the magnitude of the phenotype was less than for POT1a/b DKO cells (Fig. 2.4 A, B).

To further test the idea that polyploidization is induced under conditions where the DNA damage signal persists, we monitored the effects of continuous treatment with the DSB-inducing agent zeocin. As expected, persistent treatment with zeocin induced the accumulation of DNA damage lesions as judged by 53BP1 foci (Fig. 2.1D) and, similarly to the deletion of POT1a/b, the DNA damage appeared similar over several days. After continuous zeocin treatment for 2 or 4 days, MEFs became polyploid, showing a DNA profile characterized by discrete 8N and 16N peaks (Fig. 2.1A). Polyploidy was also induced by treatment of mouse cells with continuous doxorubicin, continuous bleomycin, or repeated UV irradiation (Fig. 2.4C-E). Moreover, tetraploidization occurred in response to activation of ATR by tamoxifen-induced expression of the TopBP1 ATR-activating domain (Fig. 2.4C). Since overexpression of this TopBP1 domain has been shown to activate ATR in the absence of DNA lesions (Toledo et al., 2008), this result argues that the DNA damage signaling

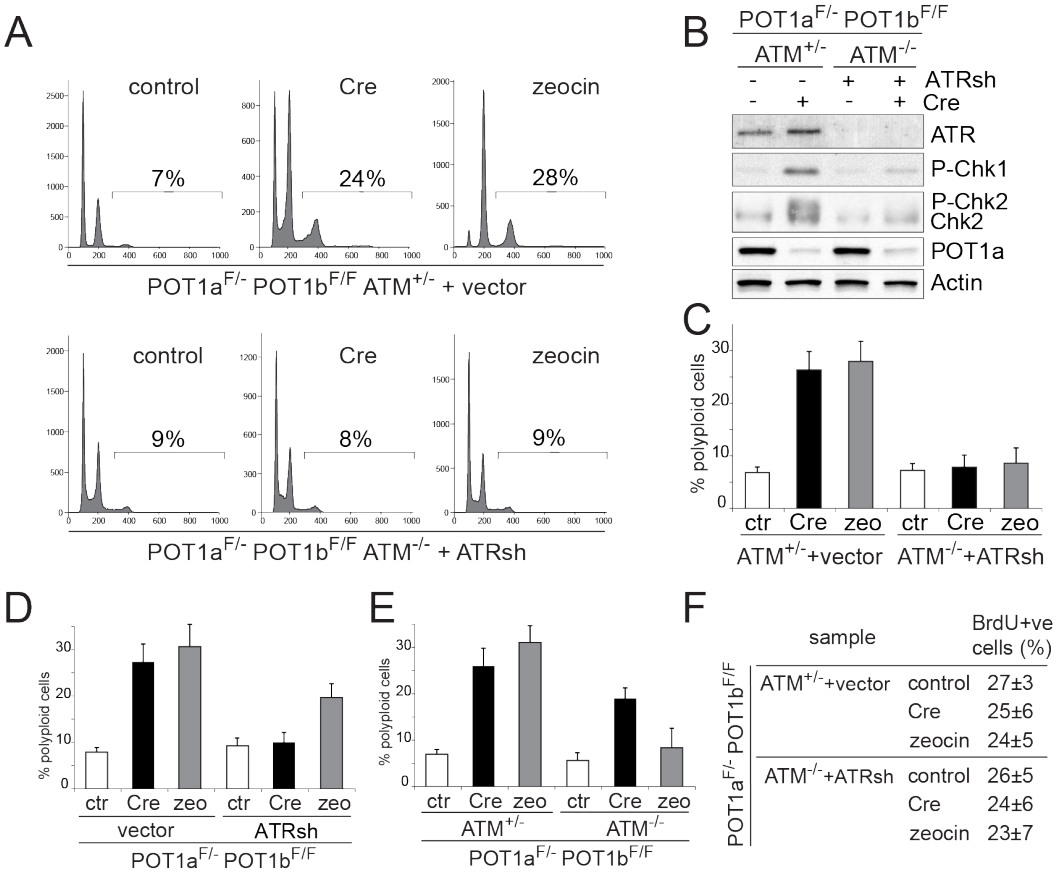

Figure 2.2: **Polyploidization depends on ATR and ATM.** (A, B, C) Diminished polyploidy after inhibition of ATM and ATR. POT1a$^{F/-}$POT1b$^{F/F}$ATM$^{-/-}$ and POT1a$^{F/-}$POT1b$^{F/F}$ATM$^{+/-}$ were treated with ATR shRNA or vector control. Polyploidy was measured as in Fig. 2.1C. FACS profiles from a representative experiment (A) and quantification of the percentage of polyploid cells in 3 independent experiments with SDs (C) are shown. Immunoblotting for ATR, P-Chk1 and Chk2 in the indicated cells is shown in (B). (G) Role of ATR in the induction of polyploidy. POT1a$^{F/-}$POT1b$^{F/F}$ MEFs were treated with ATR shRNA or vector control and polyploidy was measured by FACS after Cre expression (4 days after), zeocin treatment (48 hours after) or in cells left untreated. Quantification of the percentage of polyploid cells in 3 experiments and SDs are shown. (H) Role of ATM in the induction of polyploidy. POT1a$^{F/-}$POT1b$^{F/F}$ATM$^{-/-}$ and POT1a$^{F/-}$POT1b$^{F/F}$ATM$^{+/-}$ MEFs were treated with Cre, zeocin, or left untreated and the percentage of polyploidy was measured by FACS. Quantification of the percentage of polyploid cells in 4 independent experiments with SD is shown. (I)The indicated cells were treated as in (A). Cells were pulsed with BrdU for one hour and the percentage of BrdU positive cells was measured. Average values and SD are shown.

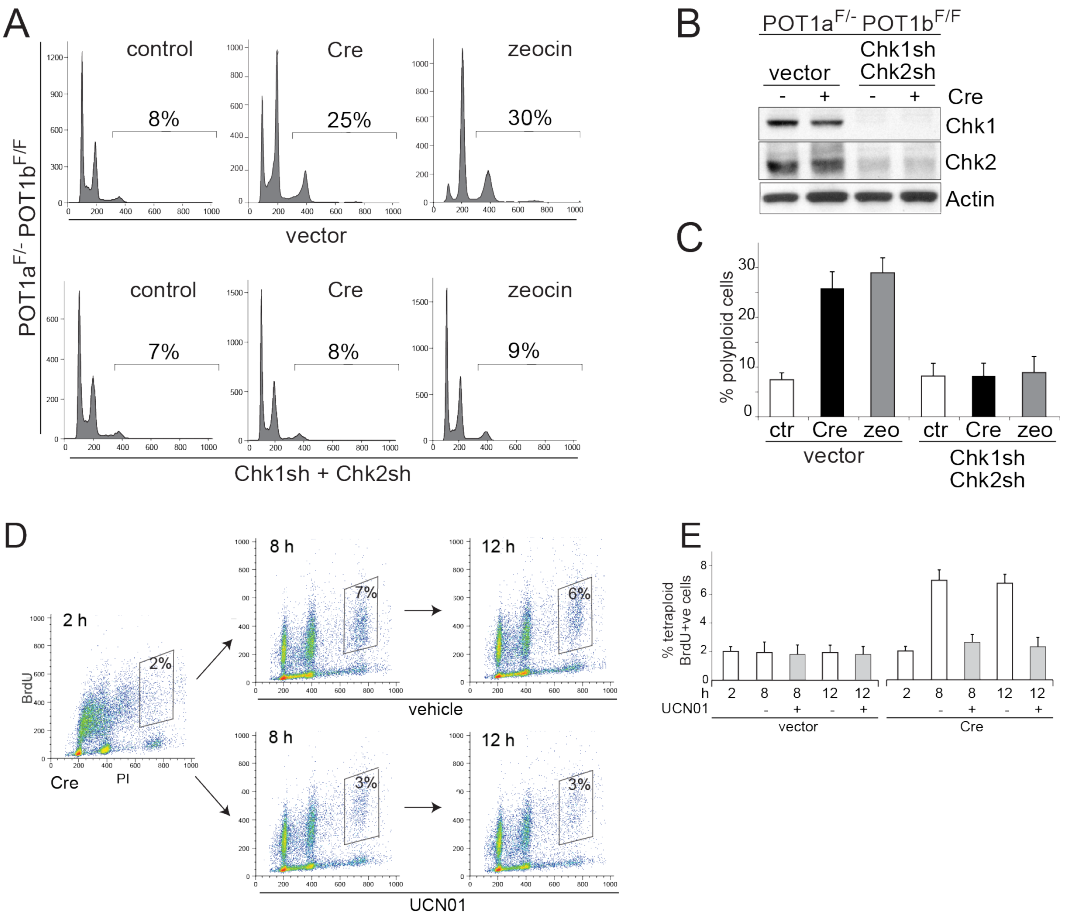

Figure 2.3: **Polyploidization depends on Chk1 and Chk2.** (A, B, C) Diminished polyploidy after impairment of Chk1 and Chk2. POT1a$^{F/-}$POT1b$^{F/F}$ MEFs were treated with Chk1 and Chk2 shRNAs (set 1) or vector control. FACS profiles from a representative experiment (A) and quantification of the percentage of polyploid cells in 3 independent experiments with SD (C) are shown. Immunoblotting showing Chk1 and Chk2 knockdown is in (B). (D, E) UCN01 decreases polyploidization in POT1a/b DKO cells. POT1a$^{F/-}$POT1b$^{F/F}$ MEFs were treated with Cre or vector and after 2 days were synchronized in G1/S by double thymidine block and released. Cells were pulsed for 1 hour (t=0h to t=1h) with BrdU in order to mark a cell population and washed. After 2 hours from release (t=2h) UCN01 (2 μ M) or vehicle was added and FACS was performed at the indicated time points (D). Bargraphs showing the average percentage of tetraploid BrdU-positive cells after treatment with 2 or 5 μM UCN01 are in (E).

rather than DNA damage per se is the primary cause of polyploidization. DNA damage induced polyploidization was not a peculiarity of the mouse cells used for generating telomere damage, as prolonged zeocin treatment of HPV-E6/E7-transformed human BJ fibroblasts also resulted in tetraploidy (Fig. 2.4F, G). Furthermore, the polyploidization was not due to the expression of viral oncoproteins since it also occurred in $p53^{-/-}$ MEFs treated with zeocin (Fig. 2.4H) and in $TRF2^{F/-}Lig4^{-/-}p53^{-/-}$ MEFs treated with Cre (Fig. 2.4A, B). In contrast, primary MEFs and BJ fibroblasts with an intact p53 pathway showed the expected cell cycle arrest in response to DNA damage and polyploidization was absent.

Figure 2.4: **Polyploidy after activation of DNA damage signaling by different sources.** (A) FACS analysis of TRF2$^{F/-}$Lig4$^{-/-}$ SV40 MEFs treated with Cre showing a mild endoreduplication phenotype. (B) Metaphase spread from TRF2$^{F/-}$Lig4$^{-/-}$p53$^{-/-}$ MEFs treated with Cre showing diplochromosomes. DAPI, red; Telomeric FISH, green. (C-E) Induction of polyploidy in mouse cells using various treatments to induce persistent DNA damage. POT1a$^{F/-}$POT1b$^{F/F}$ MEFs were continuously treated with the indicated drugs or with UV (20J2/m every 2 hours for two periods of 12 h with 12 h in between) and the percentage of polyploid cells was measured by FACS at the indicated time points. Alternatively, mouse cells expressing TopBP1-ER (Toledo et al., 2008) were treated or not with OHT for 72 hours. Representative experiments (C) and quantification in two or more independent experiments (E) are shown. Immunoblotting showing phosphorylation of Chk2 after drug treatment at the indicated time points is shown in (D). (F, G) Persistent DNA damage induces polyploidy in human cells. Human BJ fibroblasts expressing HPV E6 and E7 proteins were treated with the indicated drugs and polyploidy was measured by FACS at the indicated time points. Representative experiment (F) and quantification in 3 independent experiments (G) are shown. (H) Absence of p53 is sufficient to allow polyploidization in MEFs. p53$^{-/-}$ MEFs were treated with zeocin and polyploidy was measured by FACS at the indicated time points. Average values from 2 independent experiments with standard error of the mean (SEM) are shown.

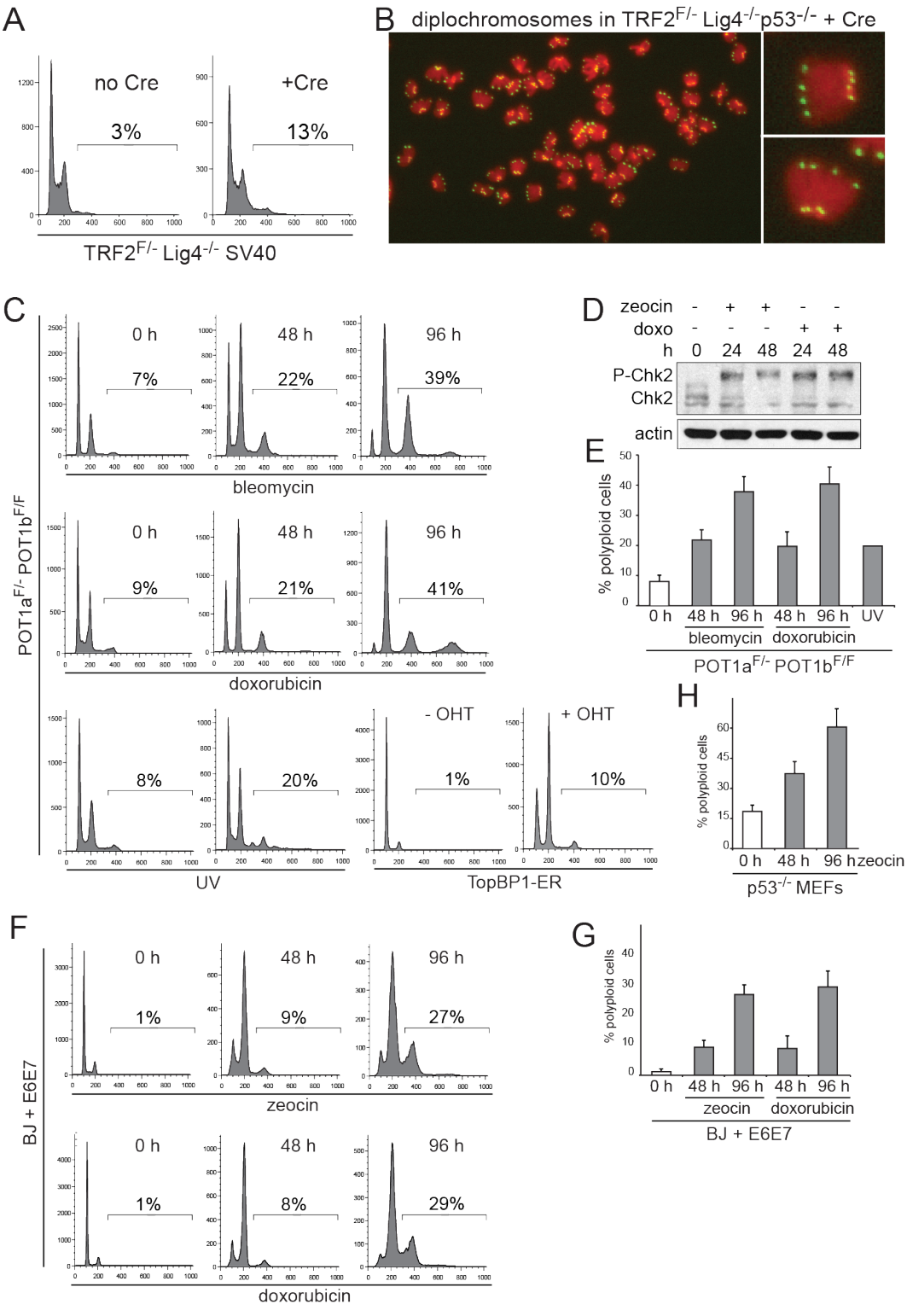
A
no Cre
3%
+Cre
13%
TRF2F/- Lig4-/- SV40
B
diplochromosomes in TRF2F/- Lig4-/-p53-/- + Cre
C
POT1aF/- POT1bF/F
0 h
7%
48 h
22%
96 h
39%
bleomycin
0 h
9%
48 h
21%
96 h
41%
doxorubicin
8%
20%
- OHT
1%
+ OHT
10%
UV
TopBP1-ER
D
zeocin - + + - -
doxo - - - + +
h 0 24 48 24 48
P-Chk2
Chk2
actin
E
% polyploid cells
0 h 48 h 96 h 48 h 96 h UV
bleomycin doxorubicin
POT1aF/- POT1bF/F
H
% polyploid cells
0 h 48 h 96 h zeocin
p53-/- MEFs
F
BJ + E6E7
0 h
1%
48 h
9%
96 h
27%
zeocin
0 h
1%
48 h
8%
96 h
29%
doxorubicin
G
% polyploid cells
0 h 48 h 96 h 48 h 96 h
zeocin doxorubicin
BJ + E6E7

Consistent with the data obtained with POT1a/b DKO cells, the induction of polyploidy by zeocin was strongly impaired when either ATR/ATM or Chk1/Chk2 were inhibited (Fig. 2.2A-F, Fig. 2.3A-C). As expected, the absence of ATM, which transduces the initial response to the DSBs, had a stronger effect than knockdown of ATR (Fig. 2.2D, E). In these experiments and those discussed below, zeocin-treated cells show a more complete depletion of 2N cells and a stronger induction of polyploidization than the POT1a/b DKO cells. This difference could be due to incomplete Cre-mediated deletion of the POT1 genes or may signify a qualitative difference, such as the nature of the DNA damage signal. Collectively, these data established that polyploidy can be induced by a persistent DNA damage signal originating from either deprotected telomeres or DNA lesions elsewhere in the genome.

2.1.2 Lack of Cdk1/CyclinB activation and stabilization of APC/Cdc20 targets

In order to determine the cell cycle alterations giving rise to polyploidization in POT1a/b DKO cells, we analyzed the kinetics of several cell cycle regulated proteins after synchronization in G1/S. Specifically, we determined the status of APC/Cdc20 targets, which are normally degraded during mitosis. Cells were synchronized in G1/S and mitotic APC targets were analyzed after release into S-phase (Fig. 2.5A). Both control and POT1a/b DKO cells entered S phase, as shown by the increase in incorporation of BrdU, although POT1a/b DKO cells progressed into S-phase somewhat slower (Fig. 2.5B). Each of the nine APC targets tested, including securin, were abnormally stabilized in POT1a/b DKO

cells (Fig. 2.5A). Thus, APC/Cdc20-mediated degradation of mitotic targets was defective and/or significantly delayed. In contrast, CyclinE, a target of SCF ubiquitin ligase, was degraded with normal kinetics in POT1a/b DKO cells (Fig. 2.5A).

We next analyzed the activity of Cdk1/CyclinB, which is required for entry into mitosis and contributes to the activation of APC/Cdc20 (Peters, 2002). Cdk1/CyclinB activation can be blocked by ATM/ATR kinase signaling through Chk1/Chk2-mediated inactivation of Cdc25 phosphatases, which removes inhibitory phosphates from Tyr14/15 of Cdk1 (Walworth, 2001). The Cdk1/CyclinB activity in synchronized POT1a/b DKO cells released into S/G2 was ∼4-fold lower than in the control and phosphorylation of Tyr14/15 was increased (Fig. 2.6A-C). Furthermore, the Cdk1/CyclinB kinase activity remained low for at least 6 days after POT1a/b deletion and during 72 hours of zeocin treatment (Fig. 2.6B). In contrast, the Cdk2/CyclinE activity was not obviously altered (Fig. 2.6D). Knockdown of Chk1 and Chk2 in POT1a/b DKO cells resulted in an increase in Cdk1/CyclinB activity and the phosphorylation of Tyr14/15 was diminished (Fig. 2.6C-E). In addition, when Chk1 and Chk2 were knocked down (Fig. 2.6C) or inhibited with UCN01 (Fig. 2.6F), the level of several APC/Cdc20 targets decreased, suggesting that APC/Cdc20 was more active. These data indicate that the activation of Chk1 and Chk2 upon POT1a/b deletion results in a failure in activation of Cdk1/CyclinB and APC/Cdc20-mediated degradation of mitotic targets.

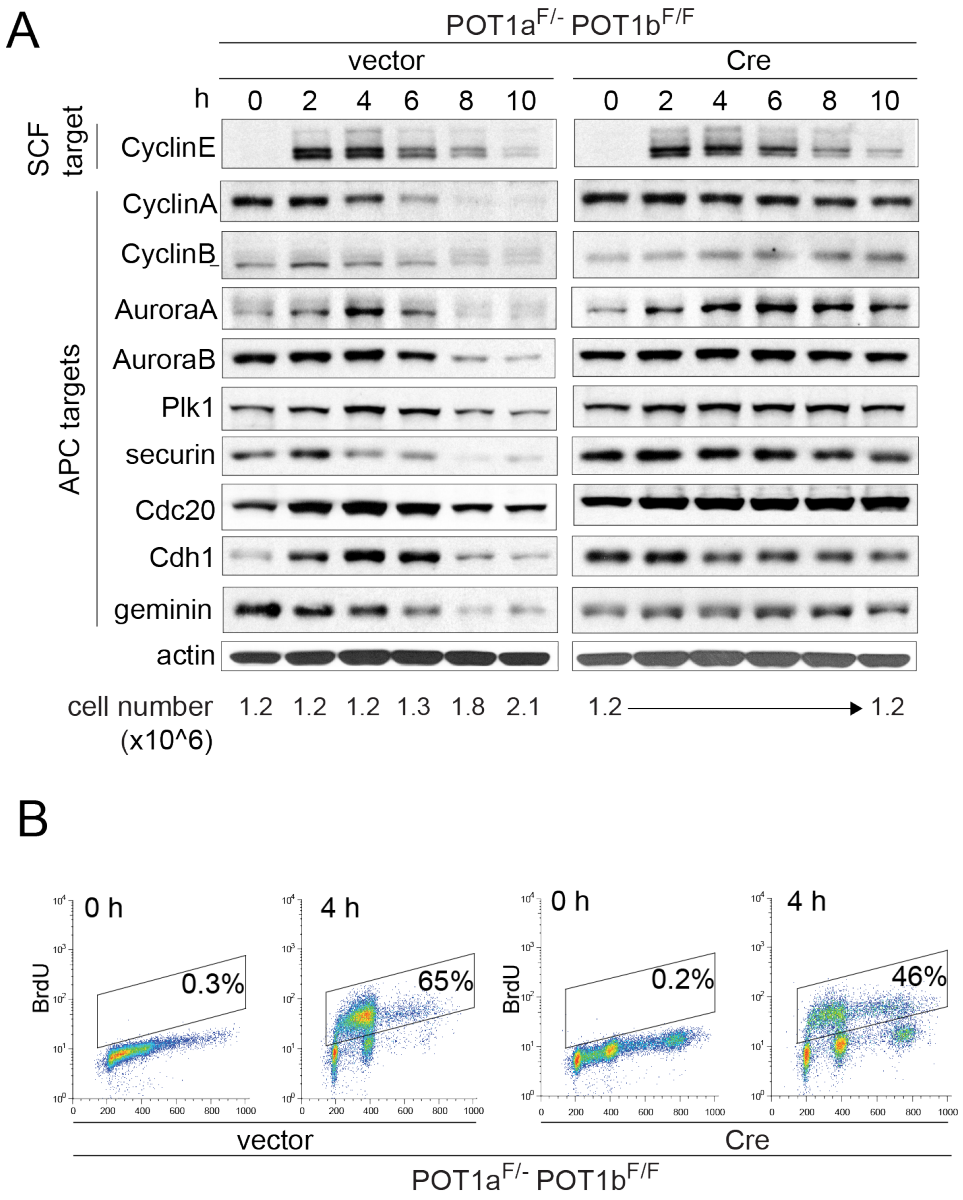

Figure 2.5: **Impaired activity of APC/Cdc20 in POT1a/b DKO cells.** (A) Abnormal stabilization of mitotic APC targets in POT1a/b DKO cells. $POT1a^{F/-}POT1b^{F/F}$ MEFs were treated with Cre and 2 days later synchronized in G1/S by double thymidine block. The indicated proteins were analyzed by immunoblotting and the cell number at the corresponding time points is indicated below the blots. (B) S phase progression of cells used in (A). FACS analysis of BrdU positive cells at 0 and 4 hours after release from double thymidine (G1/S) block.

Figure 2.6: **Impaired activity of Cdk1/CyclinB in POT1a/b DKO cells and zeocin treated cells.** (A, B, D) Reduced Cdk1/CyclinB activity in POT1a/b DKO cells. POT1a$^{F/-}$POT1b$^{F/F}$ MEFs were treated as in Fig. 2.5A and the activity of Cdk1/CyclinB (A) and Cdk2/CyclinE (D) complexes was measured by histone H1-kinase assay. Phopho-histone-H1, Coomassie staining of histone H1, immunoblotting showing Cdk1 (A) and Cdk2 (D) in IPs and quantification of kinase activity are shown. (B) Low Cdk1/CyclinB activity in POT1a/b DKO and zeocin treated cells. POT1aF/- POT1b$^{F/F}$ MEFs were treated with Cre or with continuous zeocin and Cdk1/CyclinB activity was measured at the indicated time points. Phopho-histone-H1, Coomassie staining of histone H1, immunoblotting showing Cdk1 and quantification of kinase activity are shown. (C, E) Impairment in Cdk1/CyclinB and APC/Cdc20 activation in POT1a/b DKO cells is dependent on Chk1 and/or Chk2. POT1a$^{F/-}$POT1b$^{F/F}$ MEFs were treated with Cre and two sets of Chk1 and Chk2 shRNAs. Immunoblotting for the indicated proteins is shown (C). Quantification of Cdk1/CyclinB kinase activity after knockdown of Chk1 and Chk2 (set 1) in two independent experiments is shown (E). (F) Role of Chk1/Chk2 in stabilization of mitotic APC targets. POT1a$^{F/-}$POT1b$^{F/F}$ MEFs were treated as in Fig. 1.1 and immunoblotting for the indicated proteins at the indicated time points is shown.

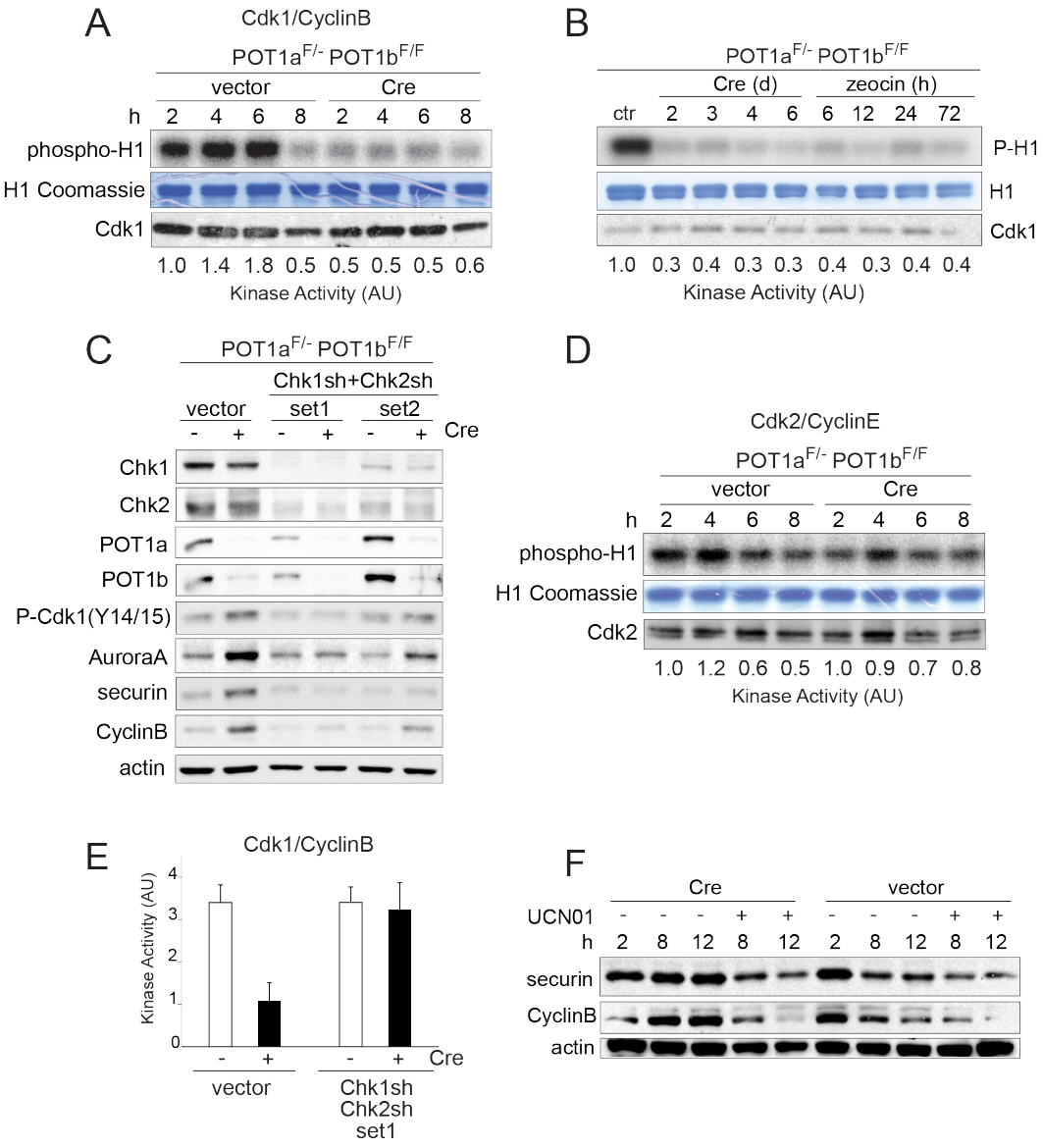
A
Cdk1/CyclinB
POT1a^F/- POT1b^F/F
vector
Cre
h 2 4 6 8 2 4 6 8
phospho-H1
H1 Coomassie
Cdk1
1.0 1.4 1.8 0.5 0.5 0.5 0.5 0.6
Kinase Activity (AU)
B
POT1a^F/- POT1b^F/F
Cre (d)
zeocin (h)
ctr 2 3 4 6 6 12 24 72
P-H1
H1
Cdk1
1.0 0.3 0.4 0.3 0.3 0.4 0.3 0.4 0.4
Kinase Activity (AU)
C
POT1a^F/- POT1b^F/F
Chk1sh+Chk2sh
vector
set1
set2
- + - + - + Cre
Chk1
Chk2
POT1a
POT1b
P-Cdk1(Y14/15)
AuroraA
securin
CyclinB
actin
D
Cdk2/CyclinE
POT1a^F/- POT1b^F/F
vector
Cre
h 2 4 6 8 2 4 6 8
phospho-H1
H1 Coomassie
Cdk2
1.0 1.2 0.6 0.5 1.0 0.9 0.7 0.8
Kinase Activity (AU)
E
Cdk1/CyclinB
Kinase Activity (AU)
0 1 2 3 4
- + - + Cre
vector
Chk1sh
Chk2sh
set1
F
Cre
vector
UCN01 - - - + + - - - + +
h 2 8 12 8 12 2 8 12 8 12
securin
CyclinB
actin

2.1.3 By-pass of mitosis in POT1a/b DKO and zeocin treated cells

To gain further insight into the cell cycle alterations during polyploidization, we used time-lapse live-cell imaging. Asynchronously growing POT1a/b DKO cells and zeocin-treated cells were imaged for two days, acquiring phase-contrast images every 15 minutes. As expected, a fraction of the cells became polyploid during this period whereas control cells divided normally, reaching confluence at the end of the 48 hours imaging period and retaining their diploid DNA content (Fig. 2.7A, B and Movie 1). On average, each cell in the control cultures went through mitosis twice (Fig. 2.7A, C). In contrast, 72% of the POT1a/b DKO cells and 86% of the zeocin-treated cells did not divide during the imaging period (Fig. 2.7A, C, Movie 1). Furthermore neither the POT1a/b DKO cells, nor the zeocin-treated cells showed signs of entering mitosis such as nuclear envelope breakdown and chromosome condensation (Fig. 2.7A, Movie 1). In comparison with control cells, POT1a/b DKO and zeocin-treated cells became larger and more flattened, displaying a senescent-like phenotype. The POT1a/b DKO cells and zeocin-treated cells showed a ∼2-fold increase in the nuclear area ($p<0.001$; Fig. 2.7D), consistent with the increase in their DNA content. We also monitored cells expressing a CyclinE-eGFP fusion in the POT1a/b DKO and zeocin-treated cells (Fig. 2.7C, Movie 2). Although the CyclinE-eGFP signals were hard to discern, ∼35% of the cells showed clear evidence of two waves of CyclinE-eGFP without intervening mitosis over a period of 48 hours. These experiments and the FUCCI imaging data presented below indicated that POT1a/b DKO and zeocin-treated cells frequently fail

to enter mitosis under conditions that induce polyploidization.

Figure 2.7: **By-pass of mitosis in POT1a/b DKO and zeocin treated cells.** (A) Time-lapse imaging of POT1a$^{F/-}$POT1b$^{F/F}$ MEFs treated with Cre, cells treated with zeocin, and the untreated controls. After 72 hours, phase contrast microscope images were taken every 15 minutes for 48 hours (Movie 1). Selected time points stills are shown. Arrows of the same color highlight the same cell over the course of the imaging session. In POT1a/b DKO and zeocin-treated cells, arrows highlight representative cells not undergoing mitosis. (B) FACS profiles of cells used in the live-cell imaging shown in (A) at the beginning (t =0h) and at the end (t = 48h) of the imaging session. Percentage of polyploid cells is shown. (C) Quantification of cells not undergoing mitosis and the average number of mitoses per cell. Cells were treated and imaged as in (A) and the movies were analyzed for the % of cells not undergoing mitosis. Cells expressing CyclinE-eGFP were also analyzed by time lapse as in (A) (Movie 2) and the percentage of cells showing CyclinE rising twice without an intervening mitosis in 48 hours is shown. At least 100 cells in each movie were analyzed for each condition. Average values and SDs were obtained from 3 independent experiments. (D) Increased nuclear area of POT1a/b DKO and zeocin treated cells. Cells were treated and imaged as in (A). For each condition, the nuclear area of 100 cells was measured at the beginning (0 h) and at the end (48 h) of the imaging session and displayed as a frequency distribution. P values based on non-parametric Krustal-Wallis test.

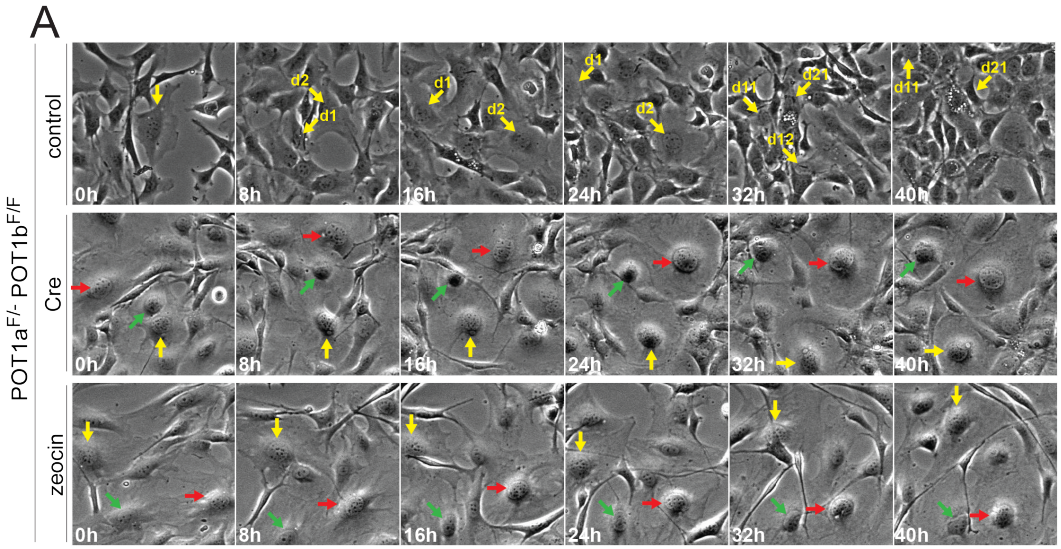

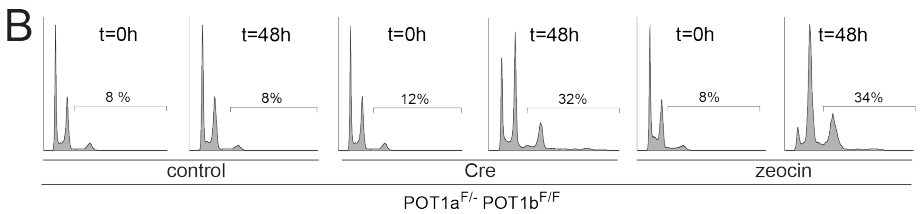

C

	% cells not going through mitosis	number of mitosis per cell	% cells showing CyclinE rising twice without mitosis
control (n≥100)	2±1	2.1±0.3	1±0.5
POT1a/b DKO (n≥100)	72±7	0.3±0.1	34±6
zeocin (n≥100)	86±5	0.1±0.05	36±5

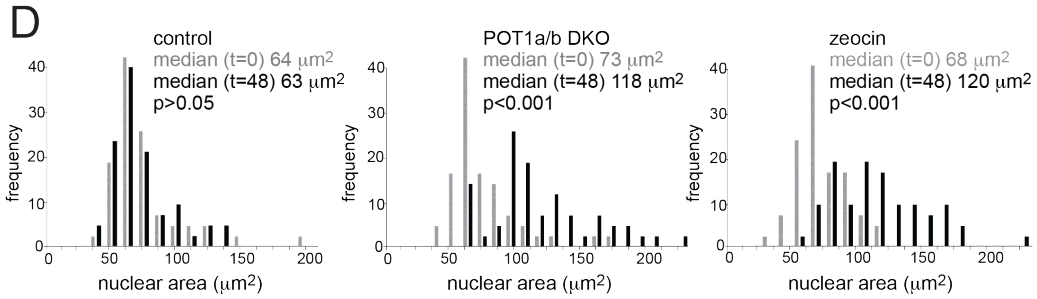

2.1.4 Alternating geminin and Cdt1 expression without mitosis

The ability of POT1a/b DKO cells to enter S phase without progression through mitosis was unexpected as the initiation of DNA replication requires degradation of the DNA replication inhibitor geminin (Blow and Dutta, 2005). In S/G2 geminin is present and inhibits re-licensing of replication origins by Cdt1. Geminin is degraded at the end of mitosis, allowing Cdt1, which rises in G1, to license replication origins. Once DNA replication is initiated, Cdt1 is degraded by SCF. This alternating expression of Cdt1 and geminin expression ensures that cells execute only one round of DNA replication per cell division cycle, a rule that is broken in the endoreduplicating cells.

To examine the fluctuations of geminin and Cdt1 in POT1a/b DKO and zeocin-treated cells, we used the FUCCI (Fluorescent Ubiquitination-based Cell Cycle Indicator) live-cell imaging system (Sakaue-Sawano et al., 2008). FUCCI imaging relies on fluorescently-tagged, truncated forms of geminin and Cdt1 (green and red, respectively) that recapitulate the degradation of the endogenous proteins. Normally cycling cells are red in G1, reflecting Cdt1 expression, become yellow upon entry into S phase when geminin begins to accumulate before Cdt1 is degraded and then are green throughout S phase and G2, due to the presence of geminin. Geminin is degraded at the end of mitosis and upon entry into G1, resulting in a brief period without either marker in early G1 before Cdt1 rises again. This sequence of events was observed in POT1a$^{F/-}$POT1b$^{F/F}$ cells not treated with Cre, showing G1 (red, $\sim$12 h), beginning of S phase (yellow, $\sim$1 h), S/G2 (green, $\sim$6 h), and disappearance

of geminin during mitosis (Fig. 2.8, Fig. 2.9A, B and Movie 3). Cre-treated POT1a/b DKO cells showed a similar Cdt1-positive G1 phase of 12-14 h, but then showed a prolonged geminin-positive S/G2 phase (∼20 h; Fig. 2.8, Fig. 2.9A, B). Importantly, S/G2 was followed by loss of geminin without mitosis, suggesting that cells returned to a G1-like state (Fig. 2.8, Fig. 2.9A, B and Movie 3). Cdt1 was undetectable until geminin was degraded but then increased over the next 12-14 h. Eventually, the POT1a/b DKO cells attained features of early S-phase, expressing both geminin and Cdt1, followed by a second period of geminin expression without Cdt1 (Fig. 2.8, Fig. 2.9B and Movie 3). Thus, the endoreduplicating POT1a/b DKO cells showed a much slower cell cycle but preserved the alternating geminin and Cdt1 expression despite the absence of mitosis.

Figure 2.8: **Geminin and Cdt1 alternate in POT1a/b DKO and zeocin treated cells.** FUCCI imaging of geminin and Cdt1. Time lapse imaging of $POT1a^{F/-}POT1b^{F/F}$ MEFs transduced with FUCCI lentiviral vectors, expressing mKO2-hCdt1 (red) and mAG-hgeminin (green). Cells were treated with Cre or vector control and imaged after 72 h. Alternatively, cells were treated with zeocin during the imaging time. Phase contrast images and fluorescent images using GFP and rhodamine filters were taken every 15 min (Movie 3). Selected time points are shown. Arrows with the same orientation highlight the same cell at different times. In control cells, arrows highlight one cell progressing through a normal cell cycle (red-yellow-green, mitosis) and its daughters until they move out of the field. In Cre-treated cells, arrows highlight two representative cells showing the color sequence red-yellow-green-red-yellow-green without intervening mitotis.

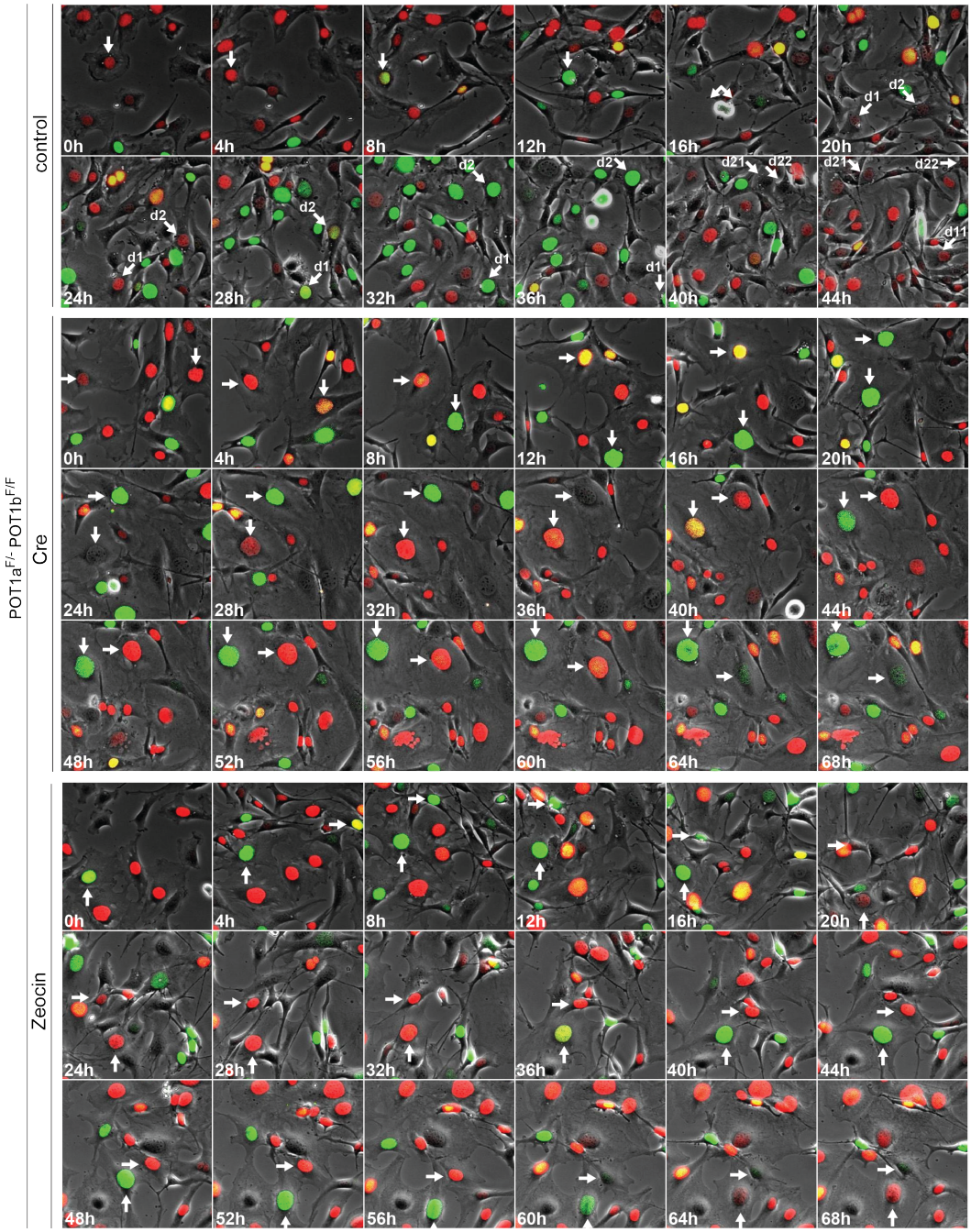
POT1a$^{F/-}$ POT1b$^{F/F}$
control
Cre
Zeocin
0h
4h
8h
12h
16h
20h
24h
28h
32h
36h
40h
44h
48h
52h
56h
60h
64h
68h
d1
d2
d11
d21
d22

The same prolonged S/G2 and mitosis-independent alternation of geminin and Cdt1 was observed with cells continuously treated with zeocin (Fig. 2.8, Fig. 2.9A, B and Movie 3). The aberrant cell cycle patterns were observed in ∼70% of the POT1a/b DKO cells and ∼83% of zeocin-treated cells compared to 1% of the controls (Fig. 2.9A). In addition, FUCCI imaging showed that zeocin treatment induced mitosis-independent geminin degradation in human BJ fibroblasts overexpressing HPV-E6/E7 or SV40-LT (Fig. 2.9C and Movie 4). During persistent treatment with zeocin, BJ cells showed an increase in mitosis-independent geminin degradation and proceeded into a second G1 phase as compared to the untreated control cells displayed a normal mitotic cycle.

Degradation of geminin without progression through mitosis and reappearance of Cdt1 was also observed in cells that were first synchronized in G1 and then allowed to progress through G1/S/G2 in the presence of zeocin (Fig. 2.10A, Movie 5). Immunoblotting of G1/S-synchronized zeocin-treated cells and POT1a/b DKO cells showed that the FUCCI system faithfully reported on the rise and fall of the endogenous Cdt1 and geminin (Fig. 2.10B, C). Data from FACS analysis was consistent with a prolonged G2 phase followed by entry into S-phase (Fig. 2.10D, E). Furthermore, zeocin-treated cells and POT1a/b DKO cells showed degradation of the APC targets CyclinA, CyclinB, and securin (Fig. 2.10B, C). However, the cohesin subunit Scc1 was stable, consistent with the occasional observation of metaphases with diplochromosomes in which the original cohesion of the sister chromatid is preserved (Hockemeyer et al., 2006). These data establish that persistent telomere-

A

	% cells showing geminin degradation without mitosis
control (n≥100)	2±1
POT1a/b DKO (n≥100)	70±7
zeocin (n≥100)	83±5

C

	% cells showing geminin degradation without mitosis
BJ E6E7 control (n≥100)	3±1
BJ E6E7+ zeocin (n≥100)	68±11

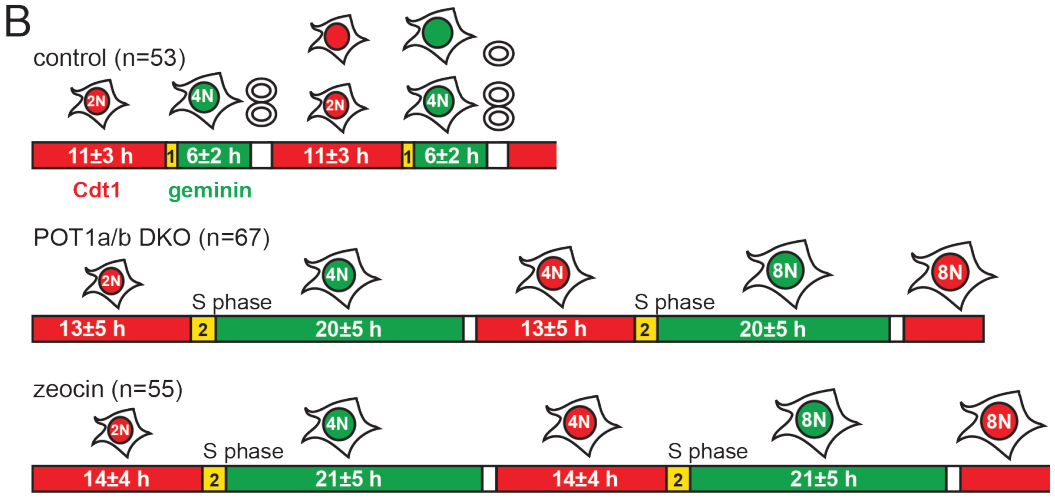

Figure 2.9: **Geminin and Cdt1 alternate in POT1a/b DKO and zeocin treated mouse and human cells.** (A) Quantification of geminin degradation in the absence of mitosis. POT1a$^{F/-}$POT1b$^{F/F}$ MEFs treated with vector control, Cre, (POT1a/b DKO) or zeocin (Movie 3) were imaged as in Fig. 2.8 and the movies were analyzed for cells showing at least one event of geminin degradation in the absence of mitosis. >100 cells were scored for each condition. Average values and SDs were obtained from 4 independent experiments. (B) Duration of alternating geminin and Cdt1 expression in endoreduplicating cells. Cells were treated and imaged as in Fig. 2.8. The indicated number of cells was followed throughout the imaging session and the length of G1 (red), entry into S phase (yellow) and S/G2 (green) was measured. Average values (h) are shown. (C) Geminin degradation in the absence of mitosis in BJ cells treated with zeocin. BJ cells were transduced with FUCCI lentiviral vectors and imaged in the absence (control) or presence of zeocin for 96 hours. The percentage of cells showing at least one event of geminin degradation in the absence of mitosis during the imaging was analyzed by scoring at least 100 cells for each condition.

derived or genome-wide DNA damage signaling induces a prolonged S/G2 after which geminin is degraded without progression through mitosis, allowing reduplication of the whole genome.

Figure 2.10: **Fluctuations of geminin, Cdt1 and other proteins in endoreduplicating cells.** (A) FUCCI imaging of synchronized cells. POT1a$^{F/-}$POT1b$^{F/F}$ MEFs expressing FUCCI vectors were synchronized in G1 by mitotic shake-off and were imaged for 72 hours in the presence or absence of zeocin, Imaging was started 10 hours after the mitotic cells were plated. Selected time points (every 6 hours) are shown from a representative experiment (Movie 5). (B) Analysis of the indicated cell cycle regulated proteins over time in zeocin treated cells. POT1a$^{F/-}$POT1b$^{F/F}$ MEFs were synchronized in G1/S by double thymidine block and released in the presence of zeocin. Immunoblotting for the indicated proteins at the indicated time points is shown. (C) Analysis of the indicated cell cycle regulated proteins in POT1a/b DKO cells. POT1a$^{F/-}$POT1b$^{F/F}$ MEFs were treated with Cre, synchronized in G1/S by double thymidine block and released. Immunoblotting for the indicated proteins is shown. (D) FACS analysis of cells treated as in (B). FACS analysis at the indicated time points is shown and the percentage of polyploid cells is indicated. (E) POT1a$^{F/-}$POT1b$^{F/F}$ MEFs were treated as in (C). FACS analysis at the indicated time points is shown and the percentage of polyploid cells is shown.

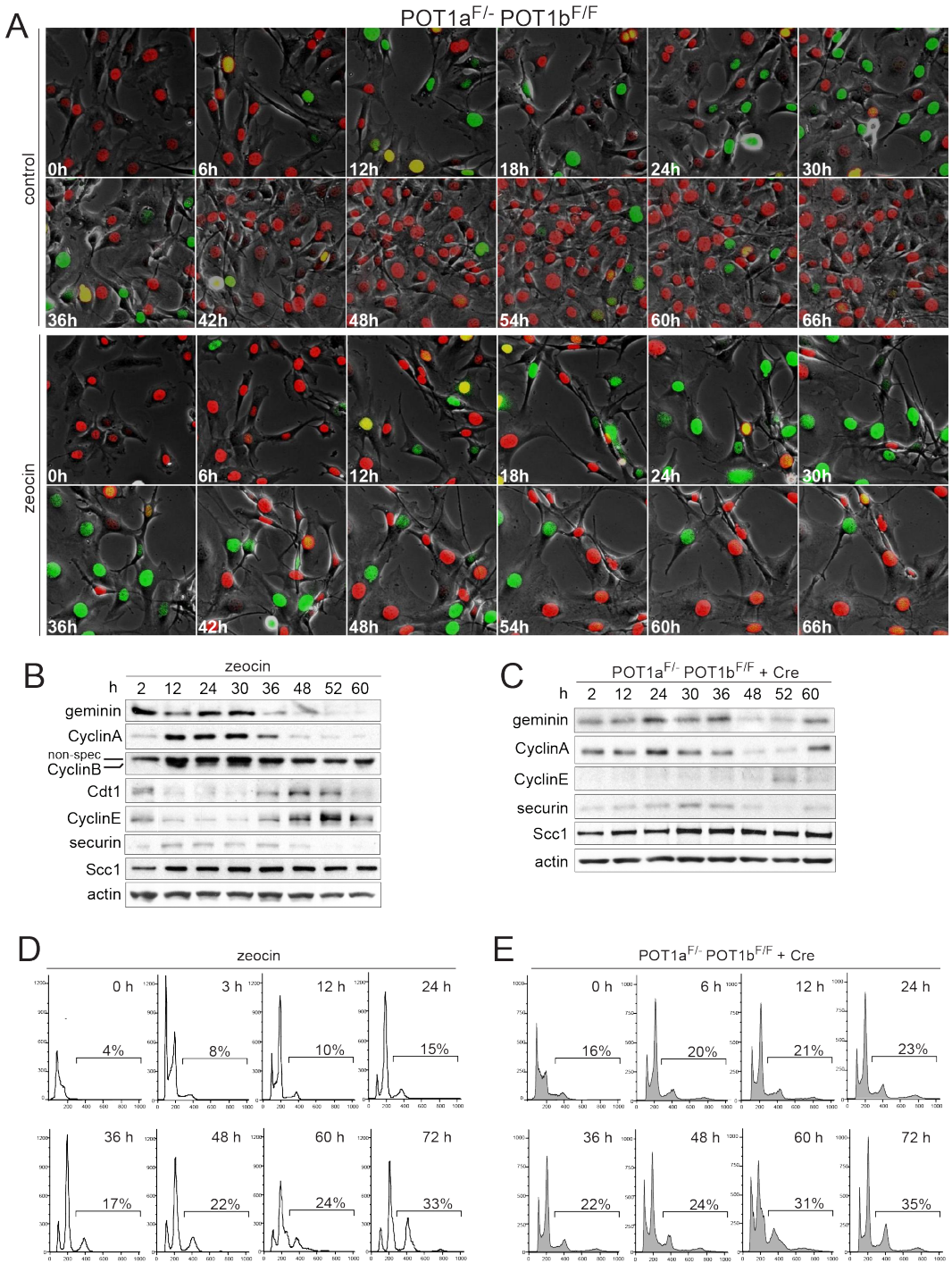
A
POT1a$^{F/-}$ POT1b$^{F/F}$
control
zeocin
0h
6h
12h
18h
24h
30h
36h
42h
48h
54h
60h
66h
B
zeocin
h 2 12 24 30 36 48 52 60
geminin
CyclinA
non-spec
CyclinB
Cdt1
CyclinE
securin
Scc1
actin
C
POT1a$^{F/-}$ POT1b$^{F/F}$ + Cre
h 2 12 24 30 36 48 52 60
geminin
CyclinA
CyclinE
securin
Scc1
actin
D
zeocin
0 h 4%
3 h 8%
12 h 10%
24 h 15%
36 h 17%
48 h 22%
60 h 24%
72 h 33%
E
POT1a$^{F/-}$ POT1b$^{F/F}$ + Cre
0 h 16%
6 h 20%
12 h 21%
24 h 23%
36 h 22%
48 h 24%
60 h 31%
72 h 35%

2.1.5 Involvement of APC/Cdh1

We next determined whether APC/Cdh1, the ubiquitin ligase responsible for degradation of geminin during normal cell cycles (McGarry and Kirschner, 1998), is involved in the endoreduplication. For both POT1a/b DKO cells and zeocin treated cells, polyploidy was decreased by knockdown of Cdh1 with an shRNA (Fig. 2.11A-C). FUCCI imaging showed that after knockdown of Cdh1, most of POT1a/b DKO cells remained blocked in G2 (green) and geminin was not degraded in these cells whereas a parallel culture of POT1a/b DKO cells showed the mitosis-independent loss of geminin noted above (Fig. 2.12A-C and Movie 6). Most of the POT1a/b DKO cells treated with Cdh1 shRNA remained blocked in G2 for 30-40 h and eventually underwent apoptosis (Fig. 2.12A, B and Movie 6). Cdh1 shRNA also had this effect on zeocin-treated cells (Fig. 2.13A-C, Movie 7) and similar results were obtained with a second Cdh1 shRNA.

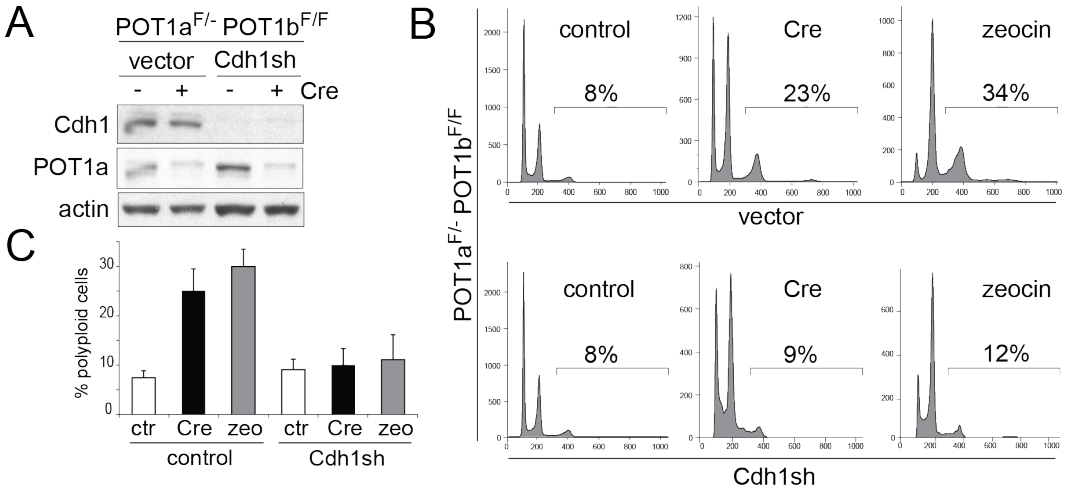

Figure 2.11: **Involvement of Cdh1 in polyploidization.** (A-C) Knockdown of Cdh1 inhibits polyploidization. POT1a$^{F/-}$POT1b$^{F/F}$ MEFs were treated with shRNA to knockdown Cdh1 and polyploidy was measured after POT1a/b deletion by Cre expression, zeocin treatment, or in untreated cells. Immunoblot is shown in (A). FACS profiles from a representative experiment (B) and quantification of the percentage of polyploid cells in 3 independent experiments with SDs (C) are shown.

Figure 2.12: **Involvement of Cdh1 in endoreduplication in POT1a/b DKO cells.** (A) Diminished geminin degradation after Cdh1 knockdown. POT1a$^{F/-}$POT1b$^{F/F}$ MEFs transduced with FUCCI vectors were treated with Cre, followed by Cdh1 shRNA or vector control infections a day later. Two days later, the cells were imaged for 60 hours (Movie 6) and selected time points of a representative experiment are shown. Arrows with the same orientation highlight the same cell over time. In Cre-treated cells two representative cells showing geminin degradation without mitosis are highlighted. In cells treated with Cre and Cdh1 shRNA, arrows highlight two cells showing prolonged arrest in G2 and persistence of geminin. (B) Schematic of FUCCI imaging data obtained on POT1a/b DKO cells treated with Cdh1 shRNA. Cells were treated and imaged as in (A). Cells treated with Cdh1 shRNA only were imaged separately (Movie 6). The indicated number of cells were followed throughout the imaging session to determine the length of G1 (red), entry into S phase (yellow), and S/G2 (green). Average values (h) are shown. (C) Table showing the effect of Cdh1 knockdown on mitosis-independent geminin degradation. Cells were treated and imaged as in (A) and (B). At least 100 cells were followed throughout the movie and the percentage of cells showing at least one event of geminin degradation without mitosis was determined. Average values and SDs were obtained from 3 independent experiments.

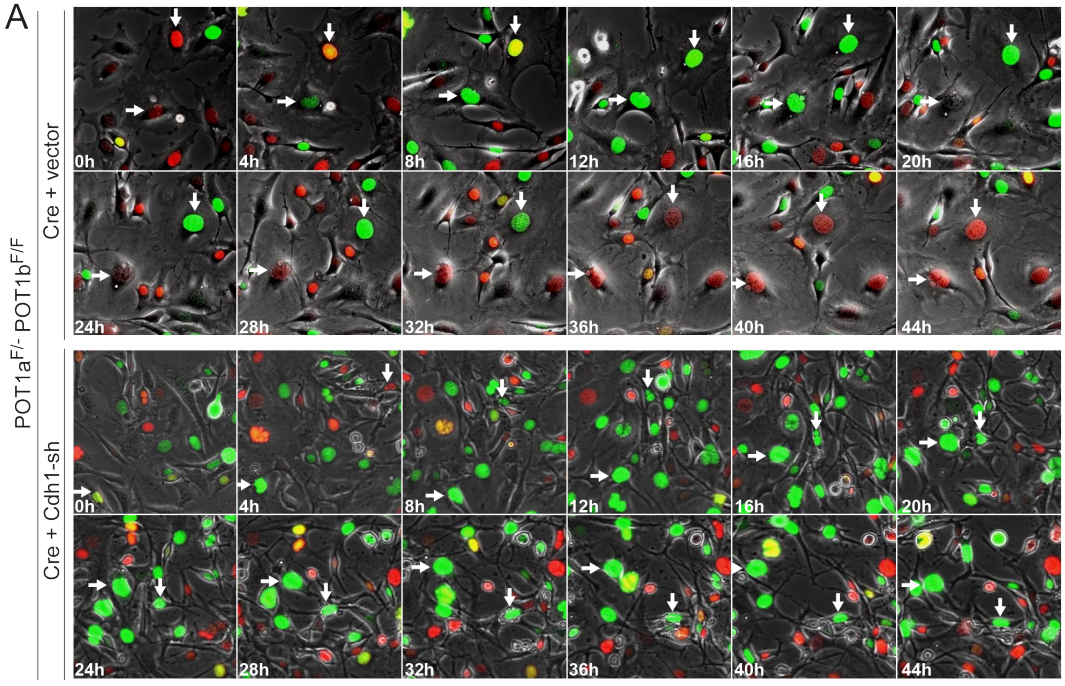

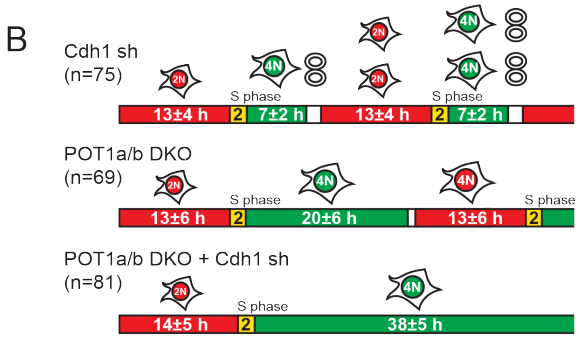

C

	% cells with geminin degradation without mitosis
Cdh1 sh (n≥100)	2±1
POT1a/b DKO (n≥100)	72±8
POT1a/b DKO + Cdh1 sh (n≥100)	8±5

The occurrence of a prolonged G2 arrest is consistent with the FACS profiles in which the ratio between the 4N and 8N peaks is higher in cells treated with Cdh1 shRNA than in the control. (Fig. 2.11B). In contrast, Cdh1 knockdown in cells that were not experiencing persistent DNA damage resulted in a nearly normal progression through the cell cycle (Movie 6 and Fig. 2.12A, B). The role of APC/Cdh1 in the degradation of geminin and endoreduplication was further confirmed with an shRNA to the APC1 subunit of the APC, which gave results similar to those with the Cdh1 shRNA in inhibiting polyploidization in POT1a/b DKO cells and zeocin-treated cells (Fig. 2.14A-C).

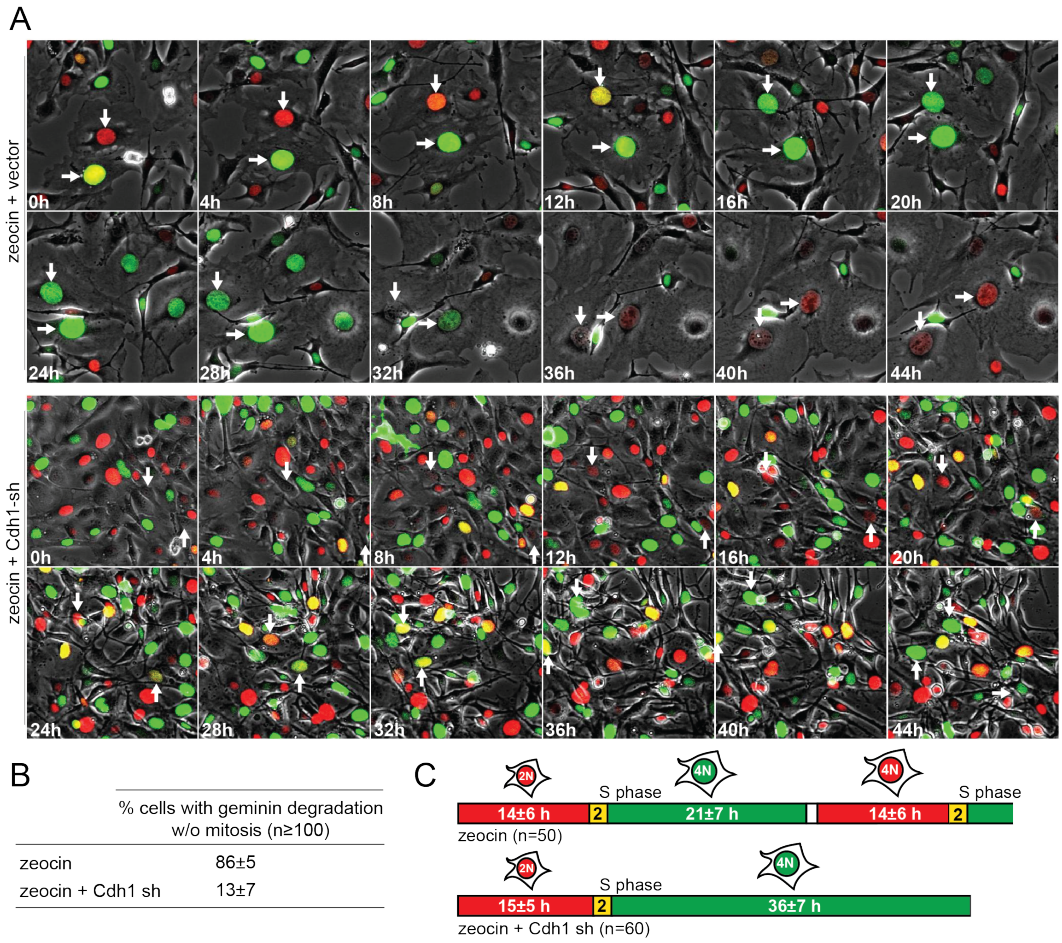

Figure 2.13: **Involvement of Cdh1 in endoreduplication in zeocin-treated cells.** (A) Cells were treated with Cdh1 shRNA or the vector control and imaged as in Fig. 2.12A in the presence of zeocin (Movie 7). Selected time points (every 4 hours) are shown. Arrows with the same orientation highlight the same cell during time. (B) Table showing the effect of Cdh1 knockdown on mitosis-independent geminin degradation in zeocin-treated cells. Cells were treated and imaged as in (A). At least 100 cells were followed throughout the movie and the percentage of cells showing at least one event of geminin degradation without mitosis was determined. Average values obtained from 3 independent experiments with SD are shown. (C) Prolonged G2 phase after Cdh1 knockdown in zeocin-treated cells. Cells were treated and imaged as in (A) and the indicated number of cells were followed throughout the imaging session to determine the length of G1 (red), entry into S phase (yellow), and S/G2 (green). Average values (h) are shown.

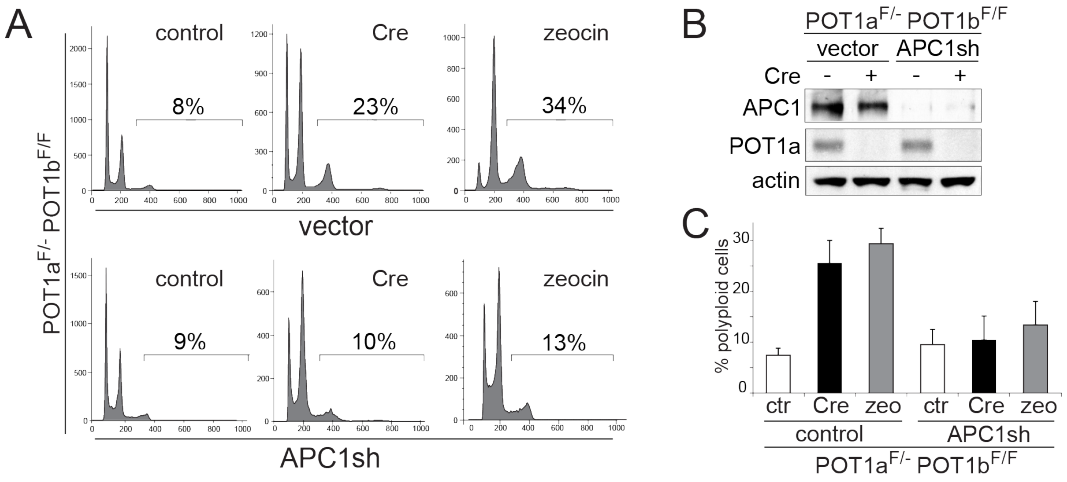

Figure 2.14: **Involvement of APC1 in endoreduplication in POT1a/b DKO and zeocin-treated cells.** (A-C) Diminished polyploidy after knockdown of APC1. POT1a$^{F/-}$POT1b$^{F/F}$ MEFs were treated with APC1 shRNA and polyploidy was measured after POT1a/b deletion with Cre, after continuous zeocin treatment, or in untreated cells. FACS profiles from a representative experiment (A) and quantification of the percentage of polyploid cells in 3 independent experiments (C) are shown. Immunoblotting showing APC1 knockdown is shown in (B).

2.2 Tetraploidization in human cells during telomere crisis

2.2.1 Telomere-driven tetraploidization occurs in human cells undergoing crisis

The data presented so far suggest that a prolonged state of telomere dysfunction, which is widespread in early tumorigenesis, may represent a source of tetraploidization. In the previous experiments, we used a genetic system where telomere dysfunction was induced by genetic inactivation of the sheltering components POT1a/b in mouse cells. We next set out to determine whether tetraploidy occurs in the cancer-relevant context of telomere crisis

(Fig. 1.5), the final stage of the last phase of human cells' lifespan, where cells experience extensive telomere shortening in the absence of p53 and Rb pathways.

To generate cells in telomere crisis, telomerase-negative human IMR90 and BJ fibroblasts were rendered p53- and Rb-deficient through expression of SV40 large T antigen (SV40-LT). As expected, the telomeres shortened progressively in these cultures (Fig. 2.15A, B), resulting in telomere crisis at PD 80-90 for IMR90-SV40LT and at PD 105-110 for BJ-SV40LT. Telomere crisis was evident from the plateau in the growth curve (Fig. 2.15A, B), the increased number of 53BP1 DNA damage foci (Fig. 2.16A), and the phosphorylation of Chk1 and Chk2 (Fig. 2.16B). FACS analysis showed that the fraction of tetraploid cells (estimated based on the fraction of cells with a DNA content >4N) progressively increased from 2-3% at early PDs to 30-35% at the time of telomere crisis (Fig. 2.16C). Similarly, BJ fibroblasts expressing HPV E6 and E7 displayed hallmarks of telomere crisis and accompanying tetraploidization at PD 90-100 (Fig. 2.17A-D).

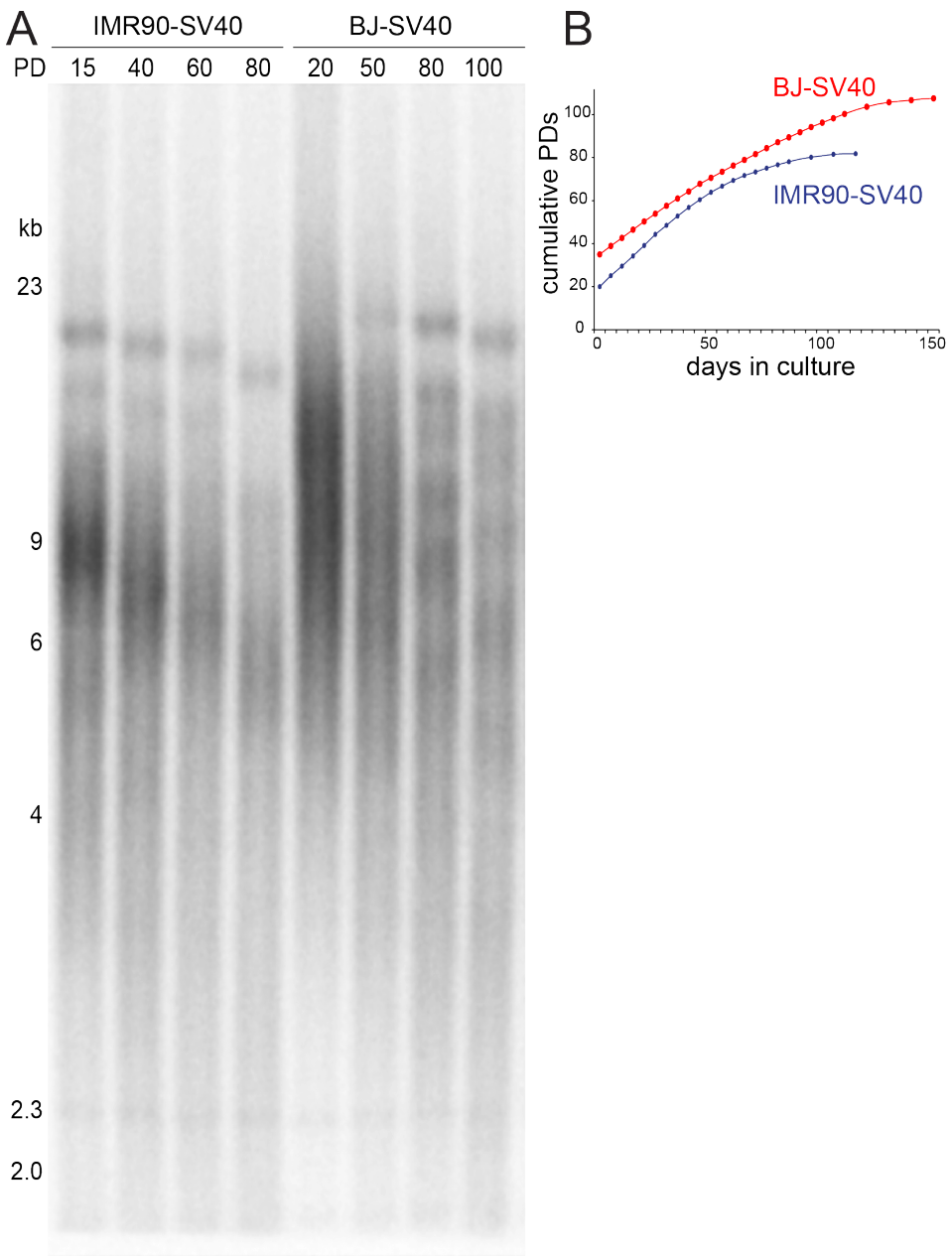

Figure 2.15: **Telomere shortening and crisis in BJ-SV40 and IMR90-SV40.** (A) Genomic blot for telomere restriction fragments of SV40-LT expressing IMR90 and BJ human fibroblasts at the indicated PD.(B) Growth curve of IMR90-SV40 and BJ-SV40 from PD 20 or 38 respectively until crisis (105-110 PDs for BJ-SV40 cells and at 80-90 for IMR90-SV40).

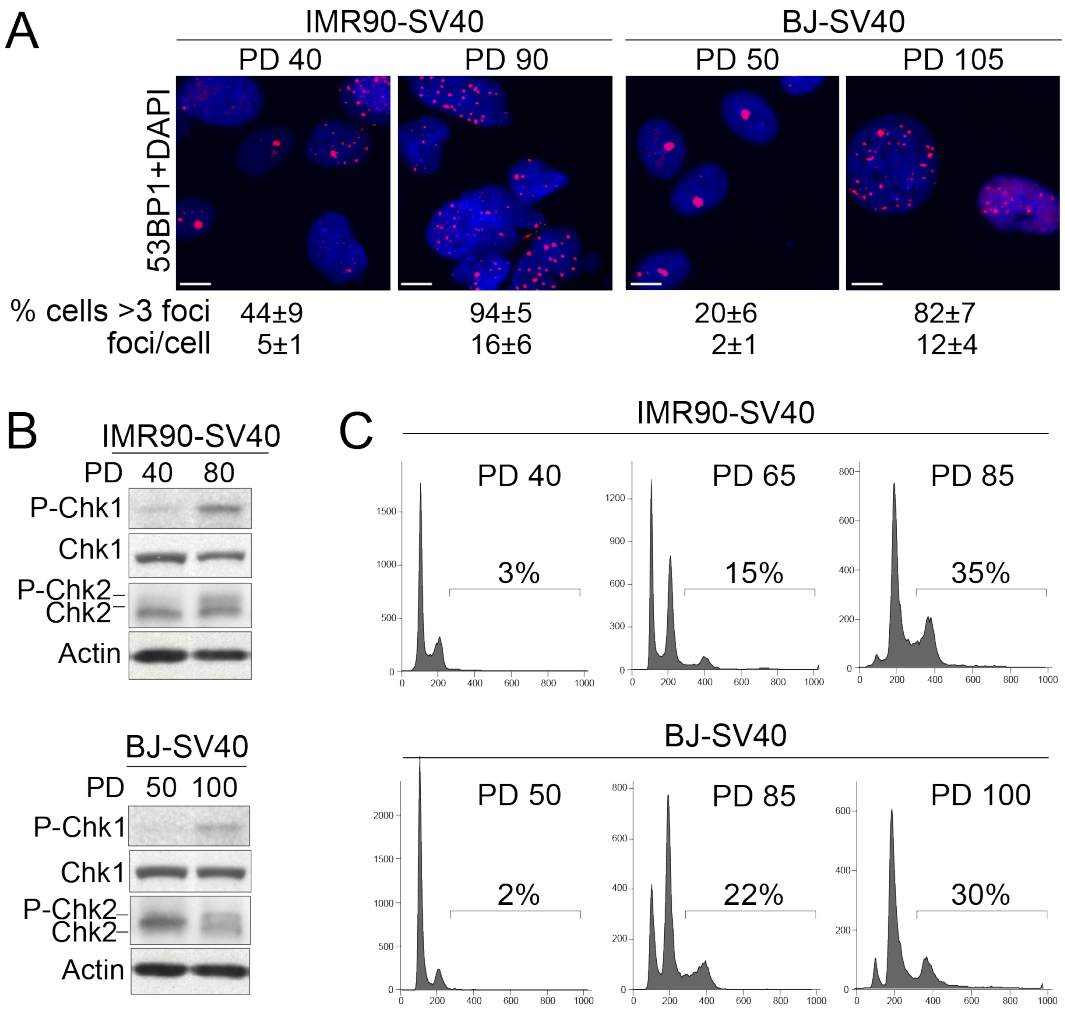

Figure 2.16: **Tetraploidization of BJ-SV40 and IMR90-SV40 in telomere crisis** (A) IF analysis of 53BP1 foci in the cells at the indicated PDs. The average number of 53BP1 foci per cell and the % of cells with >3 foci are shown with standard deviation (SD). (B) Immunoblots for P-Chk1 and P-Chk2 in the BJ-SV40 and IMR90-SV40 cells at the indicated PD. (C) FACS profiles (PI staining) of IMR90-SV40 and BJ-SV40 cells at the indicated PD. The % of cells with >4N DNA content is indicated.

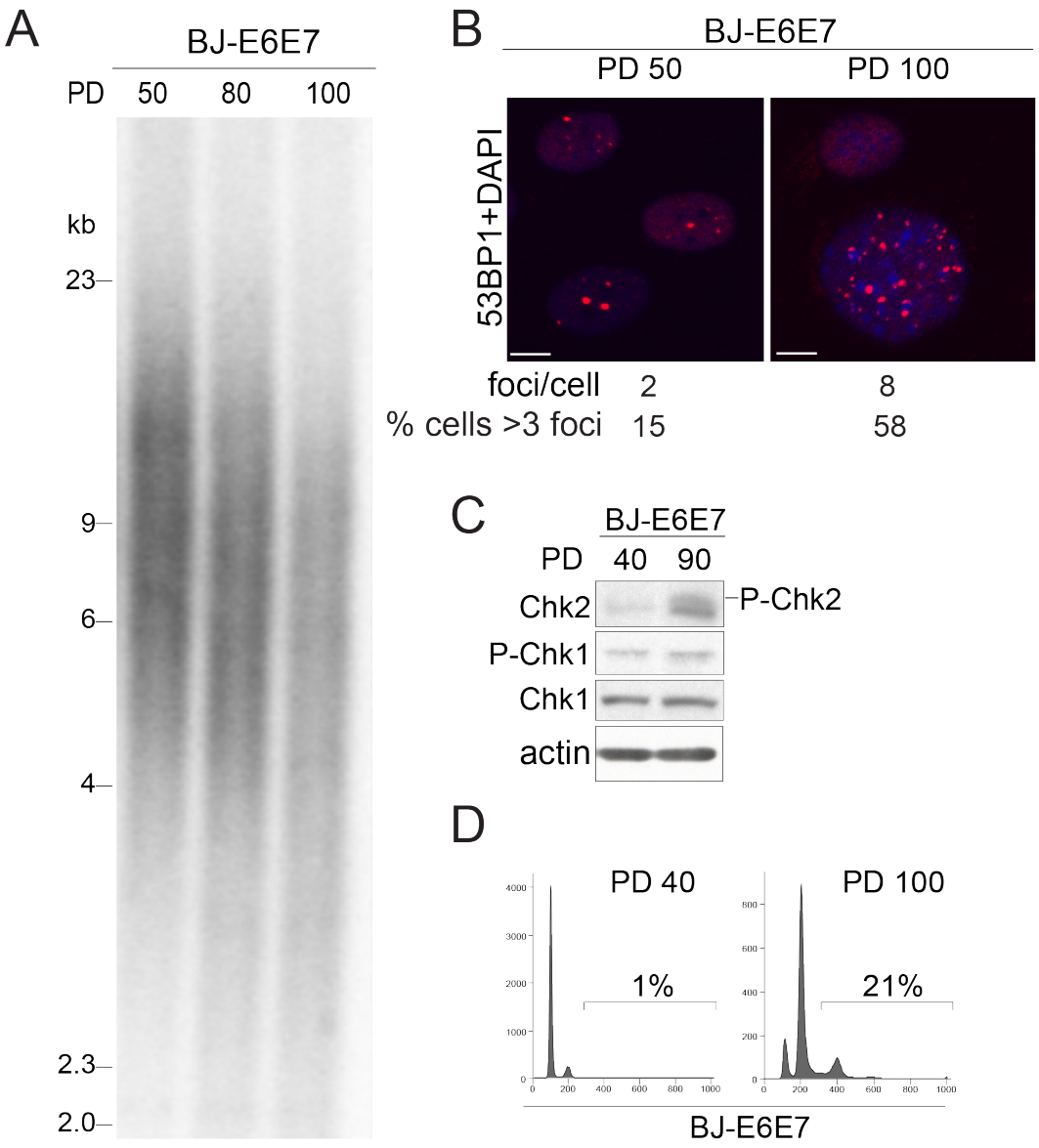

Figure 2.17: **Tetraploidization of BJ-E6E7 in telomere crisis.** (A) Genomic blot of telomere restriction fragments of BJ-E6E7 cells at the indicated PDs. (B) IF for 53BP1 foci in BJ-E6E7 cells at the indicated PDs. The average number of 53BP1 foci per cells and % of cells with >3 foci at the indicated PD is given. (C) Immunoblot showing phosphorylation of Chk1 and Chk2 in BJ-E6E7 at the indicated PD. (D) FACS analyis of BJ-E6E7 at the indicated PD. The % of cells with DNA content >4N is indicated.

Telomere crisis was also induced in two telomerase-negative human mammary epithelial cell strains (hMECs), 184BB-GSE22 and 48RS-GSE22, which lack a functional Rb pathway and express the p53 inhibitory peptide GSE22 (Romanov et al., 2001; Garbe et al., 2007). When these cells divide beyond senescence, they continue to erode their telomeres and enter a telomere crisis that is accompanied by genome instability (Romanov et al., 2001). The p53-proficient 184B and 48RS precursors were used as controls. The 184B-GSE22 and 48RS-GSE22 cultures entered telomere crisis at passage 18-20 and passage 28-32, respectively, showing shortened telomeres, an increase in the frequency of 53BP1 foci, and phosphorylation of Chk1 and Chk2 (Fig. 2.18A-D). FACS analysis showed an increase in the fraction of cells with >4N DNA content upon entry into telomere crisis in the two p53/Rb negative hMEC cultures, whereas the parallel p53-proficient counterparts showed a G1/S arrest without tetraploidization (Fig. 2.19A-D). The GSE-22 expressing hMECs, but not their p53-proficient counterparts, showed evidence for tetraploidization when pre-crisis cultures were treated with zeocin for 96 hours (Fig. 2.19A-D). Tetraploidization in telomere crisis was confirmed by analyzing the chromosome numbers of metaphase spreads (Fig. 2.20A).

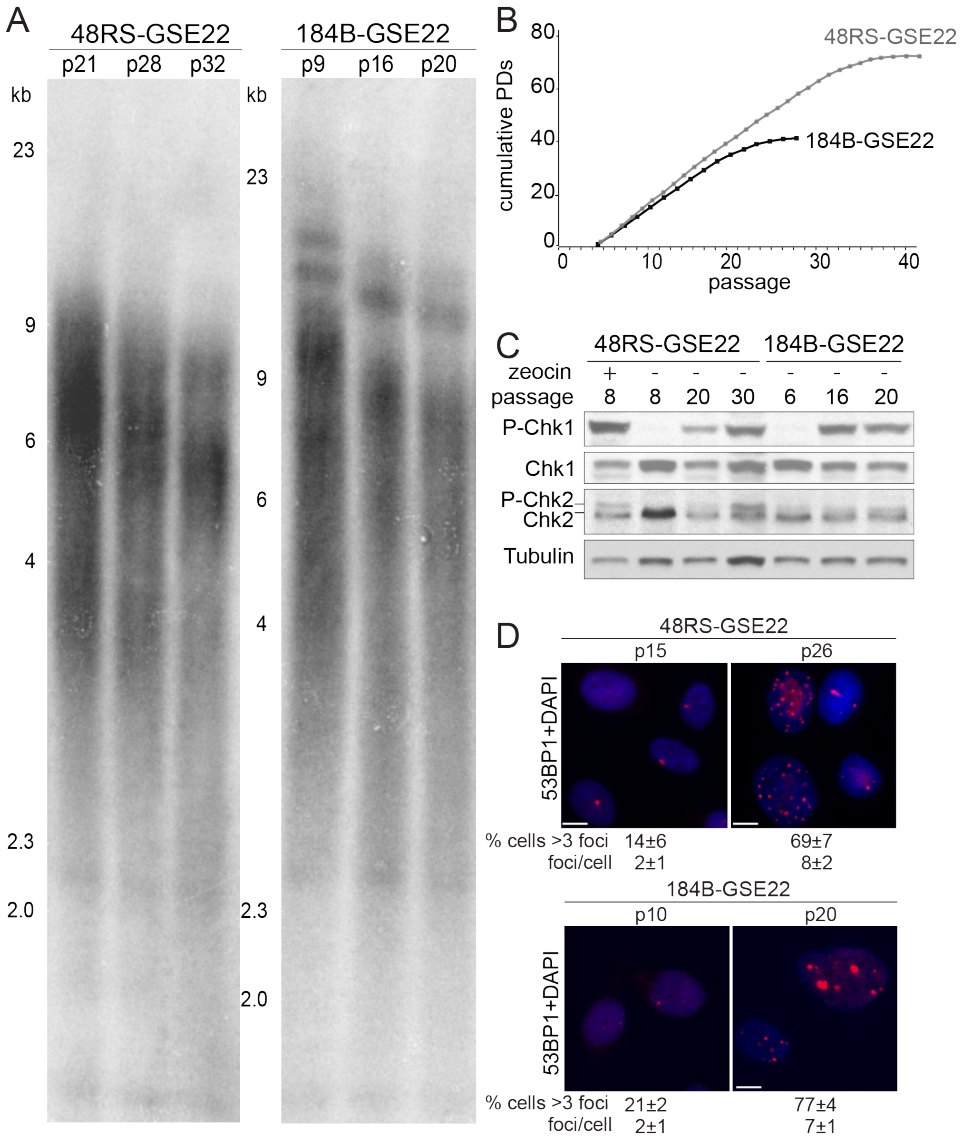

Figure 2.18: **Telomere crisis in hMECs.** (A) Genomic blot for telomere restriction fragments of 184B-GSE22 and 48RS-GSE22 at the indicated passage during the progression toward crisis. (B) Growth curves of 184B-GSE22 and 48RS-GSE22. (C) Immunoblots for Chk1 and Chk2 phosphorylation in 48RS-GSE22 and 184B-GSE22 at the indicated passage and after zeocin treatment. (D) IF for 53BP1 foci in 184B-GSE22 and 48RS-GSE22 hMECs at the indicated passages. The average number of 53BP1 foci per nucleus and the % of cells with >3 foci are given.

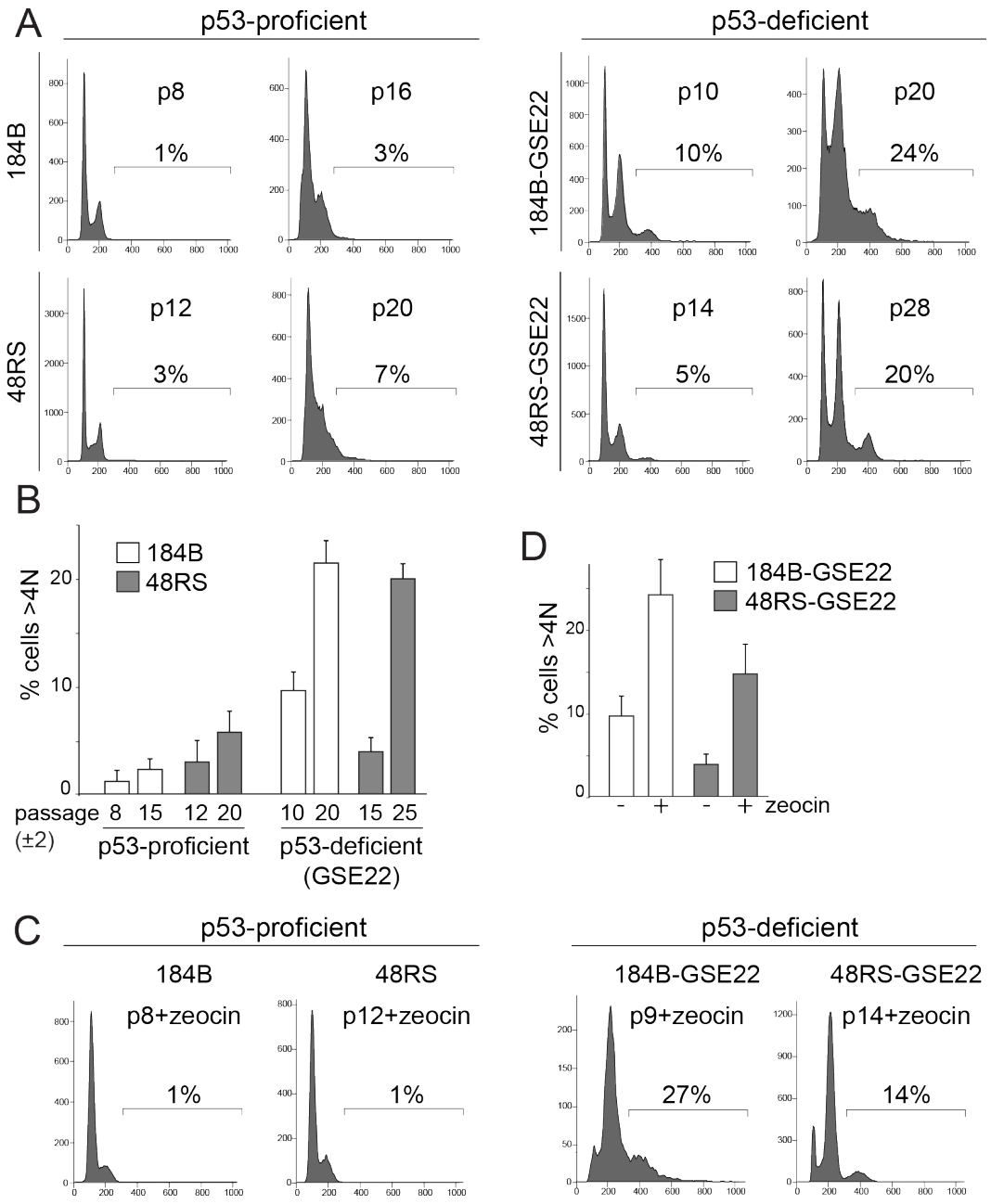

Figure 2.19: **Tetraploidization of hMECs in telomere crisis.** (A, B) FACS analysis of the indicated hMECs at the indicated passage. The % of cells with DNA content >4N is indicated. Quantification of averages of two or three independent experiments is shown in (B). (C, D) FACS analysis of 184B-GSE22 and 48RS-GSE22 at the indicated (early) passage treated with zeocin. The % of cells with a DNA content >4N is indicated. Quantification of three independent experiments is shown in (D).

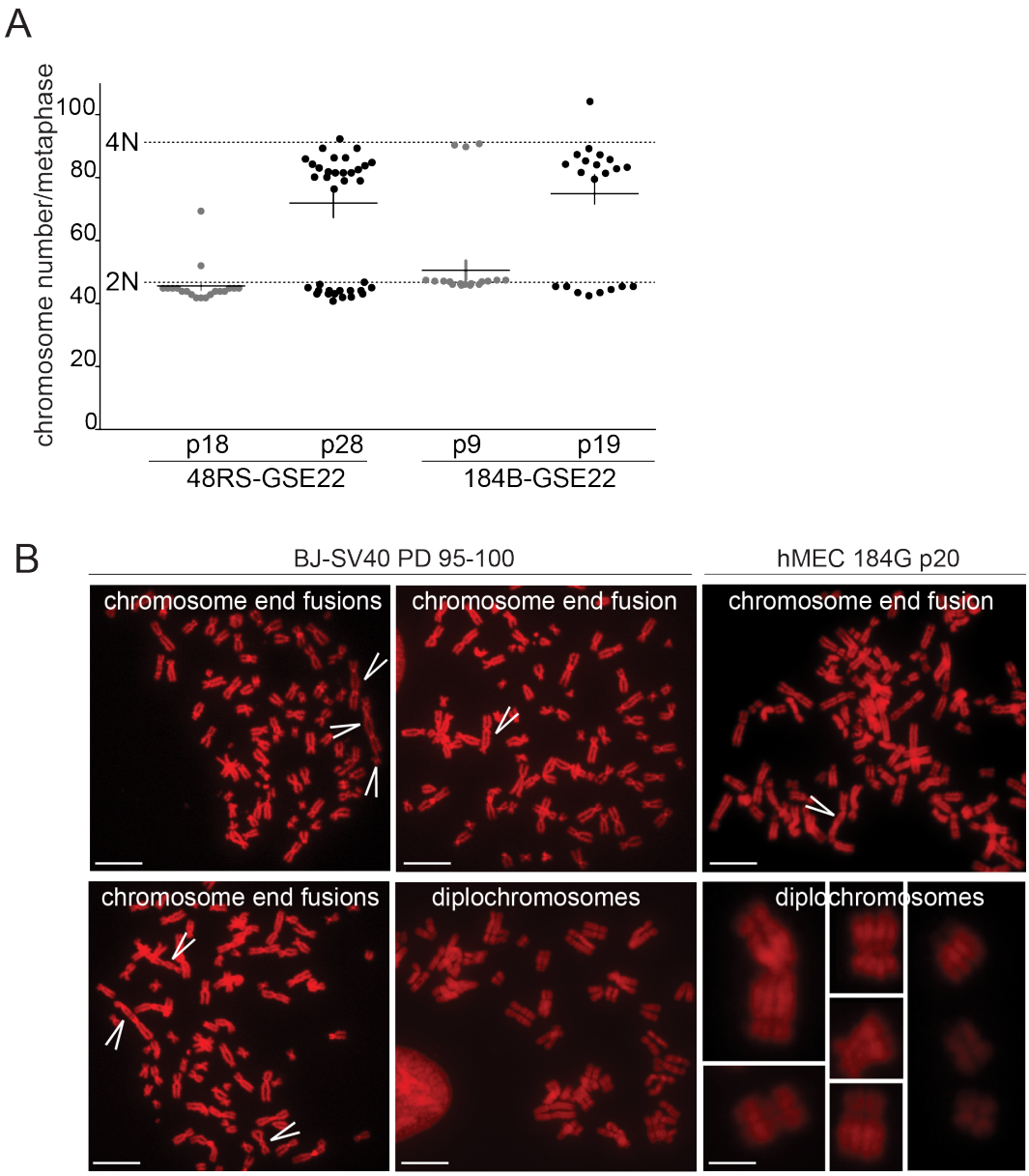

Figure 2.20: **Chromosomal abnormalities in crisis cells.** (A) Chromosome numbers of the indicated hMECs at the indicated passage (before and at crisis). (B) Examples of diplochromosomes and chromosome end fusions from metaphase spreads derived from BJ-SV40 and 184B-GSE22 in telomere crisis.

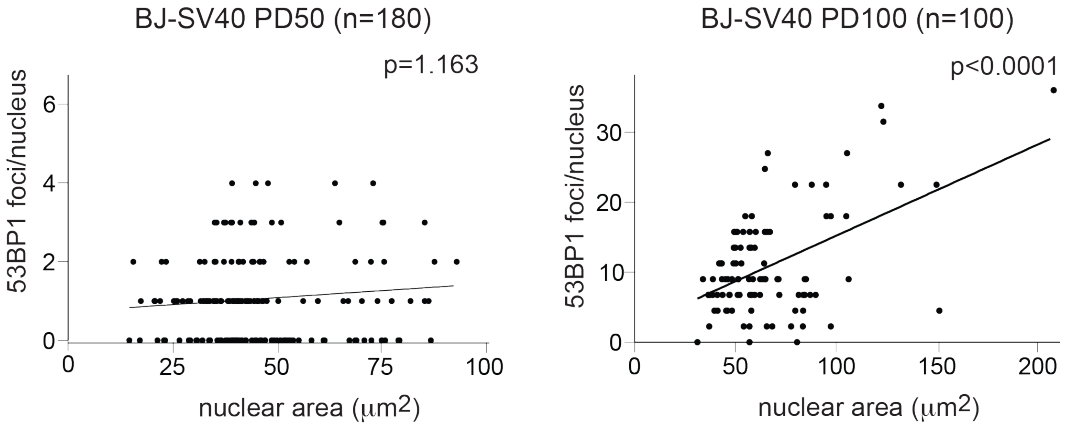

Figure 2.21: **DNA damage signal in polyploid cells.** BJ-SV40 cells at the indicated PD were stained for 53BP1 and DAPI by immunofluorescence, pictures were captured (40X objective) and analyzed using Metamorph software for nuclear area and number of 53BP1 foci per nucleus. A positive correlation ($p<0.0001$) between the nuclear area and the number of 53BP1 foci per cell was found in BJ-SV40 cells in crisis (PD 100), but not in BJ-SV40 cells at PD 50 (linear regression analysis of the data was performed using Prism 5 software).

Thus, in epithelial cells as well as in fibroblasts, telomere crisis and prolonged genome-wide DNA damage is accompanied by polyploidization resulting in tetraploid cells. While the formation of tetraploid cells is readily demonstrable, we note that the 8N peak in the FACS profiles of cells in crisis could represent octoploid cells in G1 as well as tetraploid cells in G2. As two successive aberrant cell cycles are required to generate octoploid cells, octoploidization might be too infrequent to result in a clear 16N peak in the FACS profiles. In the heterogeneous cell population in telomere crisis, tetraploidization is expected to be more frequent in cells with greater (telomeric) DNA damage signaling. In agreement, we found a positive correlation between the number of 53BP1 foci and the nuclear area of BJ-SV40 cells in telomere crisis ($p<0.0001$) but not in the same cell population at an earlier PD (Fig. 2.21).

2.2.2 Endoreduplication and mitotic failure in telomere crisis

The increased ploidy of cells in telomere crisis could be due to either endoreduplication or a failure in the late stages of mitosis, since dicentric chromosomes formed by telomere fusions (Fig. 2.20B) hinder the completion of cytokinesis. In fact if the two centromeres of a dicentric chromosome are pulled toward opposite poles of the mitotic spindle, the resulting lagging chromosome can prevent completion of mitosis (Mullins and Biesele, 1977). To distinguish between these events, we performed live-cell imaging using the FUCCI system (Sakaue-Sawano et al., 2008). In a normal mitotic cycle, geminin is degraded during mitosis, thereby re-establishing a state that is permissive to origin licensing in the daughter cells. However, as shown before, in POT1a/b DKO cells undergoing endoreduplication, geminin degradation takes place in the absence of mitosis, allowing cells to enter a G1-like state in which Cdt1 can mediate a second round of DNA replication. Thus, mitosis-independent geminin degradation is an indicator for endoreduplication (Fig. 2.22A,B and Fig. 2.23A; Movie 8). In addition, FUCCI imaging can be used to detect mitotic failure based on the breakdown of the nuclear envelope that signifies entry into mitosis and the binucleated or multinucleated cells that result from a failure in cytokinesis (Fig. 2.23A; Movie 8).

As expected, FUCCI imaging at early PDs (PD<50) of BJ-SV40 and BJ-E6/E7 fibroblasts showed that in most cells geminin degradation coincided with mitosis, whereas endocycles and mitotic failure were rare (<5%; Fig. 2.22A, B and Fig. 2.23A, B; Movie 8). However, at the late PDs when the

cells entered telomere crisis, the fraction of BJ-SV40, BJ-E6E7 and IMR90-SV40 cells undergoing geminin degradation in the absence of mitosis increased to 12-17% (Fig. 2.22A, B and Fig. 2.23A-C; Movies 8 and 9). After loss of geminin, most of these cells expressed Cdt1 and entered a second S phase as deduced from the degradation of Cdt1 and re-appearance of geminin. During these endocycles there was no evidence of nuclear envelope breakdown. The BJ-SV40 fibroblasts in telomere crisis also displayed a prolonged S/G2 phase whereas G1 was only minimally affected (Fig. 2.23C; Movie 8). In addition, the cells showed occasional metaphase spreads with diplochromosomes, a characteristic consequence of endoreduplication representing duplicated sister chromatids that are held together by the centromeric cohesin (Fig. 2.20B).

Figure 2.22: **Endoreduplication and mitotic failure in fibroblasts in telomere crisis.** (A, B) FUCCI live-cell imaging of BJ-SV40 cells (A) and IMR90-SV40 (B) at the indicated PD (Movies 8 and 9). Arrows with the same orientation highlight the same cell over time. In BJ-SV40 PD 45, the arrow highlights one cell progressing through a normal cell cycle. In BJ-SV40 cells PD 105, the white arrows highlight two cells undergoing endoreduplication; the black arrow highlights mitotic failure.

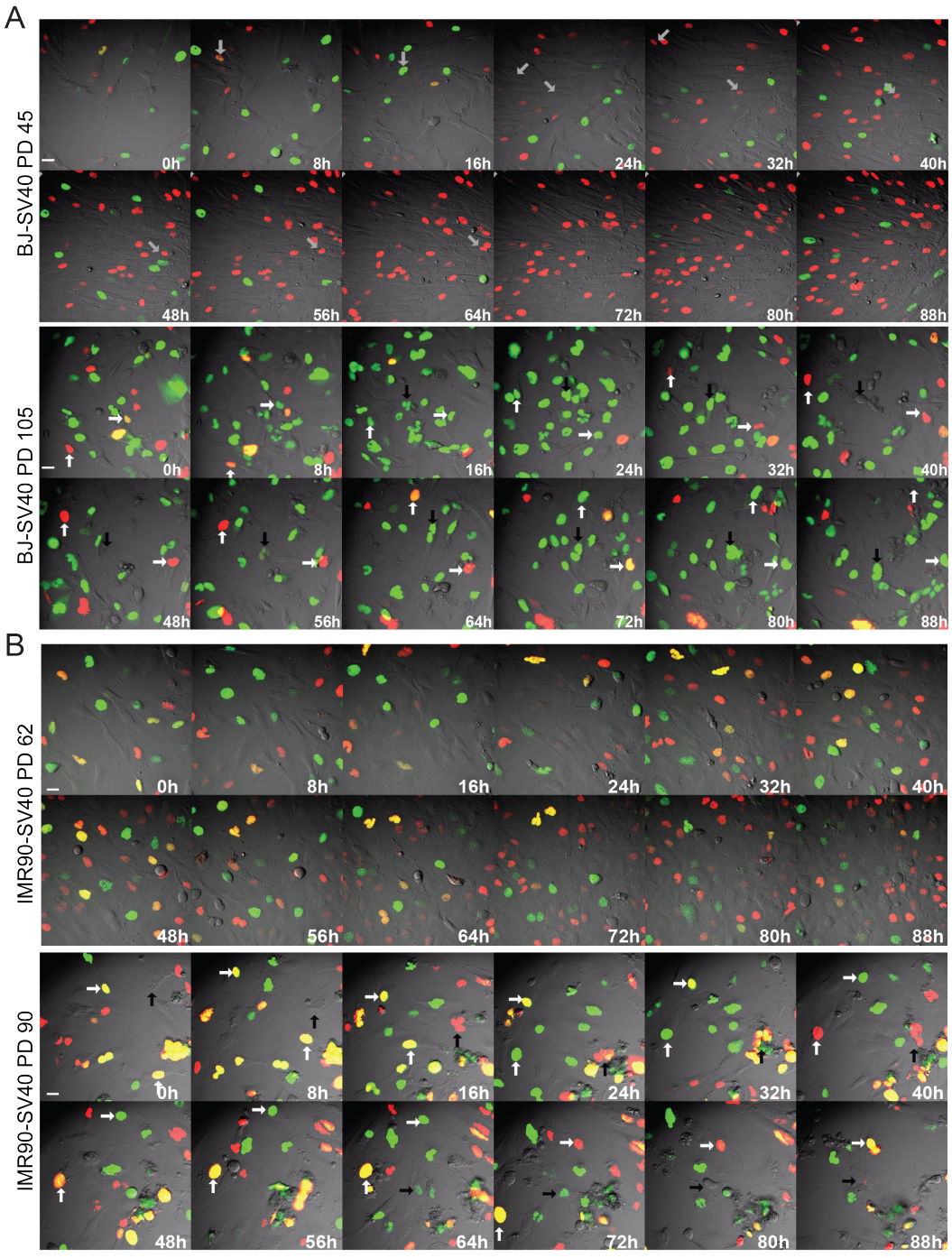
A
BJ-SV40 PD 45
0h
8h
16h
24h
32h
40h
48h
56h
64h
72h
80h
88h
BJ-SV40 PD 105
0h
8h
16h
24h
32h
40h
48h
56h
64h
72h
80h
88h
B
IMR90-SV40 PD 62
0h
8h
16h
24h
32h
40h
48h
56h
64h
72h
80h
88h
IMR90-SV40 PD 90
0h
8h
16h
24h
32h
40h
48h
56h
64h
72h
80h
88h

A

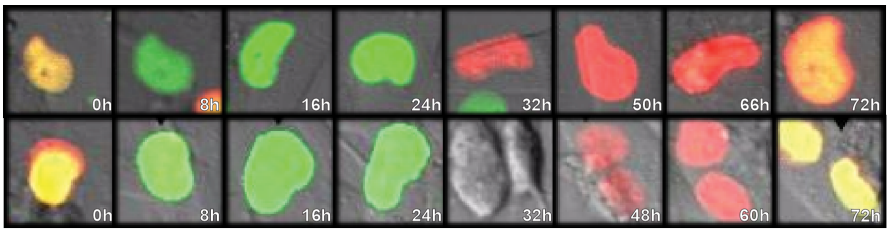

B

Cells	PD	% Endocycle	% Mitotic Failure	% >4N (FACS)
IMR90-SV40	30-40	nd	nd	5±2
	60-65	5±1	9±2	12±4
	85-90	13±2	17±2	34±8
BJ-SV40	40-50	3±1	4±1	4±2
	80-90	8±3	7±1	19±4
	100-110	17±2	14±2	32±4
BJ-E6E7	40-50	2±1	4±2	1±0.2
	95-105	12±2	7±3	17±4

C

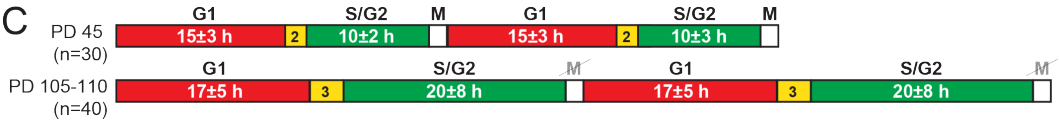

Figure 2.23: **Quantification of endoreduplication and mitotic failure in fibroblasts in crisis.** (A) Enlarged images exemplifying endoreduplication and mitotic failure. (B) Table summarizing the data derived from FUCCI imaging and FACS of BJ-SV40, IMR90-SV40, and BJ-E6E7. The average values and SD obtained from three independent experiments is given (n is the total number of cells analyzed in each case). (B) BJ-SV40 cells at the indicated PDs were imaged as in Fig. 2.22. The indicated number of cells was followed during the imaging session and the duration (hours) of the presence of geminin and Cdt1 was analyzed (average values are indicated).

In addition to endoreduplication, fibroblasts in telomere crisis showed a considerable level of mitotic failure (Fig. 2.22A, B and Fig. 2.23A, B; Movie 8 and 9). Their aberrant mitosis was presumably due to the dicentric chromosomes resulting from telomere fusions (Fig. 2.20B). The cells attempted mitosis as evidenced by their rounding up and breakdown of the nuclear envelope leading to the presence of geminin throughout the cells. However, the

execution of cytokinesis appeared to fail, resulting in binucleated or multinucleated cells (Movie 8 and 9). Endoreduplication and mitotic failure was also observed in the hMEC lines 48RS-GSE22 and 184B-GSE22 in telomere crisis and upon continuous treatment with zeocin (Fig. 2.24 and Fig. 2.25 A, B; Movie 10). Mitotic failure appeared to be more frequent in the hMECs compared to the BJ and IMR90 fibroblasts. For instance, in the presence of zeocin, BJ fibroblasts predominantly show endoreduplication whereas hMECs also show mitotic failure events (Fig. 2.25A, B; Movie 10).

Figure 2.24: **Endoreduplication and mitotic failure in hMECs in telomere crisis and after zeocin.** FUCCI imaging of 48RS-GSE22 at the indicated passages untreated or treated with zeocin. Indicated time points are from Movie 10. Arrows with the same orientation highlight the same cell over time. In 48RS-GSE22 p32, the white arrows highlight cells showing endoreduplication and the black arrows highlight cells undergoing mitotic failure.

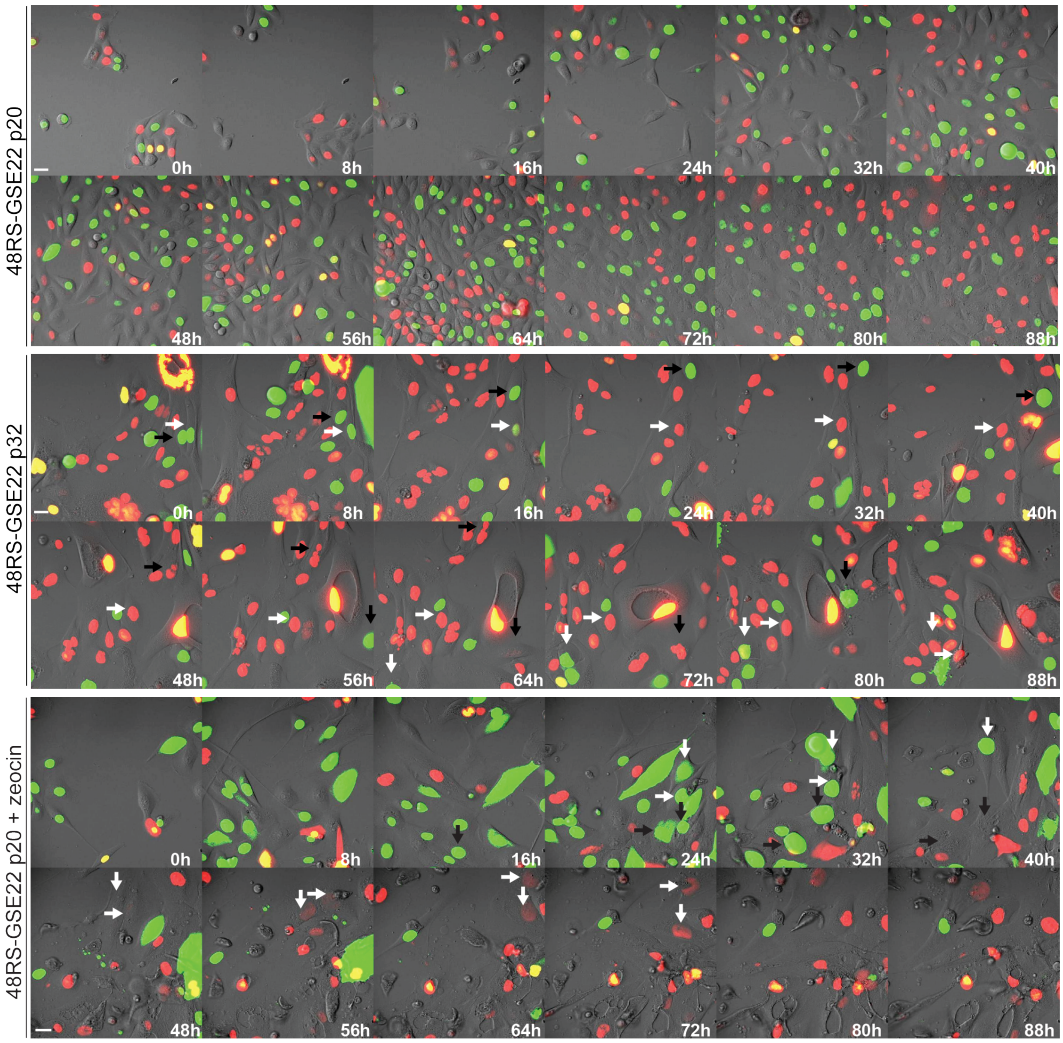
48RS-GSE22 p20
0h
8h
16h
24h
32h
40h
48h
56h
64h
72h
80h
88h
48RS-GSE22 p32
0h
8h
16h
24h
32h
40h
48h
56h
64h
72h
80h
88h
48RS-GSE22 p20 + zeocin
0h
8h
16h
24h
32h
40h
48h
56h
64h
72h
80h
88h

			FUCCI data	
Cells	passage	% >4N (FACS)	% Endocycle	% Mitotic Failure
48RS-GSE22	15-20	3±2	1±0.5	2±1
	28-35	20±3	7±2	15±2
	18-20 + zeocin	16±5	20±6	16±5
184B-GSE22	10-12	9±2	3±1	7±1
	18-20	25±5	9±2	18±5

Figure 2.25: **Quantification of endoreduplication and mitotic failure in hMECs in telomere crisis and after zeocin.** Table summarizing data derived from FUCCI imaging (Movie 10) and FACS (Fig. 2.24). The average and SD obtained from three independent experiments is given.

2.2.3 Role of Rb in blocking telomere-driven tetraploidization

In human cells, activation of the Rb pathway contributes to the cell cycle arrest in response to a genome-wide or telomere-derived DNA damage signal (Jacobs and de Lange, 2004; Shay et al., 1991; Smogorzewska and de Lange, 2002; Shay and Wright, 2005). In order to determine whether the Rb pathway can block tetraploidization, we analyzed telomerase-negative BJ fibroblasts with an unaltered Rb pathway. The p53 dominant negative allele (p53dn, p53175H) was used to abrogate the p53 response to DNA damage (p53dn, (Baker et al., 1990; Jacobs and de Lange, 2004).

To measure their propensity for tetraploidization, the BJ-p53dn cells were either subjected to continuous zeocin treatment or extensive replicative telomere shortening (PD 70-80; Fig. 2.26A-C; Fig. 2.27A-C). As compared to PD 30, at PD 70-80 the BJ-p53dn cells showed a small increase in the fraction

of tetraploid cells (<1% to ∼7%; Fig. 2.26A, B). The DNA damage response was active in BJ-p53dn cells at PD 70-80, as shown by Chk1 phosphorylation and an increased number of 53BP1 foci compared to earlier PDs (Fig. 2.26C, Fig. 2.27C). FACS analysis indicated that BJ-p53dn showed fewer tetraploid cells and a lower fraction of cells in G2 compared to BJ-SV40 at the same PD (Fig. 2.16C, Fig. 2.26A, B). Furthermore, after 96 hours of zeocin treatment, only ∼9% of BJ-p53dn cells had a DNA content >4N, whereas 20-25% of BJ-SV40 became tetraploid after zeocin treatment (Fig. 2.26A, B).

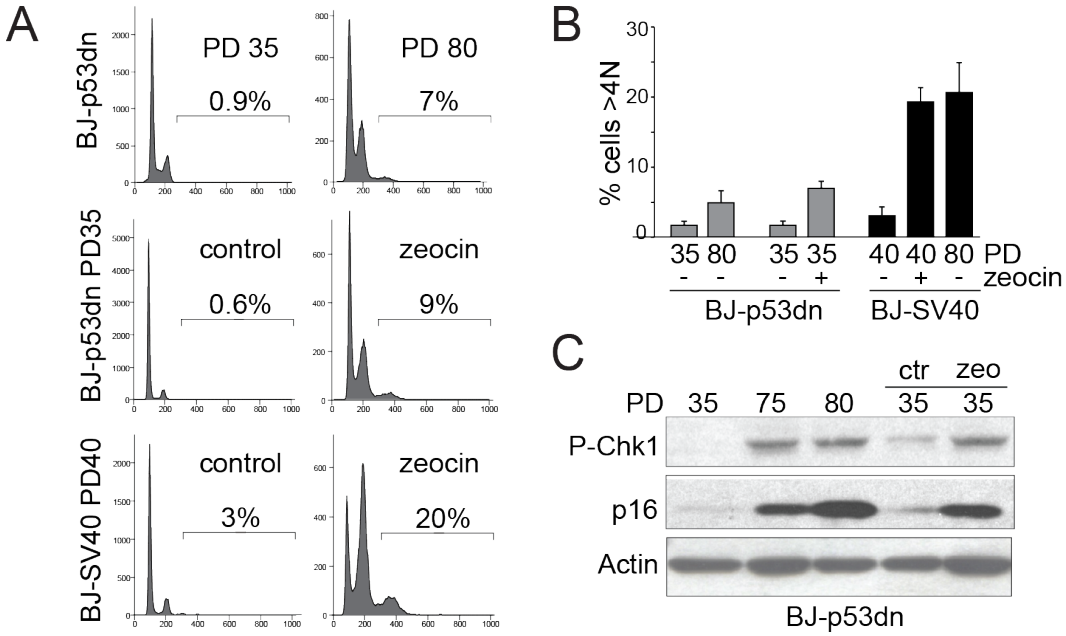

Figure 2.26: **Rb-mediated inhibition of tetraploidization in BJ cells.** (A) FACS analysis of BJ cells expressing p53175H (p53dn) or SV40-LT at the indicated PD with or without treatment with zeocin. (B) Quantification of the FACS data in (A). (C) Immunoblot for Chk1 phosphorylation and p16 expression in BJ-p53dn at the indicated PD or after treatment with zeocin.

Figure 2.27: **Telomere shortening and DNA damage after prolonged proliferation in BJ-p53dn.** (A) Genomic blot of telomere restriction fragments of BJ-p53dn cells at the indicated PDs. (B) Growth curve of BJ-p53dn cells. (C) IF for 53BP1 foci in BJ-p53dn cells at the indicated PD. The average number of 53BP1 foci per nucleus is indicated.

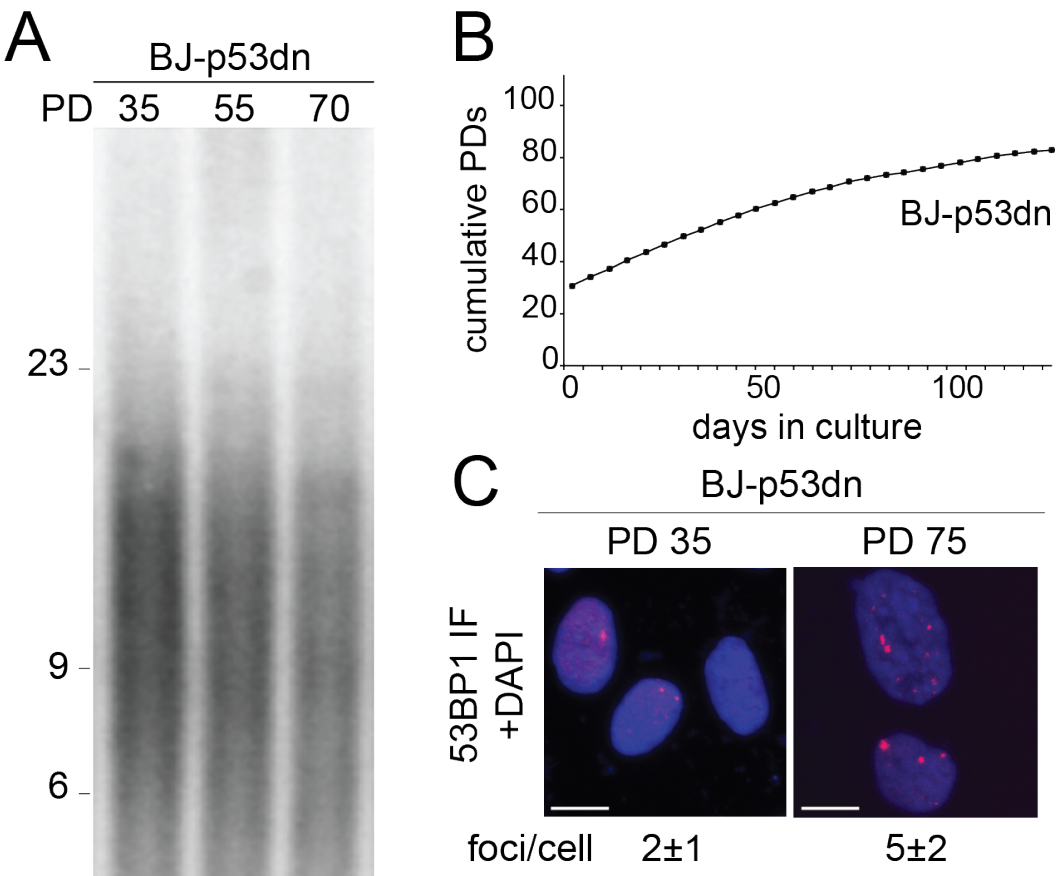
A
BJ-p53dn
PD 35 55 70
23
9
6
4
2.3
2.0
B
cumulative PDs
100
80
60
40
20
0
0
50
100
days in culture
BJ-p53dn
C
BJ-p53dn
PD 35
PD 75
53BP1 IF
+DAPI
foci/cell 2±1
5±2

Similar data were obtained using RPE (retinal pigment epithelial) cells lacking p53 function (Fig. 2.28A, B) whereas tetraploidy was not induced in primary cells, which arrested in G1/S (Fig. 2.28 A, B). Consistent with a role of the Rb pathway in mediating a G1/S arrest in response to telomere and genome-wide DNA damage, the level of p16 increased at increasing PDs and after zeocin treatment (Fig. 2.26C). These data suggest that the activation of the Rb/p16 pathway contributes to the repression of tetraploidization in cells experiencing a persistent DNA damage response.

The low level of residual tetraploidization in the Rb-proficient cells could be explained if the Rb pathway led to a block in G1 but not in G2. We therefore isolated FACS-sorted G1 and S/G2 cells, subjected them to zeocin treatment soon after plating, and then used FUCCI imaging to determine their tendency to undergo cell cycle progression and/or tetraploidization. Approximately 60% of the G1-sorted BJ-p53dn cells treated with zeocin remained in G1/S phase of the cell cycle (red or yellow) throughout the 96 hour imaging session (Fig. 2.29; Movie 11) whereas only 25-30% of G1-sorted BJ-SV40 cells arrested in G1/S after zeocin treatment (Fig. 2.29; Movie 11). In contrast, approximately 75% of the BJ-p53dn S/G2 cells underwent endoreduplication, showing mitosis-independent geminin degradation and re-entry into G1 (Fig. 2.29; Movie 12). BJ-SV40 cells in S/G2 showed the same percentage of endoreduplication, indicating that Rb status does not affect tetraploidization of cells experiencing prolonged DNA damage in S/G2. Although we cannot exclude other aspects of SV40 large T antigen expression, these data suggest that activation of the Rb/p16 pathway blocks entry into S phase in cells that experience a DNA

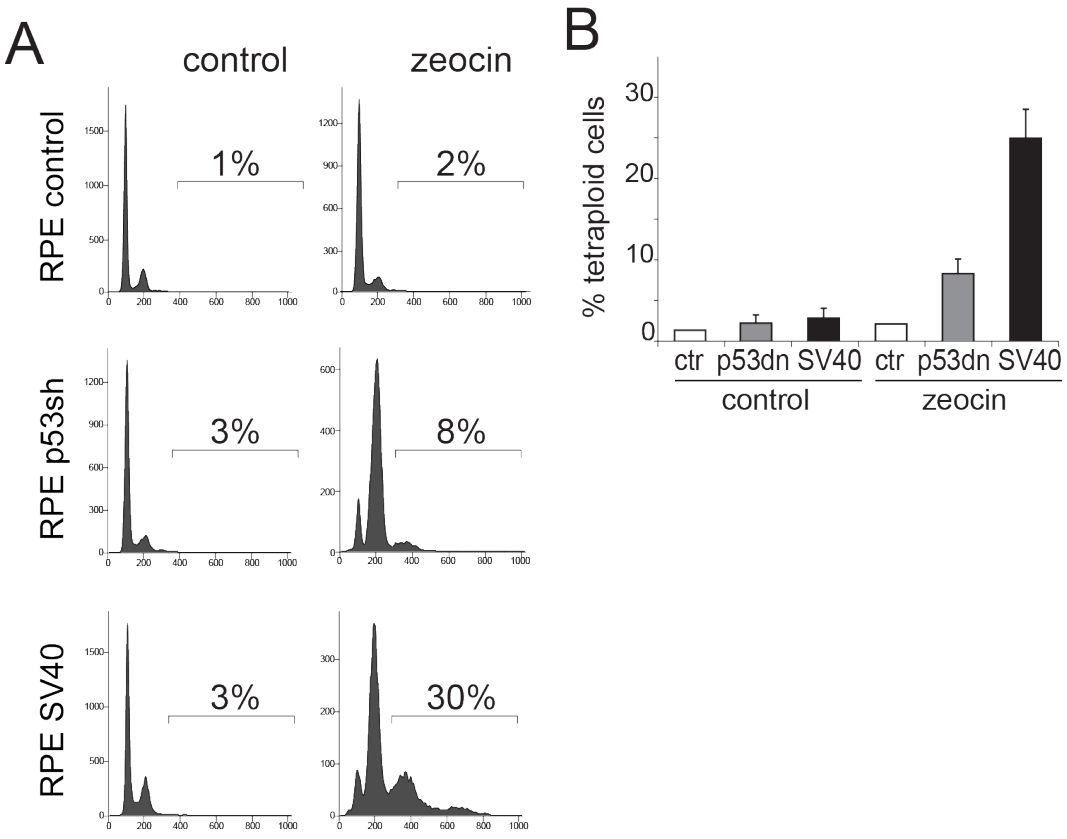

Figure 2.28: **Rb-mediated G1 arrest represses of tetraploidization in RPE cells.** (A, B) Human retinal pigment epithelial (RPE) cells at PD 10 were transduced with vectors expressing p53 shRNA or SV40-LT or an empty vector. The indicated cells were treated for 96 hours with zeocin or left untreated and were analyzed by FACS. The % of cells with a >4N DNA content is indicated. Quantification of three independent experiments is shown in B.

damage signal in G1, thereby limiting the occurrence of tetraploidization. In contrast, the Rb/p16 pathway alone is not capable of preventing endoreduplication when the DNA damage takes place in G2.

Figure 2.29: **Rb-mediated G1 arrest inhibits tetraploidization.** FUCCI imaging of BJ-p53dn PD 35 and BJ-SV40 PD 40 cells that were first FACS sorted for G1 (Cdt1, red) or S/G2 (geminin, green) and then imaged in the presence of zeocin (Movie 11, Movie 12). Selected time points are shown. Quantification of the Movie is shown below the images. The number of cells that remain arrested in G1/S (red/yellow color) throughout the imaging session and the cells showing geminin degradation in the absence of mitosis were scored in the indicated cases. Average numbers obtained in two experiments are shown.

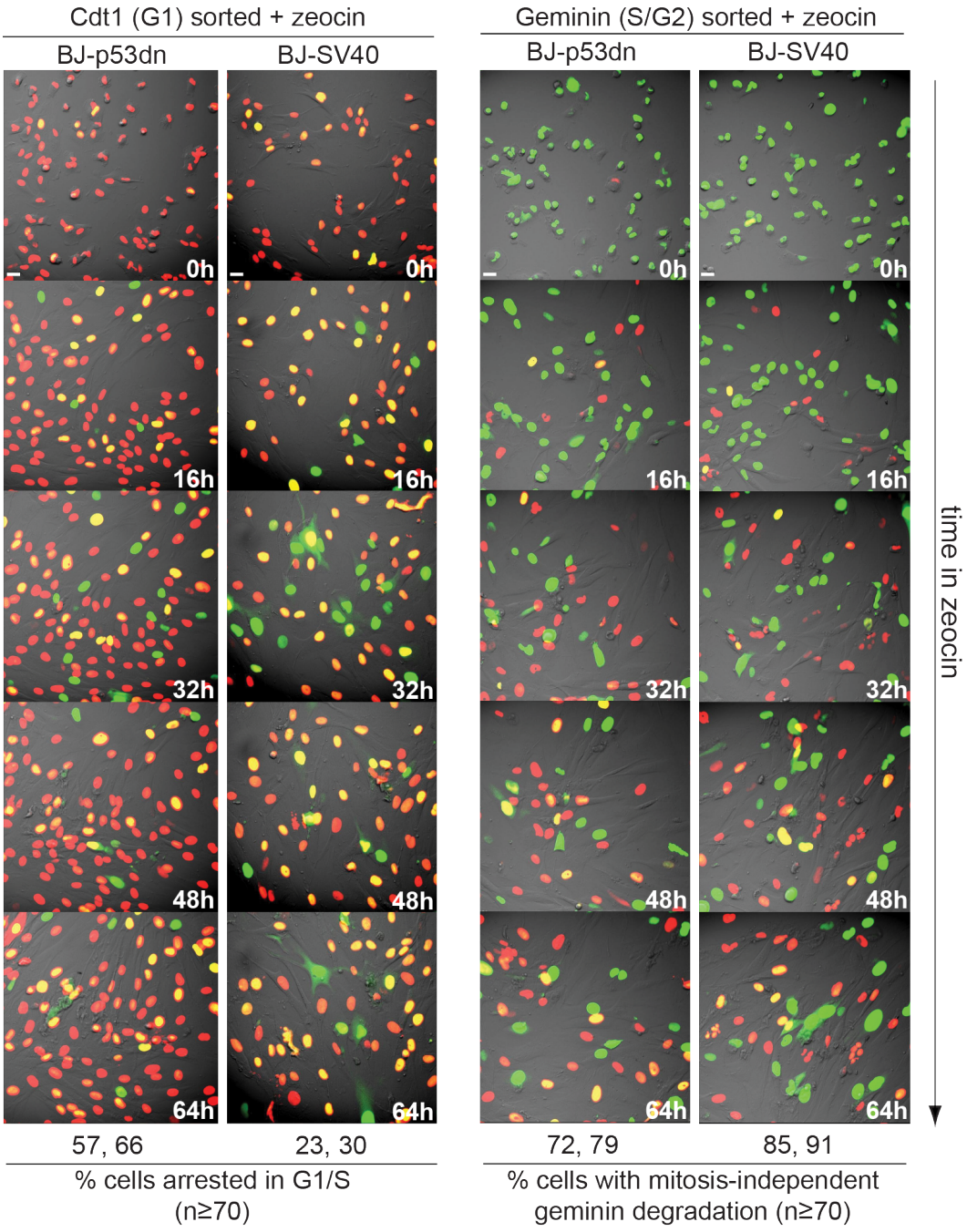
Cdt1 (G1) sorted + zeocin
BJ-p53dn
BJ-SV40
Geminin (S/G2) sorted + zeocin
BJ-p53dn
BJ-SV40
0h
16h
32h
48h
64h
time in zeocin
57, 66
23, 30
% cells arrested in G1/S
(n≥70)
72, 79
85, 91
% cells with mitosis-independent
geminin degradation (n≥70)

2.2.4 DNA damage signal threshold for the induction of tetraploidy.

A question relevant to the induction of polyploidization during telomere crisis is how many dysfunctional telomeres are required for this phenomenon and, in more general terms, whether there is a threshold for the induction of endoreduplication by DNA damage. This point was addressed by the work of Gloria Wu, an MD. PhD. student who rotated in the lab under my guidance. We treated mouse or human cells with increasing amounts of zeocin from 2 to 50-100 ug/ml for 72 hours and then analyzed the cells for polyploidy (fraction of cells with a DNA content >4N) and number of 53BP1 foci, as a quantification of the DNA damage level (Fig. 2.30 and Fig. 2.31). We noticed that the FACS profile of MEFs SV40 treated with 2 or 5 ug/ml was very similar to the untreated cells, with almost no increase in the cells with a DNA content >4N. At zeocin concentration of 10 ug/ml, we started to detect a significant increase in polyploidy from 3 to 11%, corresponding to a clear tetraploid peak in the FACS profile. Higher concentration of 20 ug/ml zeocin further increased the fraction of polyploid cells, and finally, at 50 ug/ml extensive polyploidization in almost half of the cell population (45%) was observed. The number of 53BP1 foci per cell was analyzed in the same cells after 12-16 hours from the beginning of the zeocin treatment as a quantification of the DNA damage level (Fig. 2.30). MEFs treated with zeocin concentrations of 2 and 5 ug/ml showed an homogeneous distribution of around 3 53BP1 foci per cell, with very few cells showing more than 10 foci. At higher concentrations of 10 and 20 ug/ml, the fraction of cells with more than 10 foci increased, accordingly

to the increase in polyploidy. In MEFs treated with the 50 ug/ml of zeocin almost half of the cells showed more than 10-15 foci, and these cells most likely represent the fraction of polyploid cells seen in the FACS profile (45%) Thus, from this data we can infer that, in mouse cells a minimum level of 10-15 53BP1 foci is necessary for the induction of endoreduplication in mouse fibroblasts (Fig. 2.30).

A similar experiment was performed in human BJ SV40 fibroblasts at PD30. We noticed that in BJ SV40 cells, the lowest zeocin concentration necessary for polyploidy was higher than in mouse cells (Fig. 2.31). In fact, for zeocin concentration up to 10 ug/ml, the fraction of polyploid BJ SV40 cells was not significantly higher than untreated cells. Overt polyploidization was observed only at 50 and 100 ug/ml of zeocin. The distribution of 53BP1 foci in zeocin-treated BJ SV40 cells seemed to be more homogeneous than in mouse cells, with less clear distinction of the population with high number of 53BP1 foci, most likely representing polyploid cells. Nevertheless, we were able to estimate a threshold of 15-20 DNA damage foci for the induction of polyploidy in human fibroblasts. These data indicate that a DNA damage threshold for the induction of polyploidy indeed exists, since even a prolonged treatment with low zeocin concentrations is not sufficient for polyploidy to occur. Most likely, in this case the balance between the induction of DNA lesions by zeocin and the activity of the repair machinery results in a net level of damage that is not sufficient to induce a prolonged G2 cell cycle arrest. It is likely that these cells experience a delay in G1 and/or G2 phases of the cell cycle, still being able to complete a regular mitotic cycle. Similarly, the

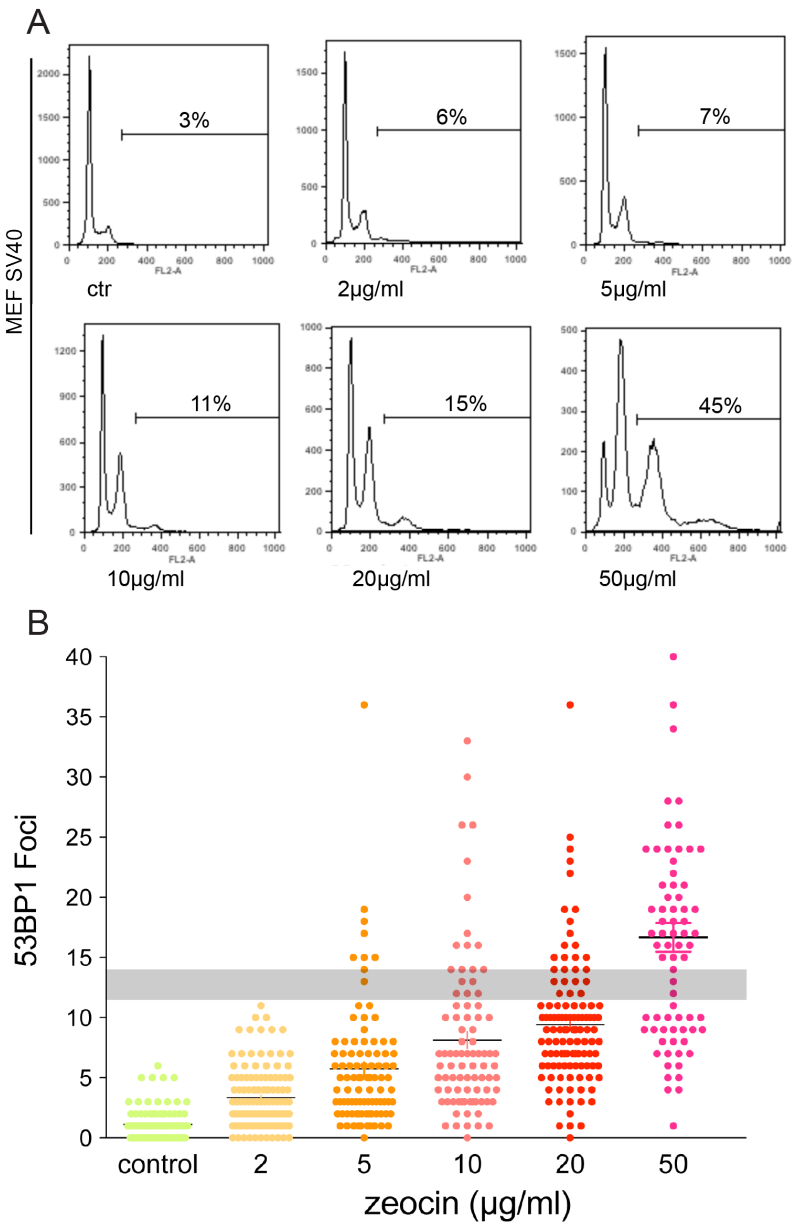

Figure 2.30: **DNA damage threshold for tetraploidization in MEF SV40.** (A) MEF SV40 were continuously treated with zeocin at the indicated concentration and analyzed by FACS after 72 hours (representative experiment is shown). (B) MEF SV40 were treated as in (A) and analyzed by IF for 53BP1 foci. The grey bar show the estimated threshold of the number of 53BP1 foci necessary to induce tetraploidy.

lower fraction of polyploid cells in human fibroblasts as compared to mouse cells treated with the same zeocin concentration might reflect differences in the regulation of the cell cycle checkpoint in G2 and/or in the re-entry into S phase, necessary for tetraploidization.

We next asked whether in BJ SV40 cells in crisis, the level of DNA damage required for polyploidization was reached in a certain fraction of cells, and whether this value is in agreement with the percentage of polyploid cells measured by FACS. Due to the low amount of telomeric DNA in crisis cells, colocalization analysis of 53BP1 DNA and telomeric DNA is very difficult. Thus, we considered the number of 53BP1 foci as an estimate of the number of dysfunctional telomeres in crisis cells (d'Adda di Fagagna et al., 2003). Quantification of 53BP1 foci in BJ SV40 cells in crisis (PD100) showed that about 15-20% of cells displayed a number of 53BP1 foci higher than 15-20 foci (Fig. 2.31), the previously estimated threshold for the induction of polyploidy in human cells. The fraction of polyploid cells in BJ SV40 in crisis measured by FACS is about 30%, higher than this value (Fig. 2.23). However, polyploid cells include both endoreduplicating cells and cells undergoing mitotic failure, in almost similar ratio (Fig. 2.23) and it is plausible that endoreduplicating cells will have more ongoing damage than cells undergoing mitotic failure. Based on this consideration, the estimated fraction of cells with high number of 53BP1 foci seems to be consistent with the % of cells undergoing endoreduplication in this context. Finally, it is also important to note that our way to assess polyploidy might be an underestimate, as the tetraploid G1 cells are not included in the polyploid fraction, therefore the threshold of 53BP1

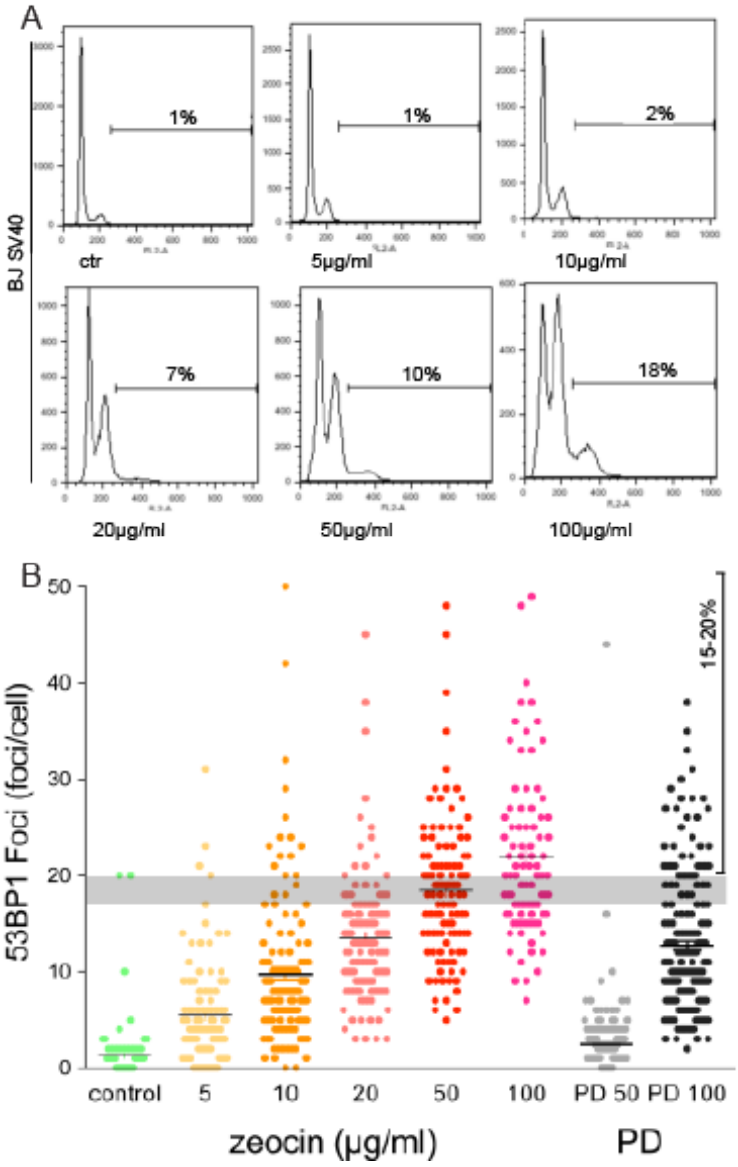

Figure 2.31: **DNA damage threshold for tetraploidization in BJ-SV40.** (A) BJ-SV40 were continuously treated with zeocin at the indicated concentration and analyzed by FACS after 72 hours (representative experiment is shown). (B) BJ SV40 were treated as in (A) and analyzed by IF for the number 53BP1 foci. BJ-SV0 before and during crisis were also analyzed in the same way. The grey bar show the estimated threshold of the number of 53BP1 foci necessary to induce tetraploidy. The fraction of predicted tetraploid cells in BJ SV40 in crisis is shown.

foci required for tetraploidy may be lower. This would be particularly true for the short term damage in zeocin-treated cells, where some cells might not have enough time to endoreduplicate during the 72-hours experiment, as compared to the 'long-term' telomere damage during crisis.

2.3 Telomere-dependent tetraploidy promotes transformation in mouse cells.

2.3.1 Re-establishment of cell division cycles after telomere-dependent tetraploidization

To address the trasformation potential of telomere-dependent tetraploidization, we created a POT1atet-OFF system to elicit transient telomere dysfunction, mimicking the temporary loss of telomere protection that is thought to occur early in tumorigenesis before telomerase activation. A tetracycline-inducible system was used to control POT1a expression in $POT1a^{F/-}POT1b^{F/F}$ MEFs. After induction of POT1a, the endogenous POT1a/b proteins were removed with Cre, clones were derived and two of them were chosen for further analysis, clone 19 and 26. Cells lacking POT1b have excessive single-stranded DNA at their telomeres but the telomeres do not elicit a DNA damage response and the cells proliferate normally (Hockemeyer et al., 2006). As expected, the loss of POT1a was accompanied by the accumulation of 53BP1 at telomeres as judged by the increase in number of colocalizations between telomeric DNA and 53BP1 or TIFs (telomere-dysfunction induced foci), phosphorylation of Chk1 and tetraploidization as measured by FACS (Fig. 2.32A, B). Tetraploidization was also evident in these cells from the supernumerary centrosomes and telomere clustering in interphase which are consistent with chromosome reduplication without chromosome segregation (Hockemeyer et al., 2006; Fig. 2.33A, B).

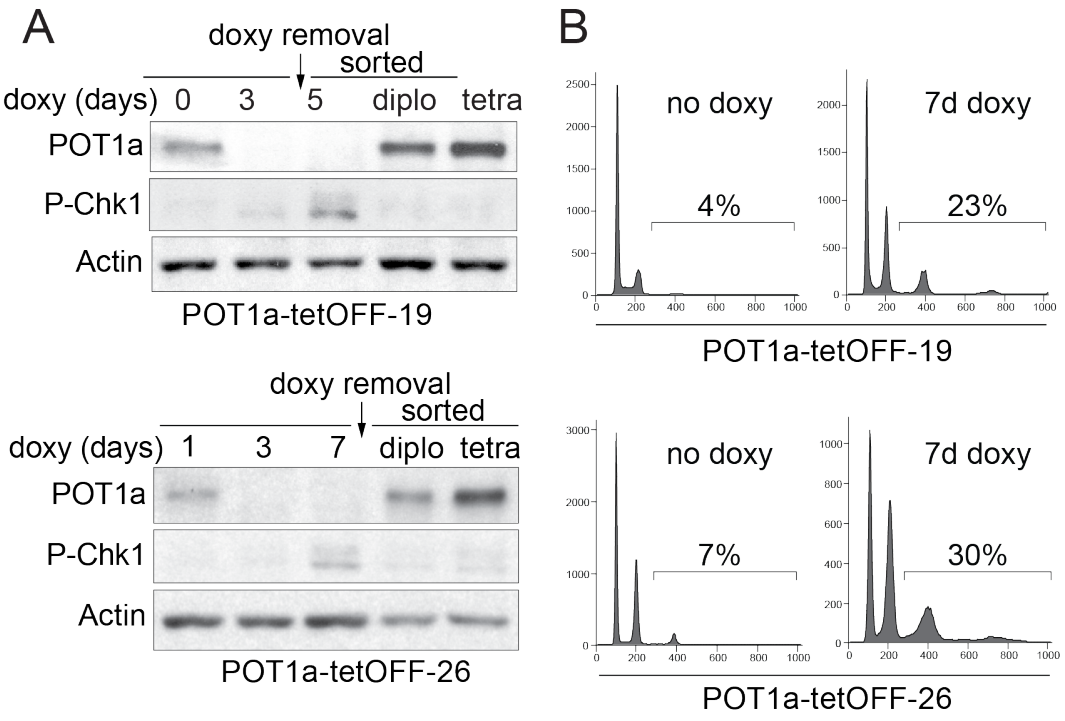

Figure 2.32: **Tet-OFF system for inducible expression of POT1a in MEFs.** (A, B) Immunoblot for Chk1 phosphorylation and POT1a in POT1a-tetOFF-19 and -26 cells (SV40-LT expressing MEFs) at the indicated time points after treatment with doxycycline and after release of the FACS-sorted diploid and tetraploid cells. POT1a-tetOFF clones 19 and 26 were treated with doxycycline for 10 days, FACS sorted after Hoechst 33342 staining, and cultured in the absence of doxycycline. (B) FACS analysis of POT1a-tetOFF-19 and -26 cells treated as in (A). The % of cells with >4N DNA content is indicated.

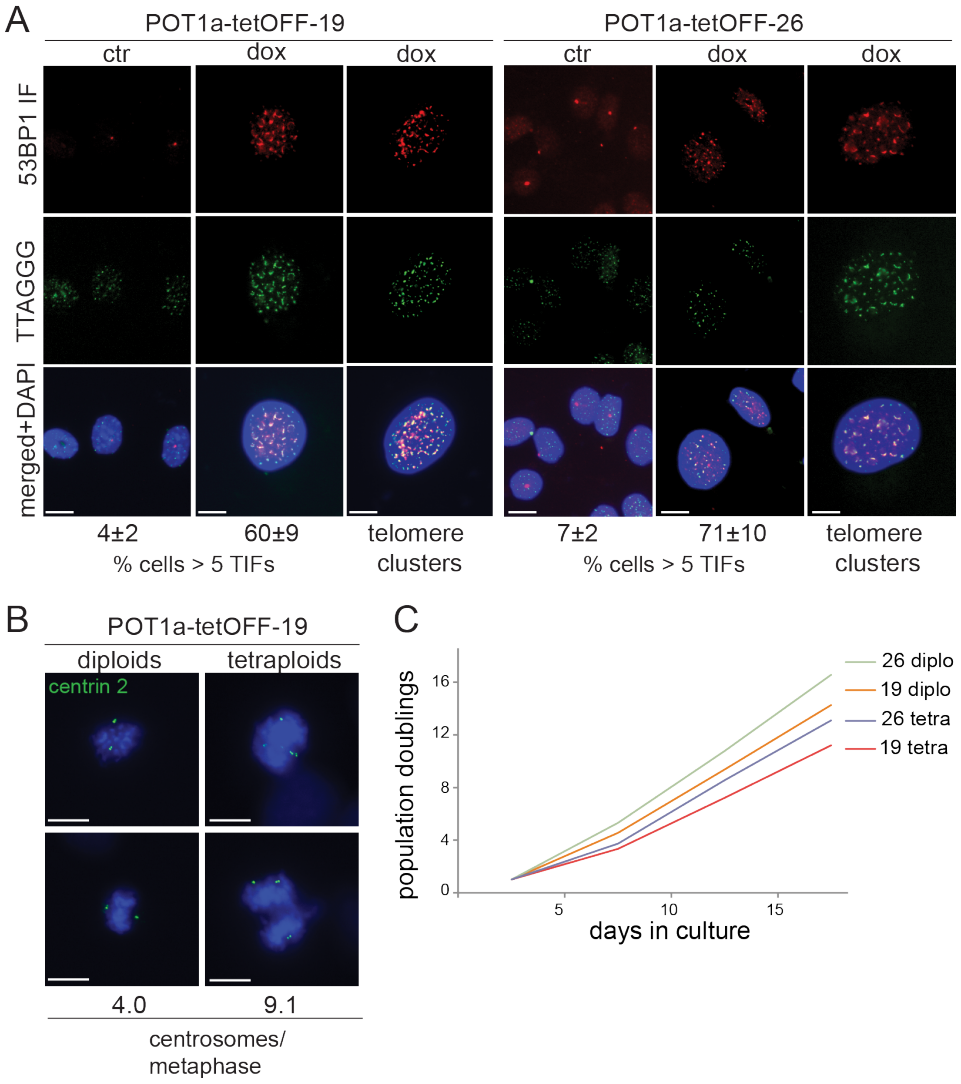

Figure 2.33: **Analysis of diploid and tetraploid cells derived from POT1a-tetOFF-19 and -26** (A) IF-FISH to detect telomere dysfunction in POT1a-tetOFF-19 and -26. Cells were treated with doxycycline and analyzed by IF for 53BP1 and telomeric FISH. Representative IF-FISH image and average % of cells with > 5 TIFs (Telomere Dysfunction Induced foci) for the indicated cells is shown. Examples of cells showing telomere clusters after doxycycline treatment are also shown for the two POT1atetOFF cell lines (right panels). (B) Centrosome amplification in tetraploid cells derived from POT1a-tetOFF-19 cells treated with doxycycline. Cells were analyzed by IF for centrin-2 staining and the average centrosome number is indicated. (C) Diploid and tetraploid cells derived from POT1a-tetOFF-19 and -26 were derived as in Fig. 2.32 and the shown growth curve was started after 5-7 days after sorting.

This system was used to test the ability of diploid and tetraploid cells to proliferate after restoration of telomere protection by POT1a. After 7 days of doxycycline treatment to repress POT1a, diploid (2N) and tetraploid (8N) cells were isolated by FACS-sorting (Fig. 2.34A). Removal of doxycycline allowed re-expression of POT1a and repressed Chk1 phosphorylation (Fig. 2.32A, B), indicative of restoration of telomere protection. The cell division cycles of the tetraploid and diploid populations were monitored by time lapse imaging using H2B-GFP to visualize chromatin (Fig. 2.34B, Movie 13). Approximately 90% of the diploid cells and ∼70% of tetraploid cells were able to progress through an apparently normal cell division cycle and gave rise to a viable progeny. Tetraploid cells proliferate at a slightly lower rate than diploid ones (Fig. 2.33C). Thus, the tetraploid cells generated by persistent telomere damage can re-establish normal cell division cycles and proliferate. As expected from the presence of supernumerary centrosomes in these cells (Fig. 2.1E and Fig. 2.33B), some of the tetraploid cell divisions showed multipolar spindles (Fig. 2.34B), predicting a greater rate of chromosome mis-segregation in these clones and higher rate of cell death.

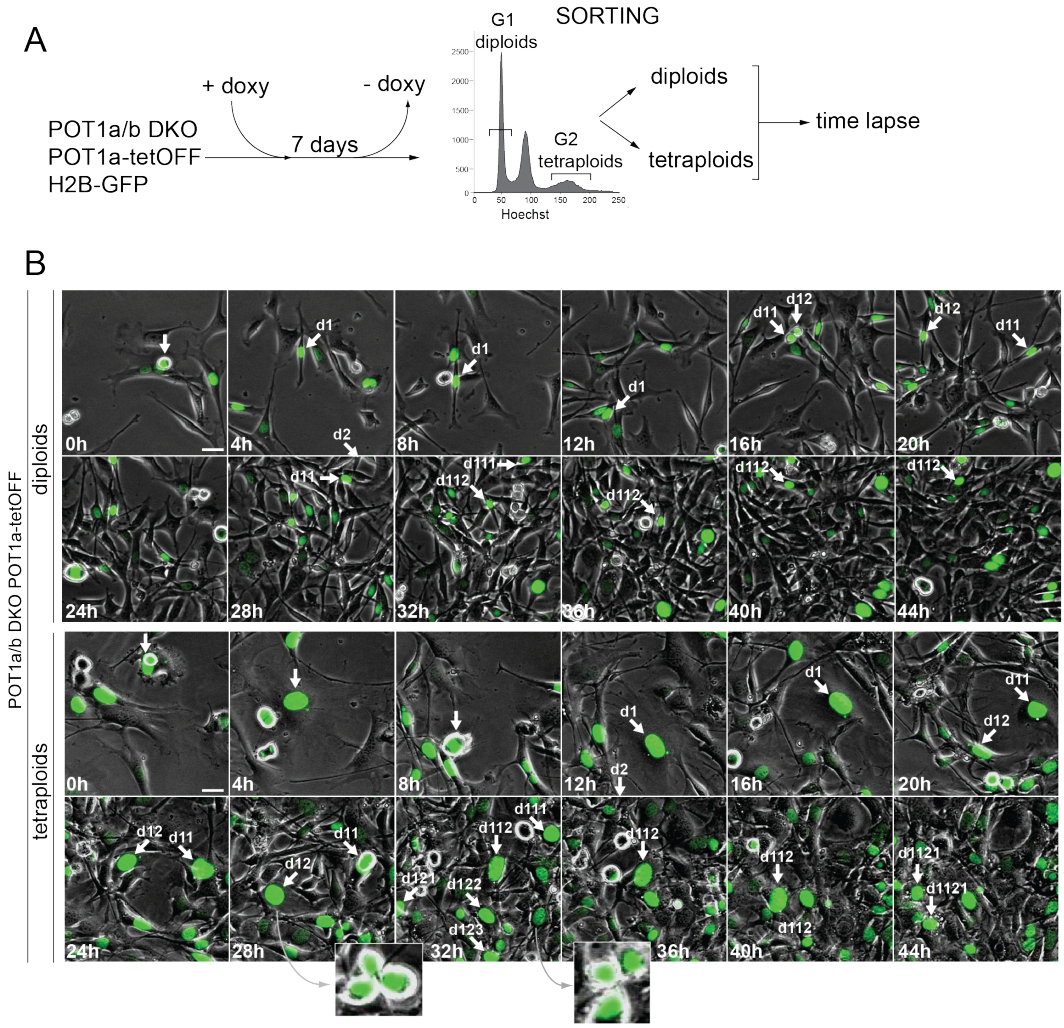

Figure 2.34: **Re-establishment of cell division cycles after tetraploidization.** (A) Schematics of the experimental approach. H2B-GFP expressing POT1a-tetOFF-19 cells were treated with doxycycline for 7 days to repress POT1a and stained with Hoechst and FACS-sorted for DNA content. G1 diploid cells (2N peak) and G2 tetraploid cells (8N peak) were separated, plated in the absence of doxycycline and monitored by time lapse imaging. (B) Cell divisions of diploid and tetraploid cells derived from clone 19 after re-expression of POT1a. Time lapse imaging of diploid and tetraploid cells expressing H2B-GFP was started 24 hours after doxyxcycline removal. Phase contrast and GFP-fluorescent images were taken every 15 minutes (Movie 13). Selected time points are shown. Arrows highlight a cell performing multiple cell divisions during the imaging session. Insets show evidence for multipolar mitoses.

2.3.2 Telomere-driven tetraploidization promotes transformation in mouse cells

We next used the POT1a-tetOFF system to determined the transformation potential of tetraploid cells generated after transient telomere damage. After doxycycline treatment, POT1a-tetOFF-19 and -26 cells were FACS-sorted based on Hoechst-staining for DNA content to derive tetraploid and diploid cells. The diploid and tetraploid cells were cultured for either 2 or 5-6 weeks in the absence of doxycycline, allowing POT1a re-expression (Fig. 2.32A). The results at these two time points were essentially the same.The resulting diploid and tetraploid cultures were tested for their ability to form colonies in soft-agar and tumors in nude mice (Fig. 2.35A, B). For both POT1a-tetOFF-19 and -26, the tetraploid descendants were more transformed based on both assays. The transformation efficiency after long term culture (5-6 weeks) was slightly higher than the one after short term culture (2 weeks). Overexpression of c-Myc further enhanced the transformation of diploid and tetraploid POT1a-tetOFF cells but even without this oncogene, the greater tumorigenic potential of the tetraploid population was significant (Fig. 2.32A, B). POT1atetOFF control cells not treated with doxycycline transformed at a rate similar to the sorted diploid cells. The increased transformation potential in the tetraploid cells was not due to increased proliferation rate, since the tetraploid cells grew slower than their diploid counterparts (Fig. 2.33C).

Figure 2.35: **Telomere-driven tetraploidy promotes cellular transformation in mouse cells.** (A, B) POT1a-tetOFF-19 and -26 with or without pBabe-Myc-ER were treated as in Fig. 2.32. FACS sorted diploid and tetraploid cells were expanded for 2 weeks or for 6-8 weeks and plated in soft-agar (A) or injected into nude mice (B). The soft-agar colonies were counted after 4 to 6 weeks. Myc-ER was induced with 0.5 μ M OHT. The average frequencies of tumor formation and latencies are indicated with standard deviation (3 or 4 experiments, 5 or 10 mice per experiment). Stars indicate a statistically significant difference ($p<0.05$ after paired Students t-test). (C, D) POT1a-tetOFF-19 cell line was stably transduced with H2B-GFP and treated as in (B). Tumors derived from diploid or tetraploid cells were harvested and GFP+ cells were FACS sorted. FACS analysis of unsorted cells derived from tumors formed by diploid or tetraploid cells (C) and sorted (GFP-positive and -negative) cells derived from a tumor formed by tetraploid cells (D) are shown. The GFP-negative cells are most likely cells derived from the host.

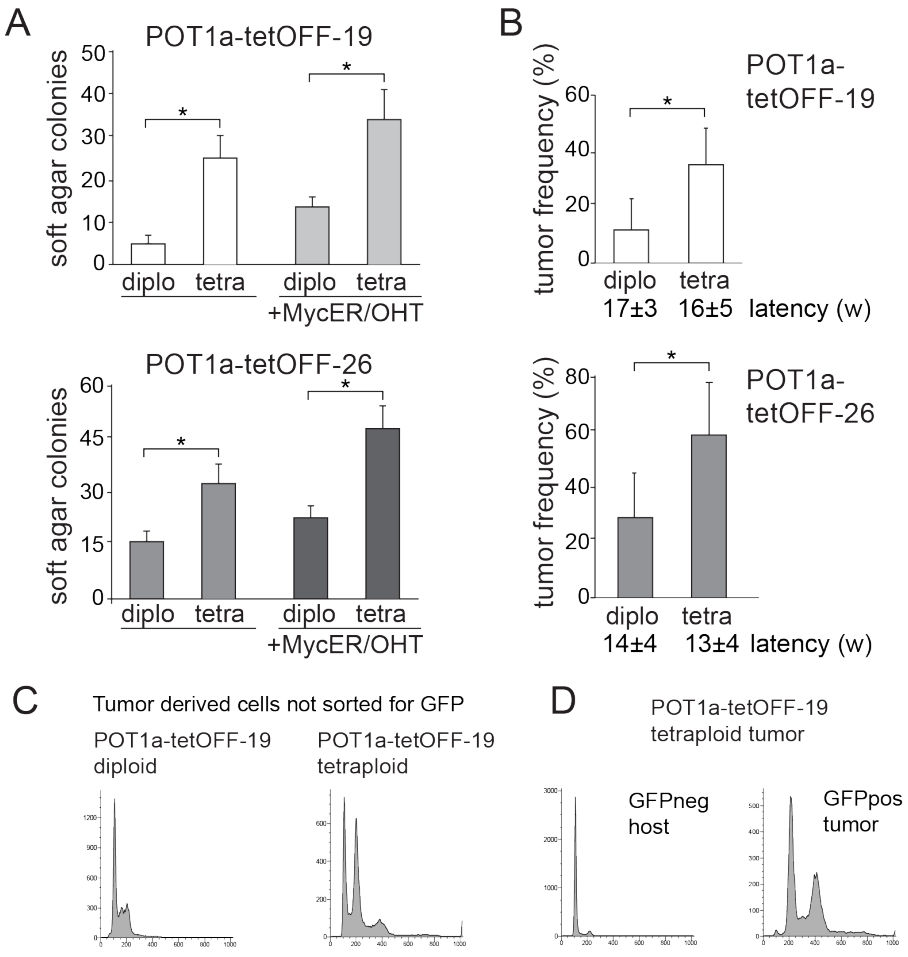
A
POT1a-tetOFF-19
soft agar colonies
50
40
30
20
10
0
*
*
diplo
tetra
diplo
tetra
+MycER/OHT
POT1a-tetOFF-26
soft agar colonies
60
45
30
15
0
*
*
diplo
tetra
diplo
tetra
+MycER/OHT
B
tumor frequency (%)
60
40
20
0
*
POT1a-
tetOFF-19
diplo
tetra
17±3
16±5
latency (w)
tumor frequency (%)
80
60
40
20
0
*
POT1a-
tetOFF-26
diplo
tetra
14±4
13±4
latency (w)
C
Tumor derived cells not sorted for GFP
POT1a-tetOFF-19
diploid
POT1a-tetOFF-19
tetraploid
D
POT1a-tetOFF-19
tetraploid tumor
GFPneg
host
GFPpos
tumor

2.3.3 Evolution of sub-tetraploid karyotypes

In order to monitor the karyotypic changes during tumor outgrowth, we established cell lines from tumors formed upon injection of diploid and tetraploid mouse cells. Prior to injection into nude mice, the cells were infected with the histone H2B-GFP construct allowing separation of tumor cells from host-derived cells present in the tumor mass. GFP-positive cells of tumors derived from injected tetraploid cells showed a tetraploid-like profile, consistent with their cells of origin (Fig. 2.35C, D). As expected, the host-derived GFP-negative cells showed a diploid-like profile. A total of eight GFP-positive cell lines were derived from tumors formed by the POT1a-tetOFF-19 and -26 tetraploid cells. Their chromosome numbers, determined after propagation of the cells for 7-10 days in culture revealed subtetraploid karyotypes, with the exception of one line which was hyper-tetraploid (chromosome number $\sim$120, Fig. 2.36A, B). Evolution of subtetraploid karyotypes had also occurred in three of four cell lines derived from soft-agar colonies formed by tetraploid POT1a-tetOFF-26 cells (Fig. 2.36C). As a control, cell lines established from a soft-agar colony and a tumor formed by diploid cells had a near-diploid karyotype (Fig. 2.36B, C). These results indicate that tetraploid cells generated through telomere dysfunction have a high rate of chromosome loss. In collaboration with Dr. Anna Jauch (University of Heidelberg) we performed spectral karyotyping (SKY) analysis of some of the tumor-derived cell lines. This analysis did not show any specific chromosome or group of chromosomes to be preferentially lost (Fig. 2.37). In addition, SKY analysis showed occasional translocations (Fig. 2.37), probably due to the low level of telomeric

fusions occurring in POT1a/b DKO cells.

Figure 2.36: **Evolution of subtetraploid karyotypes.** (A, B) Graphs indicating the number of chromosomes/metaphase in cells derived from tumors formed by diploid and tetraploid POT1a-tetOFF-19 and -26 cells (as in Fig. 2.35B). Cell lines were derived from tumors and metaphase spreads were analyzed after 7-10 day. The distribution of the chromosome number of POT1a-tetOFF diploid and tetraploid cells before injection and of cell lines derived from the indicated tumors derived from injected diploid or tetraploid cells is shown. (C) Graph indicating the number of chromosomes/metaphase in cells derived from soft-agar colonies formed by POT1a-tetOFF-26 (as in Fig. 2.35A). Statistical analysis (one-way ANOVA, Prism software) did not shown any preferential loss of a specific chromosome or group of chromosomes.

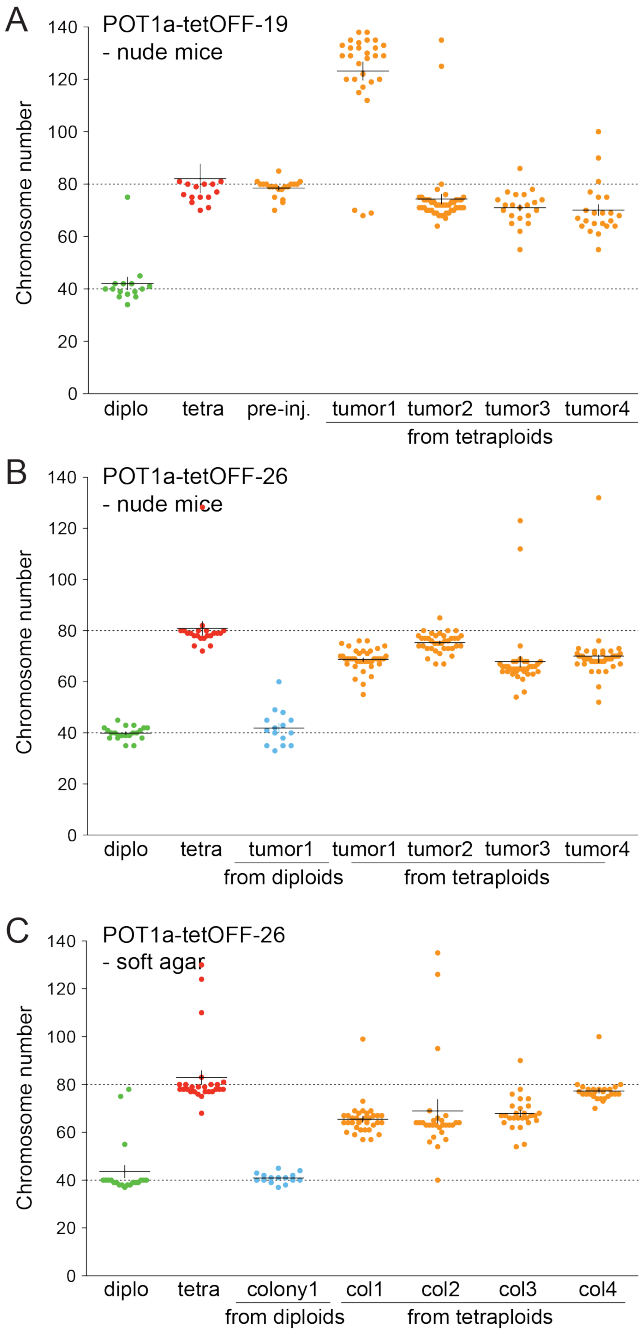
A
POT1a-tetOFF-19
- nude mice
Chromosome number
140
120
100
80
60
40
20
0
diplo
tetra
pre-inj.
tumor1
tumor2
tumor3
tumor4
from tetraploids
B
POT1a-tetOFF-26
- nude mice
Chromosome number
diplo
tetra
tumor1
tumor1
tumor2
tumor3
tumor4
from diploids
from tetraploids
C
POT1a-tetOFF-26
- soft agar
Chromosome number
diplo
tetra
colony1
col1
col2
col3
col4
from diploids
from tetraploids

It is interesting to note that subtetraploidy was also observed in in hMEC cells in telomere crisis. While 48RS-GSE22 p20 (early passage before crisis) showed a normal near-diploid chromosome number, when the same cells were analyzed during their progression through crisis (p26) we noticed an increase in the cells containing a near-tetraploid chromosome number, in agreement with FACS analysis (Fig. 2.38A and Fig. 2.19). Analysis of the chromosome number of 48RS-GSE22 cells progressing toward the plateau phase of crisis showed a decrease in the average number of chromosomes per cell, with most of the cells displaying a subtetraploid karyotype. Furthermore, we FACS sorted diploid and tetraploid cells by Hoechst staining from 48RS-GSE22 p25 and followed their growth in culture (Fig. 2.38B). Interestingly, while the growth curve of diploid cells plateaued 5-7 passages after the sorting, the tetraploid cell population was able to grow for about 10 additional passages before entering in the plateau phase (Fig. 2.38B). This result suggests that tetraploid cells can better sustain the genome instability deriving from telomere crisis, in agreement with the hypothesis of higher mutational robustness of polyploids compared to diploids. These data also suggest that clones potentially emerging from post crisis cells after hTERT activation or different mechanisms of telomere maintenance will be likely to display a subtetraploid karyotype.

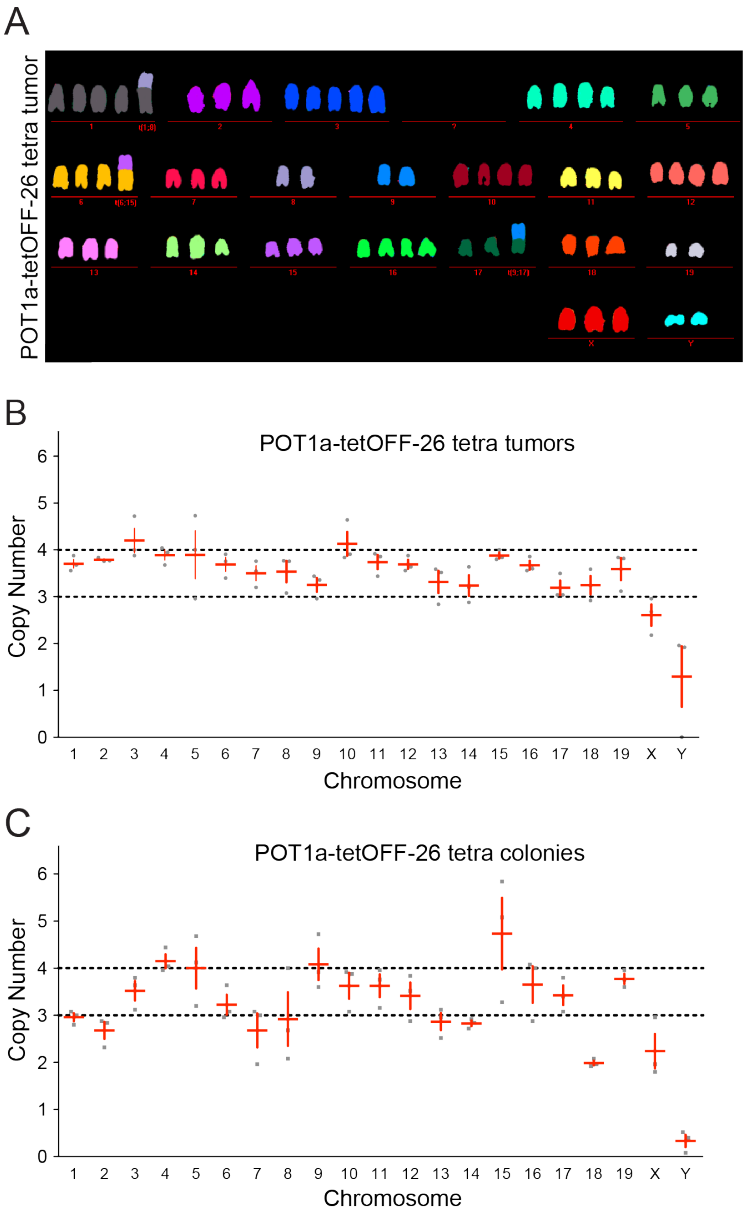

Figure 2.37: **SKY analysis of subtetraploid tumor-derived and colony-derived cell lines.** (A) Example of SKY analysis of POT1a-tetOFF-26-tetra tumor-1 cell line. (B) Cell lines derived from POT1atetOFF 26 tetra tumor 1, 2 and 3 were analyzed using SKY. The copy number for each chromosome was scored in each metaphase and is shown (grey spots). In red is the average value with standard deviation. (C) Cell lines derived from POT1atetOFF 26 tetra colonies 1, 2 and 4 were analyzed and plotted as in B.

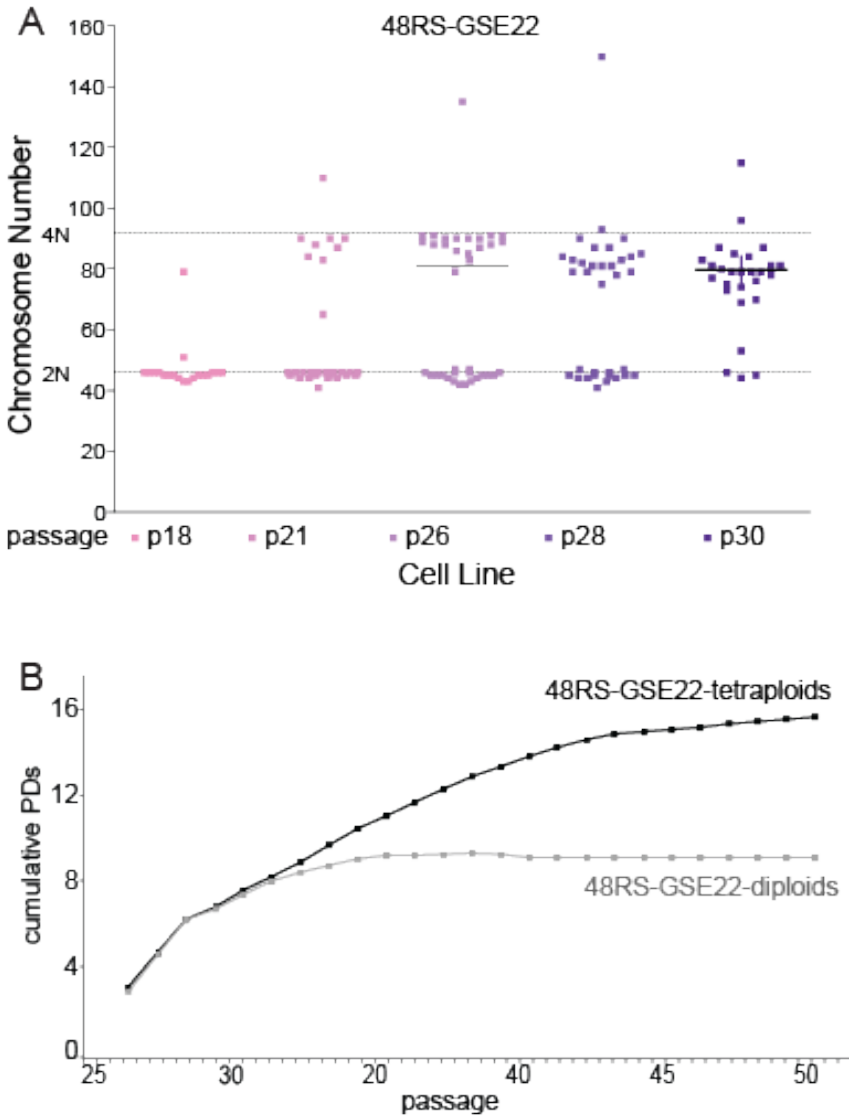

Figure 2.38: **Analysis of tetraploidy in hMECs in telomere crisis.** (A) hMECs 48RS GSE22 at the indicated passage were analyzed for chromosome number. (B) Diploid and tetraploid cells were FACS sorted from hMECs 48RS-GSE22 p26 and analyzed for proliferation. The growth curve is shown.

2.4 Evidence for telomere crisis in cancer cell lines with high chromosome number

If telomere dysfunction is the source of tetraploidy and subtetraploidy during tumorigenesis, it is expected that tumors with high chromosome numbers show features of prior telomere crisis. In order to test this hypothesis, we adapted a recently described method to amplify telomeric fusions (Capper et al., 2007; Letsolo et al., 2010; Lin et al., 2010). This method, called fusion PCR, is a PCR-based method to amplify products derived from end-to-end fusion of human chromosomes. The PCR is mediated by primers specific to the subtelomeres, DNA sequences immediately adjacent to terminal TTAGGG repeats in human chromosomes (Riethman et al., 2003). The PCR utilizes at least two subtelomere-specific primers, 5'-3'oriented toward the chromosome terminus, so that if an end-to-end fusion is present between the two chromosomes, a fusion product will be amplified, spanning from one subtelomere to the other, with the two head-to-head fused telomeres in between. The amplified telomeric fusions are then detected by Southern blotting with a subtelomeric specific probe (Fig. 2.39A). In human cells with a normal karyotype, no product amplification is expected, while in cells in telomere crisis, telomeric fusions should be amplified. The conditions for the PCR reaction are optimized for the amplification of long amplicons, however the amplification of smaller products containing a shorter tract of telomeric DNA will be anyway favored in the PCR reaction. The first described version of the fusion PCR made use of primers specific for the subtelomeres XpYp and 17p (Fig. 2.39A, (Capper

et al., 2007). The assay was proved to efficiently amplify fusion products in human cells in crisis, however it was limited to the detection of one type of telomeric fusion, occurring between two human chromosome arms. Ideally, a fusion PCR assay designed to estimate the frequency of telomeric fusions, should amplify all the possible fusions between human chromosomes. However, this is practically impossible since increasing the number of subtelomeric primers would also enormously increase the nonspecific products. A recently described modified version of the fusion PCR assay was designed to simultaneously detect multiple types of fusions by taking advantage of the fact that groups of human subtelomeres share the same or similar sequence (Riethman et al., 2003, Letsolo et al., 2010). Specifically, there are two families of subtelomeres sharing similar low-copy repetitive regions, called Tel Bam11 and Tel Bam 3.4 (Riethman et al., 2003).

Due to the presence of nonspecific bands and to the absence of an internal control in this assay, we set out to optimize the assay. We included the two well characterized primers specific for XpYp and 17p subtelomeres. We designed an internal control, represented by a 0.5 kb region amplified on the XpYp subtelomere by the XpYpM (primer also used to amplify fusions) and an additional reverse primer (XpYp-ctr2, Fig. 2.39B). Then we designed new primers and probes specific to the Tel Bam11 family of subtelomeres (called 21q family, which includes 21q, 5q, 10q, 17q and 22q) and the Tel Bam 3.4 family (called 16p family, which includes 16p, 9p, 15q and XqYq) (Fig. 2.39B). We tested these primers by using DNA extracted from hMECs 184B-GSE22 p20 in telomere crisis and the same cells immortalized at passage 9 by over-

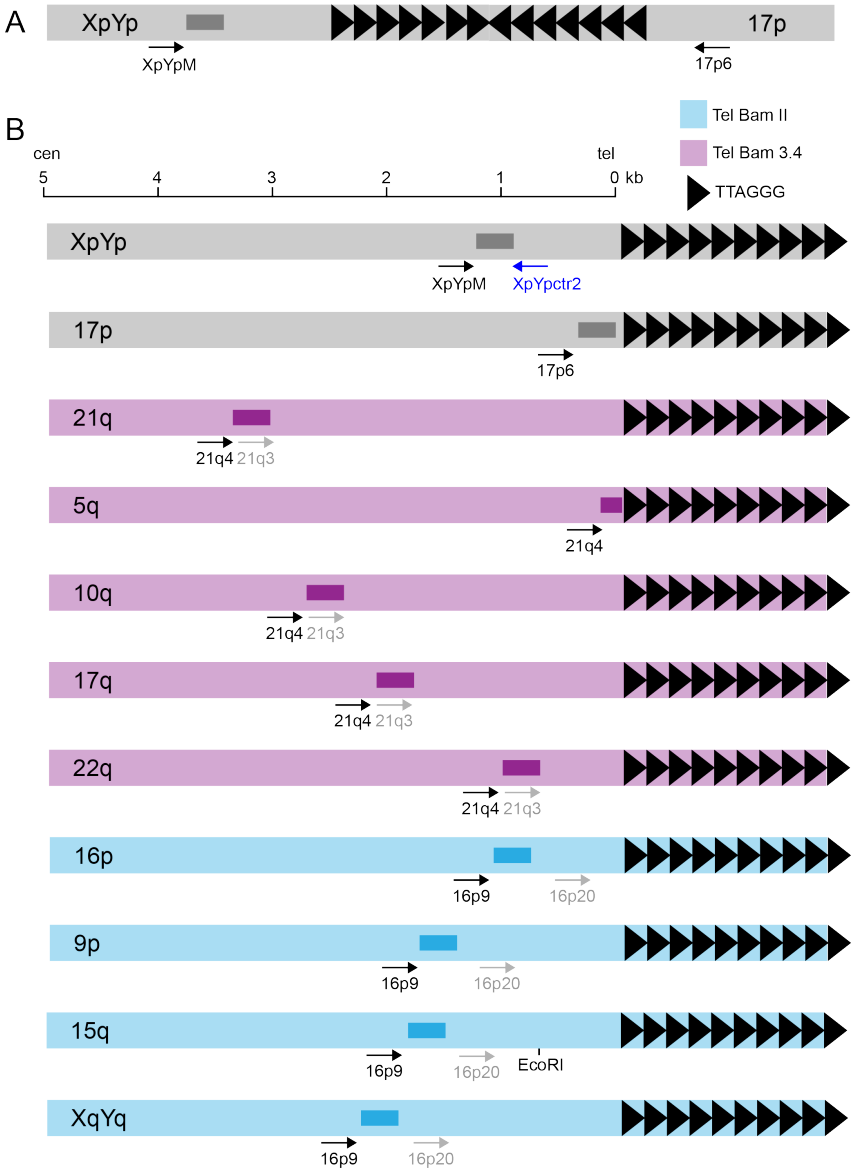

Figure 2.39: **Fusion PCR to detect telomeric fusions.** (A) Simplest version of the fusion PCR assay where two subtelomere specific primers, one specific for XpYp and the other specific for 17p are used together to detect potential fusions between these two chromosomes. The box in dark grey represents the XpYp specific probe. (B) Optimized fusion PCR assay. Primers for Tel Bam11 (21q) and Tel Bam3.4 (16p) subtelomere families are shown in black. Primers in grey are the primers used in the nested fusion PCR. Boxes in dark represents the probes used in the assay (for primers see Exp. Procedures). Distance of the primers from the start of the telomeric repeats is shown. The only EcoRI site in these subtelomeric regions is shown.

expression of telomerase (184B-GSE22 hTERT), which as expected resulted in telomere elongation. The primers were evaluated based on their ability to amplify telomeric fusions in crisis cells in the absence of nonspecific products in hTERT immortalized cells. As shown in Fig. 2.40A-B, the fusion PCR can amplify fusion products in 184B-GSE22 p20 in crisis, while no products are amplified by using DNA from 184B-GSE22 hTERT. In addition, progressively higher frequency of fusions are detected in 48RS-GSE22 hMECs progressing through crisis Fig. 2.40C. The internal control product on the XpYp arm shows that the efficiency of the PCR was similar in the different reactions.

Figure 2.40: **Increased telomere fusions in hMECs progressing through crisis.** (A) Fusions PCR assay using XpYp, 17p, 21q, 16p and XpYp-ctr primers in the indicated hMEC cell lines, expressing hTERT or in crisis (multiple repeats were performed in each case). 21q probe and XpYp probe (for the control) were used as shown. In the first two lanes of 184B GSE hTERT and 184B GSE p20, the PCR was performed without the control primer XpYp-ctr2. (B) Telomere blot for hMECs 184B GSE22 p9 before or after hTERT over-expression showing telomere elongation after hTERT expression. (C) Fusion PCR assay as in (A) in the indicated hMECs progressing through crisis.

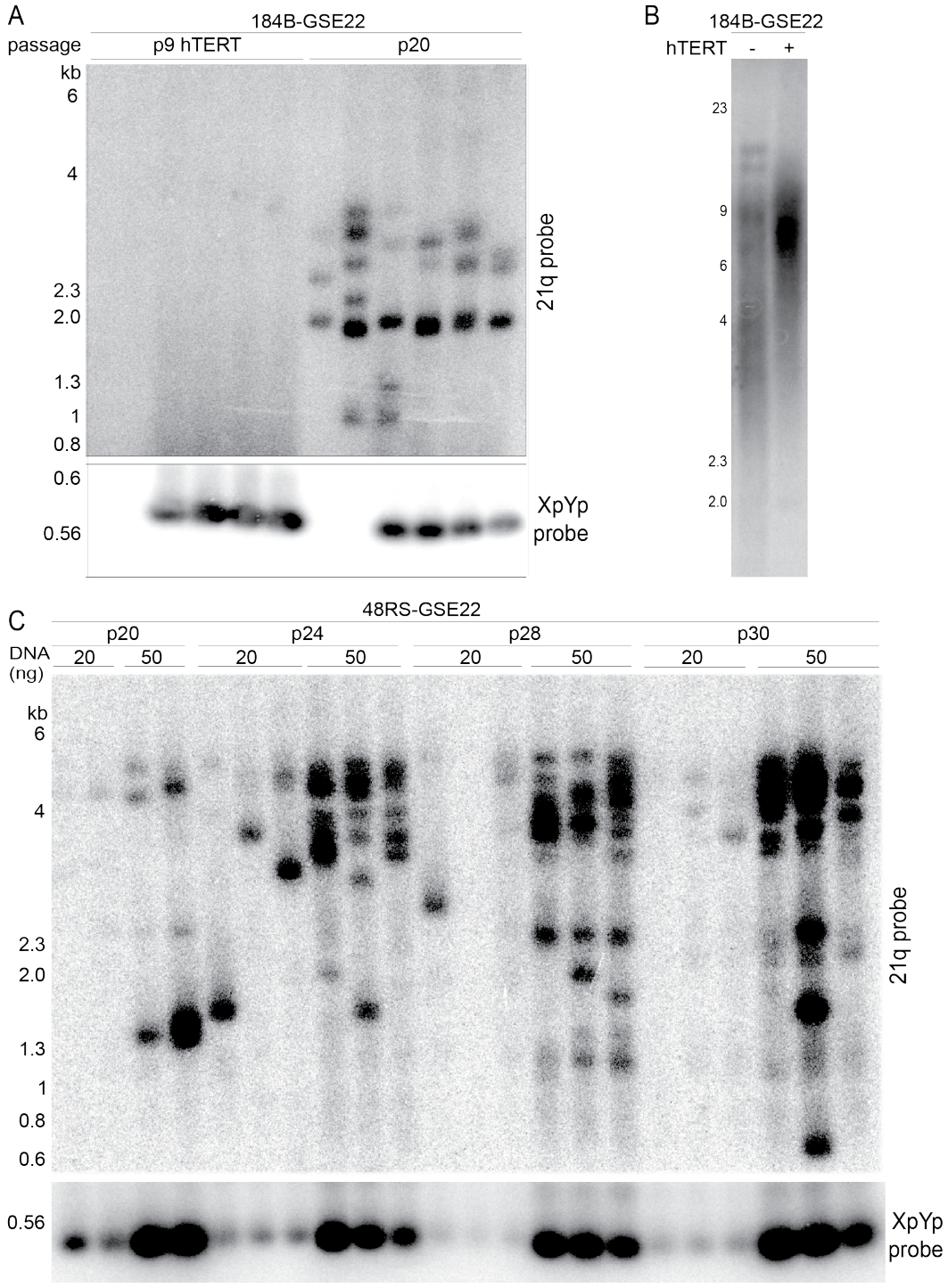
A
184B-GSE22
passage
p9 hTERT
p20
kb
6
4
2.3
2.0
1.3
1
0.8
0.6
0.56
21q probe
XpYp
probe
B
184B-GSE22
hTERT - +
23
9
6
4
2.3
2.0
C
48RS-GSE22
p20
p24
p28
p30
DNA
(ng)
20
50
20
50
20
50
20
50
kb
6
4
2.3
2.0
1.3
1
0.8
0.6
0.56
21q probe
XpYp
probe

Finally, to further verify the specificity of these products for subtelomeric and telomeric regions, we used nested PCR amplification of the fusion PCR product (Fig. 2.41). For each subtelomere family, nested primers were designed in the region adjacent to the primary primers 5'-3' oriented toward the telomere end (Fig. 2.41). Nested PCR was performed on the diluted PCR product of the primary PCR reaction. Also in this case, 184B GSE p20 or 184B GSE hTERT cells were used in parallel to test the specificity of the designed fusion PCR primers (Fig. 2.41). In some cases, the products of the nested PCR were sequenced in order to verify that they contained subtelomeric and telomeric regions. It is important to note that, even if we can readily amplify fusions from crisis cells, the efficiency of the method in detecting potential fusions is still low. In fact, the number of all possible fusions in a diploid human cell is 4560 (two by two combinations of the 92 telomeres), while the fusion PCR assay (using XpYp, 17p, 21q and 16p primers and 21q probe) theoretically detects only 165 potential fusions (1 in 28).

In order to apply the optimized fusion PCR to cancer-derived cell lines, we selected breast cancer cell lines with near-diploid or high chromosome numbers (Fig. 2.42). The near-diploid lines had an average chromosome number of 43-48, while the high chromosome number lines had an average chromosome number of 64 to 90 (one exception with 60 chromosomes). All the cell lines are derived from carcinoma of the breast, either from the primary site (breast) or from a metastatic site (pleural effusion). The cases known to be hereditary were excluded as well as cases where the patient was previously subjected to chemotherapy or radiation therapy.

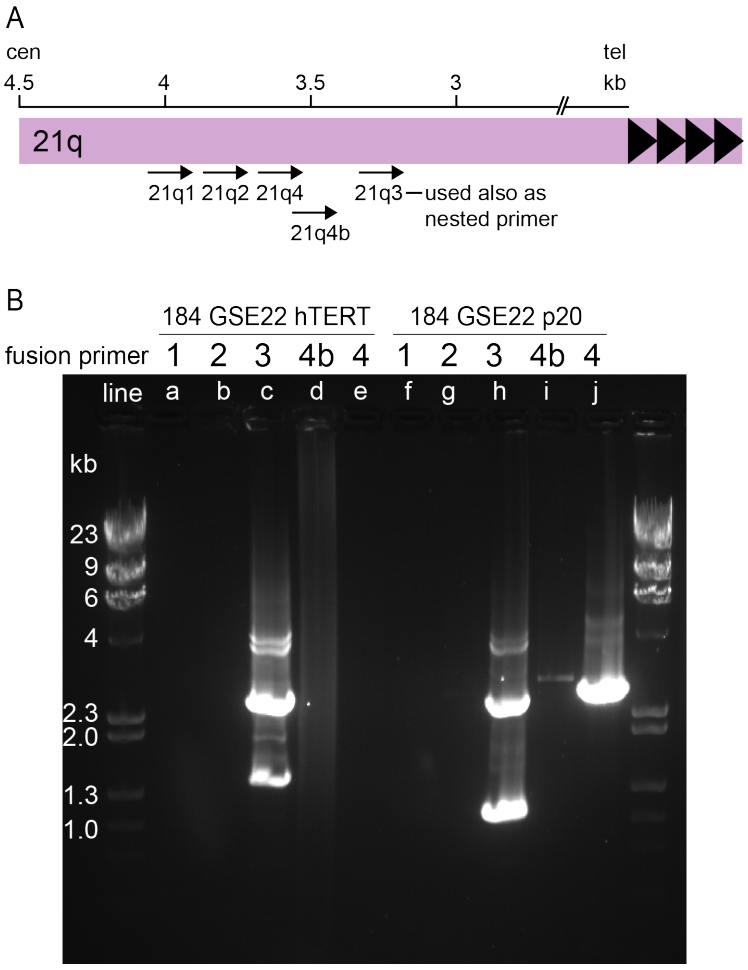

Figure 2.41: **Nested PCR to validate fusion PCR.** Fusion PCR was performed using only one of the 21q primers (recognizing telomeres in the Tel Bam11 family) represented in (A). A nested PCR was performed on of the product from the primary PCR using the 21q3 as a nested primer. The indicated cell lines were used, 184B GSE p20 in crisis and 184B GSE hTERT as negative control. The 5 primers used in the primary PCR were evaluated based on the presence of fusion products in crisis cells (p20) and absence of nonspecific products in the PCR performed on 184B GSE22 hTERT cells. PCR using 21q1 and 21q2 primers does not show products in cells in crisis (lines a, b, f, g) while primer 21q4b shows a product in the crisis cells but also some non specific products in hTERT expressing cells (lines d and i). The primer 21q4 is able to amplify a specific band from crisis cells in the absence of specific products in hTERT expressing cells (lines e and j) and is therefore the most specific.

Cell Line	ATCC#	Chromosome Number	Disease[a]	Site of Origin	Age (years)
HCC1500	CRL2329	near-diploid	IDC IIB	duct	32
MDA-MB-134-VI	HTB-23	43	DC	pleural effusion	47
MDA-MB-436	HTB-130	45	AC	pleural effusion	43
BT-20	HTB-19	43-53	DC	duct	74
BT-549	HTB-122	73-80	DC	duct	72
DU4475	HTB-123	85-95	DC	mammary gland	70
HCC1806	CRL-2335	65-79	SCC IIB	mammary gland	60
Hs 578T	HTB-126	50-77	Carc	mammary gland	74
MDA-231	HTB-26	52-68	AC	pleural effusion	51
MDA-468	HTB-132	60-67	AC	mammary gland	51
MCF-7	HTB-122	66-87	AC	pleural effusion	69
SK-BR-3	HTB-30	84	AC	pleural effusion	43

[a] IDC: invasive ductal carcinoma; DC: ductal carcinoma not specified; AC: adenocarcinoma; Carc: carcinoma IIB refers to the stage of the disease

Blue: near-diploid

Red: high chromosome number

Figure 2.42: **Breast cancer cel lines near diploid and with high chromosome numbers.** List of the breast cancer cell lines near diploid (blue) and with high chromosome number (red) and the corresponding chromosome number, type of cancer, site of origin and age. IDC: invasive ductal carcinoma; DC: ductal carcinoma not specified; AC: adenocarcinoma; Carc: carcinoma. IIB refers to the stage of the disease

Fusion PCR reactions were performed using the validated primers (Fig. 2.43 and Fig. 2.44). In order to quantify the number of telomeric fusions present in each cell line, we scored the number of bands appearing in each PCR reaction (performed in multiple repeats) and calculate the average number of fusions Fig. 2.45. Fusion PCR on these cell lines using different primer combinations showed a higher number of telomeric fusions in the cell lines with high chromosome numbers as compared to the near-diploid lines (Fig. 2.43 and Fig. 2.44). Quantification of the fusions products indicates that this difference is significant (Fig. 2.45).There was no correlation between the frequency of fusions and the stage or the origin of the cell line, being the primary tumor site or the metastatic one.

It is important to note that in many cases multiple repeats of the same PCR reaction did not result in the amplification of the same pattern of bands. This is probably due to the low efficiency of fusion detection by this assay and to the heterogeneity of the cancer cell population, which most likely contains multiple clonal cell populations, each with a different frequency of telomere fusions. When we estimated the 'real' number of fusions, considering the efficiency of the assay (detection of one fusion every 28), the number of fusions estimated was lower than 1 fusion per cell, even in the cell line with the highest number of fusions, BT 549 (1 estimated fusion every 80 cells). This result suggests that, if our estimate is correct, even in the cell lines that most likely have undergone crisis, only a small fraction of cells still contain telomeric fusions.

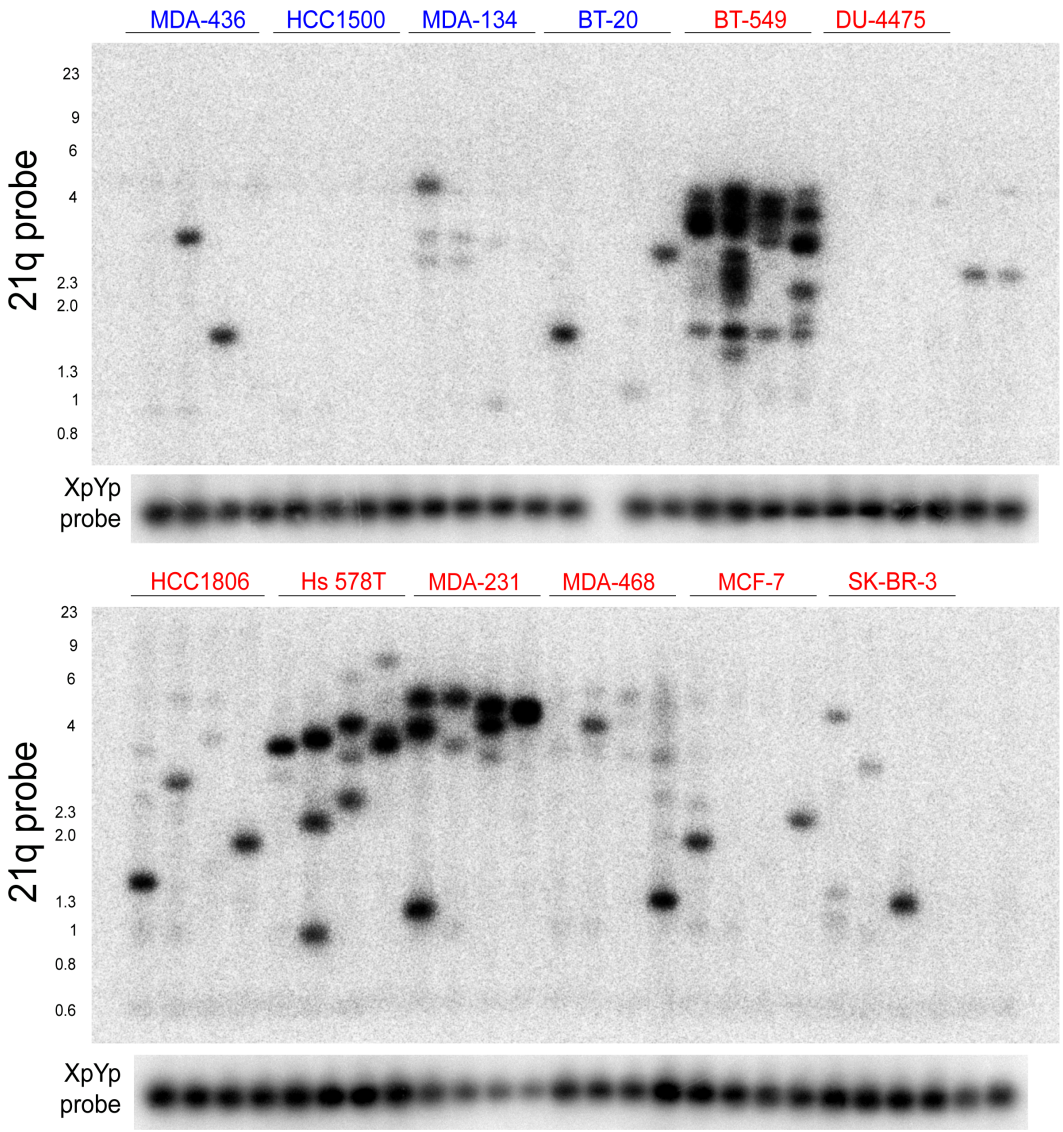

Figure 2.43: **First fusion PCR on breast cancer cell lines.** Fusion PCR was performed on breast cancer cell lines using primers specific for XpYp, 17p, 21q and XpYp-ctr. The indicated probes were used.

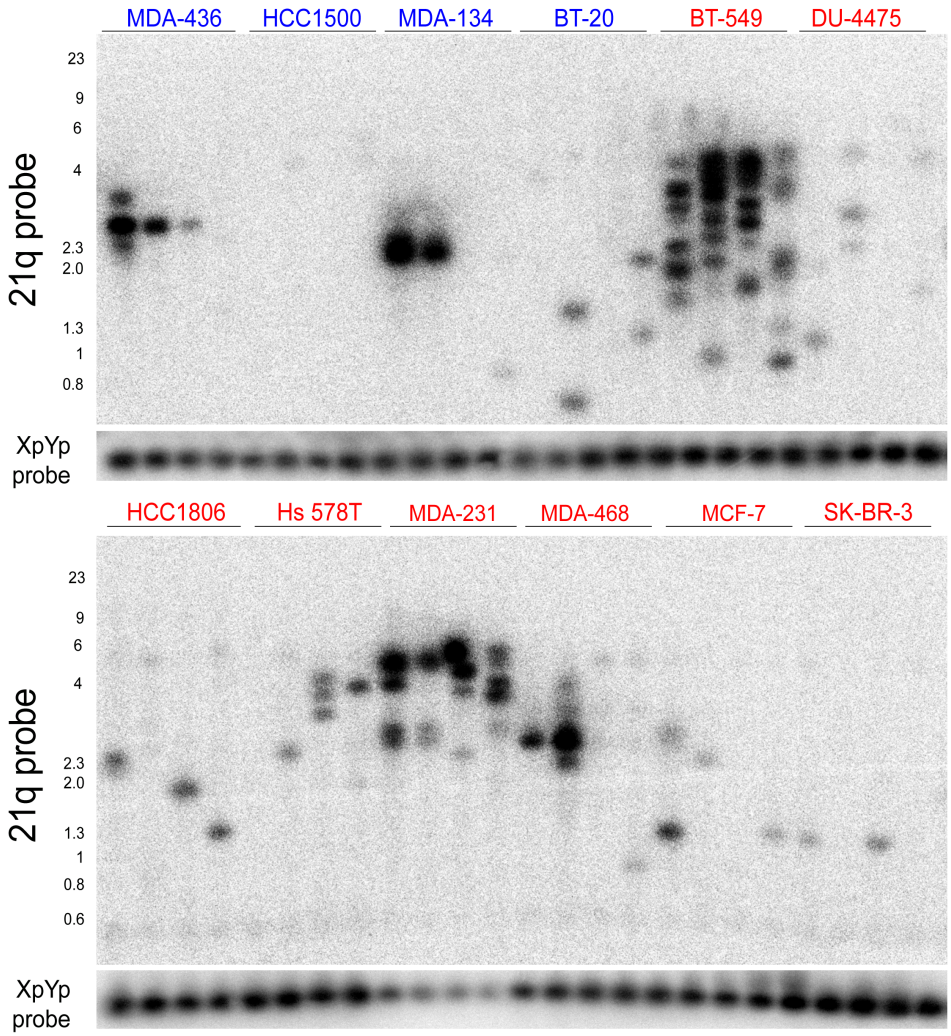

Figure 2.44: **Second fusion PCR on breast cancer cell lines.** Fusion PCR was performed on breast cancer cell lines using primers specific for XpYp, 17p, 21q, 16p and XpYp-ctr. The indicated probes were used.

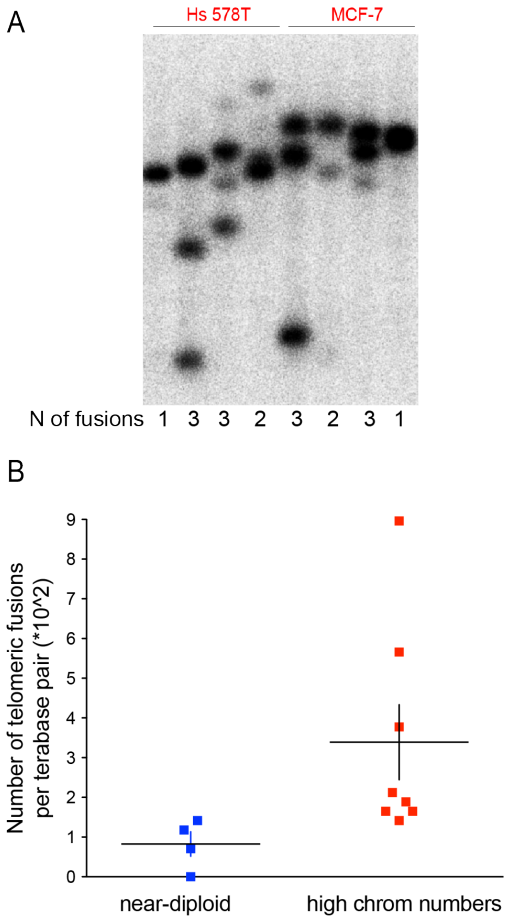

Figure 2.45: **Quantification of telomere fusions in breast cancer cell lines.** (A) Example of quantification of the number of telomeric fusions in two cancer cell lines. The quantification of the number of fusions is shown for each lane below the blot (each lane represents a repeat of the same fusion PCR reaction). The signal intensity of each band was quantified (ImageJ) and a minimum threshold of signal was applied (in each Southern blot) in order to decide whether to consider or not a band as a fusion or discard as background or nonspecific signal. (B) Quantification and statistical analysis of telomere fusions in breast cancer cell lines. Experiments shown in Fig. 2.43 and Fig. 2.44 were quantified as in (A) and the average number of fusions (per tera base-pair) was calculated for each cell line. T-test (Mann-Withney test) was applied (p=0.010).

Cell Line	ATCC#	Chromosome Number	Disease[a]	Site of Origin	Age (years)	Fusions (100Tb)	Est. Fusions (10^3 cells)	Est. Tel. Length (kb)
HCC1500	CRL2329	near-diploid	IDC IIB	duct	32	1.2	1.0	4-6
MDA-MB-134-VI	HTB-23	43	DC	pleural effusion	47	0	0	5-8
MDA-MB-436	HTB-130	45	AC	pleural effusion	43	0.7	0.6	4-6
BT-20	HTB-19	43-53	DC	duct	74	1.4	1.3	5-9
BT-549	HTB-122	73-80	DC	duct	72	8.9	13.2	2.5-5
DU4475	HTB-123	85-95	DC	mammary gland	70	1.9	3.2	3-6
HCC1806	CRL-2335	65-79	SCC IIB	mammary gland	60	1.6	2.3	3-5
Hs 578T	HTB-126	50-77	Carc	mammary gland	74	3.8	4.6	2.5-5
MDA-231	HTB-26	52-68	AC	pleural effusion	51	5.7	8.3	2.5-4
MDA-468	HTB-132	60-67	AC	mammary gland	51	2.1	2.4	2.5-4
MCF-7	HTB-122	66-87	AC	pleural effusion	69	1.6	2.0	3-5
SK-BR-3	HTB-30	84	AC	pleural effusion	43	1.4	2.2	5-9

[a] IDC: invasive ductal carcinoma; DC: ductal carcinoma not specified; AC: adenocarcinoma; Carc: carcinoma IIB refers to the stage of the disease

Blue: near-diploid

Red: high chromosome number

Figure 2.46: **Analysis of telomere fusions analysis in breast cancer cell lines.** For each cell line the average number of telomeric fusions was calculated as in Fig. 2.45. In addition, the average number of fusions per cell line was also calculated considering their ploidy (average number of chromosomes). The estimated number of fusions per line was calculated by multiplying the calculated number of fusions by 28, as the efficiency of fusion detection by this assay was calculated to be 1 in 28.

2.5 Telomere-independent sources of endoreduplication in cancer

Since endoreduplication seems to originate from the prolonged activation of the DNA damage signaling pathway independently of its source, we reasoned that other possible sources of persistent DNA damage might result in tetraploidy. Two cancer-relevant pathways resulting in DNA damage activation are defects in DNA damage repair factors such as BRCA1 and BRCA2 (required for homology-directed repair) inactivated in many hereditary breast and ovarian cancers, and abnormal activation of oncogenes such as Myc or Ras (Negrini et al., 2010). We set out to determined whether deregulation of these pathways was sufficient to induce endoreduplication-mediated polyploidy. We made use of MEFs conditionally deficient for BRCA2 ($BRCA2^{F/-}$ and littermate controls $BRCA2^{F/+}$), where BRCA2 genes can be conditionally inactivated after expression of Cre recombinase (Badie et al., 2010). $BRCA2^{F/-}$ and $BRCA2^{F/+}$ MEFs were immortalized by overexpression of TBX2, a suppressor of p16 and p19 pathways (Jacobs et al., 2000). BRCA2 deletion resulted in progressive increase of polyploidy from 1% to 12% or 18%, 10 or 12 days after Cre, respectively. Cre treatment had no effect on the level of polyploidy in control $BRCA2^{F/+}$, which remained at a basal level of 1-2% (Fig. 2.47A-B). As expected, treatment of $BRCA2^{F/-}$ cells with Cre resulted in accumulation of DNA damage lesions as judged by the accumulation of 53BP1 foci (Fig. 2.47C). FUCCI live cell imaging showed an increase from 2 to 14% of cells undergoing mitosis-independent geminin degradation, consistent with endoreduplication

cycles (Fig. 2.47D). No significant increase in mitotic failure was observed after BRCA2 loss (Fig. 2.47D and Movie 14).

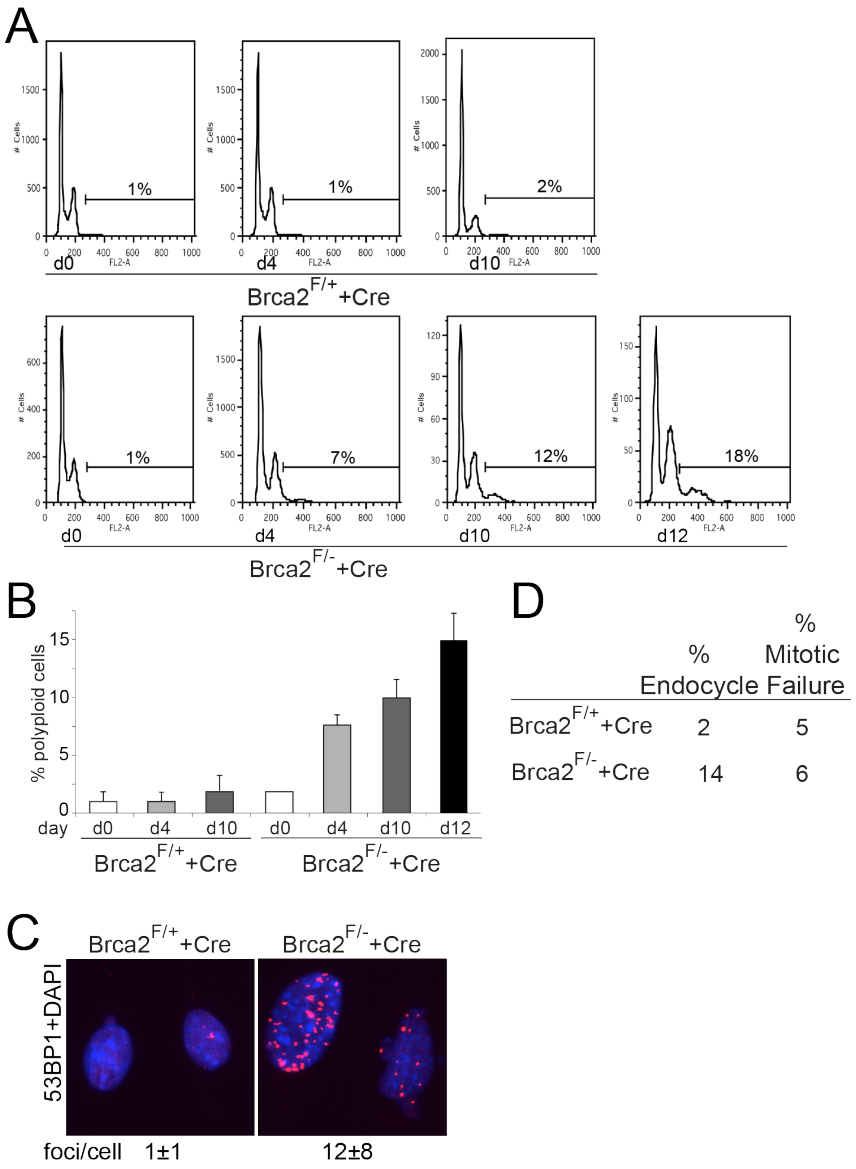

Figure 2.47: **BRCA2 deletion induces endoreduplication and tetraploidy.** (A, B) BRCA2$^{F/+}$ and BRCA2$^{F/-}$ MEFs overexpressing TBX2 (Badie et al., 2010) were treated with Cre and analyzed by FACS at the indicated time points. Quantification of three experiments is shown in B. (C) 53BP1 staining and quantification of the number of DNA damage foci per cell in the indicated cells. (D) Cells were treated as in (A) and analyzed with FUCCI imaging at day 8. Quantification of endoreduplication and mitotic cycles is shown.

We next examined the role of aberrant oncogene activation in inducing tetraploidization. The mutant form RasG12V (RasV12, Serrano et al., 1997), a constitutively active form, was overexpressed in human RPE cells. In order to inactivate p53 and Rb pathways, RPE cells were previously transduced with SV40-LT or with p21 shRNA and Rb shRNA. Overexpression of RasV12 in RPE cells lead to an accumulation of polyploid cells, whose percentage in the cell population increased from 2% to 14-17% (Fig. 2.48A-B). This result was expected since increase in tetraploidy has been described previously after Ras hyperactivation in human fibroblasts (Chicas et al., 2010). Activation of the DNA damage singnaling was confirmed by the increase of 53BP1 foci per cell in RasV12 overexpressing cells as compared to control cells (Fig. 2.48C). In order to determine the mechanism of polyploidization, RasV12 expressing cells and control cells were analyzed by live cell imaging. We observed an increase in endocycles after Ras overexpression, as suggested by the increase mitosis-independent geminin degradation events, from 4 to 12% (Fig. 2.48D and Movie15). In addition, we observed an increase in mitotic failure events from 5 to 10%, resulting in binucleated or multinucleated cells after RasV12 expression (Fig. 2.48D and Movie 15).

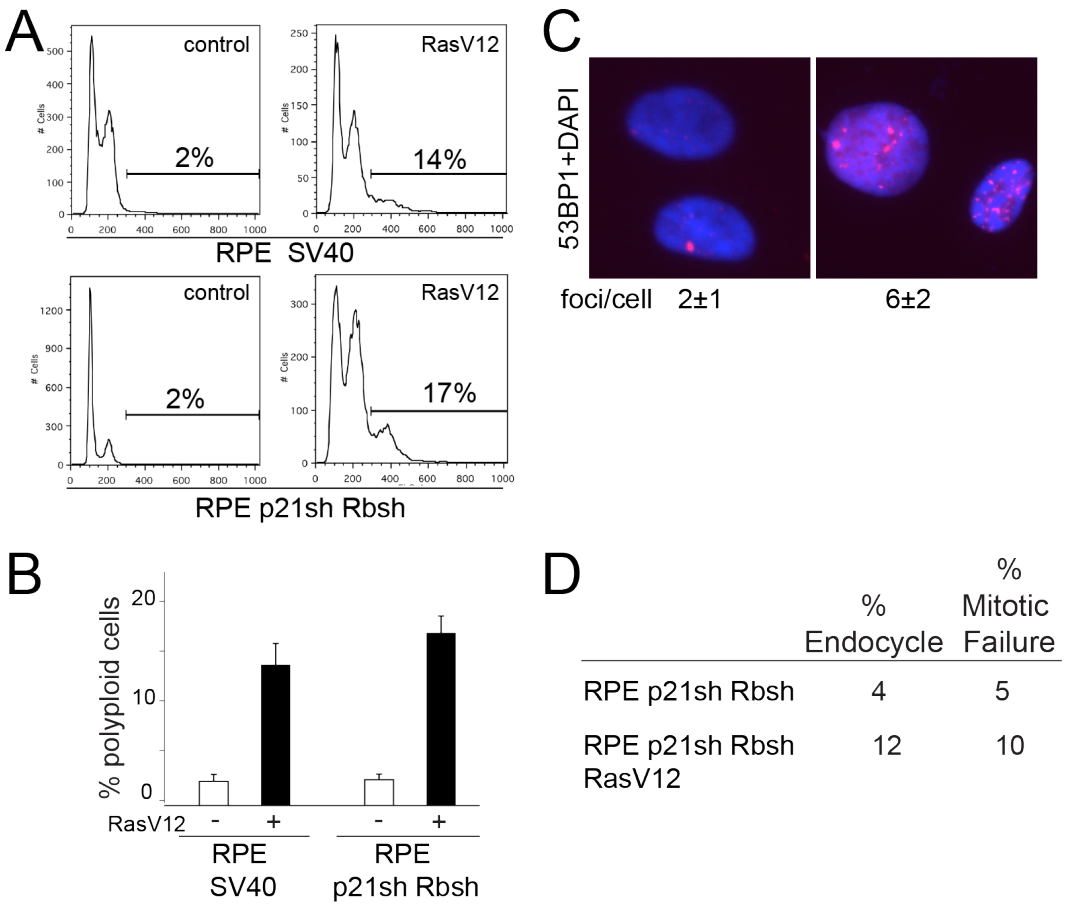

	% Endocycle	% Mitotic Failure
RPE p21sh Rbsh	4	5
RPE p21sh Rbsh RasV12	12	10

Figure 2.48: **Analysis of polyploidy after RasV12 over-expression.** (A) Human RPE cells were first transduced with SV40-LT or p21sh and Rbsh. Then cells were transduced for RasV12 overexpression and FACS analysis was performed 10 days after. (B) Quantification of polyploidy in three independent experiments is shown. (C) IF staining for 53BP1 positive DNA damage foci in the indicated cells. (D) Cells were treated as in (A) and analyzed by FUCCI live cell imaging starting one week after transduction with RasV12. Quantification of endoreduplication and mitotic failure is shown.

Chapter 3

Discussion

3.1 Model of telomere-induced tetraploidy during tumorigenesis

These data show that persistent telomere dysfunction can lead to tetraploidization and suggest a plausible scenario for the generation of aneuploid cancer cells with a sub-tetraploid chromosome number (Fig. 3.1). During the early stages of tumorigenesis, aberrant proliferation of precancerous cells leads to excessive telomere shortening. Very short telomeres will no longer contain sufficient telomeric DNA for their full protection resulting in activation of ATM and/or ATR mediated DNA damage signal (d'Adda di Fagagna et al., 2003). Such cells are normally expected to undergo permanent cell cycle arrest, with accompanying senescence or apoptosis. However, if cells can bypass this arrest, due to inactivation of the p53 and Rb pathways, cells will eventually enter telomere crisis which can eventually lead to tetraploidization. Tetraploidy dur-

ing telomere crisis in early tumorigenesis can result from endoreduplication cycles or failure in mitosis caused due to dicentric chromosomes (Fig. 3.1). We suggest that reactivation of telomerase (or other mechanisms of telomere maintenance) will allow the tetraploid clone to expand and evolve into a fully transformed cancerous state. The chromosome instability due to prior telomere dysfunction and the inherent high rate of chromosome mis-segregation of tetraploid cells will foster the evolution of a rearranged subtetraploid cancer karyotype.

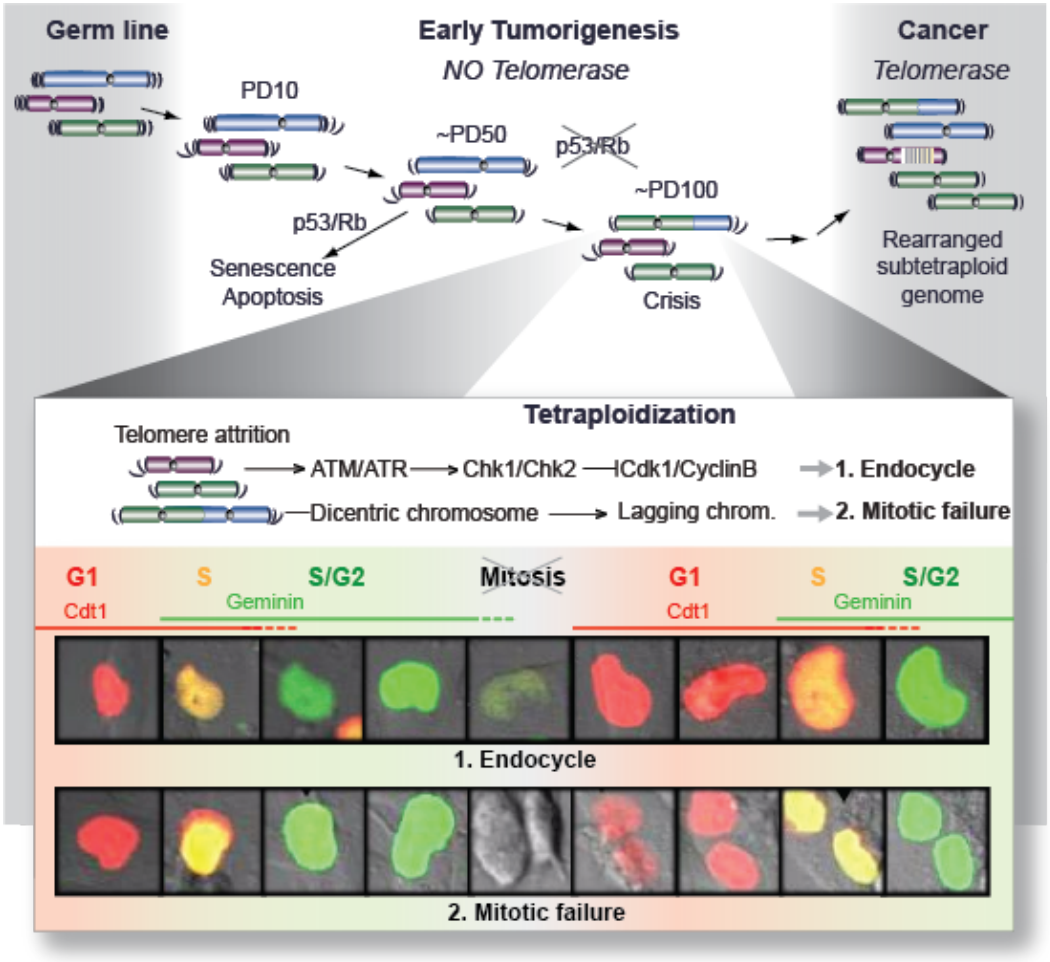

Figure 3.1: **Telomere-dependent tetraploidization during tumorigenesis.** The figure illustrates the process of telomere shortening in human somatic cells and its consequences for the development of an aneuploid tumor. Extensive telomere attrition in the absence of p53/Rb pathways can lead to tetraploidy through endoreduplication or mitotic failure. Photographs from FUCCI live-cell imaging of human cells in crisis undergoing endoreduplication or mitotic failure are shown. The endocycle, due to persistent telomere dysfunction, is characterized by alternating oscillations of Cdt1 (G1/early S) and geminin (S/G2) and by mitosis-independent geminin degradation. Mitotic failure, due to the presence of dicentric chromosomes, involves normal entry into mitosis and geminin degradation during anaphase, but cytokinesis is not completed resulting in a binucleated cell. In cancer, telomerase reactivation may allow proliferation of the tetraploid cells by reestablishing telomere protection. (PD, population doubling).

3.2 Endoreduplication cycles after POT1a/b deletion or prolonged genome-wide DNA damage

Normally when a cell experiences a DNA damage insult, the cell cycle is temporarily paused and DNA damage repair occurs. Once the DNA damage is repaired, the cell cycle resumes, a process called checkpoint recovery. This phenomenon is usually observed when cells are treated for a short period of time with a DNA damage-inducing agent or with sub-lethal doses of ionizing radiation (IR; van Vugt et al., 2004; Macurek et al., 2008; Geng et al., 2007). When DNA damage persists, a prolonged p53 and/or Rb mediated arrest occurs, resulting in senescence or apoptosis. Our data show that, if the DNA damage signal persists in the absence of functional p53 and Rb pathways, whole genome duplication can occur. Polyploidization is independent on the source of the damage, whether it is telomere-specific after POT1a/b loss or genome-wide induced by zeocin or other DNA damage inducing agents. In addition to being persistent, our data indicate that the DNA damage level must reach a threshold that we estimated to be around 15-20 lesions per cell. Several reports in literature are consistent with our findings, showing polyploidy after persistent exposure to DNA damage inducing agents (Bulavin et al., 1999; Illidge et al., 2000; Ivanov et al., 2003; Cortes and Pastor, 2003; Cantero et al., 2006; Puig et al., 2008; Cosimi et al., 2009; Nakayama et al., 2009). Our data are also in agreement with early observations on the uncoupling of S and M phase in IR-treated p21-deficient cells (Waldman et al., 1996; Lanni and

Jacks, 1998).

One point that is not completely clear and would require further investigation is why tetraploidy is more evident after POT1a/b deletion as compared to other genetic backgrounds where prolonged telomere dysfunction is induced such as after TRF2 deletion in Lig4-/- cells or after TRF1 inactivation (Sfeir et al., 2009). Upon POT1a/b depletion, ATR is activated resulting in both Chk1 and Chk2 activation. In the case of TRF2 deletion in Lig4-/- cells, the DNA damage signal depends only on ATM (not ATR), which activates Chk2, but not Chk1 (Denchi and de Lange, 2007). It is possible that the lack of ATR and Chk1 activation accounts for the lower level of tetraploidy after TRF2 deletion. On the other hand, TRF1 deletion does result in ATR and Chk1 activation due to replication fork stalling at telomeres (Sfeir et al., 2009). In this case, there are two possible reasons why tetraploidy is not induced. First, it is not completely clear whether the level of DNA damage signal persists during the cell cycle or, instead, the number of telomeres rendered dysfunctional by replication problems is higher during S-phase and decreases at the end of S-phase and in G1/G2. Second, the replication-induced DNA damage signal, which in the case of TRF1 depletion does not induce Chk2 activation, might be quantitatively different from the case of POT1a/b deletion and not sufficient to block of mitosis. Overall we can argue that the activation of both Chk1 and Chk2 and the persistence of the DNA damage through the cell cycle are necessary for the induction of endoreduplication, but further investigations would be necessary to fully understand the precise requirements of endoreduplication after DNA damage.

Our data shed light on the mechanism of tetraploidization induced after persistent activation of the DNA damage response. The endoreduplication cycle depends on the activation of ATM/ATR and downstream effector kinases Chk1 and Chk2. Chk1/Chk2 inhibit the phosphatase Cdc25C, normally required to remove the inhibitory phosphorylation on the mitotic kinase Cdk1/CyclinB. As a result, cells cannot enter mitosis and are blocked in G2. After a prolonged G2 phase, cells eventually switch to a state that is more similar to G1. Importantly, the DNA replication inhibitor geminin, which prevents re-replication in G2, is degraded despite the absence of mitosis. As a result of this altered state, cells re-enter S phase, despite the lack of progression through mitosis. Our findings are consistent with work in fission yeast and in human cells showing re-replication upon inhibition of the mitotic kinase Cdk/cyclin (Hayles et al., 1994; Kiang et al., 2009; Itzhaki et al., 1997). In addition, relicensing of replication origins in late G1 normally depends on low Cdk activity (Diffley, 2004). Thus, in our setting, a persistent state of low Cdk1/CyclinB activity can allow re-replication. We also find that Cdh1 is important for endoreduplication, most likely because it mediates the degradation of geminin. An unsolved question is how APC/Cdh1 is activated in this setting. Previous work indicates that APC/Cdh1 can be activated by the DNA damage response through a mechanism involving Cdc14B phosphatase (Bassermann et al., 2008). In the context of telomere damage, however, the degradation of geminin may simply be due to a gradual rise in APC/Cdh1 activity during the prolonged post-replication period without Cdk1/CyclinB. Normally, during mitosis Cdk1/CyclinB dependent phosphorylation promotes APC/Cdc20 ac-

tivation (Lukas et al., 1999; Kraft et al., 2003) but strongly inhibits APC/Cdh1 (Zachariae et al., 1998), allowing their sequential activation in the cell cycle. In fact, at the beginning of mitosis, the high activity of Cdk1/CyclinB promotes the activation of APC/Cdc20 complex while it inhibits APC/Cdh1 activation. APC/Cdc20-mediated degradation of CyclinB at the metaphase-to-anaphase transition leads to the inhibition of Cdk1/CyclinB, allowing the activation of APC/Cdh1 complex at the end of mitosis and in early G1. Therefore, our context, where Cdk1 activity is continuously low, is expected to be permissive for APC/Cdh1 activation, while APC/Cdc20 activation is prevented. The regulation of the kinetics of APC/Cdh1 activation and geminin degradation during the DNA damage-induced endoreduplication cycle remain to be determined.

Many similarities appear between the developmentally planned endocycles in placental trophoblasts and the endocycle induced after telomere dysfunction (Ullah et al., 2009). First, in both cases, the transition to endocycle is initiated by inhibition of the mitotic kinase Cdk1/CyclinB, mediated by the increased levels of the inhibitor p57 in trophoblasts (Ullah et al., 2008) and by the DNA damage checkpoint after telomere dysfunction. Second, APC/Cdh1 activity plays a significant role in both kinds of endocycles allowing degradation of the replication inhibitor geminin and re-entry in the absence of mitosis. Importantly, Cdh1 is required for the endocycle of placental trophoblasts and in the Drosophila salivary gland (Garcia-Higuera et al., 2008; Narbonne-Reveau et al., 2008; Zielke et al., 2008; Li et al., 2008). Finally, activity of the S-phase complex Cdk2/CyclinE is important for endoreduplication to mediate periodic DNA re-replication (Geng et al., 2003; Ullah et al., 2008). Based on

these similarities, we can argue that a developmentally planned variation of the cell cycle, might be aberrantly triggered by persistent DNA damage in somatic cells, if p53 and Rb are inactive.

3.3 Mechanism of tetraploidization after natural telomere shortening

Our data indicate that tetraploidization is not restricted to telomere deprotection after inactivation of POT1a/b (or TRF2), but can occur in the cancer relevant context of telomere crisis. Not only fibroblasts, but also epithelial cells, which are more likely to represent the cell of origin of solid tumors, can undergo polyploidization after telomere erosion. In agreement with our findings, polyploidy occurs in human cancer cells after impairment of telomerase (Pantic et al., 2006), although here the mechanism is not known. Similarly, an increase in polyploidy has been reported in human cells after extensived telomere shortening (Shay and Wright, 1989; der-Sarkissian et al., 2004; Shay et al., 1993). Consistent with a role of p53 and Rb in blocking tetraploidization, polyploidy is rare in senescence, where most of the cells arrest in a G1-like state (Saksela and Moorhead, 1963; Benn, 1976).

There are a number of differences between crisis cells and POT1a/b DKO cells. For instance, removal of POT1a from mouse telomeres exposes the single-stranded DNA and permanently activates the ATR kinase pathway whereas critically shortened telomeres may be expected to lose several (or all) shelterin proteins rather than POT1 alone and are known to activate both ATM and

ATR signaling (d'Adda di Fagagna et al., 2003). It is also unlikely that all telomeres in crisis become dysfunctional at the same time so that the overall level of the DNA damage signal elicited by telomere crisis might be less than in the POT1a knockout cells. Furthermore, rather than the irreparable damage at all telomeres generated by POT1a deletion, critically shortened telomeres are likely to be repaired by end-to-end fusion and the resulting damage signal at each telomere is therefore expected to be transient. These differences can explain the mechanism of tetraploidization of crisis cells, compared to POT1a/b DKO cells. Human cells in crisis undergo tetraploidization not only through endoreduplication, but also through mitotic failure. Epithelial cells are more prone to mitotic failure than endoreduplication, while the opposite is true for fibroblasts.

Which are the factors determining the frequency of endoreduplication versus mitotic failure? First, the DNA damage threshold necessary for a Chk1/Chk2-mediated block of Cdk1/CyclinB and entry into mitosis will important in determining whether a cell in crisis will bypass mitosis and enter endocycle or will enter mitosis. Compared to the p53/Rb mediated G1/S arrest in senescence, a higher number of dysfunctional telomeres is probably necessary for the Chk1/Chk2-mediated arrest in G2 (Jeyapalan et al., 2007; Deckbar et al., 2007). In fibroblasts we estimate a threshold for endocycle, and thus for prolonged arrest in G2 and block of mitosis, of 15-20 DNA damage foci per cell. This threshold seems to be reached in a fraction of the fibroblasts in crisis, most likely undergoing endoreduplication. This DNA damage threshold is likely to be cell type specific and our data suggest that it might be higher

in epithelial cells, which are less prone to undergo endoreduplication than fibroblasts after zeocin treatment or in telomere crisis. If this threshold is not reached, it is possible that the cells will continue

Second, the occurrence of mitotic failure versus endoreduplication in crisis will depend on the occurrence of telomeric fusions. The accumulation of critically short unprotected telomeres will promote prolonged activation of the DNA damage response signal and endocycle entry. Conversely, chromosome fusion would silence the DNA damage signal, promote entry into mitosis and mitotic failure. The two scenarios are outlined by TRF2 versus POT1a/b deletion. In TRF2 deficient cells, the unprotected telomeres are aberrantly repaired by NHEJ-mediated fusion and polyploidization is mostly due to failure in mitosis, as evident by frequent anaphase bridges in mitotic cells (van Steensel et al., 1998; Celli and de Lange, 2005; Lazzerini Denchi et al., 2006). This NHEJ reaction quickly silence the telomeric DNA damage signal in TRF2 deficient cells. Instead, the DNA damage created by POT1a/b loss at telomeres can not be repaired since the presence of TRF2 continues to block NHEJ, thus the signal persists. The mechanism of fusions of very short telomeres is unclear both in human and mouse cells (in late generation Terc-/- mice), where it does not depend on the classical NHEJ pathway (Maser et al., 2007).

Third, an important point relates to the consequences of dicentric chromosomes in mitosis. If the dicentric breaks before or during mitosis, the cell will complete mitosis and undergo a BFB cycle, while if the dicentric remains intact, it can impede mitotic furrow completion, resulting in tetraploidy. In S. cerevisiae, an elegant analysis of the fate of a single dicentric chromosome

suggest that dicentrics have the tendency to break, and preferentially do so at the telomere fusion point. This pathway would allow fused chromosomes to be segregated normally, avoiding chromosome imbalances in the daughter cells (Pobiega and Marcand, 2010). No failure in mitosis was described in this study and the mechanism and the cell cycle stage where the break is induced is not known. In mammals, tracing a dicentric is impossible due to the lack of appropriate genetic systems. The only possible approach that was followed involved the integration of a plasmid containing a negative selection marker close to the telomere of one chromosome in a cancer cell line. Analysis of clones that had lost the selection marker (due to telomere loss) allowed studying the fate of a single dysfunctional telomere (Fouladi et al., 2000; Lo et al., 2002). A similar approach was used in mouse ES cells, where a break could be induced close to the telomere ends of two chromosomes (Lo et al., 2002). The most frequent outcome of the induction of one or two dysfunctional telomeres was the formation of dicentric chromosomes most likely due sister-chromatid fusions. Non reciprocal translocations and fusions to different chromosomes was also observed, albeit with less frequency. In these studies, polyploidy was not evident, suggesting that one (or possibly two in mouse cells) is probably insufficient to induce failure in mitosis. However, a more detailed analysis of the consequences of one or more dicentric chromosomes in mitosis during one or two cell cycles (for example by time lapse imaging) is necessary to derive any conclusion.

In our imaging experiments, we noticed that in some cases after mitosis, the two daughter cells remained linked by a sort of bridge, presumably formed by

a dicentric, until the following G1 phase. Interestingly, sometimes this bridge disappeared in the following G1 or S phase and the daughter cells separated, while in other cases the cells were pulled together to form a binucleated cell. We can speculate that dicentrics can break in G1 or S phase and this would determine whether two diploid cells or a single binucleated tetraploid cell would form. Finally, an unsolved question is how the mechanism of tetraploidy (endocycle or mitotic failure) can influence the viability and proliferation of the cell progeny. This could be investigated by live-cell imaging, even though it would require very long imaging time, which can be technically challenging.

3.4 Transformation potential of tetraploid cells

Tetraploidization was initially shown to promote transformation in mouse epithelial cells with inactive p53 (Fujiwara et al., 2005). In that study, tetraploidy was induced by failure in cytokinesis after treatment with an actin inhibitor. Subsequently, tetraploidy was shown to promote transformation in a variety of different contexts and model systems. For example, polyploidy induced after overexpression of the oncogenic kinase Pim1 was shown to promote tumorigenesis in human prostate and mammary epithelial cells (Roh et al., 2008). Inactivation of the APC inhibitor Emi1 in zebrafish induces endoreduplication and cooperates with p53 in tumor development (Rhodes et al., 2009). Similarly, a mutant form of separase in the same model organism induces polyploidy and increases susceptibility to epithelial carcinogenesis with near-tetraploid karyotypes (Shepard et al., 2007). Our data show that also in the

case of telomere-driven tetraploidy, once telomere protection is re-established, the tetraploid cells can proliferate and have a higher transformation potential compared to diploid cells. Interestingly, the karyotype of the tumor-derived cell lines displayed subtetraploid chromosome number, resembling human tumors with high chromosome numbers. Additionally, in human hMECs during telomere crisis we found frequent metaphases containing subtetraploid chromosome numbers. Subtetraploid karyotypes (75-85 chromosomes) in hMECs in crisis are likely to derive from transient tetraploidization followed by chromosome loss and not from accumulation of chromosome gains in diploid cells as tetraploidization precedes the occurrence of subtetraploidy during crisis and intermediate chromosome numbers between diploid and subtetraploid values are rare.

One question that remains is why tetraploid cells have a greater transformation potential than diploid ones and how they evolve toward aneuploidy. Chromosomal instability (CIN) in tetraploid cells has been proposed as an important factor in promoting transformation and tumorigenesis ((Boveri, T., 1914, Shackney et al., 1989, Fujiwara et al., 2005). In the context of telomere crisis, tetraploidy is coupled with other kinds of telomere dysfunction-related genome instability so it is difficult to distinguish between these two interrelated phenomena (Artandi et al., 2000; Maser and DePinho, 2002). In our case of transient POT1a depletion, tetraploidization occurs through endocycle and telomere fusions are rare in this setting (Hockemeyer et al., 2006). However, we cannot formally rule out the possibility that telomere fusions contribute to transformation in this setting as occasional fusion events are observed by SKY

in the tumor-derived subtetraploid cell lines.

The increased number of centrosomes deriving from tetraploidy has been proposed as a source of CIN since Theodore Boveris idea nearly 100 years ago (Boveri, T., 1914). In recent years, a molecular mechanism for the occurrence of chromosomal instability in tetraploid cells has been demonstrated (Ganem et al., 2009; Silkworth et al., 2009). In most tetraploid cells analyzed, multiple centrosomes form a transient multipolar spindle before clustering at the opposite poles of a bipolar spindle. This temporary multipolar spindle results in increased rate of merotelic kinetochore-microtubule attachments, lagging chromosomes and unequal chromosome segregation in tetraploid cells with multiple centrosomes compared to genetically matched tetraploids with a normal centrosome number. In addition, the mere induction of centrosome reduplication in otherwise normal diploid cells leads to multipolar spindles and missegregation. It is likely that this type of chromosomal instability promotes tumorigenic transformation of tetraploid cells. However, it has not been formally proven that chromosomally stable tetraploid cells (with a normal centrosome number) have a lower transformation potential than genetically matched tetraploid cells with multiple centrosomes. It is important to note that, in a p53-deficient background (required for efficient proliferation), even a transient state of supernumerary centrosomes can potentially result in a prolonged state of chromosome instability. In fact, in a recent study, it has been shown that in the absence of p53, a transient period of chromosome missegregation can originate a permanent state of chromosome instability (Thompson and Compton, 2010). In that study, transient treatment with a kinesin inhibitor generates

viable aneuploidy cells only when p53 is not functional. Interestingly, clones derived many generation after release from the drug treatment are still chromosomally unstable. The molecular mechanism of this phenomenon is not known, but if this finding is generally true for different cell types, a transient state of supernumerary centrosomes might generate an aneuploid state that is chromosomally unstable in the absence of p53. Therefore, a careful study of not only centrosome number but also progressive chromosome number changes is necessary to formally prove that chromosomal instability is required for tumorigenesis of tetraploid cells.

In addition to chromosome missegregation and instability, an important factor in the transformation potential of tetraploid cells relates to the occurrence of endogenous DNA damage, the ability of the cells to repair the lesions and the consequence of genotoxic stress for cellular viability. The aberrant regulation of these three pathways can contribute to a mutator phenotype in tetraploids. One source of endogenous chromosome breaks that has been recently recognized is again related to chromosome missegregation (Crasta et al, 2012). Lagging chromosomes in mitosis can give rise to micronuclei in the daughter cells. These micronuclei are characterized by higher endogenous damage and can lead to massive chromosome fragmentation. Since this phenomenon is dependent on chromosome missegregation, it is predicted to occur in tetraploids with supernumerary centrosomes.

Different question is whether higher endogenous damage might be the consequence of the sole state of having a duplicated genome. Tetraploid yeasts, with an unaltered centrosome number, are much more sensitive to the inhi-

bition of homology-directed DNA repair pathway and show increased endogenous DNA damage lesions in mitosis (Storchova et al., 2006). The increased persistence of unrepaired damage might reflect a higher frequency of DNA damage lesions during the replication of the double-sized genome and/or to defects in the DNA damage repair pathways. Whether a similar phenomenon occurs in mammalian cells in not known. In human cells, studies of the response of tetraploid cells to genotoxic agents suggest a different scenario. As compared to control diploid cells, tetraploids were more resistant to apoptosis induced by treatment with genotoxic agents such as camptothecin, etopoxide, IR and UV irradiation (Castedo et al., 2006). For other drugs such as doxorubicin or hydroxyurea, no difference was noticed between tetraploids and diploids (Castedo et al., 2006). The molecular mechanism of this phenomenon and whether it depends on the integrity of the p53 pathway (as it has been suggested) are not clear. In agreement, we found that tetraploid cells have a longer lifespan than diploid cells after telomere crisis, where the mutational load is determined by the endogenous telomere-dependent genome instability. Overall these data are in agreement with increased mutational robustness after polyploidization in mammalian cells.

It is likely that in steady-state conditions, polyploid cells have lower fitness than diploid cells, as suggested by the slightly lower proliferation rate in culture dish, as indicated by our and previous data (our data, Fujiwara et al., 2005). However, in the presence of a selective pressure or mutator phenotype, as for example in the transformation assay after injection into nude mice or as it might be during telomere crisis, polyploidy confers an evolutionary ad-

vantage. In our case of telomere-derived tetraploidy after transient depletion of POT1a/b, the low level of chromosome fusions might also contribute to the higher transformation potential of tetraploids.

3.5 Telomere dysfunction as a widespread source of tetraploidy in cancer

Different sources of polyploidy have been proposed in cancer, such as virus-mediated cell fusion or failure in mitosis or cytokinesis due to deregulation of mitotic factors such as APC, Mad2 or Emi1 (Caldwell et al., 2007; Sotillo et al., 2007; Dikovskaya et al., 2007). Telomere-derived tetraploidy is relevant because telomere dysfunction represents a widespread phenomenon in the early stages of human tumorigenesis. Telomere dysfunction depends on overproliferation of preneoplastic cells and, as genetic alterations, it requires only Rb loss, which is a frequent event in solid tumors, in addition to p53 loss. Interestingly, there is a strong correlation between the occurrence of near-tetraploid karyotypes and the frequency of inactivation of the Rb pathway in different types of human solid tumors (Fig. 3.2), suggesting an important role for Rb loss in tetraploidization during tumorigenesis (see next section for the timing of p53 and Rb loss and tetraploidy). Moreover, among the potentially pervasive sources of genome instability in cancer, an episode of telomere dysfunction stands out due its potential aggregate effect. In p53-deficient cells, BFB cycles can promote the main genomic alterations observed in cancer: loss of heterozygosity, gene amplication, and non-reciprocal translocations (Artandi

et al., 2000; Maser and DePinho, 2002; de Lange, 1995). The telomere-driven tetraploidization is likely to provide a considerable advantage to precancerous cells experiencing this type of genome instability since it diminishes the chance that an essential gene function is lost. Furthermore, the DNA damage signal that induces tetraploidization is a temporary phenomenon, dissipating when telomere protection is restored by activation of telomerase or alternative mechanism of telomere maintenance.

Even if the role of of telomere dysfunction in polyploidy during tumorigenesis seems to be important, experimental evidence of its significance in human tumors is still lacking. First of all it would be important to assess whether tetraploidy actually occurs in early cancer lesions and it correlates with the evidence of DNA damage activation. Activation of the DNA damage response is frequently observed in hyperproliferative preneoplastic lesions which usually show high levels of γ-H2AX, P-Chk2 P-ATM and also of the inhibitory phosphorylation of Cdk1 (Gorgoulis et al., 2005; Bartkova et al., 2005). Simultaneous analysis of DNA damage response and tetraploidy may be useful, but the transient nature of the presumed tetraploidy most likely would render this task difficult. Nevertheless, our preliminary analysis of telomeric fusions in breast cancer cell lines showed a higher frequency of fusions in cell lines with high chromosome numbers, compared to near-diploid cell lines, in agreement with our hypothesis. It will be important to extend our analysis to primary human tumors. Analysis of telomere fusions has been successful in primary samples from chronic lymphocytic leukemia, demonstrating telomere crisis in the later stages of the disease and opening the way to a similar analysis in

human solid tumors (Lin et al., 2010).

Finally, the hypothesis of telomere-derived tetraploidy in tumorigenesis could be tested in an experimental system using human cell lines experiencing telomere crisis. Overexpression of telomerase in hMECs as the cells enter crisis might allow isolating post-crisis cells, immortalized after they experienced telomere crisis. These post-crisis cell lines can be analyzed for the evolution of their karyotype and for their transformation potential. This approach would also allow creation of a model system for the study of potential crisis-associated features and vulnerabilities.

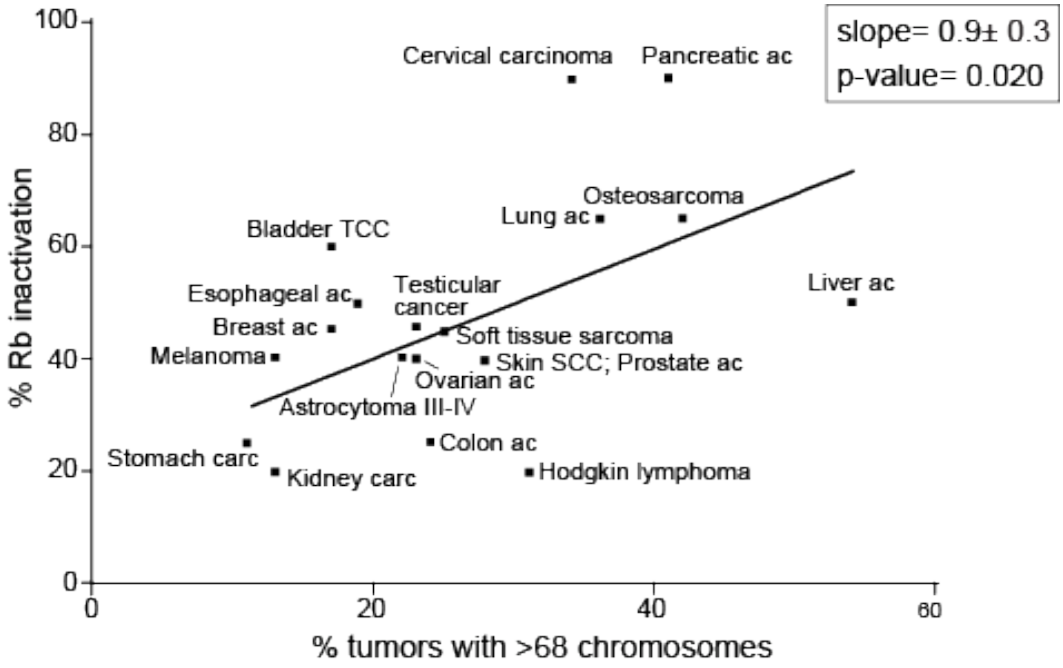

Figure 3.2: **Correlation between the frequency of Rb inactivation and near-tetraploid karyotypes.** The graphs shows the correlation between the frequency of inactivation of the Rb pathway and the percentage of karyotypes with high chromosome number (hypertriploid karyotypes, data from Fig. 1.7) for the indicated cancers. Analysis of linear regression shows significant correlation (slope and p-value are reported, from F-test using Prism-5 software). TCC: transitional cell carcinoma; SCC: squamous cell carcinoma; ac: adenocarcinoma; carc: carcinoma

3.6 Timing of tetraploidization during tumorigenesis and order of the events

The outgrowth of all tetraploid clones is blocked by the p53 pathway (Andreassen et al., 2001; Meraldi et al., 2002; Fujiwara et al., 2005) and, in the case of telomere-derived tetraploidization, also by the p16/Rb pathway. Therefore, tetraploidization is more likely to contribute to those cancers in which the relevant tumor suppressor pathways are frequently inactivated at an early stage, before the emergence of the tetraploidization stimulus. Although much of the relevant information is missing, I will consider here, for each possible mechanism of tetraploidization, the potential order of the relevant events in cancer types in which tetraploidization is observed (Fig. 3.3).

In the case of virally-induced cell fusion, the presumed causative agent is elusive. The exception is HPV-induced cervical cancer in which viral infection could both induce fusion and, through the action of HPV E6, inactivate p53 (Moody and Laimins, 2010), creating a permissive setting for the proliferation of tetraploid cells (Fig. 3.3). Tetraploidization induced by the failure in progression through mitosis represents a more complex scenario since mitotic failure can be induced in a variety of ways (Fig. 1.4). In the case of APC mutations in colon carcinoma, p53 loss is a later event (Fodde et al., 2001), suggesting that mitotic failure might take place early on but will only result in viable tetraploid clones at a later stage. Similarly, for Mad2 and Emi1, overexpression due to inactivation of the Rb pathway, the mitotic problems induced by Mad2 or Emi1 are unlikely to give rise to tetraploid clones unless p53 is inac-

tivated. For instance, in lung adenocarcinoma, inactivation of Rb precedes the loss of p53, which occurs at the time that invasive cancer develops (Noguchi, 2010; Fig. 3.3). Therefore, the development of tetraploid clones induced by overexpression of Mad2 or Emi1 are most likely to arise at the transition to invasive cancer (Garber et al., 2001; Lehman et al., 2007). In a fraction of breast cancer both the p53 and the Rb pathway are inactivated early, allowing Mad2- or Emi1-driven tetraploidization events to contribute to tumor progression at a pre-invasive stage (Shackney and Silverman, 2003; van 't Veer et al., 2002; Lehman et al., 2007; Fig. 3.3). Other sources of cytokinesis failure such as inhibition of LATS1 or AuroraA overexpression are more difficult to evaluate since the timing of these changes are not known. An exceptional case is liver adenocarcinoma. Since hepatocytes are prone to undergo tetraploidization despite a functional p53 pathway (Fig. 1.2), Mad2/Emi1-induced tetraploidization may well occur at an early stage when Rb is inactivated but p53 is not (Martin and Dufour, 2008; Teramoto et al., 1994; Hui et al., 1998; Fig. 3.3).

Figure 3.3: **Timing of loss of p53/Rb, activation of telomerase, and tetraploidization in select human cancers.** For a subset of cancers with evidence for tetraploidization, the potential causes of tetraploidy (OE: overexpression), the incidence of karyotypes with high chromosome numbers (hypertriploid karyotypes, from Fig. 1.7), the timing of loss of p53 and Rb pathways (% from Fig. 1.7), activation of telomerase, and tetraploidization are indicated. Four stages of neoplastic progression are considered: dysplasia, in situ cancer lesion, invasive cancer, and advanced/metastatic cancer. Evidence for tetraploidization includes data on chromosome number in metaphase spreads, FACS analysis of the DNA content, and supernumerary centrosomes.

Tumor type	Potential causes of tetraploidy	Incidence and sequence of events Dysplasia / Cancer in situ / Invasive cancer / Advanced/ metastatic	Hyper-triploid tumors
Liver adenocarcinoma	Mad2 OE (80%)[53] Emi1 OE (80%)[19] AuroraA OE (50%)[19] Telomere shortening[42]	Tetraploidy [4] p53 inactive (30–60%)[26,50] Rb inactive (40–60%)[16,26] Telomerase active[42]	54%
Pancreatic adenocarcinoma	AuroraA OE[19] Telomere shortening[52]	Tetraploidy[49,41] p53 inactive (50–75%)[24] Rb inactive (80–95%)[24] Telomerase active[24,47]	41%
Lung adenocarcinoma	Mad2 OE[12] Emi1 OE (65%)[19] Telomere shortening[9]	Tetraploidy[23] p53 inactive (40–60%)[36] Rb inactive (50–80%)[36] Telomerase active[9]	36%
Cervical carcinoma	HPV infection (>90%)[34] Emi1 OE (80%)[19] AuroraA OE (50%)[19] Telomere shortening[28]	Tetraploidy[18,37] p53 inactive (>90%)[34] Rb inactive (>90%)[34] Telomerase active[13]	34%
Prostate adenocarcinoma	Telomere shortening[27]	Tetraploidy[5,33] p53 inactive (20–30%)[1] Rb inactive (30–50%)[1] Telomerase active[29]	28%
Colon adenocarcinoma	APC mut (50–70%)[40] Mad2 OE[10] AuroraA OE (60%)[19] Telomere shortening[26]	Tetraploidy[14,20] p53 inactive (60–70%)[8] Rb inactive (20–30%)[8] Telomerase active[7,46]	24%
Ovarian adenocarcinoma	Emi1 OE (60–100%)[19] AuroraA OE (60%)[19] Telomere shortening[35]	Tetraploidy[3,17] p53 inactive (50–70%)[2] Rb inactive (30–50%)[2] Telomerase active[35]	23%
Esophageal adenocarcinoma	Telomere shortening[28]	Tetraploidy[11,37] p53 inactive (40–50%)[25] Rb inactive (40–60%)[25] Telomerase active[25]	19%
Breast adenocarcinoma	Mad2 OE[51] Emi1 OE (45%)[19] AuroraA OE[32] LATS1 downreg.[48] Telomere shortening[30]	Tetraploidy[6,38,43] p53 inactive (20–30%)[6,45,43] Rb inactive (40–50%)[45] Telomerase active[15,46]	17%
Bladder transitional cell carcinoma	Emi1 OE (45%)[19] Telomere shortening[28]	Tetraploidy[44] p53 inactive (30–50%)[31] Rb inactive (40–70%)[31] Telomerase active[22]	17%

[1]Abate-Shen & Shen 2000
[2]Bast et al. 2009
[3]Braly & Klevecz 1993
[4]Celton-Morizur & Desdouets 2010
[5]Deitch et al. 1993
[6]Dutrillaux et al. 1991
[7]Engelhardt et al. 1997
[8]Fearon 2010
[9]Fernandez-Garcia et al. 2008
[10]Friederichs et al. 2005
[11]Galipeau et al. 1996
[12]Garber et al. 2001
[13]Gupta et al. 2010
[14]Hamada et al. 1988
[15]Herbert et al. 2001
[16]Hui et al. 1998
[17]Kallioniemi et al. 1988
[18]Kirkland et al. 1967
[19]Lehman et al. 2007
[20]Levine et al. 1991
[21]Li et al. 2003
[22]Lin et al. 1996
[23]Lothschutz et al. 2002
[24]Maitra & Hruban 2008
[25]Maley 2007
[26]Martin & Dufour 2008
[27]Meeker et al. 2002
[28]Meeker et al. 2004
[29]Meeker 2006
[30]Meeker & Argani 2004
[31]Mitra & Cote 2009
[32]Miyoshi et al. 2001
[33]Montgomery et al. 1990
[34]Moody & Laimins 2010
[35]Murakami et al. 1997
[36]Noguchi 2010
[37]Olaharski et al. 2006
[38]Ottesen, 2003
[39]Reid et al. 1996
[40]Samowitz et al. 2007
[41]Sato et al. 1999
[42]Satyanarayana et al. 2004
[43]Shackney et al. 1995
[44]Shackney et al. 2003
[45]Shackney & Silverman 2003
[46]Shay & Bacchetti 1997
[47]Suehara et al. 1997
[48]Takahashi et al. 2005
[49]Tanaka et al. 1984
[50]Teramoto et al. 1994
[51]van 't Veer et al. 2002
[52]van Heek et al. 2002
[53]Zhang et al. 2008

The third potential cause of tetraploidization, endoreduplication or mitotic failure due to dysfunctional telomeres, requires the correct order of three events. First, the p53 and p16/Rb pathways need to be disabled to allow cell to proliferate to the point of telomere crisis; second, tetraploidization needs to occur; and third, telomerase has to be activated to restore telomere function and avoid further telomere shortening. Telomere shortening is notable in the pre-invasive stages of most epithelial cancers (Meeker et al., 2002; van Heek et al., 2002; Meeker et al., 2004; Meeker and Argani, 2004), which also represents the approximate timing of inactivation of the p53 and Rb pathways in many tumors (Fig. 3.3). For instance, in esophageal carcinoma, Rb inactivation is an early event that is followed by p53 dysfunction and telomerase activation at the pre-invasive stage when tetraploidy arises (Maley, 2007; Reid et al., 1996). In breast cancer, tetraploidization occurs at the DCIS stage when the p53 and Rb pathways are inactivated and telomerase is increasingly detectable (Shackney and Silverman, 2003; Shay and Bacchetti, 1997; Herbert et al., 2001). In addition, there is good evidence for telomere crisis in DCIS followed by stabilization of the genome due to telomerase-mediated telomere restoration (Chin et al., 2004). In pancreatic adenocarcinoma, frequent inactivation of Rb and p53 pathways also takes place before the activation of telomerase at an early stage (usually in intra-epithelial/in situ neoplasia) when tetraploidy is observed (Maitra and Hruban, 2008; van Heek et al., 2002; Suehara et al., 1997; Tanaka et al., 1984; Sato et al., 1999). In bladder, ovarian and prostate cancer, inactivation of Rb/p53 pathways and telomerase reactivation occur approximately at the same time, at the transition from in situ to invasive cancer,

where there is evidence of tetraploidy (Mitra and Cote, 2009; Lin et al., 1996; Shackney et al., 1995; Bast et al., 2009; Murakami et al., 1997; Kallioniemi et al., 1988; Braly and Klevecz, 1993; Abate-Shen and Shen, 2000; Koeneman et al., 1998; Montgomery et al., 1990). In summary, in a number of tumor types with evidence for tetraploidization (Fig. 3.3), the order of p53/Rb inactivation, occurrence of tetraploidy, and telomerase upregulation is in agreement with telomere dysfunction as the stimulus for tetraploidization. This contrasts with other cancers in which the correct order of events is unlikely to occur. For instance, in kidney carcinoma, inactivation of p53 and Rb pathways is rare and occurs late, often in advanced or metastatic tumors (Ibrahim and Haluska, 2009). Indeed, the near-diploid karyotype of most kidney carcinomas argue against tetraploidization in the formation of this cancer type. Similarly, tetraploidization is rare in human tumors arising from telomerase competent cells in which telomerase activation presumably precedes other events. Near-diploid karyotypes are present in most human leukemias and some lymphomas, which originate from telomerase competent cells (Hilgenfeld et al., 1999; Broccoli et al., 1995).

3.7 Telomere-independent origin of tetraploidy in cancer

Our data indicate that at least two telomere-independent sources of prolonged DNA damage signaling relevant for cancer can lead to tetraploidization in p53 and Rb deficient cells. The first source of DNA damage is represented

by defects in homology-directed repair (HDR) due to BRCA2 inactivation. When HDR is diminished, unresolved S phase problems can elicit a persistent DNA damage signal in G2 and induce tetraploidization. In agreement, XRCC3-deficient cells, which have impaired HDR, show a low frequency of endoreduplication (Yoshihara et al., 2004). Furthermore, overexpression of RPA, or deletion of Nbs1 and Rad17 results in polyploidy, most likely because of persistent unrepaired DNA damage (Reina-San-Martin et al., 2005; Wang et al., 2003). The relevance of these observations to tetraploidization in human cancer remains to be determined but it is noteworthy that p53-deficient breast cancers lacking the HDR protein BRCA2 are often polyploid (Gretarsdottir et al., 1998). The second possible cause of DNA damage-induced tetraploidization is replication stress induced by aberrant oncogene activation. Activation of the DNA damage response, presumably due to unscheduled DNA replication, is frequently observed in hyperproliferative preneoplastic lesions and a DNA damage response is induced upon oncogene expression in cultured cells (Gorgoulis et al., 2005; Bartkova et al., 2005; Bartkova et al., 2006; Di Micco et al., 2006). We found that overexpression of the constitutively active RasV12 mutant can lead to tetraploidy both through endoreduplication or mitotic failure in human epithelial cells. Mitotic failure in this setting might be due to the formation of dicentrics or other chromosomal structural abnormalities due to aberrant repair of the DSBs induced in S -phase. In agreement with our data, previous reports also showed polyploidy after oncogene overeexpression in U2OS osteosarcoma (CyclinE) cells and IMR90 fibroblasts (Ras; Bartkova et al., 2006; Chicas et al., 2010).

While telomere dysfunction is a transient state buffered later in tumorigenesis by telomerase reactivation, oncogene activation is usually a permanent genetic lesions occurring relatively early in tumorigenesis and persisting during tumor development. In this context, the switch from the endocycle to the mitotic cycle might be mediated by inactivation of the ATM/ATR and Chk1/Chk2 pathways. Interestingly, in bladder cancer, high Chk2 phosphorylation in early lesions with low genomic instability is decreased in more advanced lesions with higher genome instability, suggesting that the Chk1/Chk2 checkpoint activation is transient and precedes aneuploidy (Bartkova et al., 2006). Moreover, mutations in ATM or Chk2 correlate with the transition from early genomically stable tumors to later more unstable ones. In some cases of advanced stage melanomas and lung cancers, absence of active downstream effector P-Chk2 was observed in the presence of active upstream DNA damage factor γ-H2AX (Gorgoulis et al., 2005), reflecting the presence of ongoing DNA damage but inactive downstream checkpoint.

Besides oncogene-induced senescence and replicative senescence, other mechanisms have been implicated as sources of DNA damage signal in early cancerous lesions, such as hypoxia, reactive oxygen species and inflammatory cytokines (d'Adda di Fagagna, 2008). In addition to cancer-causing sources, induction of DNA damage is relevant to the context of commonly used cancer therapies, such as chemotherapy or radiation therapy (Helleday et al., 2008). Our data would suggest that, if the DNA damage signal is sufficiently intense and prolonged, chemotherapic treatment might result in polyploidy in p53 and Rb deficient tumor cells. During or after treatment, most of tumor cells,

including polyploid cells, are expected to undergo apoptosis or mitotic catastrophe due to high levels of chromosomal aberrations. However, if a polyploid cancer clone can survive this stage, it might be able to more rapidly acquire resistance or ability to colonize new niches. It would be interesting to monitor changes in ploidy during cancer treatment, tumor relapse, therapy-related secondary tumors and metastasis formation in the (mouse) clinic.

3.8 Future directions

A better insight into the pervasive pathway of tetraploidization toward aneuploidy can better illuminate the nature of genome instability in cancer and may reveal cancer-specific vulnerabilities that can be exploited in the clinic. It is likely that progression through a tetraploid intermediate requires adaptations that may become permanent in the developing cancer lineage. An example of polyploidy-specific adaptation of tumor cells is centrosome clustering to allow bipolar spindle formation (Kwon et al., 2008). Other adaptations are likely to be specific for the mechanism of polyploidization and in this regard, it will be important to identify the mechanisms/instigators of the whole genome duplication for each cancer type. For example, progression through telomere crisis by precancerous cells might be associated with specific genetic or epigenetic features allowing cells to progress through crisis before evolution of a tumorigenic clone. Furthermore, a deeper knowledge of the causes and consequences of tetraploidization in cancer could deliver diagnostic tools to parse subsets of cancers based on their route to aneuploidy. As a first step in

this direction, PCR-mediated analysis of telomeric fusions in tumor samples represents a method to distinguish between tumors that did or did not undergo telomere crisis in their natural history. This and similar approaches may be useful to optimize cancer diagnosis and treatment based on the mechanism of past polyploidization.

Chapter 4

Experimental Procedures

4.1 Constructs

Cre-recombinased was transduced into the cells by retroviral vectors using pWZL-hygro-Cre and pWZL empty vector as negative control. Alternatively, pMMP Hit&Run Cre (Silver and Livingston, 2001) was used and mock infection as negative control in this case. For pLPC-CyclinE-eGFP, the C-terminus of full length hCyclinE (provided by Dr. J. Pines) was fused in frame to the eGFP in pLPC retroviral vector, using the Gateway cloning system (Invitrogen). The following primers were used: CycE-fw: 5'-CACCGCCACCATGGAGGAGGACGGCGGC-3'; CycE-rv: 5'-CTCGAGCGCCATTTCCGGCCCGCTGCT-3'; eGFP-fw: 5'-CTCGAGGTGAGCAAGGGCGAGCTG-3'; eGFP-rv: 5'-CTCGAGTCACTTGTACAGCTCGTCCATGCC-3'. pBabe-Puro-Myc was gently provided by Dr. Pier Giuseppe Pelicci. Full-length hTERT was cloned into the bicistronic lentiviral vector pLVX-IRES-Hygro (Clonetech,

632182). pWZL-Hygro-RasV12 and pLM2P-shRB.698-p21.890 (for the simultaneous knock-down of p21 and Rb) were kindly provided by Dr. Scott Lowe (Chicas et al., 2010). TopBP1-ER was provided by Dr. Oscar Fernandez-Capetillo (Toledo et al., 2008). For the POT1atetOFF system, full-length mouse POT1a was cloned into P-TRE-Tight (Clonetech, 631059) using BamH1 and EcoR1 restriction sites and the following primers: POT1a-fw: 5'-ATGCGG ATCCACCATGTCTTTGGTTTCAACA-3'and POT1a-rv: 5'-ATGCGAATT CCTAGACAACATTTTCTGC
AACTGT-3'. P-TRE-TIGHT was used in combination with P-Tet-Off-Advanced (Clonetech, 630934) to develop the inducible system in POT1a/b DKO MEFs. FUCCI lentiviral vectors were generously provided by Atsushi Miyawaki (Sakaue-Sawano et al., 2008). The FUCCI system is made of two lentiviral vectors expressing the two fluorescently-tagged cell cycle markers: CSII-EF-MCS-mKO2-hCdt1(30-120) and CSII-EF-MCS-mAG-hgeminin(1-100). For overexpression of SV40-LT, pBabe-neo-SV40LT or pLPC SV40LT retroviral vectors were used. Sh-RNA mediated knock-down of the following endogenous proteins was performed by using lentiviral vectors purchased from Openbiosystem: empty vector as control (pLK0.1), vectors for Chk1 shRNA (RMM3981-9580337 (set1) and RMM3981-9580340 (set2)), vectors for Chk2 shRNA (RMM 3981-9580345 (set1) and RMM3981-9580346 (set2)), vector for Cdh1 shRNA (RMM3981-9593724) and vector for APC1 shRNA (RMM3981-97076474). The ATR shRNA retroviral vector was as described (Denchi and de Lange, 2007). pBabe-neo-p53175H and pSuper-retro-hygro-p53sh were previously described in Jacobs and de Lange, 2004.

4.2 Isolation of MEFs

POT1a/b DKO MEFs lacking ATM were generated by intercrosses of POT1a$^{F/-}$ POT1b $^{F/F}$ (Hockemeyer et al., 2006) and ATM$^{+/-}$ (Barlow et al., 1996) mice. MEFs were isolated, from E13.5 embryos of timed pregnancies using standard techniques and were grown in DMEM containing 15% Fetal Bovine Serum (Gibco), supplemented with 100 U/ml penicillin (Sigma), 0.1 μg/ml of streptomycin (Sigma), 2 mM L-glutamine (Invitrogen), 0.1 mM non-essential amino acids (Invitrogen), 1 mM sodium pyruvate (Sigma), and 50 mM b-mercaptoethanol (Chemicon). Primary MEFs were immortalized by overexpression of SV40-LT at passage 2. BRCA2$^{F/+}$ and BRCA2$^{F/-}$ MEFs overexpressing TBX2 (Badie et al. 2010) were a gift from Dr. J. Jonkers.

4.3 Cell culture procedures

SV40-LT immortalized MEFs, IMR90 lung fibroblasts (ATCC), were grown in DMEM supplemented with 100 U/ml penicillin (Sigma), 0.1 μg/ml of streptomycin (Sigma), 2 mM L-glutamine (Invitrogen), 0.1 mM non-essential amino acids (Invitrogen), and 10% Fetal Bovine Serum (Gibco). BJ fibroblasts (ATCC) and retinal epithelial cells (RPE, ATCC) were grown in the same culture medium described above except that the base medium was composed of 80% DMEM and 20% Medium199 for BJ cells and DMEM/F12 medium for RPE cells. Pheonix ecotropic or amphotropic packaging cell line (ATCC) and 293T cells (ATCC) were grown in DMEM supplemented as above except for the serum which was replaced with 10% Bovine Calf Serum (HyClone).

Human mammary epithelial cell lines 184B and 48RS (Romanov et al., 2001), expressing or not the GSE22 peptide (GSE), acting as a p53 dominant negative (Garbe et al., 2007) were kindly provided by Dr. Martha Stampfer. hMEC cells were grown in MEMG (Lonza, CC-3051A) supplemented with bovine pituitary extract (BPE, Lonza, CC-4009), 10μM isoproterenol (Sigma, I-5627) and 5μg/ml of transferrin (Sigma, T-2252). hMECs were cultured according to the procedures described by Martha Stampfer on this website: $http://hmec.lbl.gov/mindex.html$. All cells were grown at 3737°C in the presence of 5% CO2 and 95% humidity. Breast cancer cell lines were purchased from ATCC (30-4500K) and each of the lines was cultured using to the recommended medium and culture conditions. A list of all the cell lines is provided in the Appendix C.

4.4 Viral gene delivery

For retroviral and lentiviral infections, phoenix cells (retro) or 293T (lenti) cells were transfected with 10-20 μg of the transgene-expressing plasmid (in addition to lentiviral packaging vectors in the case of 293T). Starting 36 hours after transfection, supernatants from transfected packaging cells were filtered (45μm filter unit) added with polybrene (2-4 μg/ml final concentration) and used to infect targeting cells. Medium was replaced on the transfected cells and the supernatant was used again for subsequent infections, performed in the same way. A total of 3-4 consecutive infections delivered at 6-12h intervals for each experimental condition. In some cases, filtered viral supernatant

were frozen using liquid nitrogen and stored at -80°C. 24-48 hours after the last infection, cells were split into fresh media, which contained antibiotics for selection if a selection marker was present in the vectors used (puromycin 2 μg/ml, hygromycin 90 μg/ml). Selection was maintained for 3-6 days, until uninfected control cells had died. Cre recombinase was introduced through retroviral infection. MEFs were infected 3 times at 12 h intervals with retrovirus vector pWzl-hygro-Cre or empty vector, as a negative control, followed by hygromycin selection. Alternatively, pMMP Hit&Run Cre retroviral vector (Silver and Livingston, 2001) was used and no selection was applied. The experimental time-points were counted as h or days after the last retroviral infection. For the two lentiviral vectors of the FUCCI system, 2 infections or 4-5 hours each were performed with each vector during two consecutive days. No selection marker is contained in these vectors, so no selection was applied. In some cases the cells were FACS-sorted for expression of both transgenes (mKO2 and mAG double-positive cells).

4.5 G1/S synchronization by double thymidine block

MEFs at 25-30% confluence were incubated with culture medium containing 2mM thymidine for 16-18h (first block). The next day, thymidine was removed by washing three times with PBS and fresh culture medium was added to allow the cells to progress through the cell cycle. After 8-10h, 2mM thymidine was added to the medium and incubated for other 16-18h (second block). Finally,

after the second block, cells were released into the cell cycle by removing the thymidine containing medium and washing 3 times with PBS. After the double-thymidine block cells are synchronized in G1/S and after release they progress through S-phase (lasting around 4 hours in SV40 MEFs), G2 (lasting around 2 hours), mitosis and subsequent G1 phase.

4.6 Treatment with drugs and with UV

Zeocin (Invitrogen, R250-01, stock solution) was used at a concentration varying from 2 to 100 ug/ml as indicated. Doxorubicin (Sigma, D1515) was dissolved in water and used at 1 μM. Bleomycin (Sigma, B5507) was dissolved in water and used at the concentration of 50 μg/ml. These three DNA damage inducing agents were used to treat the cells continuously for 72h or 96h by adding the drug every 24-48 h. Doxycycline (Sigma, D9891) was dissolved in water and used at 2 ug/ml. 4-hydroxytamoxifen (OHT, Sigma, H7904) was dissolved in ethanol and used to treat the cells at a final concentration of 0.5 μM. For UV treatment, MEFs were first washed with PBS and treated with 20J/m2 UV every 2 hours for two periods of 12 h with 12 h in between.

4.7 FACS analysis and FACS sorting

For FACS analysis of the cell cycle with BrdU and propidium iodide (PI) staining, cells were grown at 50-70% confluence and treated with 10 μM BrdU (Sigma, 5002) for 1 hour prior to harvesting. Cells were harvested by trypsinization, counted and fixed by adding -20°C cold ethanol while vortex-

ing. Cells were stored overnight at -20°C and then at 4°C. For FACS analysis, 2-5 10^5 cells were used for each sample. Cells were first incubated with 2N HCl/Triton-X-100 0.5% (added while vortexing) for 30 min at R.T. to denature the DNA. Cells were then re-suspended in 0.1M Na2B4O7X10H2O pH 8.5. Next cells were resuspended in blocking buffer (PBS containing 0.5%Tween20/0.5%BSA). Staining with FITC-conjugated anti-BrdU (BD, Biosciences, 347583) was performed by incubating the cells in the blocking buffer containing anti-BrdU antibody (diluted 1:10) for 30 min in the dark. Cells were finally washed 3 times in the blocking buffer and resuspended in PBS containing 0.5% BSA, 5μg/ml PI and 200 μg/ml RNA-ase. Flow cytometry was performed using the FACSCalibur (Becton Dickinson) and data was analyzed using FlowJo 8.7.1 software. To calculate the % of polyploid cells (DNA content >4N), cell doublets and sub-G1 apoptotic cells were first excluded, then a gate was draw to include the cells with a DNA content >4N (based on the PI profile). FACS sorting of diploid can tetraploid cells was performed at the FCRC Facility of the Rockefeller University. Before sorting, the cells were incubated with 10-12 μM of Hoechst 33342 (AnaSpec Inc., 83218) for 30 min. Cells were then harvested by trypsinization, counted, washed with PBS and resuspended in cold PBS for FACS sorting. Sorted G1 diploid cells and G2 teraploid cells were then washed in PBS twice and plated in the appropriate medium. Usually a sample of 2-3 10^5 cells was fixed in ethanol and used for PI-mediated cell cycle analysis. Other FACS sorting, for example for FUCCI infected cells or for cell populations isolated from tumors, were performed using standard procedures by preparing single cell suspension of the sample to

be sorted in PBS.

4.8 Cell lysate and immunoblotting

Cells were lysed in $2X$ Laemmli buffer (100 mM Tris-HCl, pH 6.8, 200 mM DTT, 3% SDS, 20% glycerol, 0.05% bromophenol blue) at 10^6 cells per 100 μl, denatured for 7 min at 100°C, and sheared with a 28 gauge insulin needle. Lysate deriving from before loading the equivalent of 2-3 10^5 cells per lane. Protein samples were separated by SDS-PAGE and blotted onto nitrocellulose membranes. Membranes were blocked in 5% milk in TBST (0.5% Tween-20 in 50mM Tris, 150mM NaCl, pH 7.6) for 30 min at RT and incubated with primary antibodies in 1 or 5% milk containing TBST overnight at 4°C or for 2 hours at RT. Membranes were washed 3 times in TBST, 5 min each and incubated with secondary antibody in TBST for 30-45 min at RT, and washed 3 times with PBST at RT. Blots were developed with enhanced chemiluminescence system (Amersham).

4.9 Immunofluorescence (IF)

Cells were grown on coverslips. Cells were rinsed with PBS, fixed with 2% paraformaldehyde in PBS for 10 min at RT and washed three times with PBS for 5 min each. Alternatively, cells were fixed in -20°C cold methanol (Sigma, 154903) for 10 minutes and washed with PBS. Cells were either stored in PBS with the addition of 10 mM sodium azide or processed immediately. Cells were blocked with PBG (0.2% (w/v) cold water fish gelatin (Sigma),

0.5% (w/v) BSA (Sigma) in PBS) for 1 h at RT. Cells were incubated with primary antibody diluted in PBG for 2 h at RT or overnight at 4°C, washed 3 times with PBG at RT, incubated with secondary antibody diluted 1:250 in PBG for 1 h at RT, and washed 3 times with PBS. To the second PBS wash 0.1 μg/ml 4,6-diamidino-2-phenylindole (DAPI) was added. Coverslips were sealed onto glass sides with embedding media (ProLong Gold Antifade Reagent, Invitrogen). Digital images were captured with a Zeiss Axioplan II microscope with a Hamamatsu C4742-95 camera using Improvision OpenLab software.

4.10 Fluorescence *In situ* Hybridization-Immunofluorescence (FISH-IF)

Cells were grown on coverslips and fixed for 10 min in 2% paraformaldehyde at room temperature followed by PBS washes. Coverslips were blocked for 30 min in blocking solution (1 mg/ml BSA, 3% goat serum, 0.1% Triton X-100, 1 mM EDTA in PBS). Next, the cells were incubated with primary antibodies diluted in blocking solution for 1 h at room temperature. After PBS washes, coverslips were incubated with Alexa 488- or Rhodamine-Red-X-labelled secondary antibody raised against mouse or rabbit (Jackson) for 30 min and washed in PBS. At this point, coverslips were dehydrated consecutively in 70%, 95% and 100% ethanol for 5 min each, and allowed to dry completely. Hybridizing solution (70% formamide, 1 mg/ml blocking reagent (Roche), 10 mM Tris-HCl, pH 7.2, containing PNA probe FITC-OO-(AATCCC)3 (Applied Biosystems)

was added to each coverslip and the cells were denatured by heating for 10 min at 80°C on a heat block. After 2 h or overnight incubation at room temperature in the dark, cells were washed twice with washing solution (70% formamide, 10 mM Tris-HCl, pH 7.2) and three times in PBS. To the second PBS wash 0.1 μg/ml DAPI was added. Coverslips were sealed onto glass sides with embedding media (ProLong Gold Antifade Reagent, Invitrogen). Digital images were captured with a Zeiss Axioplan II microscope with a Hamamatsu C4742-95 camera using Improvision OpenLab software.

4.11 Metaphase chromosome spreads

Cells were grown to approximately 70-80% confluence on 10 cm dishes and incubated for 1-2 h in 0.1 μg/ml colcemide (Sigma) for human cells and 0.2 μg/ml colcemide (Sigma) for mouse cells. For spectral karyotyping(SKY) analysis, colcemid treatment was performed for 3-5 hours. Cells were harvested by trypsinization, washed in PBS and resuspended in 10 ml of 0.075M KCl prewarmed to 37°C. Cells were incubated at 37°C for 20-30 min. 200μl of fixative solution (-20°C cold 3:1 methanol:glacial acetic acid) was added to each sample (10 ml) and cells were centrifuged and the supernatant was decanted. Cell pellets were loosened by tapping and 1 ml of -20°C cold d fixative was added dropwise during gentle vortexing. For SKY analysis cells were washed five times with cold fixative. Tubes were then filled to 10 ml with the fixative and stored at 4C overnight. For metaphase spreads, cells were centrifuged and resuspended in 600-800μl of freshly prepared fixative. 100μl

were dropped from approximately 20 cm onto glass slides, which had been soaked in cold water and dried. Slides were washed with fresh fixative twice and dried at RT overnight. Alternatively, 100 ml of cells resuspended in fixative were dropped on dry slides in a temperature-controlled chamber (settings at 20°C and 50% humidity, Thermotron). To perform chromosome counts in metaphase spreads, DAPI staining was performed. Slides were rehydrated in PBS for 5 min, stained with DAPI in PBS for 5 min, washed in PBS for 5 min, and allowed to dry before mounting. For FISH on metaphase spreads, slides were washed in PBS twice, dehydrated by consecutive 5-min incubations in 70%, 95% and 100% ethanol. After air-drying, Hybridizing Solution (70% formamide, 1 mg/ml blocking reagent (Roche), 10 mM Tris-HCl, pH 7.2) containing FIu-OO-(AATCCC)3 PNA probe (peptide nucleic acid , Applied Biosystems) was added and spreads were denatured by heating for 10 min at 80°C on a heat block. Spreads were then allowed to hybridize in the dark for 2 h or overnight at room temperature. Two 15-min washes were performed in a washing buffer made of 70% formamide, 10 mM Tris-HCl, pH 7.0. Slides were then washed three times in PBS. To the second PBS wash 0.1 μg/ml DAPI was added. Coverslips were sealed onto glass sides with embedding media (ProLong Gold Antifade Reagent, Invitrogen). Digital images were captured with a Zeiss Axioplan II microscope with a Hamamatsu C4742-95 camera using Improvision OpenLab software. Dropping of metaphase spreads, staining and image analysis of metaphase spreads for SKY analysis was performed in collaboration with the laboratory of Dr. Anna Jauch at the University of Heidelberg, Germany.

4.12 Cdk kinase assay

10^6 cells were plated the day before in a 10cm dish. The next day cells were washed once with ice-cold PBS and harvested by cell scraping. Cells were lysed in cold IP lysis buffer (0.3% Triton X-100, 50 mM sodium phosphate pH 7.2, 2 mM EDTA, 2 mM EGTA, 25 mM NaF, 100 μM $NaVO_4$, 25 mM 2-glycerophosphate, 1 mM PMSF, and a protease inhibitor cocktail (Roche Diagnostics) and frozen in liquid nitrogen. Thawed extracts were sonicated, cleared after incubation with Protein G Sepharose (GE Healthcare), and incubated with anti-CyclinB1 (sc-245, Santa Cruz), anti-CyclinE M-20 (sc-481, Santa Cruz), or control IgG for 2 h. After 45 min with Protein G Sepharose beads, IPs were collected and washed 3 times in IP lysis buffer. Kinase activities were determined by incubating beads with histone H1 (5 μg, Roche) in kinase reaction buffer (50 mM HEPES pH 7.5, 10 mM MgCl2, 50 mM 2-glycerophosphate, 0.1% Triton X-100, 1 mM DTT) with 150 $\gamma - ^{32} P - ATP$ (10 μCi/μl) for 10 min at 30°C. Laemmli buffer was added and samples were fractionated on SDS-PAGE. H1-P was detected using a Storm PhosphorImager (Amersham). Kinase activity was quantified using ImageQuant software and normalized to the amounts of H1 and Cdk1 or Cdk2 in the IPs (ImageJ software).

4.13 Growth analysis

For growth curves of human fibroblasts BJ-SV40, IMR90-SV40, BJ-E6E7, BJ-p53dn and hMECs cells were plated at a density of 0.5 10^5 cells per 10 cm

dish and after 72 or 96h the cells were harvested, counted, and replated at the same density. This process was repeated until the cell population underwent telomere crisis. Growth curve was presented as cumulative population doublings (PD) plotted against time. PDs were determined by the following formula, where N is the number of cells at the indicated PD and n is the passage number: $PD_n = PD_{n-1} + \log_2(N_{PD_n}/N_{PD_{n-1}})$. For hMECs cell lines, the the initial passage number was known but not the initial PD, which was set arbitrarily to 0, in order to count the PD from the beginning of the experiment. hMECs were split every 4 days (one split corresponds to one passage) and in this case growth curves were presented as cumulative number of PDs plotted against the number of passages.

4.14 Live-cell imaging

For FUCCI live cell imaging, the cells were previously transduced with FUCCI vectors (Sakaue-Sawano et al., 2008) and in some cases sorted for expression of both the cell cycle fluorescent markers. For CyclinE-eGFP and H2B-GFP live cell imaging, MEFs were previously transduced with the corresponding retroviral constructs. For the analysis of POT1a/b deletion, MEFs of the indicated genotype were infected with Cre and/or shRNA expressing vector 2-4 days before the beginning of the imaging session. Live-cell imaging was started at day 3 after Cre and/or 2 days after treatment with Cdh1 shrine. For BRCA2$^{F/+}$ and BRCA2$^{F/F}$ MEFs and RPE over expressing RasV12, cells were analyzed by FUCCI imaging starting at day 8 after Cre or after expres-

sion of RasV12, respectively. Cells were plated 24h before the imaging session at 40-50% confluence in 4-chambered coverglass (LabTek) or in glass bottom plates (MatTek). Regular medium was replaced 1 h before the imaging session by phenol red-free Liebovitzs L-15 medium (GIBCO) containing 10-15% FBS100 U/ml penicillin (Sigma), and 0.1 μg/ml of streptomycin (Sigma) 2 mM L-glutamine (Invitrogen). In the cases of continuous zeocin treatment, zeocin was also added one hour before the imaging session and maintained in the medium. Time-lapse live-cell imaging was performed using an Olympus IX71 inverted microscope (Olympus) or by LCV110 "VivaView" Incubator Microscope (Olympus) for 72 or 96 hours at the Bioimaging Facility of the Rockefeller University. Phase contrast and fluorescent (GFP and RFP filters) images were acquired every 15-20 min with a 10X objective. MetaMorph software (Universal Imaging, Media, PA) and ImageJ software were used for data analysis. For CyclinE-eGFP live cell imagine, a 20X objective was used. Nuclear size was calculated from digital images using the Openlab (Improvision) measure module and statistical analysis was performed using a non-parametric Krustal-Wallis test (Prism software). After adjustment of the contrast in all the channels, all the images corresponding to one imaged field were assembled into a movie. In order to score the fraction of cells undergoing failure to complete mitosis or mitosis-independent geminin degradation (as an indicator of endoreduplication) in each movie, I used the following method. First the cells at the beginning, middle and end of the movie were scored: the average of these three numbers was considered as the total number of cells. Alternatively, the total number of cells was considered as the sum of the green-positive

(expressing geminin) cells every 8 hours. The number obtained with the two methods is similar. Next, I scored the number of cells showing mitotic failure through out the movie and the cells undergoing mitosis-independent geminin degradation and reversion to a G1-like state (expression of Cdt1). The cases in which binucleated or multinucleated cells underwent mitosis-independent geminin degradation were scored as endocycle events.

4.15 *In vitro* soft agar transformation assay

Soft agar colony-forming assay was performed in 6-well dishes. SeaPlaque agarose (Lonza) was dissolved in water at a concentration of 4.5%. Each well contained a bottom layer (2ml, 0.9% agarose) and a top layer (2ml, 0.45% agarose). First the bottom layer was prepared by preparing culture medium containing 0.9% agarose (2ml per well) and allowed it to solidify. MEFs were harvested by trypsinization, counted (twice, before and after dilution) and diluted to 10^5 cells per ml. 10^4 cells were seeded in each well in the upper layer by quickly mixing the diluted cell suspension in agar containing medium pre-warmed at 37°C. After seeding the cells, the upper layer was allowed to solidify at 4°C for 30 min. For each sample, 3 or 6 replicates (each well correspond to one replicate) were plated and analyzed. Cells were incubated at 37°Cand 300-500 μl of complete medium was added to each well once a week. When desired, 4-hydroxytamoxifen was added to the top soft-agar top layer and to the culture medium. After 4-6 weeks, colonies were stained with nitro-blue tetrazolium and the number of colonies was scored. In order to

derive cell lines from soft-agar colonies, the colonies were not stained and the biggest colonies were picked, trypsinized for 5-10 minutes at 37°C and plated in 48-well dishes.

4.16 *In vivo* transformation assay

In vivo tumorigenic assay was performed by subcutaneous injection in nude mice with the expert help of Devon White. MEFs were harvested by trypsinization, counted and resuspended in PBS. 5 10^5 diploid or tetraploid cells were resuspended in 150 ul of PBS and injected into the contra-lateral sides of NCR-Foxn1$^{nu/nu}$ female mice (Taconic). In some cases, two spots per side were injected. Injections were performed by Devon White or by me with Devons assistance after transiently anhestetizing the animals with isoflurane. The recipient mice were checked once or twice a week for tumor formation and euthanized when tumors reached 1 cm of diameter, in accordance with institutional procedures. Latency of the tumor was considered as the number of weeks prior to the development of a tumor of approximately 1 cm in diameter. When cell lines were derived from the tumors, the tumor mass was excised and dissociated in culture into single cells by treatment with collagenase A (Roche) at 250 units/ml in DMEM for 3 hours at 37°C or with collagenaseD/dispase neural protease (4mg/ml of each in DMEM, Boeringher Mannheim cat 1088858 and 165859) for 1 hour. Cells were then plated in complete medium for MEFs in 6-well dishes and expanded. All experiments involving mice were performed in accordance with the institutional regulations

and ethical guidelines, and have been authorized by the Institutional Animal Care and Use Committee (IACUC) at Rockefeller University.

4.17 Telomere length analysis

For genomic blotting, cells were harvested at the indicated PD, DNA was isolated by phenol-chloroform extraction using standard technique and digested with AluI and MboI restriction enzymes (New Engnd BioLabs). After measurement of the DNA concentration by fluorometer (Hoechst staining), 4 ug of DNA were size-fractionated on a 0.7% agarose gel and transferred to a Hybond membrane for hyridization using an 800-bp telomeric DNA probe from pSP73Sty11 labeled with [CCCTAA]3-primed Klenow polymerase and $\alpha -^{32} P - dCTP$. Blots were exposed to a phosphor-imaging screen and analyzed using ImageQuant software.

4.18 Fusion PCR Assay

DNA from 10^7 cells was first isolated by phenol-chloroform extraction (standard method), digested with EcoRI or XhoI restriction enzymes overnight at 37°C and analyzed for DNA concentration with fluorometer using Hoechst. Fusion PCR was performed using the following primer concentrations (primer sequence is given in the Appendix B): 1uM 21q1, 0.5uM 16p9, 0.25uM XpYpM, 0.25uM 17p6 and 0.05uM XpYp-ctr2 (in some cases the primer 16p9 was omitted). Each reaction was performed in a final volume of 20μl, containing 20-100ng of DNA, 2X Failsafe Buffer H (Epicenter, FSP995H) and 0.8μl of Failsafe

Enzyme Mix (Epicenter, FS99100). PCR cycles were as follow: 25 cycles of 94°C for 20 sec, 59°C for 20 sec and 68°C for 10 min, with a final extension time of 10 min at 68°C. Products of PCR reactions were resolved by 0.7% TAE (40 mM Tris acetate 1 mM EDTA pH 8) agarose gel electrophoresis and detection by Southern hybridization with random-primed probe labeled with $\alpha -^{32} P - dCTP$. 21q specific probe (21q probe) was made using 21q4 and 21q-seq-rev primers (Appendix B). The 0.5 kb product amplified by XpYpM and XpYp-ctr-2 was used as internal control and detected using a probe generated by XpYpO and XpYpB2 primers (XpYp probe). Nested PCR reactions for 21q primers were performed using 1 ul of 1:20 diluted primary PCR product and 21q3 primer as nested primer on the 21q subtelomere. Nested PCR was performed using the same PCR buffer/enzyme and the same thermal-cycling conditions described for the primary fusion PCR except that 35 cycles were performed. Blots were exposed to a phosphor-imaging screen and analyzed using ImageQuant software. For quantification of the fusion bands, ImageJ software was used to quantify the intensity of each band. An arbitrary threshold was decided for each Southern blot, in order to decide in each case whether to consider the band as a telomeric product or background or nonspecific product.

4.19 Tet-Off inducible system for POT1a expression

POT1a cloned into P-TRE-Tight and P-Tet-Off-Advanced (Clonetech) were transduced into POT1aF/-POT1bF/F MEFs. After treatment with Cre, clones were isolated with cloning cylinders and analyzed by PCR for the deletion of the endogenous POT1a. Clones were tested for doxycycline (2μg/ml) inducible depletion of POT1a and tetraploidy. Two clones were selected for further analysis, clones 19 and 26.

4.20 List of antibodies

POT1a (1221) and POT1b (1223) (Hockemeyer et al., 2006); ATR N-19 (sc-1887, Santa Cruz); Chk1 (sc-8408, Santa Cruz); Chk1 pS345 (2348, Cell Signaling Technology); Chk2 (611570, BD Biosciences); CyclinE M-20 (sc-481, Santa Cruz); CyclinA (sc-596, Santa Cruz), CyclinB1 (sc-245, Santa Cruz); AuroraA (ab13824, Abcam); AuroraB (ab2254, Abcam); Plk1 (06-813, Upstate); securin (K0090-3, MBL); Cdc20 (ab64877, Abcam); Cdh1 (ab5483, Abcam); geminin (sc-13015, Santa Cruz); β-actin (I-19) (sc-1616, Santa Cruz); Cdk1 (cc16, Calbiochem); Cdk2 (M2) (sc-163, Santa Cruz); APC1 (NB 100-86985, Novus Biologicals); Cdt1 (P26A6, a gift from A. Ballabeni (Ballabeni et al., 2004); Cdk1 P-Tyr14/15 (9111, Cell Signaling); pericentrin (ab4448 Abcam); Scc1 (K0202-3, MBL) ; p16 (C-20) (Santa Cruz). IF for 53BP1 was performed with Ab 100-304A (Novus Biologicals).

Appendix A

List of Movies

Movie 1

Chapter 1. Phase contrast imaging of control cells

POT1a$^{F/-}$POT1b$^{F/F}$ MEFs were infected with vector control an imaged (phase contrast, objective 10X) every 15 min for 48 h. Arrows highlight one dividing cell and its daughters. Selected frames from this movie are shown in Fig. 2.7A.

Chapter 2. Phase contrast imaging of POT1a/b DKO cells

POT1a$^{F/-}$POT1b$^{F/F}$ MEFs were treated with Cre and were imaged as in Chapter 1 (imaging started 72 h after introduction of Cre). Arrows highlight 3 representative cells that do not perform mitosis during the imaging session. Selected frames from this movie are shown in Fig. 2.7A.

Chapter 3. Phase contrast imaging of zeocin-treated cells

POT1a$^{F/-}$POT1b$^{F/F}$ MEFs were imaged as in Chapter 1 in the presence of zeocin (added two hours before starting imaging session and maintained in culture medium during the imaging session). Arrows highlight 3 representa-

tive cells not dividing during the session. Selected frames from this movie are shown in Fig. 2.7A.

Movie 2

Chapter 1. Imaging of control cells expressing CyclinE-eGFP

POT1a$^{F/-}$POT1b$^{F/F}$ MEFs were transduced with CyclinE-eGFP expressing vector and then treated with vector control. Cells were imaged (phase contrast and GFP channel, 20X objective) every 15 min. Arrows highlight representative cells showing raise in CyclinE-eGFP followed by mitosis.

Chapter 2. Imaging of POT1a/b DKO cells expressing CyclinE-eGFP

POT1a$^{F/-}$POT1b$^{F/F}$ MEFs were transduced with CyclinE-eGFP expressing vectors and then treated with Cre. After 72 h, cells were imaged as in Chapter 1. Arrows highlight representative cells showing CyclinE rising multiple times without an intervening mitosis.

Movie 3

Chapter 1. FUCCI imaging of control cells

POT1a$^{F/-}$POT1b$^{F/F}$ MEFs transduced with FUCCI vectors were treated with vector control and imaged (phase contrast, GFP and rhodamine channels) every 15 min for 72 h (10X objective). Arrows highlight a representative cell. Selected frames from this movie are shown in Fig. 2.8.

Chapter 2. FUCCI imaging of POT1a/b DKO cells

POT1a$^{F/-}$POT1b$^{F/F}$ MEFs transduced with FUCCI vectors were treated with

Cre and imaged as in Chapter 1 (imaging started 72 h after introduction of Cre). Arrows highlight representative cells showing geminin and Cdt1 oscillation in the absence of mitotic events. Selected frames from this movie are shown in Fig. 2.8.

Chapter 3. FUCCI imaging of zeocin-treated cells

POT1a$^{F/-}$POT1b$^{F/F}$ MEFs transduced with FUCCI vectors were imaged as in Chapter 1 in the presence of zeocin (added before the beginning of the session and maintained on the cells). Arrows highlight representative cells showing geminin and Cdt1 oscillation in the absence of mitotic events. Selected frames from this movie are shown in Fig. 2.8.

Movie 4

Chapter 1. FUCCI imaging of control BJ-SV40 cells

BJ human fibroblasts expressing SV40-LT transduced with FUCCI vectors were imaged (phase contrast, GFP and rhodamine channels) every 15 min for 96 h (10X objective). Arrow highlights a representative cell dividing during time.

Chapter 2. FUCCI imaging of BJ-SV40 cells treated with zeocin

BJ human fibroblasts expressing SV40-LT transduced with FUCCI vectors were imaged as in Chapter 1 in the presence of zeocin. Arrows highlight representative cells showing geminin and Cdt1 fluctuation in the absence of mitotic events.

Movie 5

Chapter 1. FUCCI imaging of synchronized control cells

POT1a$^{F/-}$POT1b$^{F/F}$ MEFs transduced with FUCCI vectors were synchronized in G1 by mitotic shake-off. Mitotic cells were plated and 10 h later, cells were imaged as in Movie 3. Selected frames from this movie are shown in Fig. 2.10A.

Chapter 2. FUCCI imaging of synchronized cells treated with zeocin

POT1a$^{F/-}$POT1b$^{F/F}$ MEFs transduced with FUCCI vectors were synchronized in G1 by mitotic shake-off. Mitotic cells were imaged as in Chapter 1 in the presence of zeocin (added 2 hours before the imaging session and maintained throughout). Selected frames from this movie are shown in Fig. 2.10A.

Movie 6

Chapter 1. FUCCI imaging of cells treated with Cdh1 shRNA

POT1a$^{F/-}$POT1b$^{F/F}$ MEFs transduced with FUCCI vectors were treated with Cdh1 shRNA and imaged (phase contrast, GFP and rhodamine channels, 10X objective) every 15 min over a period of 60 h. Arrow shows a representative cell dividing during the imaging session.

Chapter 2. FUCCI imaging of POT1a/b DKO cells treated with vector control for Cdh1 shRNA

POT1a$^{F/-}$POT1b$^{F/F}$ MEFs transduced with FUCCI vectors were treated with Cre and the day after with empty vector (pLK0.1) used for the Cdh1 shRNA. Cells were imaged (at 72 h after introduction of Cre) as in Chapter 1. Arrows highlight representative cells. Selected time points from this movie are shown in Fig. 2.12A.

Chapter 3. FUCCI imaging of POT1a/b DKO cells treated with Cdh1 shRNA

POT1a$^{F/-}$POT1b$^{F/F}$ MEFs transduced with FUCCI vectors were treated with Cre and the day after with Cdh1 shRNA. At 72 h after introduction of Cre, cells were imaged as in Chapter 1. Arrows highlight representative cells showing prolonged arrest in G2 without geminin degradation. Selected time points from this movie are shown in Fig. 2.12A.

Movie 7

Chapter 1. FUCCI imaging of zeocin-treated cells infected with vector control for Cdh1 shRNA

POT1aF/-POT1bF/F MEFs transduced with FUCCI vectors were treated with the empty vector (pLK0.1) used for Cdh1 shRNA. Cells were imaged as in Movie 6 in the presence of zeocin. Zeocin was added 2 h before the session and maintained on the cells. Arrows highlight representative cells over time. Selected time points from this movie are shown in Fig. 2.13A.

Chapter 2. FUCCI imaging of zeocin-treated cells infected with the Cdh1 shRNA

POT1a$^{F/-}$POT1b$^{F/F}$ MEFs transduced with FUCCI vectors were infected with Cdh1 shRNA and imaged in the presence of zeocin as in Chapter 1. Arrows highlight representative cells over time showing prolonged arrest in G2 without geminin degradation. Selected time points from this movie are shown in Fig. 2.13A.

Movie 8

Chapter 1. FUCCI imaging of BJ-SV40 cells PD 45

BJ-SV40 cells at PD45 were stably transduced with FUCCI vectors and imaged (phase contrast, GFP and rhodamine channels) for 96 hours every 20 min (10X objective). Most of the cells perform a normal mitotic cell cycle where the green geminin is degraded as the cell goes through mitosis. Selected frames of this movie are shown in Fig. 2.22A.

Chapter 2. FUCCI imaging of BJ-SV40 cells PD 105

BJ-SV40 cells PD105 stably expressing the FUCCI markers were imaged as in Chapter 1. Arrows highlight representative cells becoming tetraploid during the imaging. White arrows highlight representative cells undergoing endoreduplication, and black arrows highlight cells undergoing mitotic failure. Selected frames of this movie are shown in Fig. 2.22A.

Chapter 3. FUCCI imaging of BJ-SV40 cells PD 100

BJ-SV40 cells PD100 (experiment independent from the one shown in Chapter 2) stably expressing the FUCCI markers were imaged as in Chapter 1. Arrows highlight representative cells becoming tetraploid during the imaging. White arrows highlight representative cells undergoing endoreduplication, black arrows highlight cells undergoing mitotic failure.

Movie 9

Chapter 1. FUCCI imaging of IMR90-SV40 cells PD 62

IMR90-SV40 cells PD62 were stably transduced with FUCCI vectors and analyzed by live cell imaging as in Movie 8. Selected frames of this movie are

shown in Fig. 2.22B.

Chapter 2. FUCCI imaging of IMR90-SV40 cells PD 90

IMR90-SV40 cells PD90 stably expressing FUCCI vectors were analyzed by live-cell imaging as in Movie 8. Arrows highlight representative cells becoming tetraploid during the imaging. White arrows highlight representative cells undergoing endoreduplication and black arrows highlight cells undergoing mitotic failure (as in Movie 8). Selected frames of this movie are shown in Fig. 2.22B.

Movie 10

Chapter 1. FUCCI imaging of hMECs 48RS-GSE22 p20

hMECs 48RS-GSE22 passage 20 (early passage) stably expressing FUCCI markers were imaged as in Movie 8. Selected frames of this are shown in Fig. 2.24.

Chapter 2. FUCCI imaging of hMECs 48RS-GSE22 p32

hMECs 48RS-GSE22 passage 32 (telomere crisis) stably expressing FUCCI markers were imaged as in Movie 8. White arrows highlight representative cells undergoing endoreduplication, and black arrows highlight cells undergoing mitotic failure Selected frames of this movie are shown in Fig. 2.24.

Chapter 3. FUCCI imaging of hMECs p20 48RS-GSE22 p20 treated with zeocin

hMECs 48RS-GSE22 passage 20 stably expressing FUCCI markers were imaged in the presence of zeocin. White arrows highlight endocycle events and black arrows highlight mitotic failure events. Selected frames of this movie are shown in Fig. 2.24.

Movie 11

Chapter 1. FUCCI imaging of G1-sorted BJ-p53dn cells treated with zeocin

BJ-p53dn cells at PD35 transduced with the FUCCI vectors were FACS sorted to isolate the cells in G1 (Cdt1, red). Sorted BJ-p53dn G1 cells were imaged in the presence of zeocin. Selected frames are shown in Fig. 2.29.

Chapter 2. FUCCI imaging of G1-sorted BJ-SV40 cells treated with zeocin

BJ-SV40 cells at PD40 transduced with the FUCCI vectors were FACS sorted for the cells in G1 (Cdt1, red) and imaged as in Chapter1 in the presence of zeocin. Selected frames are shown in Fig. 2.29.

Movie 12

Chapter 1. FUCCI imaging of G2-sorted BJ-p53dn cells treated with zeocin

BJ-p53dn cells at PD35 transduced with the FUCCI vectors were FACS sorted for selection of cells in late S/G2 (geminin, green). S/G2-sorted cells were imaged as in Movie 12 in the presence of zeocin. Selected frames are shown in Fig. 2.29.

Chapter 2. FUCCI imaging of G2-sorted BJ-SV40 cells treated with zeocin

BJ-SV40 cells at PD40 transduced with the FUCCI vectors were FACS sorted for cells in late S/G2 (geminin, green). S/G2-sorted cells were imaged as in

Movie 11 in the presence of zeocin. Selected frames are shown in Fig. 2.29.

Movie 13

Chapter 1 Imaging of sorted diploid cells after re-expression of POT1a

H2B-GFP expressing POT1a-tetOFF cell line 19 was treated as described in Fig. 2.34A and after sorting diploid cells were imaged in the absence of doxycycline (phase contrast and GFP channel) every 15 min for 72 hours. Arrows highlight a representative cell dividing multiple times. Selected time points from this movie are shown in Fig. 2.34B.

Chapter 2 Imaging of sorted tetraploid cells after re-expression of POT1a

H2B-GFP expressing POT1a-tetOFF cell line 19 was treated as described in Fig. 2.34A and after sorting tetraploid cells were imaged as in Chapter 1. Arrows highlight representative cells dividing during time. Cells showing evidence of multipolar spindles are marked with three red arrows. Selected time points from this movie are shown in Fig. 2.34B.

Movie 14

Chapter 1. FUCCI imaging of BRCA2$^{F/+}$ MEFs treated with Cre

BRCA2$^{F/+}$ MEFs were treated with Cre as in Fig. 2.47 and analyzed by FUCCI imaging at day 8 after Cre. Arrows indicate cells undergoing endoreduplication.

Chapter 2. FUCCI imaging of BRCA2$^{F/-}$ MEFs treated with Cre

BRCA2$^{F/-}$ MEFs were treated with Cre as in Fig. 2.47 and analyzed by FUCCI

imaging at day 8 after Cre. Arrows indicate endoreduplicating cells.

Movie 15

Chapter 1. FUCCI imaging of RPE SV40 cells

RPE SV40 control cells were analyzed by FUCCI imaging.

Chapter 2. FUCCI imaging of RPE SV40 cells overexpressing RasV12

RPE SV40 cells were transduced to overexpress RasV12 as in Fig. 2.48 and analyzed by FUCCI imaging after 8 days.

Appendix B

Fusion PCR primers

The following figure shows the sequence of the primers used in the Fusion PCR assay.

Primer	Sequence	Use
XpYpM	ACCAGGTTTTCCAGTGTGTT	fusion PCR
17p6	GGCTGAACTATAGCCTCTGC	fusion PCR
21q4	GGGACATATTTTGGGGTTGC	fusion PCR and 21q probe
16p9	CCGGATTTCCTTTGCTGTTCC	fusion PCR and 16p probe
XpYpctr2	GCTATGGCTTCTTGGGGC	internal control in fusion PCR
XpYpO	CCTGTAACGCTGT TAGGTAC	XpYp probe
XpYpG	AATTCCAGACACACTAGGACCCTGA	XpYp probe
17p2	GAGTCAATGATTCCATTCCTA	17p probe
17p7	CCTGGCATGGTATTGACATG	17p probe
16p-seq-rev12	CATGTGTGCATTAGGAATGCTG	16p probe
21q-seq-rev2	ACACAGAAGGTTGATATACACAG	21q probe

Figure B.1: **Sequence of the primers used in the fusion PCR assay.**

Appendix C

List of cell Lines

The following list includes the the cell lines used in this work.

Cell Lines	Organism, organ	Notes
293T	Human, kidney	lentiviral system
Phoenix, eco	Human, epithelial	293T derivative, retroviral system
Phoenix, ampho	Huma, epithelial	293T derivative, retroviral system
BJ	Human, foreskin	primary fibroblasts
IMR90	Human, lung	primary fibroblasts
RPE	Human, retinal pigment epithelium	primary epithelial cells
48RS	Human, mammary gland	Romanov et al., 2001
48RS GSE22	Human, mammary gland	Romanov et al., 2001
184B	Human, mammary gland	Garbe et al., 2007
184B GSE22	Human, mammary gland	Garbe et al., 2007
ATCC30-4500K	Human, breast cancer	some of the lines were used in this study
$POT1a^{F/-}$ $POT1b^{F/F}$	Mouse, E13.5 MEF	Hockemeyer et al., 2006; this work
$POT1a^{F/-}$ $POT1b^{F/F}$ $ATM^{+/-}$	Mouse, E13.5 MEF	this work
$POT1a^{F/-}$ $POT1b^{F/F}$ $ATM^{-/-}$	Mouse, E13.5 MEF	this work
$BRCA2^{F/F}$; $BRCA2^{F/-}$	Mouse, mouse embryo	Badie et al., 2010

Figure C.1: **List of the cell lines used.** List of the cell lines used in this work including the organism and organ of origin and the reference, if not produced in this work.

Bibliography

Abate-Shen, C., and Shen, M. M. (2000). Molecular genetics of prostate cancer. Genes Dev 14, 2410-2434.

Adler, C. P., and Costabel, U. (1975). Cell number in human heart in atrophy, hypertrophy, and under the influence of cytostatics. Recent Adv Stud Cardiac Struct Metab 6, 343-355.

Andalis, A. A., Storchova, Z., Styles, C., Galitski, T., Pellman, D., and Fink, G. R. (2004). Defects arising from whole-genome duplications in Saccharomyces cerevisiae. Genetics 167, 1109-1121.

Anderson, J. B., Sirjusingh, C., Parsons, A. B., Boone, C., Wickens, C., Cowen, L. E., and Kohn, L. M. (2003). Mode of selection and experimental evolution of antifungal drug resistance in Saccharomyces cerevisiae. Genetics 163, 1287-1298.

Anderson, J. B., Sirjusingh, C., and Ricker, N. (2004). Haploidy, diploidy and evolution of antifungal drug resistance in Saccharomyces cerevisiae. Genetics 168, 1915-1923.

Andreassen, P. R., Lohez, O. D., Lacroix, F. B., and Margolis, R. L. (2001).

Tetraploid state induces p53-dependent arrest of nontransformed mammalian cells in G1. Mol Biol Cell 12, 1315-1328.

Arias, E. E., and Walter, J. C. (2005). Replication-dependent destruction of Cdt1 limits DNA replication to a single round per cell cycle in Xenopus egg extracts. Genes Dev 19, 114-126.

Artandi, S. E., Chang, S., Lee, S. L., Alson, S., Gottlieb, G. J., Chin, L., and DePinho, R. A. (2000). Telomere dysfunction promotes non-reciprocal translocations and epithelial cancers in mice. Nature 406, 641-645.

Atkin, N. B., and Richards B. M. (1956). Deoxyribonucleic acid in human tumours as measured by microspectrophotometry of Feulgen stain: a comparison of tumours arising at different sites. Br J Cancer 10, 769-786.

Badie, S., Escandell, J. M., Bouwman, P., Carlos, A. R., Thanasoula, M., Gallardo, M. M., Suram, A., Jaco, I., Benitez, J., Herbig, U., Blasco, M. A., Jonkers, J., and Tarsounas, M. (2010). BRCA2 acts as a RAD51 loader to facilitate telomere replication and capping. Nat Struct Mol Biol 17, 1461-1469.

Baker, S. J., Preisinger, A. C., Jessup, J. M., Paraskeva, C., Markowitz, S., Willson, J. K., Hamilton, S., and Vogelstein, B. (1990). p53 gene mutations occur in combination with 17p allelic deletions as late events in colorectal tumorigenesis. Cancer Res 50, 7717-7722.

Ballabeni, A., Melixetian, M., Zamponi, R., Masiero, L., Marinoni, F., and Helin, K. (2004). Human geminin promotes pre-RC formation and DNA replication by stabilizing CDT1 in mitosis. EMBO J 23, 3122-3132.

Barlow, C., Hirotsune, S., Paylor, R., Liyanage, M., Eckhaus, M., Collins, F., Shiloh, Y., Crawley, J. N., Ried, T., Tagle, D., and Wynshaw-Boris, A. (1996). Atm-deficient mice: a paradigm of ataxia telangiectasia. Cell 86, 159-171.

Bartkova, J., Horejsi, Z., Koed, K., Kramer, A., Tort, F., Zieger, K., Guldberg, P., Sehested, M., Nesland, J. M., Lukas, C., Orntoft, T., Lukas, J., and Bartek, J. (2005). DNA damage response as a candidate anti-cancer barrier in early human tumorigenesis. Nature 434, 864-870.

Bartkova, J., Rezaei, N., Liontos, M., Karakaidos, P., Kletsas, D., Issaeva, N., Vassiliou, L. V., Kolettas, E., Niforou, K., Zoumpourlis, V. C., Takaoka, M., Nakagawa, H., Tort, F., Fugger, K., Johansson, F., Sehested, M., Andersen, C. L., Dyrskjot, L., Orntoft, T., Lukas, J., Kittas, C., Helleday, T., Halazonetis, T. D., Bartek, J., and Gorgoulis, V. G. (2006). Oncogene-induced senescence is part of the tumorigenesis barrier imposed by DNA damage checkpoints. Nature 444, 633-637.

Bassermann, F., Frescas, D., Guardavaccaro, D., Busino, L., Peschiaroli, A., and Pagano, M. (2008). The Cdc14B-Cdh1-Plk1 axis controls the G2 DNA-

damage-response checkpoint. Cell 134, 256-267.

Bast, R. C. J., Hennessy, B., and Mills, G. B. (2009). The biology of ovarian cancer: new opportunities for translation. Nat Rev Cancer 9, 415-428.

Baumann, P., and Cech, T. R. (2000). Protection of telomeres by the Ku protein in fission yeast. Mol Biol Cell 11, 3265-3275.

Baumann, P., and Cech, T. R. (2001). Pot1, the putative telomere end-binding protein in fission yeast and humans. Science 292, 1171-1175.

Benn, P. A. (1976). Specific chromosome aberrations in senescent fibroblast cell lines derived from human embryos. Am J Hum Genet 28, 465-473.

Bianchi, A., Smith, S., Chong, L., Elias, P., and de Lange, T. (1997). TRF1 is a dimer and bends telomeric DNA. Embo J 16, 1785-1794.

Biesterfeld, S., Gerres, K., Fischer-Wein, G., and Bocking, A. (1994). Polyploidy in non-neoplastic tissues. J Clin Pathol 47, 38-42.

Bilaud, T., Brun, C., Ancelin, K., Koering, C. E., Laroche, T., and Gilson, E. (1997). Telomeric localization of TRF2, a novel human telobox protein. Nat Genet 17, 236-239.

Bischoff, J. R., Anderson, L., Zhu, Y., Mossie, K., Ng, L., Souza, B., Schryver, B., Flanagan, P., Clairvoyant, F., Ginther, C., Chan, C. S., Novotny, M., Slamon, D. J., and Plowman, G. D. (1998). A homologue of Drosophila aurora kinase is oncogenic and amplified in human colorectal cancers. EMBO J 17, 3052-3065.

Blow, J. J., and Dutta, A. (2005). Preventing re-replication of chromosomal DNA. Nat Rev Mol Cell Biol 6, 476-486.

Bodnar, A. G., Ouellette, M., Frolkis, M., Holt, S. E., Chiu, C. P., Morin, G. B., Harley, C. B., Shay, J. W., Lichtsteiner, S., and Wright, W. E. (1998). Extension of life-span by introduction of telomerase into normal human cells. Science 279, 349-352.

Boveri, T. (1914), Zur Frage der Entstehung maligner Tumoren. (Gustav Fisher Verlag, Jena, Germany

Braly, P. S., and Klevecz, R. R. (1993). Flow cytometric evaluation of ovarian cancer. Cancer 71, 1621-1628.

Broccoli, D., Smogorzewska, A., Chong, L., and de Lange, T. (1997). Human telomeres contain two distinct Myb-related proteins, TRF1 and TRF2. Nat Genet 17, 231-235.

Broccoli, D., Young, J. W., and de Lange, T. (1995). Telomerase activity in normal and malignant hematopoietic cells. Proc Natl Acad Sci USA 92, 9082-9086.

Bryan, T. M., Englezou, A., Dalla-Pozza, L., Dunham, M. A., and Reddel, R. R. (1997). Evidence for an alternative mechanism for maintaining telomere length in human tumors and tumor-derived cell lines. Nat Med 3, 1271-1274.

Bryan, T. M., Englezou, A., Gupta, J., Bacchetti, S., and Reddel, R. R. (1995). Telomere elongation in immortal human cells without detectable telomerase activity. Embo J 14, 4240-4248.

Bulavin, D. V., Tararova, N. D., Aksenov, N. D., Pospelov, V. A., and Pospelova, T. V. (1999). Deregulation of p53/p21Cip1/Waf1 pathway contributes to polyploidy and apoptosis of E1A+cHa-ras transformed cells after gamma-irradiation. Oncogene 18, 5611-5619.

Caldwell, C. M., Green, R. A., and Kaplan, K. B. (2007). APC mutations lead to cytokinetic failures in vitro and tetraploid genotypes in Min mice. J Cell Biol 178, 1109-1120.

Cantero, G., Pastor, N., Mateos, S., Campanella, C., and Cortes, F. (2006). Cisplatin-induced endoreduplication in CHO cells: DNA damage and inhibition of topoisomerase II. Mutat Res 599, 160-166.

Capper, R., Britt-Compton, B., Tankimanova, M., Rowson, J., Letsolo, B., Man, S., Haughton, M., and Baird, D. M. (2007). The nature of telomere fusion and a definition of the critical telomere length in human cells. Genes Dev 21, 2495-2508.

Carder, P., Wyllie, A. H., Purdie, C. A., Morris, R. G., White, S., Piris, J., and Bird, C. C. (1993). Stabilised p53 facilitates aneuploid clonal divergence in colorectal cancer. Oncogene 8, 1397-1401.

Castedo, M., Coquelle, A., Vitale, I., Vivet, S., Mouhamad, S., Viaud, S., Zitvogel, L., and Kroemer, G. (2006). Selective resistance of tetraploid cancer cells against DNA damage-induced apoptosis. Ann N Y Acad Sci 1090, 35-49.

Celli, G. B., and de Lange, T. (2005). DNA processing is not required for ATM-mediated telomere damage response after TRF2 deletion. Nat Cell Biol 7, 712-718.

Celton-Morizur, S., and Desdouets, C. (2010). Polyploidization of liver cells. Adv Exp Med Biol 676, 123-135.

Celton-Morizur, S., Merlen, G., Couton, D., and Desdouets, C. (2010). Polyploidy and liver proliferation: central role of insulin signaling. Cell Cycle 9, 460-466.

Chicas, A., Wang, X., Zhang, C., McCurrach, M., Zhao, Z., Mert, O., Dickins, R. A., Narita, M., Zhang, M., and Lowe, S. W. (2010). Dissecting the unique role of the retinoblastoma tumor suppressor during cellular senescence. Cancer Cell 17, 376-387.

Chin, K., De Solorzano, C. O., Knowles, D., Jones, A., Chou, W., Rodriguez, E. G., Kuo, W. L., Ljung, B. M., Chew, K., Myambo, K., Miranda, M., Krig, S., Garbe, J., Stampfer, M., Yaswen, P., Gray, J. W., and Lockett, S. J. (2004). In situ analyses of genome instability in breast cancer. Nat Genet 36, 984-988.

Chong, L., van Steensel, B., Broccoli, D., Erdjument-Bromage, H., Hanish, J., Tempst, P., and de Lange, T. (1995). A human telomeric protein. Science 270, 1663-1667.

Ciccia, A., and Elledge, S. J. (2010). The DNA damage response: making it safe to play with knives. Mol Cell 40, 179-204.

Colegrave, N., and Collins, S. (2008). Experimental evolution: experimental evolution and evolvability. Heredity 100, 464-470.

Comai, L. (2005). The advantages and disadvantages of being polyploid. Nat Rev Genet 6, 836-846.

Comai, L., Tyagi, A. P., Winter, K., Holmes-Davis, R., Reynolds, S. H., Stevens, Y., and Byers, B. (2000). Phenotypic instability and rapid gene silencing in newly formed arabidopsis allotetraploids. Plant Cell 12, 1551-1568.

Cortes, F., and Pastor, N. (2003). Induction of endoreduplication by topoisomerase II catalytic inhibitors. Mutagenesis 18, 105-112.

Coschi, C. H., Martens, A. L., Ritchie, K., Francis, S. M., Chakrabarti, S., Berube, N. G., and Dick, F. A. (2010). Mitotic chromosome condensation mediated by the retinoblastoma protein is tumor-suppressive. Genes Dev 24, 1351-1363.

Cosimi, S., Orta, L., Mateos, S., and Cortes, F. (2009). The mycotoxin ochratoxin A inhibits DNA topoisomerase II and induces polyploidy in cultured CHO cells. Toxicol In Vitro 23, 1110-1115.

Crasta, K., Ganem, N. J., Dagher, R., Lantermann, A. B., Ivanova, E. V., Pan, Y., Nezi, L., Protopopov, A., Chowdhury, D., and Pellman, D. (2012). DNA breaks and chromosome pulverization from errors in mitosis. Nature 482, 53-58.

Creasy, M. R., Crolla, J. A., and Alberman, E. D. (1976). A cytogenetic study of human spontaneous abortions using banding techniques. Hum Genet 31, 177-196.

Crow, K. D., and Wagner, G. P. (2006). Proceedings of the SMBE Tri-National Young Investigators' Workshop 2005. What is the role of genome duplication in the evolution of complexity and diversity? Mol Biol Evol 23, 887-892.

d'Adda di Fagagna, F. (2008). Living on a break: cellular senescence as a DNA-damage response. Nat Rev Cancer 8, 512-522.

d'Adda di Fagagna, F., Reaper, P. M., Clay-Farrace, L., Fiegler, H., Carr, P., Von Zglinicki, T., Saretzki, G., Carter, N. P., and Jackson, S. P. (2003). A DNA damage checkpoint response in telomere-initiated senescence. Nature 426, 194-198.

Davoli, T., Denchi, E. L., and de Lange, T. (2010). Persistent telomere damage induces bypass of mitosis and tetraploidy. Cell 141, 81-93.

de Lange, T. (1995). Telomere dynamics and genome instability in human cancer. In Telomeres, Greider, E. H. B. a. C. W., ed. (CSH: CSH press), pp. 265-293.

de Lange, T. (2005). Telomere-related Genome Instability in Cancer. Cold Spring Harb Symp Quant Biol 70, 197-204.

de Lange, T., Shiue, L., Myers, R. M., Cox, D. R., Naylor, S. L., Killery, A.

M., and Varmus, H. E. (1990). Structure and variability of human chromosome ends. Mol Cell Biol 10, 518-527.

Deckbar, D., Birraux, J., Krempler, A., Tchouandong, L., Beucher, A., Walker, S., Stiff, T., Jeggo, P., and Lobrich, M. (2007). Chromosome breakage after G2 checkpoint release. J Cell Biol 176, 749-755.

Deitch, A. D., Miller, G. J., and deVere White, R. W. (1993). Significance of abnormal diploid DNA histograms in localized prostate cancer and adjacent benign prostatic tissue. Cancer 72, 1692-1700.

Denchi, E. L., and de Lange, T. (2007). Protection of telomeres through independent control of ATM and ATR by TRF2 and POT1. Nature 448, 1068-1071.

der-Sarkissian, H., Bacchetti, S., Cazes, L., and Londono-Vallejo, J. A. (2004). The shortest telomeres drive karyotype evolution in transformed cells. Oncogene 23, 1221-1228.

Di Micco, R., Fumagalli, M., Cicalese, A., Piccinin, S., Gasparini, P., Luise, C., Schurra, C., Garre', M., Nuciforo, P. G., Bensimon, A., Maestro, R., Pelicci, P. G., and d'Adda di Fagagna, F. (2006). Oncogene-induced senescence is a DNA damage response triggered by DNA hyper-replication. Nature 444, 638-642.

Diffley, J. F. (2004). Regulation of early events in chromosome replication. Curr Biol 14, R778-86.

Dikovskaya, D., Newton, I. P., and Nathke, I. S. (2004). The adenomatous polyposis coli protein is required for the formation of robust spindles formed in CSF Xenopus extracts. Mol Biol Cell 15, 2978-2991.

Dikovskaya, D., Schiffmann, D., Newton, I. P., Oakley, A., Kroboth, K., Sansom, O., Jamieson, T. J., Meniel, V., Clarke, A., and Nathke, I. S. (2007). Loss of APC induces polyploidy as a result of a combination of defects in mitosis and apoptosis. J Cell Biol 176, 183-195.

Ding, Z., Wu, C. J., Jaskelioff, M., Ivanova, E., Kost-Alimova, M., Protopopov, A., Chu, G. C., Wang, G., Lu, X., Labrot, E. S., Hu, J., Wang, W., Xiao, Y., Zhang, H., Zhang, J., Zhang, J., Gan, B., Perry, S. R., Jiang, S., Li, L., Horner, J. W., Wang, Y. A., Chin, L., and DePinho, R. A. (2012). Telomerase reactivation following telomere dysfunction yields murine prostate tumors with bone metastases. Cell 148, 896-907.

Draviam, V. M., Shapiro, I., Aldridge, B., and Sorger, P. K. (2006). Misorientation and reduced stretching of aligned sister kinetochores promote chromosome missegregation in EB1- or APC-depleted cells. EMBO J 25, 2814-2827.

Duelli, D., and Lazebnik, Y. (2007). Cell-to-cell fusion as a link between viruses and cancer. Nat Rev Cancer 7, 968-976.

Duelli, D. M., Padilla-Nash, H. M., Berman, D., Murphy, K. M., Ried, T., and Lazebnik, Y. (2007). A virus causes cancer by inducing massive chromosomal instability through cell fusion. Curr Biol 17, 431-437.

Duncan, A. W., Hickey, R. D., Paulk, N. K., Culberson, A. J., Olson, S. B., Finegold, M. J., and Grompe, M. (2009). Ploidy reductions in murine fusion-derived hepatocytes. PLoS Genet 5, e1000385.

Duncan, A. W., Taylor, M. H., Hickey, R. D., Hanlon Newell, A. E., Lenzi, M. L., Olson, S. B., Finegold, M. J., and Grompe, M. (2010). The ploidy conveyor of mature hepatocytes as a source of genetic variation. Nature 467, 707-710.

Dutrillaux, B., Gerbault-Seureau, M., Remvikos, Y., Zafrani, B., and Prieur, M. (1991). Breast cancer genetic evolution: I. Data from cytogenetics and DNA content. Breast Cancer Res Treat 19, 245-255.

Fei, P., Bernhard, E. J., and El-Deiry, W. S. (2002). Tissue-specific induction of p53 targets in vivo. Cancer Res 62, 7316-7327.

Finley, J. C., Reid, B. J., Odze, R. D., Sanchez, C. A., Galipeau, P., Li, X.,

Self, S. G., Gollahon, K. A., Blount, P. L., and Rabinovitch, P. S. (2006). Chromosomal instability in Barrett's esophagus is related to telomere shortening. Cancer Epidemiol Biomarkers Prev 15, 1451-1457.

Fodde, R., Kuipers, J., Rosenberg, C., Smits, R., Kielman, M., Gaspar, C., van Es, J. H., Breukel, C., Wiegant, J., Giles, R. H., and Clevers, H. (2001a). Mutations in the APC tumour suppressor gene cause chromosomal instability. Nat Cell Biol 3, 433-438.

Fodde, R., Smits, R., and Clevers, H. (2001b). APC, signal transduction and genetic instability in colorectal cancer. Nat Rev Cancer 1, 55-67.

Fouladi, B., Sabatier, L., Miller, D., Pottier, G., and Murnane, J. P. (2000). The relationship between spontaneous telomere loss and chromosome instability in a human tumor cell line. Neoplasia 2, 540-554.

Freeling, M., and Thomas, B. C. (2006). Gene-balanced duplications, like tetraploidy, provide predictable drive to increase morphological complexity. Genome Res 16, 805-814.

Fujiwara, T., Bandi, M., Nitta, M., Ivanova, E. V., Bronson, R. T., and Pellman, D. (2005). Cytokinesis failure generating tetraploids promotes tumorigenesis in p53-null cells. Nature 437, 1043-1047.

Galbraith, D. W., Harkins, K. R., and Knapp, S. (1991). Systemic Endopolyploidy in Arabidopsis thaliana. Plant Physiol 96, 985-989.

Galipeau, P. C., Cowan, D. S., Sanchez, C. A., Barrett, M. T., Emond, M. J., Levine, D. S., Rabinovitch, P. S., and Reid, B. J. (1996). 17p (p53) allelic losses, 4N (G2/tetraploid) populations, and progression to aneuploidy in Barrett's esophagus. Proc Natl Acad Sci U S A 93, 7081-7084.

Ganem, N. J., Godinho, S. A., and Pellman, D. (2009). A mechanism linking extra centrosomes to chromosomal instability. Nature 460, 278-282.

Gao, P., and Zheng, J. (2010). High-risk HPV E5-induced cell fusion: a critical initiating event in the early stage of HPV-associated cervical cancer. Virology Journal 7, 238.

Garbe, J. C., Holst, C. R., Bassett, E., Tlsty, T., and Stampfer, M. R. (2007). Inactivation of p53 function in cultured human mammary epithelial cells turns the telomere-length dependent senescence barrier from agonescence into crisis. Cell Cycle 6, 1927-1936.

Garber, M. E., Troyanskaya, O. G., Schluens, K., Petersen, S., Thaesler, Z., Pacyna-Gengelbach, M., van de Rijn, M., Rosen, G. D., Perou, C. M., Whyte, R. I., Altman, R. B., Brown, P. O., Botstein, D., and Petersen, I. (2001). Diversity of gene expression in adenocarcinoma of the lung. Proc Natl Acad

Sci U S A 98, 13784-13789.

Garcia-Higuera, I., Manchado, E., Dubus, P., Canamero, M., Mendez, J., Moreno, S., and Malumbres, M. (2008). Genomic stability and tumour suppression by the APC/C cofactor Cdh1. Nat Cell Biol 10, 802-811.

Gardner, R. L., and Davies, T. J. (1993). Lack of coupling between onset of giant transformation and genome endoreduplication in the mural trophectoderm of the mouse blastocyst. J Exp Zool 265, 54-60.

Geng, L., Zhang, X., Zheng, S., and Legerski, R. J. (2007). Artemis links ATM to G2/M checkpoint recovery via regulation of Cdk1-cyclin B. Mol Cell Biol 27, 2625-2635.

Geng, Y., Yu, Q., Sicinska, E., Das, M., Schneider, J. E., Bhattacharya, S., Rideout, W. M., Bronson, R. T., Gardner, H., and Sicinski, P. (2003). Cyclin E ablation in the mouse. Cell 114, 431-443.

Gil, J., and Peters, G. (2006). Regulation of the INK4b-ARF-INK4a tumour suppressor locus: all for one or one for all. Nat Rev Mol Cell Biol 7, 667-677.

Godinho, S. A., Kwon, M., and Pellman, D. (2009). Centrosomes and cancer: how cancer cells divide with too many centrosomes. Cancer Metastasis Rev 28, 85-98.

Goncalves, C. R., Antonini, S., Vianna-Morgante, A. M., Machado-Santelli, G. M., and Bevilacqua, E. (2003). Developmental changes in the ploidy of mouse implanting trophoblast cells in vitro. Histochem Cell Biol 119, 189-198.

Gong, Y., and de Lange, T. (2010). A Shld1-controlled POT1a provides support for repression of ATR signaling at telomeres through RPA exclusion. Mol Cell 40, 377-387.

Gonzalez-Suarez, E., Samper, E., Flores, J. M., and Blasco, M. A. (2000). Telomerase-deficient mice with short telomeres are resistant to skin tumorigenesis. Nat Genet 26, 114-117.

Gonzalez, M. A., Tachibana, K. E., Adams, D. J., van der Weyden, L., Hemberger, M., Coleman, N., Bradley, A., and Laskey, R. A. (2006). Geminin is essential to prevent endoreduplication and to form pluripotent cells during mammalian development. Genes Dev 20, 1880-1884.

Gorgoulis, V. G., Vassiliou, L. V., Karakaidos, P., Zacharatos, P., Kotsinas, A., Liloglou, T., Venere, M., Ditullio, R. A. J., Kastrinakis, N. G., Levy, B., Kletsas, D., Yoneta, A., Herlyn, M., Kittas, C., and Halazonetis, T. D. (2005). Activation of the DNA damage checkpoint and genomic instability in human precancerous lesions. Nature 434, 907-913.

Gorla, G. R., Malhi, H., and Gupta, S. (2001). Polyploidy associated with oxidative injury attenuates proliferative potential of cells. J Cell Sci 114, 2943-2951.

Greenberg, R. A., Chin, L., Femino, A., Lee, K. H., Gottlieb, G. J., Singer, R. H., Greider, C. W., and DePinho, R. A. (1999). Short dysfunctional telomeres impair tumorigenesis in the INK4a(delta2/3) cancer-prone mouse. Cell 97, 515-525.

Gretarsdottir, S., Thorlacius, S., Valgardsdottir, R., Gudlaugsdottir, S., Sigurdsson, S., Steinarsdottir, M., Jonasson, J. G., Anamthawat-Jonsson, K., and Eyfjord, J. E. (1998). BRCA2 and p53 mutations in primary breast cancer in relation to genetic instability. Cancer Res 58, 859-862.

Griffith, J. D., Comeau, L., Rosenfield, S., Stansel, R. M., Bianchi, A., Moss, H., and de Lange, T. (1999). Mammalian telomeres end in a large duplex loop. Cell 97, 503-514.

Guidotti, J. E., Bregerie, O., Robert, A., Debey, P., Brechot, C., and Desdouets, C. (2003). Liver cell polyploidization: a pivotal role for binuclear hepatocytes. J Biol Chem 278, 19095-19101.

Hahn, W. C., Stewart, S. A., Brooks, M. W., York, S. G., Eaton, E., Kurachi, A., Beijersbergen, R. L., Knoll, J. H., Meyerson, M., and Weinberg, R. A.

(1999). Inhibition of telomerase limits the growth of human cancer cells. Nat Med 5, 1164-1170.

Hamada, S., Itoh, R., and Fujita, S. (1988). DNA distribution pattern of the so-called severe dysplasias and small carcinomas of the colon and rectum and its possible significance in the tumor progression. Cancer 61, 1555-1562.

Hashimoto, M. W., Nikaido, O., Kobayashi, N., Chang, C. C., Trosko, J. E., and Mori, T. (1996). A comparison of the propensity for gene amplification between near-tetraploid and near-diploid V79 clones resistant to 150 nM methotrexate. Carcinogenesis 17, 389-394.

Hastie, N. D., Dempster, M., Dunlop, M. G., Thompson, A. M., Green, D. K., and Allshire, R. C. (1990). Telomere reduction in human colorectal carcinoma and with ageing. Nature 346, 866-868.

Hattori, N., Davies, T. C., Anson-Cartwright, L., and Cross, J. C. (2000). Periodic expression of the cyclin-dependent kinase inhibitor p57(Kip2) in trophoblast giant cells defines a G2-like gap phase of the endocycle. Mol Biol Cell 11, 1037-1045.

Hayles, J., Fisher, D., Woollard, A., and Nurse, P. (1994). Temporal order of S phase and mitosis in fission yeast is determined by the state of the p34cdc2-mitotic B cyclin complex. Cell 78, 813-822.

Helleday, T., Petermann, E., Lundin, C., Hodgson, B., and Sharma, R. A. (2008). DNA repair pathways as targets for cancer therapy. Nat Rev Cancer 8, 193-204.

Henery, C. C., Bard, J. B. L., and Kaufman, M. H. (1992). Tetraploidy in mice, embryonic cell number, and the grain of the developmental map. Developmental biology 152, 233-241.

Herbert, B. S., Wright, W. E., and Shay, J. W. (2001). Telomerase and breast cancer. Breast Cancer Res 3, 146-149.

Hilgenfeld, E., Padilla-Nash, H., Schrock, E., and Ried, T. (1999). Analysis of B-cell neoplasias by spectral karyotyping (SKY). Curr Top Microbiol Immunol 246, 169-174.

Hisaoka, M., Tanaka, A., and Hashimoto, H. (2002). Molecular alterations of h-warts/LATS1 tumor suppressor in human soft tissue sarcoma. Lab Invest 82, 1427-1435.

Hixon, M. L., and Gualberto, A. (2003). Vascular smooth muscle polyploidization–from mitotic checkpoints to hypertension. Cell Cycle 2, 105-110.

Hockemeyer, D., Daniels, J. P., Takai, H., and de Lange, T. (2006). Recent

expansion of the telomeric complex in rodents: Two distinct POT1 proteins protect mouse telomeres. Cell 126, 63-77.

Hockemeyer, D., Palm, W., Else, T., Daniels, J. P., Takai, K. K., Ye, J. Z., Keegan, C. E., de Lange, T., and Hammer, G. D. (2007). Telomere protection by mammalian POT1 requires interaction with TPP1. Nat Struct Mol Biol 14, 754-761.

Holland, A. J., and Cleveland, D. W. (2009). Boveri revisited: chromosomal instability, aneuploidy and tumorigenesis. Nat Rev Mol Cell Biol 10, 478-487.

Houghtaling, B. R., Cuttonaro, L., Chang, W., and Smith, S. (2004). A dynamic molecular link between the telomere length regulator TRF1 and the chromosome end protector TRF2. Curr Biol 14, 1621-1631.

Hu, L., Plafker, K., Vorozhko, V., Zuna, R. E., Hanigan, M. H., Gorbsky, G. J., Plafker, S. M., Angeletti, P. C., and Ceresa, B. P. (2009). Human papillomavirus 16 E5 induces bi-nucleated cell formation by cell-cell fusion. Virology 384, 125-134.

Hui, A. M., Makuuchi, M., and Li, X. (1998). Cell cycle regulators and human hepatocarcinogenesis. Hepatogastroenterology 45, 1635-1642.

Ibrahim, N., and Haluska, F. G. (2009). Molecular pathogenesis of cutaneous

melanocytic neoplasms. Annu Rev Pathol 4, 551-579.

Ilgren, E. B. (1981). On the control of the trophoblastic giant-cell transformation in the mouse: homotypic cellular interactions and polyploidy. J Embryol Exp Morphol 62, 183-202.

Illidge, T. M., Cragg, M. S., Fringes, B., Olive, P., and Erenpreisa, J. A. (2000). Polyploid giant cells provide a survival mechanism for p53 mutant cells after DNA damage. Cell Biol Int 24, 621-633.

Itzhaki, J. E., Gilbert, C. S., and Porter, A. C. (1997). Construction by gene targeting in human cells of a "conditional' CDC2 mutant that rereplicates its DNA. Nat Genet 15, 258-265.

Ivanov, A., Cragg, M. S., Erenpreisa, J., Emzinsh, D., Lukman, H., and Illidge, T. M. (2003). Endopolyploid cells produced after severe genotoxic damage have the potential to repair DNA double strand breaks. J Cell Sci 116, 4095-4106.

Levan A. (1956). Chromosomes in cancer tissue. Ann N Y Acad Sci 63, 774-792.

Jacobs, J. J., and de Lange, T. (2004). Significant Role for p16(INK4a) in p53-Independent Telomere-Directed Senescence. Curr Biol 14, 2302-2308.

Jacobs, J. J., Keblusek, P., Robanus-Maandag, E., Kristel, P., Lingbeek, M., Nederlof, P. M., van Welsem, T., van de Vijver, M. J., Koh, E. Y., Daley, G. Q., and van Lohuizen, M. (2000). Senescence bypass screen identifies TBX2, which represses Cdkn2a (p19(ARF)) and is amplified in a subset of human breast cancers. Nat Genet 26, 291-299.

Jaillon, O., Aury, J. M., Brunet, F., Petit, J. L., Stange-Thomann, N., Mauceli, E., Bouneau, L., Fischer, C., Ozouf-Costaz, C., Bernot, A., Nicaud, S., Jaffe, D., Fisher, S., Lutfalla, G., Dossat, C., Segurens, B., Dasilva, C., Salanoubat, M., Levy, M., Boudet, N., Castellano, S., Anthouard, V., Jubin, C., Castelli, V., Katinka, M., Vacherie, B., Biemont, C., Skalli, Z., Cattolico, L., Poulain, J., De Berardinis, V., Cruaud, C., Duprat, S., Brottier, P., Coutanceau, J. P., Gouzy, J., Parra, G., Lardier, G., Chapple, C., McKernan, K. J., McEwan, P., Bosak, S., Kellis, M., Volff, J. N., Guigo, R., Zody, M. C., Mesirov, J., Lindblad-Toh, K., Birren, B., Nusbaum, C., Kahn, D., Robinson-Rechavi, M., Laudet, V., Schachter, V., Quetier, F., Saurin, W., Scarpelli, C., Wincker, P., Lander, E. S., Weissenbach, J., and Roest Crollius, H. (2004). Genome duplication in the teleost fish Tetraodon nigroviridis reveals the early vertebrate proto-karyotype. Nature 431, 946-957.

Jeyapalan, J. C., Ferreira, M., Sedivy, J. M., and Herbig, U. (2007). Accumulation of senescent cells in mitotic tissue of aging primates. Mech Ageing Dev 128, 36-44.

Jiang, Z., Li, X., Hu, J., Zhou, W., Jiang, Y., Li, G., and Lu, D. (2006). Promoter hypermethylation-mediated down-regulation of LATS1 and LATS2 in human astrocytoma. Neurosci Res 56, 450-458.

Joubes, J., and Chevalier, C. (2000). Endoreduplication in higher plants. Plant Mol Biol 43, 735-745.

Kallioniemi, O. P., Punnonen, R., Mattila, J., Lehtinen, M., and Koivula, T. (1988). Prognostic significance of DNA index, multiploidy, and S-phase fraction in ovarian cancer. Cancer 61, 334-339.

Kaplan, K. B., Burds, A. A., Swedlow, J. R., Bekir, S. S., Sorger, P. K., and Nathke, I. S. (2001). A role for the Adenomatous Polyposis Coli protein in chromosome segregation. Nat Cell Biol 3, 429-432.

Karlseder, J., Broccoli, D., Dai, Y., Hardy, S., and de Lange, T. (1999). p53- and ATM-dependent apoptosis induced by telomeres lacking TRF2. Science 283, 1321-1325.

Kasahara, M. (2007). The 2R hypothesis: an update. Curr Opin Immunol 19, 547-552.

Kiang, L., Heichinger, C., Watt, S., Bahler, J., and Nurse, P. (2009). Cyclin-

dependent kinase inhibits reinitiation of a normal S-phase program during G2 in fission yeast. Mol Cell Biol 29, 4025-4032.

Kibe, T., Osawa, G. A., Keegan, C. E., and de Lange, T. (2010). Telomere Protection by TPP1 Is Mediated by POT1a and POT1b. Mol Cell Biol 30, 1059-1066.

Kim, N. W., Piatyszek, M. A., Prowse, K. R., Harley, C. B., West, M. D., Ho, P. L., Coviello, G. M., Wright, W. E., Weinrich, S. L., and Shay, J. W. (1994). Specific association of human telomerase activity with immortal cells and cancer. Science 266, 2011-2015.

Kim, S. H., Kaminker, P., and Campisi, J. (1999). TIN2, a new regulator of telomere length in human cells. Nat Genet 23, 405-412.

Kirkland, J. A., Stanley, M. A., and Cellier, K. M. (1967). Comparative study of histologic and chromosomal abnormalities in cervical neoplasia. Cancer 20, 1934-1952.

Koeneman, K. S., Pan, C. X., Jin, J. K., Pyle, J. M. r., Flanigan, R. C., Shankey, T. V., and Diaz, M. O. (1998). Telomerase activity, telomere length, and DNA ploidy in prostatic intraepithelial neoplasia (PIN). J Urol 160, 1533-1539.

Kraft, C., Herzog, F., Gieffers, C., Mechtler, K., Hagting, A., Pines, J., and Peters, J. M. (2003). Mitotic regulation of the human anaphase-promoting complex by phosphorylation. EMBO J 22, 6598-6609.

Kwon, M., Godinho, S. A., Chandhok, N. S., Ganem, N. J., Azioune, A., Thery, M., and Pellman, D. (2008). Mechanisms to suppress multipolar divisions in cancer cells with extra centrosomes. Genes Dev 22, 2189-2203.

Lanni, J. S., and Jacks, T. (1998). Characterization of the p53-dependent postmitotic checkpoint following spindle disruption. Mol Cell Biol 18, 1055-1064.

Lazzerini Denchi, E., Celli, G., and de Lange, T. (2006). Hepatocytes with extensive telomere deprotection and fusion remain viable and regenerate liver mass through endoreduplication. Genes Dev 20, 2648-2653.

Lee, H. O., Davidson, J. M., and Duronio, R. J. (2009). Endoreplication: polyploidy with purpose. Genes Dev 23, 2461-2477.

Lee, S. H., McCormick, F., and Saya, H. (2010). Mad2 inhibits the mitotic kinesin MKlp2. J Cell Biol 191, 1069-1077.

Lehman, N. L., Tibshirani, R., Hsu, J. Y., Natkunam, Y., Harris, B. T., West, R. B., Masek, M. A., Montgomery, K., van de Rijn, M., and Jackson, P.

K. (2007). Oncogenic regulators and substrates of the anaphase promoting complex/cyclosome are frequently overexpressed in malignant tumors. Am J Pathol 170, 1793-1805.

Lehman, N. L., Verschuren, E. W., Hsu, J. Y., Cherry, A. M., and Jackson, P. K. (2006). Overexpression of the anaphase promoting complex/cyclosome inhibitor Emi1 leads to tetraploidy and genomic instability of p53-deficient cells. Cell Cycle 5, 1569-1573.

Lei, M., Podell, E. R., and Cech, T. R. (2004). Structure of human POT1 bound to telomeric single-stranded DNA provides a model for chromosome end-protection. Nat Struct Mol Biol 11, 1223-1229.

Lengauer, C., Kinzler, K. W., and Vogelstein, B. (1997). Genetic instability in colorectal cancers. Nature 386, 623-627.

Letsolo, B. T., Rowson, J., and Baird, D. M. (2010). Fusion of short telomeres in human cells is characterized by extensive deletion and microhomology, and can result in complex rearrangements. Nucleic Acids Res 38, 1841-1852.

Levine, D. S., Rabinovitch, P. S., Haggitt, R. C., Blount, P. L., Dean, P. J., Rubin, C. E., and Reid, B. J. (1991). Distribution of aneuploid cell populations in ulcerative colitis with dysplasia or cancer. Gastroenterology 101, 1198-1210.

Li, B., Oestreich, S., and de Lange, T. (2000). Identification of human Rap1: implications for telomere evolution. Cell 101, 471-483.

Lin, T. T., Letsolo, B. T., Jones, R. E., Rowson, J., Pratt, G., Hewamana, S., Fegan, C., Pepper, C., and Baird, D. M. (2010). Telomere dysfunction and fusion during the progression of chronic lymphocytic leukemia: evidence for a telomere crisis. Blood 116, 1899-1907.

Lin, Y., Miyamoto, H., Fujinami, K., Uemura, H., Hosaka, M., Iwasaki, Y., and Kubota, Y. (1996). Telomerase activity in human bladder cancer. Clin Cancer Res 2, 929-932.

Lingle, W. L., Barrett, S. L., Negron, V. C., D'Assoro, A. B., Boeneman, K., Liu, W., Whitehead, C. M., Reynolds, C., and Salisbury, J. L. (2002). Centrosome amplification drives chromosomal instability in breast tumor development. Proc Natl Acad Sci U S A 99, 1978-1983.

Lingle, W. L., Lukasiewicz, K., and Salisbury, J. L. (2005). Deregulation of the centrosome cycle and the origin of chromosomal instability in cancer. Adv Exp Med Biol 570, 393-421.

Lingle, W. L., Lutz, W. H., Ingle, J. N., Maihle, N. J., and Salisbury, J. L. (1998). Centrosome hypertrophy in human breast tumors: implications for

genomic stability and cell polarity. Proc Natl Acad Sci U S A 95, 2950-2955.

Liu, D., Safari, A., O'Connor, M. S., Chan, D. W., Laegeler, A., Qin, J., and Songyang, Z. (2004). PTOP interacts with POT1 and regulates its localization to telomeres. Nat Cell Biol 6, 673-680.

Lo, A. W., Sabatier, L., Fouladi, B., Pottier, G., Ricoul, M., and Murnane, J. P. (2002a). DNA amplification by breakage/fusion/bridge cycles initiated by spontaneous telomere loss in a human cancer cell line. Neoplasia 4, 531-538.

Lo, A. W., Sprung, C. N., Fouladi, B., Pedram, M., Sabatier, L., Ricoul, M., Reynolds, G. E., and Murnane, J. P. (2002b). Chromosome Instability as a Result of Double-Strand Breaks near Telomeres in Mouse Embryonic Stem Cells. Mol Cell Biol 22, 4836-4850.

Loayza, D., Parsons, H., Donigian, J., Hoke, K., and de Lange, T. (2004). DNA binding features of human POT1: A nonamer 5'-TAGGGTTAG-3' minimal binding site, sequence specificity, and internal binding to multimeric sites. J Biol Chem 279, 13241-13248.

Lothschutz, D., Jennewein, M., Pahl, S., Lausberg, H. F., Eichler, A., Mutschler, W., Hanselmann, R. G., and Oberringer, M. (2002). Polyploidization and centrosome hyperamplification in inflammatory bronchi. Inflamm Res 51, 416-422.

Lukas, C., Sorensen, C. S., Kramer, E., Santoni-Rugiu, E., Lindeneg, C., Peters, J. M., Bartek, J., and Lukas, J. (1999). Accumulation of cyclin B1 requires E2F and cyclin-A-dependent rearrangement of the anaphase-promoting complex. Nature 401, 815-818.

Lundblad, V., and Blackburn, E. H. (1993). An alternative pathway for yeast telomere maintenance rescues est1- senescence. Cell 73, 347-360.

Lutzker, S. G., and Levine, A. J. (1996). Apoptosis and cancer chemotherapy. Cancer Treat Res 87, 345-356.

Macurek, L., Lindqvist, A., Lim, D., Lampson, M. A., Klompmaker, R., Freire, R., Clouin, C., Taylor, S. S., Yaffe, M. B., and Medema, R. H. (2008). Polo-like kinase-1 is activated by aurora A to promote checkpoint recovery. Nature 455, 119-123.

Maitra, A., and Hruban, R. H. (2008). Pancreatic cancer. Annu Rev Pathol 3, 157-188.

Maley, C. C. (2007). Multistage carcinogenesis in Barrett's esophagus. Cancer Lett 245, 22-32.

Manning, A. L., Longworth, M. S., and Dyson, N. J. (2010). Loss of pRB

causes centromere dysfunction and chromosomal instability. Genes Dev 24, 1364-1376.

Margall-Ducos, G., Celton-Morizur, S., Couton, D., Bregerie, O., and Desdouets, C. (2007). Liver tetraploidization is controlled by a new process of incomplete cytokinesis. J Cell Sci 120, 3633-3639.

Margolis, R. L., Lohez, O. D., and Andreassen, P. R. (2003). G1 tetraploidy checkpoint and the suppression of tumorigenesis. J Cell Biochem 88, 673-683.

Martin, J., and Dufour, J. F. (2008). Tumor suppressor and hepatocellular carcinoma. World J Gastroenterol 14, 1720-1733.

Maser, R. S., and DePinho, R. A. (2002). Connecting chromosomes, crisis, and cancer. Science 297, 565-569.

Maser, R. S., Wong, K. K., Sahin, E., Xia, H., Naylor, M., Hedberg, H. M., Artandi, S. E., and DePinho, R. A. (2007). DNA-dependent protein kinase catalytic subunit is not required for dysfunctional telomere fusion and checkpoint response in the telomerase-deficient mouse. Mol Cell Biol 27, 2253-2265.

Masterson, J. (1994). Stomatal size in fossil plants: evidence for polyploidy in majority of angiosperms. Science 264, 421-424.

Mayer, V. W., and Aguilera, A. (1990). High levels of chromosome instability in polyploids of Saccharomyces cerevisiae. Mutat Res 231, 177-186.

McClintock, B. (1941). The stability of broken ends of chromosomes in Zea mays. Genetics 26, 234-282.

McGarry, T. J., and Kirschner, M. W. (1998). Geminin, an inhibitor of DNA replication, is degraded during mitosis. Cell 93, 1043-1053.

Meeker, A. K., and Argani, P. (2004). Telomere shortening occurs early during breast tumorigenesis: a cause of chromosome destabilization underlying malignant transformation? J Mammary Gland Biol Neoplasia 9, 285-296.

Meeker, A. K., Hicks, J. L., Iacobuzio-Donahue, C. A., Montgomery, E. A., Westra, W. H., Chan, T. Y., Ronnett, B. M., and De Marzo, A. M. (2004). Telomere length abnormalities occur early in the initiation of epithelial carcinogenesis. Clin Cancer Res 10, 3317-3326.

Meeker, A. K., Hicks, J. L., Platz, E. A., March, G. E., Bennett, C. J., Delannoy, M. J., and De Marzo, A. M. (2002). Telomere shortening is an early somatic DNA alteration in human prostate tumorigenesis. Cancer Res 62, 6405-6409.

Meraldi, P., Honda, R., and Nigg, E. A. (2002). Aurora-A overexpression re-

veals tetraploidization as a major route to centrosome amplification in p53-/- cells. EMBO J 21, 483-492.

Mitra, A. P., and Cote, R. J. (2009). Molecular pathogenesis and diagnostics of bladder cancer. Annu Rev Pathol 4, 251-285.

Miura, N., Horikawa, I., Nishimoto, A., Ohmura, H., Ito, H., Hirohashi, S., Shay, J. W., and Oshimura, M. (1997). Progressive telomere shortening and telomerase reactivation during hepatocellular carcinogenesis. Cancer Genet Cytogenet 93, 56-62.

Montgomery, B. T., Nativ, O., Blute, M. L., Farrow, G. M., Myers, R. P., Zincke, H., Therneau, T. M., and Lieber, M. M. (1990). Stage B prostate adenocarcinoma. Flow cytometric nuclear DNA ploidy analysis. Arch Surg 125, 327-331.

Moody, C. A., and Laimins, L. A. (2010). Human papillomavirus oncoproteins: pathways to transformation. Nat Rev Cancer 10, 550-560.

Mortimer, R. K. (1958). Radiobiological and genetic studies on a polyploid series (haploid to hexaploid) of Saccharomyces cerevisiae. Radiat Res 9, 312-326.

Mullins, J. M., and Biesele, J. J. (1977). Terminal phase of cytokinesis in

D-98s cells. J Cell Biol 73, 672-684.

Murakami, J., Nagai, N., Ohama, K., Tahara, H., and Ide, T. (1997). Telomerase activity in ovarian tumors. Cancer 80, 1085-1092.

Musacchio, A., and Salmon, E. D. (2007). The spindle-assembly checkpoint in space and time. Nat Rev Mol Cell Biol 8, 379-393.

Nakayama, Y., Igarashi, A., Kikuchi, I., Obata, Y., Fukumoto, Y., and Yamaguchi, N. (2009). Bleomycin-induced over-replication involves sustained inhibition of mitotic entry through the ATM/ATR pathway. Exp Cell Res 315, 2515-2528.

Narbonne-Reveau, K., Senger, S., Pal, M., Herr, A., Richardson, H. E., Asano, M., Deak, P., and Lilly, M. A. (2008). APC/CFzr/Cdh1 promotes cell cycle progression during the Drosophila endocycle. Development 135, 1451-1461.

Negrini, S., Gorgoulis, V. G., and Halazonetis, T. D. (2010). Genomic instability–an evolving hallmark of cancer. Nat Rev Mol Cell Biol 11, 220-228.

Noguchi, M. (2010). Stepwise progression of pulmonary adenocarcinoma–clinical and molecular implications. Cancer Metastasis Rev 29, 15-21.

O'Connor, M. S., Safari, A., Xin, H., Liu, D., and Songyang, Z. (2006). A

critical role for TPP1 and TIN2 interaction in high-order telomeric complex assembly. Proc Natl Acad Sci USA 103, 11874-11879.

O'Sullivan, J. N., Bronner, M. P., Brentnall, T. A., Finley, J. C., Shen, W. T., Emerson, S., Emond, M. J., Gollahon, K. A., Moskovitz, A. H., Crispin, D. A., Potter, J. D., and Rabinovitch, P. S. (2002). Chromosomal instability in ulcerative colitis is related to telomere shortening. Nat Genet 32, 280-284.

Oberringer, M., Lothschutz, D., Jennewein, M., Koschnick, M., Mutschler, W., and Hanselmann, R. G. (1999). Centrosome multiplication accompanies a transient clustering of polyploid cells during tissue repair. Mol Cell Biol Res Commun 2, 190-196.

Olaharski, A. J., Sotelo, R., Solorza-Luna, G., Gonsebatt, M. E., Guzman, P., Mohar, A., and Eastmond, D. A. (2006). c. Carcinogenesis 27, 337-343.

Ohno, S. (1970). Evolution By Gene Duplication Allen & Unwin

Ottesen, G. L. (2003). Carcinoma in situ of the female breast. A clinico-pathological, immunohistological, and DNA ploidy study. APMIS Suppl 1-67.

Otto, S. P., and Whitton, J. (2000). Polyploid incidence and evolution. Annu Rev Genet 34, 401-437.

Palazon, L. S., Davies, T. J., and Gardner, R. L. (1998). Translational inhibition of cyclin B1 and appearance of cyclin D1 very early in the differentiation of mouse trophoblast giant cells. Mol Hum Reprod 4, 1013-1020.

Pantic, M., Zimmermann, S., El Daly, H., Opitz, O. G., Popp, S., Boukamp, P., and Martens, U. M. (2006). Telomere dysfunction and loss of p53 cooperate in defective mitotic segregation of chromosomes in cancer cells. Oncogene 25, 4413-4420.

Paquin, C., and Adams, J. (1983). Frequency of fixation of adaptive mutations is higher in evolving diploid than haploid yeast populations. Nature 302, 495-500.

Peters, J. M. (2002). The anaphase-promoting complex: proteolysis in mitosis and beyond. Mol Cell 9, 931-943.

Pihan, G. A., Purohit, A., Wallace, J., Knecht, H., Woda, B., Quesenberry, P., and Doxsey, S. J. (1998). Centrosome defects and genetic instability in malignant tumors. Cancer Res 58, 3974-3985.

Pihan, G. A., Purohit, A., Wallace, J., Malhotra, R., Liotta, L., and Doxsey, S. J. (2001). Centrosome defects can account for cellular and genetic changes that characterize prostate cancer progression. Cancer Res 61, 2212-2219.

Pihan, G. A., Wallace, J., Zhou, Y., and Doxsey, S. J. (2003). Centrosome abnormalities and chromosome instability occur together in pre-invasive carcinomas. Cancer Res 63, 1398-1404.

Pobiega, S., and Marcand, S. (2010). Dicentric breakage at telomere fusions. Genes Dev 24, 720-733.

Puig, P. E., Guilly, M. N., Bouchot, A., Droin, N., Cathelin, D., Bouyer, F., Favier, L., Ghiringhelli, F., Kroemer, G., Solary, E., Martin, F., and Chauffert, B. (2008). Tumor cells can escape DNA-damaging cisplatin through DNA endoreduplication and reversible polyploidy. Cell Biol Int 32, 1031-1043.

Radulescu, S., Ridgway, R. A., Appleton, P., Kroboth, K., Patel, S., Woodgett, J., Taylor, S., Nathke, I. S., and Sansom, O. J. (2010). Defining the role of APC in the mitotic spindle checkpoint in vivo: APC-deficient cells are resistant to Taxol. Oncogene 29, 6418-6427.

Ravid, K., Lu, J., Zimmet, J. M., and Jones, M. R. (2002). Roads to polyploidy: the megakaryocyte example. J Cell Physiol 190, 7-20.

Reid, B. J., Barrett, M. T., Galipeau, P. C., Sanchez, C. A., Neshat, K., Cowan, D. S., and Levine, D. S. (1996). Barrett's esophagus: ordering the events that lead to cancer. Eur J Cancer Prev 5 Suppl 2, 57-65.

Reina-San-Martin, B., Nussenzweig, M. C., Nussenzweig, A., and Difilippantonio, S. (2005). Genomic instability, endoreduplication, and diminished Ig class-switch recombination in B cells lacking Nbs1. Proc Natl Acad Sci U S A 102, 1590-1595.

Remus, D., and Diffley, J. F. (2009). Eukaryotic DNA replication control: lock and load, then fire. Curr Opin Cell Biol 21, 771-777.

Rhodes, J., Amsterdam, A., Sanda, T., Moreau, L. A., McKenna, K., Heinrichs, S., Ganem, N. J., Ho, K. W., Neuberg, D. S., Johnston, A., Ahn, Y., Kutok, J. L., Hromas, R., Wray, J., Lee, C., Murphy, C., Radtke, I., Downing, J. R., Fleming, M. D., MacConaill, L. E., Amatruda, J. F., Gutierrez, A., Galinsky, I., Stone, R. M., Ross, E. A., Pellman, D. S., Kanki, J. P., and Look, A. T. (2009). Emi1 maintains genomic integrity during zebrafish embryogenesis and cooperates with p53 in tumor suppression. Mol Cell Biol 29, 5911-5922.

Riethman, H., Ambrosini, A., Castaneda, C., Finklestein, J. M., Hu, X. L., Paul, S., and Wei, J. (2003). Human subtelomeric DNA. Cold Spring Harb Symp Quant Biol 68, 39-47.

Roh, M., Franco, O. E., Hayward, S. W., van der Meer, R., and Abdulkadir, S. A. (2008). A role for polyploidy in the tumorigenicity of Pim-1-expressing human prostate and mammary epithelial cells. PLoS One 3, e2572.

Romanov, S. R., Kozakiewicz, B. K., Holst, C. R., Stampfer, M. R., Haupt, L. M., and Tlsty, T. D. (2001). Normal human mammary epithelial cells spontaneously escape senescence and acquire genomic changes. Nature 409, 633-637.

Rossant, J., and Cross, J. C. (2001). Placental development: lessons from mouse mutants. Nat Rev Genet 2, 538-548.

Rudolph, K. L., Millard, M., Bosenberg, M. W., and DePinho, R. A. (2001). Telomere dysfunction and evolution of intestinal carcinoma in mice and humans. Nat Genet 28, 155-159.

Sakaue-Sawano, A., Kurokawa, H., Morimura, T., Hanyu, A., Hama, H., Osawa, H., Kashiwagi, S., Fukami, K., Miyata, T., Miyoshi, H., Imamura, T., Ogawa, M., Masai, H., and Miyawaki, A. (2008). Visualizing spatiotemporal dynamics of multicellular cell-cycle progression. Cell 132, 487-498.

Saksela, E., and Moorhead, P. S. (1963). Aneuploidy in the degenerative phase of serial cultivation of human cell strains. Proc Natl Acad Sci U S A 50, 390-395.

Sato, N., Mizumoto, K., Nakamura, M., Nakamura, K., Kusumoto, M., Niiyama, H., Ogawa, T., and Tanaka, M. (1999). Centrosome abnormalities in pancreatic ductal carcinoma. Clin Cancer Res 5, 963-970.

Schaeffer, V., Althauser, C., Shcherbata, H. R., Deng, W. M., and Ruohola-Baker, H. (2004). Notch-dependent Fizzy-related/Hec1/Cdh1 expression is required for the mitotic-to-endocycle transition in Drosophila follicle cells. Curr Biol 14, 630-636.

Scheel, C., Schaefer, K. L., Jauch, A., Keller, M., Wai, D., Brinkschmidt, C., van Valen, F., Boecker, W., Dockhorn-Dworniczak, B., and Poremba, C. (2001). Alternative lengthening of telomeres is associated with chromosomal instability in osteosarcomas. Oncogene 20, 3835-3844.

Serrano, M., Lin, A. W., McCurrach, M. E., Beach, D., and Lowe, S. W. (1997). Oncogenic ras provokes premature cell senescence associated with accumulation of p53 and p16INK4a. Cell 88, 593-602.

Sfeir, A., Kabir, S., van Overbeek, M., Celli, G. B., and de Lange, T. (2010). Loss of Rap1 induces telomere recombination in the absence of NHEJ or a DNA damage signal. Science 327, 1657-1661.

Sfeir, A., Kosiyatrakul, S. T., Hockemeyer, D., MacRae, S. L., Karlseder, J., Schildkraut, C. L., and de Lange, T. (2009). Mammalian telomeres resemble fragile sites and require TRF1 for efficient replication. Cell 138, 90-103.

Shackney, S. E., Berg, G., Simon, S. R., Cohen, J., Amina, S., Pommersheim,

W., Yakulis, R., Wang, S., Uhl, M., Smith, C. A., and et, a. (1995a). Origins and clinical implications of aneuploidy in early bladder cancer. Cytometry 22, 307-316.

Shackney, S. E., and Silverman, J. F. (2003). Molecular evolutionary patterns in breast cancer. Adv Anat Pathol 10, 278-290.

Shackney, S. E., Singh, S. G., Yakulis, R., Smith, C. A., Pollice, A. A., Petruolo, S., Waggoner, A., and Hartsock, R. J. (1995b). Aneuploidy in breast cancer: a fluorescence in situ hybridization study. Cytometry 22, 282-291.

Shackney, S. E., Smith, C. A., Miller, B. W., Burholt, D. R., Murtha, K., Giles, H. R., Ketterer, D. M., and Pollice, A. A. (1989). Model for the genetic evolution of human solid tumors. Cancer Res 49, 3344-3354.

Shay, J. W., and Bacchetti, S. (1997). A survey of telomerase activity in human cancer. Eur J Cancer 33, 787-791.

Shay, J. W., and Wright, W. E. (1989). Quantitation of the frequency of immortalization of normal human diploid fibroblasts by SV40 large T-antigen. Exp Cell Res 184, 109-118.

Shay, J. W., Pereira-Smith, O. M., and Wright, W. E. (1991). A role for both RB and p53 in the regulation of human cellular senescence. Exp Cell Res 196,

33-39.

Shay, J. W., Van Der Haegen, B. A., Ying, Y., and Wright, W. E. (1993). The frequency of immortalization of human fibroblasts and mammary epithelial cells transfected with SV40 large T-antigen. Exp Cell Res 209, 45-52.

Shay, J. W., and Wright, W. E. (2005). Senescence and immortalization: role of telomeres and telomerase. Carcinogenesis 26, 867-874.

Shepard, J. L., Amatruda, J. F., Finkelstein, D., Ziai, J., Finley, K. R., Stern, H. M., Chiang, K., Hersey, C., Barut, B., Freeman, J. L., Lee, C., Glickman, J. N., Kutok, J. L., Aster, J. C., and Zon, L. I. (2007). A mutation in separase causes genome instability and increased susceptibility to epithelial cancer. Genes Dev 21, 55-59.

Sigrist, S. J., and Lehner, C. F. (1997). Drosophila fizzy-related down-regulates mitotic cyclins and is required for cell proliferation arrest and entry into endocycles. Cell 90, 671-681.

Silkworth, W. T., Nardi, I. K., Scholl, L. M., and Cimini, D. (2009). Multipolar spindle pole coalescence is a major source of kinetochore mis-attachment and chromosome mis-segregation in cancer cells. PLoS One 4, e6564.

Silver, D. P., and Livingston, D. M. (2001). Self-excising retroviral vectors

encoding the Cre recombinase overcome Cre-mediated cellular toxicity. Mol Cell 8, 233-243.

Smith, A. V., and Orr-Weaver, T. L. (1991). The regulation of the cell cycle during Drosophila embryogenesis: the transition to polyteny. Development 112, 997-1008.

Smogorzewska, A., and de Lange, T. (2002). Different telomere damage signaling pathways in human and mouse cells. Embo J 21, 4338-4348.

Sotillo, R., Hernando, E., Diaz-Rodriguez, E., Teruya-Feldstein, J., Cordon-Cardo, C., Lowe, S. W., and Benezra, R. (2007). Mad2 overexpression promotes aneuploidy and tumorigenesis in mice. Cancer Cell 11, 9-23.

Staiger, J., Stolze, H., and Adler, C. P. (1975). Nuclear deoxyribonucleic acid content in congenital cardiac malformations. Recent Adv Stud Cardiac Struct Metab 6, 357-363.

Stansel, R. M., de Lange, T., and Griffith, J. D. (2001). T-loop assembly in vitro involves binding of TRF2 near the 3' telomeric overhang. EMBO J 20, 5532-5540.

Steigemann, P., Wurzenberger, C., Schmitz, M. H., Held, M., Guizetti, J., Maar, S., and Gerlich, D. W. (2009). Aurora B-mediated abscission check-

point protects against tetraploidization. Cell 136, 473-484.

Stephens, P. J., Greenman, C. D., Fu, B., Yang, F., Bignell, G. R., Mudie, L. J., Pleasance, E. D., Lau, K. W., Beare, D., Stebbings, L. A., McLaren, S., Lin, M. L., McBride, D. J., Varela, I., Nik-Zainal, S., Leroy, C., Jia, M., Menzies, A., Butler, A. P., Teague, J. W., Quail, M. A., Burton, J., Swerdlow, H., Carter, N. P., Morsberger, L. A., Iacobuzio-Donahue, C., Follows, G. A., Green, A. R., Flanagan, A. M., Stratton, M. R., Futreal, P. A., and Campbell, P. J. (2011). Massive genomic rearrangement acquired in a single catastrophic event during cancer development. Cell 144, 27-40.

Storchova, Z., Breneman, A., Cande, J., Dunn, J., Burbank, K., O'Toole, E., and Pellman, D. (2006). Genome-wide genetic analysis of polyploidy in yeast. Nature 443, 541-547.

Suehara, N., Mizumoto, K., Muta, T., Tominaga, Y., Shimura, H., Kitajima, S., Hamasaki, N., Tsuneyoshi, M., and Tanaka, M. (1997). Telomerase elevation in pancreatic ductal carcinoma compared to nonmalignant pathological states. Clin Cancer Res 3, 993-998.

Takahashi, Y., Miyoshi, Y., Takahata, C., Irahara, N., Taguchi, T., Tamaki, Y., and Noguchi, S. (2005). Down-regulation of LATS1 and LATS2 mRNA expression by promoter hypermethylation and its association with biologically aggressive phenotype in human breast cancers. Clin Cancer Res 11, 1380-1385.

Takai, K. K., Hooper, S., Blackwood, S., Gandhi, R., and de Lange, T. (2010). In vivo stoichiometry of shelterin components. J Biol Chem 285, 1457-1467.

Takai, K. K., Kibe, T., Donigian, J. R., Frescas, D., and de Lange, T. (2011). Telomere protection by TPP1/POT1 requires tethering to TIN2. Mol Cell 44, 647-659.

Tanaka, T., Mori, H., Takahashi, M., and Williams, G. M. (1984). DNA content of hyperplastic and neoplastic acinar cell lesions in rat and human pancreas. J Exp Pathol 1, 315-326.

Teramoto, T., Satonaka, K., Kitazawa, S., Fujimori, T., Hayashi, K., and Maeda, S. (1994). p53 gene abnormalities are closely related to hepatoviral infections and occur at a late stage of hepatocarcinogenesis. Cancer Res 54, 231-235.

Thompson, D. A., Desai, M. M., and Murray, A. W. (2006). Ploidy controls the success of mutators and nature of mutations during budding yeast evolution. Curr Biol 16, 1581-1590.

Thompson, S. L., Bakhoum, S. F., and Compton, D. A. (2010). Mechanisms of chromosomal instability. Curr Biol 20, R285-95.

Thompson, S. L., and Compton, D. A. (2010). Proliferation of aneuploid human cells is limited by a p53-dependent mechanism. J Cell Biol 188, 369-381.

Toledo, L. I., Murga, M., Gutierrez-Martinez, P., Soria, R., and Fernandez-Capetillo, O. (2008). ATR signaling can drive cells into senescence in the absence of DNA breaks. Genes Dev 22, 297-302.

Uetake, Y., and Sluder, G. (2004). Cell cycle progression after cleavage failure: mammalian somatic cells do not possess a "tetraploidy checkpoint". J Cell Biol 165, 609-615.

Ullah, Z., Kohn, M. J., Yagi, R., Vassilev, L. T., and DePamphilis, M. L. (2008). Differentiation of trophoblast stem cells into giant cells is triggered by p57/Kip2 inhibition of CDK1 activity. Genes Dev 22, 3024-3036.

Ullah, Z., Lee, C. Y., and Depamphilis, M. L. (2009a). Cip/Kip cyclin-dependent protein kinase inhibitors and the road to polyploidy. Cell Div 4, 10.

Ullah, Z., Lee, C. Y., Lilly, M. A., and DePamphilis, M. L. (2009b). Developmentally programmed endoreduplication in animals. Cell Cycle 8, 1501-1509.

van 't Veer, L. J., Dai, H., van de Vijver, M. J., He, Y. D., Hart, A. A., Mao, M., Peterse, H. L., van der Kooy, K., Marton, M. J., Witteveen, A. T.,

Schreiber, G. J., Kerkhoven, R. M., Roberts, C., Linsley, P. S., Bernards, R., and Friend, S. H. (2002). Gene expression profiling predicts clinical outcome of breast cancer. Nature 415, 530-536.

van Harn, T., Foijer, F., van Vugt, M., Banerjee, R., Yang, F., Oostra, A., Joenje, H., and te Riele, H. (2010). Loss of Rb proteins causes genomic instability in the absence of mitogenic signaling. Genes Dev 24, 1377-1388.

van Heek, N. T., Meeker, A. K., Kern, S. E., Yeo, C. J., Lillemoe, K. D., Cameron, J. L., Offerhaus, G. J., Hicks, J. L., Wilentz, R. E., Goggins, M. G., De Marzo, A. M., Hruban, R. H., and Maitra, A. (2002). Telomere shortening is nearly universal in pancreatic intraepithelial neoplasia. Am J Pathol 161, 1541-1547.

van Steensel, B., and de Lange, T. (1997). Control of telomere length by the human telomeric protein TRF1. Nature 385, 740-743.

van Steensel, B., Smogorzewska, A., and de Lange, T. (1998). TRF2 protects human telomeres from end-to-end fusions. Cell 92, 401-413.

van Vugt, M. A., Bras, A., and Medema, R. H. (2004). Polo-like kinase-1 controls recovery from a G2 DNA damage-induced arrest in mammalian cells. Mol Cell 15, 799-811.

Vignery, A. (2000). Osteoclasts and giant cells: macrophage-macrophage fusion mechanism. Int J Exp Pathol 81, 291-304.

Wagner, M., Hampel, B., Bernhard, D., Hala, M., Zwerschke, W., and Jansen-Durr, P. (2001). Replicative senescence of human endothelial cells in vitro involves G1 arrest, polyploidization and senescence-associated apoptosis. Exp Gerontol 36, 1327-1347.

Waldman, T., Lengauer, C., Kinzler, K. W., and Vogelstein, B. (1996). Uncoupling of S phase and mitosis induced by anticancer agents in cells lacking p21. Nature 381, 713-716.

Walen, K. H. (2006). Human diploid fibroblast cells in senescence; cycling through polyploidy to mitotic cells. In Vitro Cell Dev Biol Anim 42, 216-224.

Walworth, N. C. (2001). DNA damage: Chk1 and Cdc25, more than meets the eye. Curr Opin Genet Dev 11, 78-82.

Wang, X., Zou, L., Zheng, H., Wei, Q., Elledge, S. J., and Li, L. (2003). Genomic instability and endoreduplication triggered by RAD17 deletion. Genes Dev 17, 965-970.

Watanabe, T., Shimada, H., and Tanaka, Y. (1978). Human hepatocytes and aging: a cytophotometrical analysis in 35 sudden-death cases. Virchows Arch

B Cell Pathol 27, 307-316.

Winkelmann, M., Pfitzer, P., and Schneider, W. (1987). Significance of polyploidy in megakaryocytes and other cells in health and tumor disease. Klin Wochenschr 65, 1115-1131.

Wirth, K. G., Wutz, G., Kudo, N. R., Desdouets, C., Zetterberg, A., Taghybeeglu, S., Seznec, J., Ducos, G. M., Ricci, R., Firnberg, N., Peters, J. M., and Nasmyth, K. (2006). Separase: a universal trigger for sister chromatid disjunction but not chromosome cycle progression. J Cell Biol 172, 847-860.

Wong, C., and Stearns, T. (2005). Mammalian cells lack checkpoints for tetraploidy, aberrant centrosome number, and cytokinesis failure. BMC Cell Biol 6, 6.

Wright, W. E., and Shay, J. W. (1992). The two-stage mechanism controlling cellular senescence and immortalization. Exp Gerontol 27, 383-389.

Xin, H., Liu, D., Wan, M., Safari, A., Kim, H., Sun, W., O'Connor, M. S., and Songyang, Z. (2007). TPP1 is a homologue of ciliate TEBP-beta and interacts with POT1 to recruit telomerase. Nature 445, 559-562.

Yaffe, D., and Feldman, M. (1965). The formation of hybrid multinucleated muscle fibers from myoblasts of different genetic origin* 1. Developmental Bi-

ology 11, 300-317.

Yang, X., Yu, K., Hao, Y., Li, D. M., Stewart, R., Insogna, K. L., and Xu, T. (2004). LATS1 tumour suppressor affects cytokinesis by inhibiting LIMK1. Nat Cell Biol 6, 609-617.

Ye, J. Z., Donigian, J. R., Van Overbeek, M., Loayza, D., Luo, Y., Krutchinsky, A. N., Chait, B. T., and de Lange, T. (2004). TIN2 binds TRF1 and TRF2 simultaneously and stabilizes the TRF2 complex on telomeres. J Biol Chem 279, 47264-47271.

Yoshihara, T., Ishida, M., Kinomura, A., Katsura, M., Tsuruga, T., Tashiro, S., Asahara, T., and Miyagawa, K. (2004). XRCC3 deficiency results in a defect in recombination and increased endoreduplication in human cells. Embo J 23, 670-680.

Zachariae, W., Schwab, M., Nasmyth, K., and Seufert, W. (1998). Control of cyclin ubiquitination by CDK-regulated binding of Hct1 to the anaphase promoting complex. Science 282, 1721-1724.

Zeyl, C., Vanderford, T., and Carter, M. (2003). An evolutionary advantage of haploidy in large yeast populations. Science 299, 555-558.

Zhang, A., Wang, J., Zheng, B., Fang, X., Angstrom, T., Liu, C., Li, X.,

Erlandsson, F., Bjorkholm, M., Nordenskjord, M., Gruber, A., Wallin, K. L., and Xu, D. (2004a). Telomere attrition predominantly occurs in precursor lesions during in vivo carcinogenic process of the uterine cervix. Oncogene 23, 7441-7447.

Zhang, D., Hirota, T., Marumoto, T., Shimizu, M., Kunitoku, N., Sasayama, T., Arima, Y., Feng, L., Suzuki, M., Takeya, M., and Saya, H. (2004b). Cre-loxP-controlled periodic Aurora-A overexpression induces mitotic abnormalities and hyperplasia in mammary glands of mouse models. Oncogene 23, 8720-8730.

Zhou, H., Kuang, J., Zhong, L., Kuo, W. L., Gray, J. W., Sahin, A., Brinkley, B. R., and Sen, S. (1998). Tumour amplified kinase STK15/BTAK induces centrosome amplification, aneuploidy and transformation. Nat Genet 20, 189-193.

Zielke, N., Querings, S., Rottig, C., Lehner, C., and Sprenger, F. (2008). The anaphase-promoting complex/cyclosome (APC/C) is required for rereplication control in endoreplication cycles. Genes Dev 22, 1690-1703.